Proceedings
PRO 128

Proceedings of the International Conference on Sustainable Materials, Systems and Structures (SMSS2019)

Challenges in Design and Management of Structures

Edited by
Ana Mandić Ivanković
Marija Kušter Marić
Alfred Strauss
Tomislav Kišiček

RILEM Publications S.A.R.L.

International Conference on Sustainable Materials, Systems and Structures (SMSS 2019)

Challenges in Design and Management of Structures

International Conference on Sustainable Materials, Systems and Structures (SMSS 2019)
Challenges in Design and Management of Structures
20-22 March 2019 – Rovinj, Croatia

Published by RILEM Publications S.A.R.L.
4 avenue du Recteur Poincaré 75016 Paris - France
Tel : + 33 1 42 24 64 46 Fax : + 33 9 70 29 51 20
http://www.rilem.net E-mail: dg@rilem.net

ISBN: 978-2-35158-217-6, Vol 4. 978-2-35158-226-8
e-ISBN: 978-2-35158-218-3

RILEM, The International Union of Laboratories and Experts in Construction Materials, Systems and Structures, is a non profit-making, non-governmental technical association whose vocation is to contribute to progress in the construction sciences, techniques and industries, essentially by means of the communication it fosters between research and practice. RILEM's activity therefore aims at developing the knowledge of properties of materials and performance of structures, at defining the means for their assessment in laboratory and service conditions and at unifying measurement and testing methods used with this objective.

RILEM was founded in 1947 and has a membership of over 900 in some 70 countries. It forms an institutional framework for co-operation by experts to:
• optimise and harmonise test methods for measuring properties and performance of building and civil engineering materials and structures under laboratory and service environments,
• prepare technical recommendations for testing methods,
• prepare state-of-the-art reports to identify further research needs,
• collaborate with national or international associations in realising these objectives.

RILEM members include the leading building research and testing laboratories around the world, industrial research, manufacturing and contracting interests, as well as a significant number of individual members from industry and universities. RILEM's focus is on construction materials and their use in building and civil engineering structures, covering all phases of the building process from manufacture to use and recycling of materials.

RILEM meets these objectives through the work of its technical committees. Symposia, workshops and seminars are organised to facilitate the exchange of information and dissemination of knowledge. RILEM's primary output consists of technical recommendations. RILEM also publishes the journal *Materials and Structures* which provides a further avenue for reporting the work of its committees. Many other publications, in the form of reports, monographs, symposia and workshop proceedings are produced.

International Conference on Sustainable Materials, Systems and Structures – SMSS 2019
Challenges in Design and Management of Structures

Rovinj, Croatia
20-22 March 2019

Edited by
Ana Mandić Ivanković
Marija Kušter Marić
Alfred Strauss
Tomislav Kišiček

RILEM Publications S.A.R.L.

CONFERENCE SPONSORS

RILEM Publications

The following list is presenting the global offer of RILEM Publications, sorted by series. Each publication is available in printed version and/or in online version.

RILEM PROCEEDINGS (PRO)

PRO 1: Durability of High Performance Concrete (ISBN: 2-912143-03-9); *Ed. H. Sommer*

PRO 2: Chloride Penetration into Concrete (ISBN: 2-912143-00-04); *Eds. L.-O. Nilsson and J.-P. Ollivier*

PRO 3: Evaluation and Strengthening of Existing Masonry Structures (ISBN: 2-912143-02-0); *Eds. L. Binda and C. Modena*

PRO 4: Concrete: From Material to Structure (ISBN: 2-912143-04-7); *Eds. J.-P. Bournazel and Y. Malier*

PRO 5: The Role of Admixtures in High Performance Concrete (ISBN: 2-912143-05-5); *Eds. J. G. Cabrera and R. Rivera-Villarreal*

PRO 6: High Performance Fiber Reinforced Cement Composites - HPFRCC 3 (ISBN: 2-912143-06-3); *Eds. H. W. Reinhardt and A. E. Naaman*

PRO 7: 1st International RILEM Symposium on Self-Compacting Concrete (ISBN: 2-912143-09-8); *Eds. Å. Skarendahl and Ö. Petersson*

PRO 8: International RILEM Symposium on Timber Engineering (ISBN: 2-912143-10-1); *Ed. L. Boström*

PRO 9: 2nd International RILEM Symposium on Adhesion between Polymers and Concrete ISAP ’99 (ISBN: 2-912143-11-X); *Eds. Y. Ohama and M. Puterman*

PRO 10: 3rd International RILEM Symposium on Durability of Building and Construction Sealants (ISBN: 2-912143-13-6); *Eds. A. T. Wolf*

PRO 11: 4th International RILEM Conference on Reflective Cracking in Pavements (ISBN: 2-912143-14-4); *Eds. A. O. Abd El Halim, D. A. Taylor and El H. H. Mohamed*

PRO 12: International RILEM Workshop on Historic Mortars: Characteristics and Tests (ISBN: 2-912143-15-2); *Eds. P. Bartos, C. Groot and J. J. Hughes*

PRO 13: 2nd International RILEM Symposium on Hydration and Setting (ISBN: 2-912143-16-0); *Ed. A. Nonat*

PRO 14: Integrated Life-Cycle Design of Materials and Structures - ILCDES 2000 (ISBN: 951-758-408-3); (ISSN: 0356-9403); *Ed. S. Sarja*

PRO 15: Fifth RILEM Symposium on Fibre-Reinforced Concretes (FRC) - BEFIB’2000 (ISBN: 2-912143-18-7); *Eds. P. Rossi and G. Chanvillard*

PRO 16: Life Prediction and Management of Concrete Structures (ISBN: 2-912143-19-5); *Ed. D. Naus*

PRO 17: Shrinkage of Concrete – Shrinkage 2000 (ISBN: 2-912143-20-9); *Eds. V. Baroghel-Bouny and P.-C. Aïtcin*

PRO 18: Measurement and Interpretation of the On-Site Corrosion Rate (ISBN: 2-912143-21-7); *Eds. C. Andrade, C. Alonso, J. Fullea, J. Polimon and J. Rodriguez*

PRO 19: Testing and Modelling the Chloride Ingress into Concrete (ISBN: 2-912143-22-5); *Eds. C. Andrade and J. Kropp*

PRO 20: 1st International RILEM Workshop on Microbial Impacts on Building Materials (CD 02) (e-ISBN 978-2-35158-013-4); *Ed. M. Ribas Silva*

PRO 21: International RILEM Symposium on Connections between Steel and Concrete (ISBN: 2-912143-25-X); *Ed. R. Eligehausen*

PRO 22: International RILEM Symposium on Joints in Timber Structures (ISBN: 2-912143-28-4); *Eds. S. Aicher and H.-W. Reinhardt*

PRO 23: International RILEM Conference on Early Age Cracking in Cementitious Systems (ISBN: 2-912143-29-2); *Eds. K. Kovler and A. Bentur*

PRO 24: 2nd International RILEM Workshop on Frost Resistance of Concrete (ISBN: 2-912143-30-6); *Eds. M. J. Setzer, R. Auberg and H.-J. Keck*

PRO 25: International RILEM Workshop on Frost Damage in Concrete (ISBN: 2-912143-31-4); *Eds. D. J. Janssen, M. J. Setzer and M. B. Snyder*

PRO 26: International RILEM Workshop on On-Site Control and Evaluation of Masonry Structures (ISBN: 2-912143-34-9); *Eds. L. Binda and R. C. de Vekey*

PRO 27: International RILEM Symposium on Building Joint Sealants (CD03); *Ed. A. T. Wolf*

PRO 28: 6th International RILEM Symposium on Performance Testing and Evaluation of Bituminous Materials - PTEBM'03 (ISBN: 2-912143-35-7; e-ISBN: 978-2-912143-77-8); *Ed. M. N. Partl*

PRO 29: 2nd International RILEM Workshop on Life Prediction and Ageing Management of Concrete Structures (ISBN: 2-912143-36-5); *Ed. D. J. Naus*

PRO 30: 4th International RILEM Workshop on High Performance Fiber Reinforced Cement Composites - HPFRCC 4 (ISBN: 2-912143-37-3); *Eds. A. E. Naaman and H. W. Reinhardt*

PRO 31: International RILEM Workshop on Test and Design Methods for Steel Fibre Reinforced Concrete: Background and Experiences (ISBN: 2-912143-38-1); *Eds. B. Schnütgen and L. Vandewalle*

PRO 32: International Conference on Advances in Concrete and Structures 2 vol. (ISBN (set): 2-912143-41-1); *Eds. Ying-shu Yuan, Surendra P. Shah and Heng-lin Lü*

PRO 33: 3rd International Symposium on Self-Compacting Concrete (ISBN: 2-912143-42-X); *Eds. Ó. Wallevik and I. Níelsson*

PRO 34: International RILEM Conference on Microbial Impact on Building Materials (ISBN: 2-912143-43-8); *Ed. M. Ribas Silva*

PRO 35: International RILEM TC 186-ISA on Internal Sulfate Attack and Delayed Ettringite Formation (ISBN: 2-912143-44-6); *Eds. K. Scrivener and J. Skalny*

PRO 36: International RILEM Symposium on Concrete Science and Engineering – A Tribute to Arnon Bentur (ISBN: 2-912143-46-2); *Eds. K. Kovler, J. Marchand, S. Mindess and J. Weiss*

PRO 37: 5th International RILEM Conference on Cracking in Pavements – Mitigation, Risk Assessment and Prevention (ISBN: 2-912143-47-0); *Eds. C. Petit, I. Al-Qadi and A. Millien*

PRO 38: 3rd International RILEM Workshop on Testing and Modelling the Chloride Ingress into Concrete (ISBN: 2-912143-48-9); *Eds. C. Andrade and J. Kropp*

PRO 39: 6th International RILEM Symposium on Fibre-Reinforced Concretes - BEFIB 2004 (ISBN: 2-912143-51-9); *Eds. M. Di Prisco, R. Felicetti and G. A. Plizzari*

PRO 40: International RILEM Conference on the Use of Recycled Materials in Buildings and Structures (ISBN: 2-912143-52-7); *Eds. E. Vázquez, Ch. F. Hendriks and G. M. T. Janssen*

PRO 41: RILEM International Symposium on Environment-Conscious Materials and Systems for Sustainable Development (ISBN: 2-912143-55-1); *Eds. N. Kashino and Y. Ohama*

PRO 42: SCC'2005 - China: 1st International Symposium on Design, Performance and Use of Self-Consolidating Concrete (ISBN: 2-912143-61-6); *Eds. Zhiwu Yu, Caijun Shi, Kamal Henri Khayat and Youjun Xie*

PRO 43: International RILEM Workshop on Bonded Concrete Overlays (e-ISBN: 2-912143-83-7); *Eds. J. L. Granju and J. Silfwerbrand*

PRO 44: 2nd International RILEM Workshop on Microbial Impacts on Building Materials (CD11) (e-ISBN: 2-912143-84-5); *Ed. M. Ribas Silva*

PRO 45: 2nd International Symposium on Nanotechnology in Construction, Bilbao (ISBN: 2-912143-87-X); *Eds. Peter J. M. Bartos, Yolanda de Miguel and Antonio Porro*

PRO 46: ConcreteLife'06 - International RILEM-JCI Seminar on Concrete Durability and Service Life Planning: Curing, Crack Control, Performance in Harsh Environments (ISBN: 2-912143-89-6); *Ed. K. Kovler*

PRO 47: International RILEM Workshop on Performance Based Evaluation and Indicators for Concrete Durability (ISBN: 978-2-912143-95-2); *Eds. V. Baroghel-Bouny, C. Andrade, R. Torrent and K. Scrivener*

PRO 48: 1st International RILEM Symposium on Advances in Concrete through Science and Engineering (e-ISBN: 2-912143-92-6); *Eds. J. Weiss, K. Kovler, J. Marchand, and S. Mindess*

PRO 49: International RILEM Workshop on High Performance Fiber Reinforced Cementitious Composites in Structural Applications (ISBN: 2-912143-93-4); *Eds. G. Fischer and V.C. Li*

PRO 50: 1st International RILEM Symposium on Textile Reinforced Concrete (ISBN: 2-912143-97-7); *Eds. Josef Hegger, Wolfgang Brameshuber and Norbert Will*

PRO 51: 2nd International Symposium on Advances in Concrete through Science and Engineering (ISBN: 2-35158-003-6; e-ISBN: 2-35158-002-8); *Eds. J. Marchand, B. Bissonnette, R. Gagné, M. Jolin and F. Paradis*

PRO 52: Volume Changes of Hardening Concrete: Testing and Mitigation (ISBN: 2-35158-004-4; e-ISBN: 2-35158-005-2); *Eds. O. M. Jensen, P. Lura and K. Kovler*

PRO 53: High Performance Fiber Reinforced Cement Composites - HPFRCC5 (ISBN: 978-2-35158-046-2); *Eds. H. W. Reinhardt and A. E. Naaman*

PRO 54: 5th International RILEM Symposium on Self-Compacting Concrete (ISBN: 978-2-35158-047-9); *Eds. G. De Schutter and V. Boel*

PRO 55: International RILEM Symposium Photocatalysis, Environment and Construction Materials (ISBN: 978-2-35158-056-1); *Eds. P. Baglioni and L. Cassar*

PRO56: International RILEM Workshop on Integral Service Life Modelling of Concrete Structures (ISBN 978-2-35158-058-5); *Eds. R. M. Ferreira, J. Gulikers and C. Andrade*

PRO57: RILEM Workshop on Performance of cement-based materials in aggressive aqueous environments (e-ISBN: 978-2-35158-059-2); *Ed. N. De Belie*

PRO58: International RILEM Symposium on Concrete Modelling - CONMOD'08 (ISBN: 978-2-35158-060-8); *Eds. E. Schlangen and G. De Schutter*

PRO 59: International RILEM Conference on On Site Assessment of Concrete, Masonry and Timber Structures - SACoMaTiS 2008 (ISBN set: 978-2-35158-061-5); *Eds. L. Binda, M. di Prisco and R. Felicetti*

PRO 60: Seventh RILEM International Symposium on Fibre Reinforced Concrete: Design and Applications - BEFIB 2008 (ISBN: 978-2-35158-064-6); *Ed. R. Gettu*

PRO 61: 1st International Conference on Microstructure Related Durability of Cementitious Composites 2 vol., (ISBN: 978-2-35158-065-3); *Eds. W. Sun, K. van Breugel, C. Miao, G. Ye and H. Chen*

PRO 62: NSF/ RILEM Workshop: In-situ Evaluation of Historic Wood and Masonry Structures (e-ISBN: 978-2-35158-068-4); *Eds. B. Kasal, R. Anthony and M. Drdácký*

PRO 63: Concrete in Aggressive Aqueous Environments: Performance, Testing and Modelling, 2 vol., (ISBN: 978-2-35158-071-4); *Eds. M. G. Alexander and A. Bertron*

PRO 64: Long Term Performance of Cementitious Barriers and Reinforced Concrete in Nuclear Power Plants and Waste Management - NUCPERF 2009 (ISBN: 978-2-35158-072-1); *Eds. V. L'Hostis, R. Gens, C. Gallé*

PRO 65: Design Performance and Use of Self-consolidating Concrete - SCC'2009 (ISBN: 978-2-35158-073-8); *Eds. C. Shi, Z. Yu, K. H. Khayat and P. Yan*

PRO 66: 2nd International RILEM Workshop on Concrete Durability and Service Life Planning - ConcreteLife'09 (ISBN: 978-2-35158-074-5); *Ed. K. Kovler*

PRO 67: Repairs Mortars for Historic Masonry (e-ISBN: 978-2-35158-083-7); *Ed. C. Groot*

PRO 68: Proceedings of the 3rd International RILEM Symposium on 'Rheology of Cement Suspensions such as Fresh Concrete (ISBN 978-2-35158-091-2); *Eds. O. H. Wallevik, S. Kubens and S. Oesterheld*

PRO 69: 3rd International PhD Student Workshop on 'Modelling the Durability of Reinforced Concrete (ISBN: 978-2-35158-095-0); *Eds. R. M. Ferreira, J. Gulikers and C. Andrade*

PRO 70: 2nd International Conference on 'Service Life Design for Infrastructure' (ISBN set: 978-2-35158-096-7, e-ISBN: 978-2-35158-097-4); *Ed. K. van Breugel, G. Ye and Y. Yuan*

PRO 71: Advances in Civil Engineering Materials - The 50-year Teaching Anniversary of Prof. Sun Wei' (ISBN: 978-2-35158-098-1; e-ISBN: 978-2-35158-099-8); *Eds. C. Miao, G. Ye, and H. Chen*

PRO 72: First International Conference on 'Advances in Chemically-Activated Materials – CAM'2010' (2010), 264 pp, ISBN: 978-2-35158-101-8; e-ISBN: 978-2-35158-115-5, *Eds. Caijun Shi and Xiaodong Shen*

PRO 73: 2nd International Conference on 'Waste Engineering and Management - ICWEM 2010' (2010), 894 pp, ISBN: 978-2-35158-102-5; e-ISBN: 978-2-35158-103-2, *Eds. J. Zh. Xiao, Y. Zhang, M. S. Cheung and R. Chu*

PRO 74: International RILEM Conference on 'Use of Superabsorsorbent Polymers and Other New Addditives in Concrete' (2010) 374 pp., ISBN: 978-2-35158-104-9; e-ISBN: 978-2-35158-105-6;
Eds. O.M. Jensen, M.T. Hasholt, and S. Laustsen

PRO 75: International Conference on 'Material Science - 2nd ICTRC - Textile Reinforced Concrete - Theme 1' (2010) 436 pp., ISBN: 978-2-35158-106-3; e-ISBN: 978-2-35158-107-0;
Ed. W. Brameshuber

PRO 76: International Conference on 'Material Science - HetMat - Modelling of Heterogeneous Materials - Theme 2' (2010) 255 pp., ISBN: 978-2-35158-108-7; e-ISBN: 978-2-35158-109-4; *Ed. W. Brameshuber*

PRO 77: International Conference on 'Material Science - AdIPoC - Additions Improving Properties of Concrete - Theme 3' (2010) 459 pp., ISBN: 978-2-35158-110-0; e-ISBN: 978-2-35158-111-7; *Ed. W. Brameshuber*

PRO 78: 2nd Historic Mortars Conference and RILEM TC 203-RHM Final Workshop – HMC2010 (2010) 1416 pp., e-ISBN: 978-2-35158-112-4; *Eds J. Válek, C. Groot, and J. J. Hughes*

PRO 79: International RILEM Conference on Advances in Construction Materials Through Science and Engineering (2011) 213 pp., e-ISBN: 978-2-35158-117-9; *Eds Christopher Leung and K.T. Wan*

PRO 80: 2nd International RILEM Conference on Concrete Spalling due to Fire Exposure (2011) 453 pp., ISBN: 978-2-35158-118-6, e-ISBN: 978-2-35158-119-3; *Eds E.A.B. Koenders and F. Dehn*

PRO 81: 2nd International RILEM Conference on Strain Hardening Cementitious Composites (SHCC2-Rio) (2011) 451 pp., ISBN: 978-2-35158-120-9, e-ISBN: 978-2-35158-121-6; *Eds R.D. Toledo Filho, F.A. Silva, E.A.B. Koenders and E.M.R. Fairbairn*

PRO 82: 2nd International RILEM Conference on Progress of Recycling in the Built Environment (2011) 507 pp., e-ISBN: 978-2-35158-122-3; *Eds V.M. John, E. Vazquez, S.C. Angulo and C. Ulsen*

PRO 83: 2nd International Conference on Microstructural-related Durability of Cementitious Composites (2012) 250 pp., ISBN: 978-2-35158-129-2; e-ISBN: 978-2-35158-123-0; *Eds G. Ye, K. van Breugel, W. Sun and C. Miao*

PRO 85: RILEM-JCI International Workshop on Crack Control of Mass Concrete and Related issues concerning Early-Age of Concrete Structures – ConCrack 3 – Control of Cracking in Concrete Structures 3 (2012) 237 pp., ISBN: 978-2-35158-125-4; e-ISBN: 978-2-35158-126-1; *Eds F. Toutlemonde and J.-M. Torrenti*

PRO 86: International Symposium on Life Cycle Assessment and Construction (2012) 414 pp., ISBN: 978-2-35158-127-8, e-ISBN: 978-2-35158-128-5; *Eds A. Ventura and C. de la Roche*

PRO 87: UHPFRC 2013 – RILEM-fib-AFGC International Symposium on Ultra-High Performance Fibre-Reinforced Concrete (2013), ISBN: 978-2-35158-130-8, e-ISBN: 978-2-35158-131-5; *Eds F. Toutlemonde*

PRO 88: 8th RILEM International Symposium on Fibre Reinforced Concrete (2012) 344 pp., ISBN: 978-2-35158-132-2, e-ISBN: 978-2-35158-133-9; *Eds Joaquim A.O. Barros*

PRO 89: RILEM International workshop on performance-based specification and control of concrete durability (2014) 678 pp, ISBN: 978-2-35158-135-3, e-ISBN: 978-2-35158-136-0; *Eds. D. Bjegović, H. Beushausen and M. Serdar*

PRO 90: 7th RILEM International Conference on Self-Compacting Concrete and of the 1st RILEM International Conference on Rheology and Processing of Construction Materials (2013) 396 pp, ISBN: 978-2-35158-137-7, e-ISBN: 978-2-35158-138-4; *Eds. Nicolas Roussel and Hela Bessaies-Bey*

PRO 91: CONMOD 2014 - RILEM International Symposium on Concrete Modelling (2014), ISBN: 978-2-35158-139-1; e-ISBN: 978-2-35158-140-7; *Eds. Kefei Li, Peiyu Yan and Rongwei Yang*

PRO 92: CAM 2014 - 2nd International Conference on advances in chemically-activated materials (2014) 392 pp., ISBN: 978-2-35158-141-4; e-ISBN: 978-2-35158-142-1; *Eds. Caijun Shi and Xiadong Shen*

PRO 93: SCC 2014 - 3rd International Symposium on Design, Performance and Use of Self-Consolidating Concrete (2014) 438 pp., ISBN: 978-2-35158-143-8; e-ISBN: 978-2-35158-144-5; *Eds. Caijun Shi, Zhihua Ou, Kamal H. Khayat*

PRO 94 (online version): HPFRCC-7 - 7th RILEM conference on High performance fiber reinforced cement composites (2015), e-ISBN: 978-2-35158-146-9; *Eds. H.W. Reinhardt, G.J. Parra-Montesinos, H. Garrecht*

PRO 95: International RILEM Conference on Application of superabsorbent polymers and other new admixtures in concrete construction (2014), ISBN: 978-2-35158-147-6; e-ISBN: 978-2-35158-148-3; *Eds. Viktor Mechtcherine, Christof Schroefl*

PRO 96 (online version): XIII DBMC: XIII International Conference on Durability of Building Materials and Components (2015), e-ISBN: 978-2-35158-149-0; *Eds. M. Quattrone, V.M. John*

PRO 97: SHCC3 – 3rd International RILEM Conference on Strain Hardening Cementitious Composites (2014), ISBN: 978-2-35158-150-6; e-ISBN: 978-2-35158-151-3; *Eds. E. Schlangen, M.G. Sierra Beltran, M. Lukovic, G. Ye*

PRO 98: FERRO-11 – 11th International Symposium on Ferrocement and 3rd ICTRC - International Conference on Textile Reinforced Concrete (2015), ISBN: 978-2-35158-152-0; e-ISBN: 978-2-35158-153-7; *Ed. W. Brameshuber*

PRO 99 (online version): ICBBM 2015 - 1st International Conference on Bio-Based Building Materials (2015), e-ISBN: 978-2-35158-154-4; *Eds. S. Amziane, M. Sonebi*

PRO 100: SCC16 - RILEM Self-Consolidating Concrete Conference (2016)**,** ISBN: 978-2-35158-156-8; e-ISBN: 978-2-35158-157-5

PRO 101 (online version): III Progress of Recycling in the Built Environment (2015), e-ISBN: 978-2-35158-158-2; *Eds I. Martins, C. Ulsen and S. C. Angulo*

PRO 102 (online version): RILEM Conference on Microorganisms-Cementitious Materials Interactions (2016), e-ISBN: 978-2-35158-160-5; *Eds. Alexandra Bertron, Henk Jonkers, Virginie Wiktor*

PRO 103 (online version): ACESC'16 - Advances in Civil Engineering and Sustainable Construction (2016), e-ISBN: 978-2-35158-161-2

PRO 104 (online version): SSCS'2015 - Numerical Modeling - Strategies for Sustainable Concrete Structures (2015), e-ISBN: 978-2-35158-162-9

PRO 105: 1st International Conference on UHPC Materials and Structures (2016), ISBN: 978-2-35158-164-3, e-ISBN: 978-2-35158-165-0

PRO 106: AFGC-ACI-fib-RILEM International Conference on Ultra-High-Performance Fibre-Reinforced Concrete – UHPFRC 2017 (2017), ISBN: 978-2-35158-166-7, e-ISBN: 978-2-35158-167-4; *Eds. François Toutlemonde & Jacques Resplendino*

PRO 107 (online version): XIV DBMC – 14th International Conference on Durability of Building Materials and Components (2017), e-ISBN: 978-2-35158-159-9; *Eds. Geert De Schutter, Nele De Belie, Arnold Janssens, Nathan Van Den Bossche*

PRO 108: MSSCE 2016 - Innovation of Teaching in Materials and Structures (2016), ISBN: 978-2-35158-178-0, e-ISBN: 978-2-35158-179-7; *Ed. Per Goltermann*

PRO 109 (2 volumes): MSSCE 2016 - Service Life of Cement-Based Materials and Structures (2016), ISBN Vol. 1: 978-2-35158-170-4, Vol. 2: 978-2-35158-171-4, Set Vol. 1&2: 978-2-

35158-172-8, e-ISBN: 978-2-35158-173-5; *Eds. Miguel Azenha, Ivan Gabrijel, Dirk Schlicke, Terje Kanstad and Ole Mejlhede Jensen*

PRO 110: MSSCE 2016 - Historical Masonry (2016), ISBN: 978-2-35158-178-0, e-ISBN: 978-2-35158-179-7; *Eds. Inge Rörig-Dalgaard and Ioannis Ioannou*

PRO 111: MSSCE 2016 - Electrochemistry in Civil Engineering (2016), ISBN: 978-2-35158-176-6, e-ISBN: 978-2-35158-177-3; *Ed. Lisbeth M. Ottosen*

PRO 112: MSSCE 2016 - Moisture in Materials and Structures (2016), ISBN: 978-2-35158-178-0, e-ISBN: 978-2-35158-179-7; *Eds. Kurt Kielsgaard Hansen, Carsten Rode and Lars-Olof Nilsson*

PRO 113: MSSCE 2016 - Concrete with Supplementary Cementitious Materials (2016), ISBN: 978-2-35158-178-0, e-ISBN: 978-2-35158-179-7; *Eds. Ole Mejlhede Jensen, Konstantin Kovler and Nele De Belie*

PRO 114: MSSCE 2016 - Frost Action in Concrete (2016), ISBN: 978-2-35158-182-7, e-ISBN: 978-2-35158-183-4; *Eds. Marianne Tange Hasholt, Katja Fridh and R. Doug Hooton*

PRO 115: MSSCE 2016 - Fresh Concrete (2016), ISBN: 978-2-35158-184-1, e-ISBN: 978-2-35158-185-8; *Eds. Lars N. Thrane, Claus Pade, Oldrich Svec and Nicolas Roussel*

PRO 116: BEFIB 2016 – 9th RILEM International Symposium on Fiber Reinforced Concrete (2016), ISBN: 978-2-35158-187-2, e-ISBN: 978-2-35158-186-5;

PRO 117: 3rd International RILEM Conference on Microstructure Related Durability of Cementitious Composites (2016), ISBN: 978-2-35158-188-9, e-ISBN: 978-2-35158-189-6; *Eds. Changwen Miao, Wei Sun, Jiaping Liu, Huisu Chen, Guang Ye and Klaas van Breugel*

PRO 118 (4 volumes): International Conference on Advances in Construction Materials and Systems (2017), ISBN Set: 978-2-35158-190-2, Vol. 1: 978-2-35158-193-3, Vol. 2: 978-2-35158-194-0, Vol. 3: ISBN:978-2-35158-195-7, Vol. 4: ISBN:978-2-35158-196-4, e-ISBN: 978-2-35158-191-9; *Ed. Manu Santhanam*

PRO 119 (online version): ICBBM 2017 - Second International RILEM Conference on Bio-based Building Materials, (2017), e-ISBN: 978-2-35158-192-6; *Ed. Sofiane Amziane*

PRO 120 (2 volumes): EAC-02 - 2nd International RILEM/COST Conference on Early Age Cracking and Serviceability in Cement-based Materials and Structures, (2017), Vol. 1: 978-2-35158-199-5, Vol. 2: 978-2-35158-200-8, Set: 978-2-35158-197-1, e-ISBN: 978-2-35158-198-8; *Eds. Stéphanie Staquet and Dimitrios Aggelis*

PRO 121 (2 volumes): SynerCrete18: Interdisciplinary Approaches for Cement-based Materials and Structural Concrete: Synergizing Expertise and Bridging Scales of Space and Time, (2018), Set: 978-2-35158-202-2, Vol.1: 978-2-35158-211-4, Vol.2: 978-2-35158-212-1, e-ISBN: 978-2-35158-203-9; *Ed. Miguel Azenha, Dirk Schlicke, Farid Benboudjema, Agnieszka Knoppik*

PRO 122: SCC’2018 China - Fourth International Symposium on Design, Performance and Use of Self-Consolidating Concrete, (2018), ISBN: 978-2-35158-204-6, e-ISBN: 978-2-35158-205-3

PRO 123: Final Conference of RILEM TC 253-MCI: Microorganisms-Cementitious Materials Interactions (2018), Set: 978-2-35158-207-7, Vol.1: 978-2-35158-209-1, Vol.2: 978-2-35158-210-7, e-ISBN: 978-2-35158-206-0; *Ed. Alexandra Bertron*

PRO 124 (online version): Fourth International Conference Progress of Recycling in the Built Environment (2018), e-ISBN: 978-2-35158-208-4; *Eds. Isabel M. Martins, Carina Ulsen, Yury Villagran*

PRO 125 (online version): SLD4 - 4th International Conference on Service Life Design for Infrastructures (2018), e-ISBN: 978-2-35158-213-8; *Eds. Guang Ye, Yong Yuan, Claudia Romero Rodriguez, Hongzhi Zhang, Branko Savija*

PRO 126: Workshop on Concrete Modelling and Material Behaviour in honor of Professor Klaas van Breugel (2018), ISBN: 978-2-35158-214-5, e-ISBN: 978-2-35158-215-2; *Ed. Guang Ye*

PRO 127 (online version): CONMOD2018 - Symposium on Concrete Modelling (2018), e-ISBN: 978-2-35158-216-9; *Eds. Erik Schlangen, Geert de Schutter, Branko Savija, Hongzhi Zhang, Claudia Romero Rodriguez*

RILEM REPORTS (REP)

Report 19: Considerations for Use in Managing the Aging of Nuclear Power Plant Concrete Structures (ISBN: 2-912143-07-1); *Ed. D. J. Naus*

Report 20: Engineering and Transport Properties of the Interfacial Transition Zone in Cementitious Composites (ISBN: 2-912143-08-X); *Eds. M. G. Alexander, G. Arliguie, G. Ballivy, A. Bentur and J. Marchand*

Report 21: Durability of Building Sealants (ISBN: 2-912143-12-8); *Ed. A. T. Wolf*

Report 22: Sustainable Raw Materials - Construction and Demolition Waste (ISBN: 2-912143-17-9); *Eds. C. F. Hendriks and H. S. Pietersen*

Report 23: Self-Compacting Concrete state-of-the-art report (ISBN: 2-912143-23-3); *Eds. Å. Skarendahl and Ö. Petersson*

Report 24: Workability and Rheology of Fresh Concrete: Compendium of Tests (ISBN: 2-912143-32-2); *Eds. P. J. M. Bartos, M. Sonebi and A. K. Tamimi*

Report 25: Early Age Cracking in Cementitious Systems (ISBN: 2-912143-33-0); *Ed. A. Bentur*

Report 26: Towards Sustainable Roofing (Joint Committee CIB/RILEM) (CD 07) (e-ISBN 978-2-912143-65-5); *Eds. Thomas W. Hutchinson and Keith Roberts*

Report 27: Condition Assessment of Roofs (Joint Committee CIB/RILEM) (CD 08) (e-ISBN 978-2-912143-66-2); *Ed. CIB W 83/RILEM TC166-RMS*

Report 28: Final report of RILEM TC 167-COM 'Characterisation of Old Mortars with Respect to Their Repair (ISBN: 978-2-912143-56-3); *Eds. C. Groot, G. Ashall and J. Hughes*

Report 29: Pavement Performance Prediction and Evaluation (PPPE): Interlaboratory Tests (e-ISBN: 2-912143-68-3); *Eds. M. Partl and H. Piber*

Report 30: Final Report of RILEM TC 198-URM 'Use of Recycled Materials' (ISBN: 2-912143-82-9; e-ISBN: 2-912143-69-1); *Eds. Ch. F. Hendriks, G. M. T. Janssen and E. Vázquez*

Report 31: Final Report of RILEM TC 185-ATC 'Advanced testing of cement-based materials during setting and hardening' (ISBN: 2-912143-81-0; e-ISBN: 2-912143-70-5); *Eds. H. W. Reinhardt and C. U. Grosse*

Report 32: Probabilistic Assessment of Existing Structures. A JCSS publication (ISBN 2-912143-24-1); *Ed. D. Diamantidis*

Report 33: State-of-the-Art Report of RILEM Technical Committee TC 184-IFE 'Industrial Floors' (ISBN 2-35158-006-0); *Ed. P. Seidler*

Report 34: Report of RILEM Technical Committee TC 147-FMB 'Fracture mechanics applications to anchorage and bond' Tension of Reinforced Concrete Prisms – Round Robin Analysis and Tests on Bond (e-ISBN 2-912143-91-8); *Eds. L. Elfgren and K. Noghabai*

Report 35: Final Report of RILEM Technical Committee TC 188-CSC 'Casting of Self Compacting Concrete' (ISBN 2-35158-001-X; e-ISBN: 2-912143-98-5); *Eds. Å. Skarendahl and P. Billberg*

Report 36: State-of-the-Art Report of RILEM Technical Committee TC 201-TRC 'Textile Reinforced Concrete' (ISBN 2-912143-99-3); *Ed. W. Brameshuber*

Report 37: State-of-the-Art Report of RILEM Technical Committee TC 192-ECM 'Environment-conscious construction materials and systems' (ISBN: 978-2-35158-053-0);
Eds. N. Kashino, D. Van Gemert and K. Imamoto

Report 38: State-of-the-Art Report of RILEM Technical Committee TC 205-DSC 'Durability of Self-Compacting Concrete' (ISBN: 978-2-35158-048-6); *Eds. G. De Schutter and K. Audenaert*

Report 39: Final Report of RILEM Technical Committee TC 187-SOC 'Experimental determination of the stress-crack opening curve for concrete in tension' (ISBN 978-2-35158-049-3); *Ed. J. Planas*

Report 40: State-of-the-Art Report of RILEM Technical Committee TC 189-NEC 'Non-Destructive Evaluation of the Penetrability and Thickness of the Concrete Cover' (ISBN 978-2-35158-054-7);
Eds. R. Torrent and L. Fernández Luco

Report 41: State-of-the-Art Report of RILEM Technical Committee TC 196-ICC 'Internal Curing of Concrete' (ISBN 978-2-35158-009-7); *Eds. K. Kovler and O. M. Jensen*

Report 42: 'Acoustic Emission and Related Non-destructive Evaluation Techniques for Crack Detection and Damage Evaluation in Concrete' - Final Report of RILEM Technical Committee 212-ACD (e-ISBN: 978-2-35158-100-1); *Ed. M. Ohtsu*

Report 45: Repair Mortars for Historic Masonry - State-of-the-Art Report of RILEM Technical Committee TC 203-RHM (e-ISBN: 978-2-35158-163-6); *Eds. Paul Maurenbrecher and Caspar Groot*

Report 46: Surface delamination of concrete industrial floors and other durability related aspects guide - Report of RILEM Technical Committee TC 268-SIF (e-ISBN: 978-2-35158-201-5); *Ed. Valérie Pollet*

Conference Chairs

Marijana Serdar, University of Zagreb, Faculty of Civil Engineering, Croatia
Ivana Banjad Pečur, University of Zagreb, Faculty of Civil Engineering, Croatia

Honorary president of scientific committee

Dubravka Bjegović, University of Zagreb, Faculty of Civil Engineering, Croatia

International Scientific Committee of Challenges in Design and Management of Structures

György L. Balázs
Agnieszka Bigaj-van Vliet
Jelena Bleiziffer
Joan Casas
Laurent Charpin
Eleni Chatzi
Frank Dehn
Salvatore di Bernardo
Murat Dicleli
Darko Dujmović
Cyrille Dunant
Ivica Džeba
Jan Falbr
Emmanuel Ferrier
Hitoshi Furuta
Erez Gal
Arndt Goldack
Niels Peter Høj
Dorian Janjic
Agnieszka Jędrzejewska
Terje Kanstad
Sylvia Kessler
Miloš Knežević
Renata Kotynia
Ivica Kožar
Minoru Kunieda
Giuseppe Mancini
Ippei Maruyama
Jose Matos
Stuart Matthews
Stijn Matthys
Ivana Miličević
Roger Ohayon
André Orcesi
Joško Ožbolt
Matthias Pahn
Vlastimir Radonjanjin
Vlatka Rajčić
Robert Ratay
Michael Raupach
Theodoros Rousakis
Pavel Ryjaček
Abdullah Shahrum
Davor Skejić
Miroslav Sykora
Anton Syrkov
Vivian Tam
Dil Tirimanna
Jan Vitek
Anđelko Vlašić
Slowik Volker
Jianzhuang Xiao

Jochen Köhler
Laurie Lacarriere
Oskar Larsson
Jian Yang
Stefan Zmigrodzki
Daia Zwicky

Organizing Committee of Challenges in Design and Management of Structures

Ana Mandić Ivanković, University of Zagreb, Faculty of Civil Engineering, Croatia

Marija Kušter Marić, University of Zagreb, Faculty of Civil Engineering, Croatia

Alfred Strauss, University of Vienna, Austria

Tomislav Kišiček, University of Zagreb, Faculty of Civil Engineering, Croatia

Preface

RILEM International Conference on Sustainable Materials, Systems and Structures (SMSS 2019) is a conference organised by Faculty of Civil Engineering University of Zagreb as a supporting event of RILEM Spring Convention from in Rovinj, Croatia. Both are organised in the year Faculty of Civil Engineering in Zagreb is celebrating 100 years from its establishment, making 2019 a perfect year for hosting such an important international event. The scope of the conference was to gather scientists, practitioners, members of technical committees and users of technical recommendations, to jointly at the same place discuss and envision the future sustainable development of materials, systems and structures in a holistic, global way.

SMSS 2019 conference has gathered participants from 50 countries, from Argentina to United States of America, who will exhibit a total of 290 papers. The conference was sponsored by 10 international industrial partners, supported by 6 international organisations of scientists and practitioners and organised under the patronage of 4 governmental bodies. A total of 450 contributions which arrived was reviewed by more than 150 prominent reviewers from different fields. Event was organised by 16 members of the local organising committee and 6 invited international members of organising committee.

Conference segment *Challenges in Design and Management of Structures* provides a forum for discussion on problems related to structural performance for the whole life cycle of the civil engineering structures. It covers advances in design of new and assessment of existing structures based on lessons learned from practice, from collapses, from successes, aiming optimization of structural life cycle management decisions.

Rating and weighting of performance indicators from component, through system, up to network level is a crucial for optimal management of structures aiming their safety, durability and reliability, security and serviceability, availability and maintainability.

Application of scientific achievements in linear and nonlinear analysis methods, numerical modelling and simulation, data updating and processing, semi and full probabilistic based methods with adequate treatment of uncertainties is envisaged to improve design of new and assessment and maintenance of existing infrastructures.

Editors wish to thank the authors for their efforts at producing and delivering papers of high standard. We are sure that this Proceedings will be a valued reference of research topics in this important field and that it will together with the other volumes from SMSS conference form a suitable base for discussion and suggestions for future development and research.

Ana Mandić Ivanković (University of Zagreb, Croatia)
Marija Kušter Marić (University of Zagreb, Croatia)
Alfred Strauss (University of Vienna, Austria)
Tomislav Kišiček (University of Zagreb, Croatia)

Contents

DESIGNING AND MANAGING STRUCTURES IN A LIFE-CYCLE PERSPECTIVE

André Orcesi

Université Paris-Est, MAST, EMGCU, IFSTTAR, F-77447 Marne-la-Vallée, France

Abstract

Civil engineering structures are designed to stay in service for at least several decades. Due to their significance in the political economy the request for sustainable, meaning highly advanced, cost-effective, environmentally friendly and long-living structures is outstanding.

The current practice of structural design generally focuses on optimizing the economic and performance aspects of construction. In particular for bridges, it does not enable to fully optimize the operation and end-of-life strategies. Maintenance strategies may be different from one design solution to another and one solution can appear to be more attractive at the design stage but less interesting when the entire life-cycle is considered, all the more, when user costs are also considered in the decision process. In this context, the request for sustainable structures is urgent, especially in view of a 100-year planned lifetime.

Besides, it is well known that a majority of existing bridges around the world was constructed in the 60's and 70's of the 20th century. A challenge is now to manage transportation infrastructure networks as a whole and to identify best practices and processes to assure adequate safety and serviceability levels for existing structures. Inspection and maintenance optimization based on rational life-cycle indicators then plays a crucial role to tackle structural degradation processes in the most efficient way.

For these reasons, a holistic approach is proposed to provide stakeholders with decision management tools from the construction to the end-of-life. It aims at combining economic, social and performance analyses during service lifetime, ensure that the concepts are optimal in the long term, not just at the point of construction, and deal with existing structures in an economic and sustainable way.

Case studies will be presented, considering the multi-scale (system/network, stock, bridge…) and the multicriteria complexities to illustrate several types of applications and possible outputs of life-cycle analyses.

Keywords: life-cycle analysis, bridges, networks, design, inspection, maintenance, management, decision process, optimization.

PROBABILISTIC DESIGN OF WIND TURBINE CONCRETE COMPONENTS SUBJECT TO FATIGUE

John D. Sørensen, Amol Mankar

Aalborg University, Denmark

Abstract

Wind turbines contribute significantly to the production of renewable energy. In order to minimize the Levelized Cost of Energy (LCOE) the cost of the wind turbine incl. tower and the foundation should be as low as possible but at the same time have a sufficient reliability. In this paper, focus is on wind turbine components which may be made of concrete such as tower and foundation. In traditional deterministic design based on design standards, partial safety factors are applied to obtain the design values. Improved design with a consistent reliability level for all components can be obtained by use of probabilistic design methods with explicit consideration of uncertainties connected to loads, strengths and numerical models / calculation methods. Wind turbines are basically designed based on IEC 61400-1:2019 which indicates a target reliability level that can be used for probabilistic design. In this paper, probabilistic fatigue models for concrete are presented based on the fatigue models in *fib* Model Code 2010, but extended within a stochastic modelling using a large dataset of fatigue tests. Generic uncertainty models for the fatigue load are applied. It is illustrated how reliability analyses can be performed within a probabilistic design framework.

Keywords: Wind turbines, Fatigue, Concrete, Reliability, Probabilistic design

1. INTRODUCTION

During the last decades, wind turbines for electricity production have increased significantly both in production capacity and in size; now with a rated power of 10MW, rotor diameters in the range of 160-200m and tower heights more than 100m; and even larger wind turbines are expected the next years to be installed offshore. Typically the tower and the substructure for offshore wind farms are made of structural steel, but concrete towers and substructures are been considered and also used as a cost-effective alternative to steel.

In traditional, deterministic design based on design standards, partial safety factors are applied to obtain the design values. Improved design with a consistent reliability level for all components can be obtained by use of probabilistic design methods with explicit consideration of uncertainties connected to loads, strengths and numerical models / calculation methods.

Furthermore, using a probabilistic design basis it is possible to design wind turbines such that site-specific information on climate parameters are applied. Wind turbines are basically designed based on the IEC 61400 series of standards where IEC 61400-1 ed. 4 [1] indicates a target reliability level which can be used for probabilistic design. In this paper, probabilistic fatigue models for concrete ae presented based on the basic, deterministic fatigue models in [2], but extended within a stochastic modelling framework and with parameters calibrated using a large dataset of fatigue tests. Generic uncertainty models for the fatigue load are applied.

The structural response of wind turbines is highly dependent on the wind turbulence, aerodynamics, dynamics of the structural system and of the control system applied. Further, wind turbines are manufactured in a series production based on many component tests, some subcomponent tests and a few prototype tests making it possible to update the knowledge through the design process, e.g. using a Bayesian approach.

In this paper, a general approach for probabilistic design is presented with focus on wind turbine components made of concrete such as tower and foundation, and especially the fatigue failure mode. It is illustrated how reliability analyses and probabilistic design can be performed within a probabilistic design framework considering a gravity based foundation for an offshore wind turbine.

2. PROBABILISTIC DESIGN

Structural components in wind turbines are designed considering a number of load combinations, see [1]:

- Failure during normal operation in extreme load or by fatigue (DLC 1)
- Failure under fault conditions (e.g. failure of electrical / mechanical components or loss of grid connection) due to extreme loads or by fatigue (DLC 2)
- Failure during start up, normal shut down or emergency shut down (DLC 3, 4 and 5)
- Failure when the wind turbine is idling / parked and does not produce electricity. Failure can be by extreme loads or by fatigue (DLC 6)
- Failure during transportation and installation (DLC 7)
- Failure during transport, assembly, maintenance and repair (DLC 8)

Wind turbine components can generally be divided in two groups:

1) Electrical and mechanical components modelled by the failure rate, λ. Further, the bath-tub model is often used to describe the time dependent behaviour of the failure rate / hazard rate, see e.g. [3] and [4]. Reliability of drivetrain components (e.g. the gear-box) has been considered in e.g. [5].

2) Structural components such as tower, main frame, blades and the support structure / foundation where failure modes can be described by limit state equations, $g_i(X)$. Parameters in the limit state equation $g(X)$ are assumed to be modelled by n stochastic variables $X = (X_1, \dots, X_n)$. The probability of failure, P_F can be estimated using Structural Reliability Methods, e.g. FORM / SORM / simulation methods, see e.g. [6] and [7].

For wind turbines, the risk of loss of human lives in case of failure of a structural element is generally very small. Further, it can be assumed that wind turbines are systematically reconstructed in case of collapse or end of lifetime. Therefore, an appropriate target reliability level corresponding to a minimum annual probability of failure, ΔP_F^{max} is considered be $5 \cdot 10^{-4}$

(annual reliability index equal to 3.3), see [1] and [8]. More details on probabilistic design and reliability assessment of wind turbines can be found in [9], [10], [11] and [12].

In probabilistic design, it has to be verified that $\Delta P_{F,i} \leq \Delta P_F^{max}$ or $\lambda_{F,i} \leq \Delta P_F^{max}$ for all components for all DLCs where $\Delta P_{F,i}$ and $\lambda_{F,i}$ are used where relevant. Some representative stochastic models and limit state equations can be found in e.g. [8].

3. GRAVITY BASED FOUNDATION (GBF) CASE STUDY

As a case study, a reinforced concrete GBF of an offshore wind turbine (OWT) is considered as shown in Figure 1, see [13] for details. Reliability assessment wrt. fatigue failure and ultimate strength failure in compression of the concrete shaft is considered. The critical section is assumed to be the section just above lower ring beam as shown in Figure 1.

The OWT is installed in water depth of 25m. The outer diameter of the shaft at critical section is 6.5m. The thickness of the shaft (t) is considered as a design parameter.

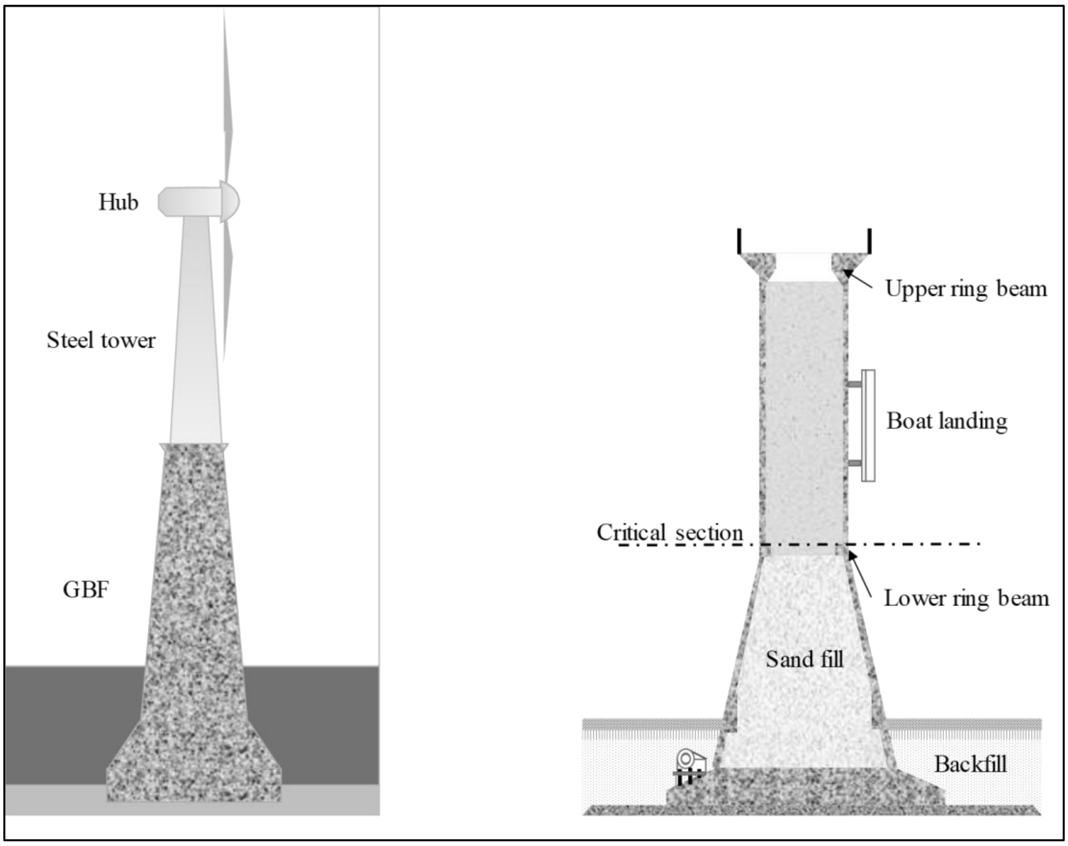

Figure 1: Typical GBF offshore wind turbine

Two limit states are considered in this paper, namely fatigue failure of the concrete in compression zone of the cross section (DLC 1.2) and extreme / ultimate strength failure of the concrete in compression (DLC 6.1). It is noted that it could also be very relevant to study yielding failure of the reinforcement in extreme storm conditions and tension fatigue failure of the concrete for cracked section given cracks in section due to extreme storm (multi-hazard scenario).

3.1 Fatigue limit state (DLC 1.2)

A probabilistic fatigue model for concrete is presented based on the basic, deterministic fatigue models in [2], but extended within a stochastic modelling framework and with parameters calibrated using a large dataset of fatigue tests, [14], [15] and [16].

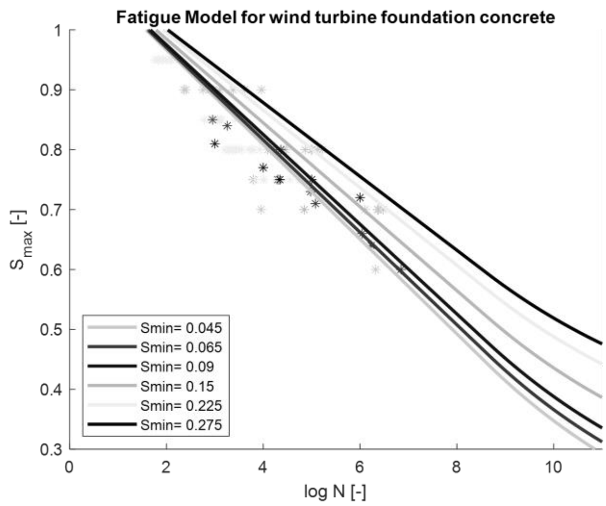

Figure 2: Fatigue strength model of concrete for GBF

Equation (1) shows a limit state equation based on Miner's rule where the number of cycles to failure is calculated based on [2] and [16]. Figure 2 shows graphical representation of fatigue strength model incl. fatigue test data while Table 1 shows the corresponding statistical parameters.

Table 1: Stochastic parameters

Parameter	Dist* Type	Parameters Mean	Parameters Std. Dev.	Ref**
X_1	N	1.13	0.03	Stochastic parameters associated with fatigue strength for compression-compression [16]
X_2	N	8.66	0.37	
ε	N	0.0	σ_ε	
σ_ε	N	0.88	0.07	
$\rho_{X_1,\sigma_\varepsilon}$	-	0.01		
$\rho_{X_2,\sigma_\varepsilon}$	-	-0.01		
ρ_{X_1,X_2}	-	-0.84		
X_W	LN	1.0	0.10	Uncertainty associated with wind loads
X_G	LN	1.0	0.05	Uncertainty associated with gravity loads
X_{PS}	LN	1.0	0.05	Uncertainty associated with pre-stressing loads
Δ	LN	1.0	0.30	[17]
X_{fc}	LN	1.0	0.14	Uncertainty in static strength of concrete
BM	G	186.7	40.4	Bending moment at critical section MN-m

$$g(t,z) = \Delta - \sum_{i=1}^{N_{\text{Windspeeds}}} \sum_{j=1}^{N_{\text{bins}}} \frac{n_{ij} t}{N_{S,ij}} \tag{1}$$

where

Δ model uncertainty associated with Miner's rule

t time in years $0 < t < T_L$

T_L design service life of the GBF structure

n_{ij} number of stress cycles per year in mean windspeed *i* in stress bin *j* (obtained by rainflow counting)

$N_{S,ij}$ number of stress cycles to failure of stress bin $S_{C,max,ij}$ and $S_{C,min,ij}$ modelled by

$$\log N_{S,ij} = \frac{X_2}{(Y - X_1)} \cdot (S_{c,max,ij} - X_1) + \epsilon \qquad \text{if } \log N_{S,ij} \leq X_2$$

$$\log N_{S,ij} = X_2 + \frac{X_2 \cdot \ln(10)}{(Y - X_1)} \cdot (Y - S_{c,min,ij}) \cdot \log\left(\frac{S_{c,max,ij} - S_{c,min,ij}}{Y - S_{c,min,ij}}\right) + \epsilon \qquad \text{if } \log N_{S,ij} > X_2 \tag{2}$$

where

$S_{c,max,ij} = |\sigma_{c,max,ij}| / f_{cfat}$

$S_{c,min,ij} = |\sigma_{c,min,ij}| / f_{cfat}$

$\sigma_{c,max,ij}$ and $\sigma_{c,min,ij}$ are maximum and minimum stresses used to obtain $S_{c,max,ij}$ and $S_{c,min,ij}$

$\sigma_{c,max,ij}(z) = X_G \cdot \sigma_G(z) + X_{PS} \cdot \sigma_P(z) + X_w \cdot \sigma_{WL_{max,ij}}(z)$

$\sigma_{c,min,ij}(z) = X_G \cdot \sigma_G(z) + X_{PS} \cdot \sigma_P(z) + X_w \cdot \sigma_{WL_{min,ij}}(z)$

$f_{cfat} = \beta_{c,sus(t,t0)} \cdot \beta_{cc(t)} \cdot f_c \cdot (1 - f_c/400)$

$f_c = X_{f_c} \cdot f_{cm}$

z design parameter

3.2 Ultimate limit state (DLC 6.1)

The ultimate limit state (ULS) for extreme storm conditions is considered, [18] with the following limit state equation for compression failure of concrete:

$$g(z) = R - S = fc - \left(\frac{BM}{I_{Cr}(z)} \cdot y + \frac{X_G \cdot G}{A_{Eq}(z)} + \frac{X_{PS} \cdot A_P \cdot f_{pa}}{A_{Eq}(z)}\right) \tag{3}$$

where

R stochastic compression strength of concrete $= f_{cm} \cdot X_{fc}$

S action effects, e.g. lateral bending moment, gravity forces, and pre-stressing force

BM annual maximum storm bending moment at critical section due to lateral loads (wind and wave), Gumbel distributed, [18]

y extreme fibre distance (outer radius of concrete shaft)

G gravity forces on wind turbine, [18]

I_{Cr} moment of inertia of cracked section obtained using by considering rectangular stress block of concrete in compression zone

A_{Eq} $= A_c + A_R \cdot (m - 1)$, equivalent concrete area

A_c, A_R, A_P area of concrete, reinforcement and pre-stressing (m^2) respectively
f_{pa} maximum pre-stressing stress
m $= E_s/E_c$, modular ratio, ratio of modulus of elasticity of steel to concrete

3.3 Results and discussions

Reliability analyses as basis for probabilistic design are performed using the First Order Reliability Method (FORM), see [19] resulting in an estimate of the annual probability of failure P_F and the corresponding annual reliability index $\Delta\beta$.

The thickness of the GBF shaft (t) is considered as design parameter (denoted z in above section). Figure 3 shows the annual reliability index $(\Delta\beta)$ as function of thickness of the shaft (t) for different values of the reinforcement. It is noted that increase of the thickness of the shaft increases both fatigue and ultimate reliability indices increase, and also that an increase of the reinforcement (A_R) increases both fatigue and ultimate reliability indices. For all cases, ULS is governing.

Figure 4 shows the annual reliability index $(\Delta\beta)$as function of thickness of the shaft (t) with variation of pre-stressing. Increase in pre-stressing (A_P) induces additional pressure on concrete and thus reduces the reliability against fatigue as well ultimate strength failure. For all cases, ULS is governing. From Figure 3 and Figure 4 it is seen that to satisfy a minimum reliability requirement with an annual reliability index equal to 3.3, a design would require GBF shaft with thickness of 550 mm (minimum), reinforcement area of 0.2 m^2 (minimum) and pre-stressing area of 0.1 m^2 (maximum).

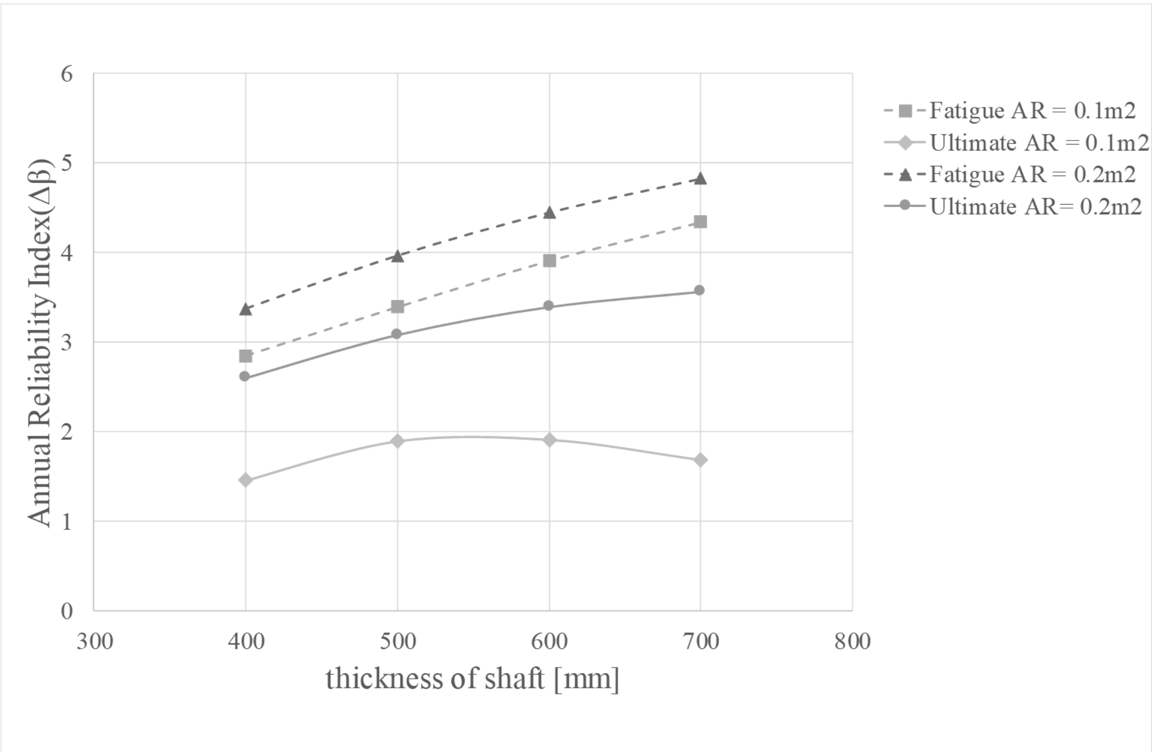

Figure 3: Sensitivity of reliability index to area reinforcement $A_P = 0.1$ m^2

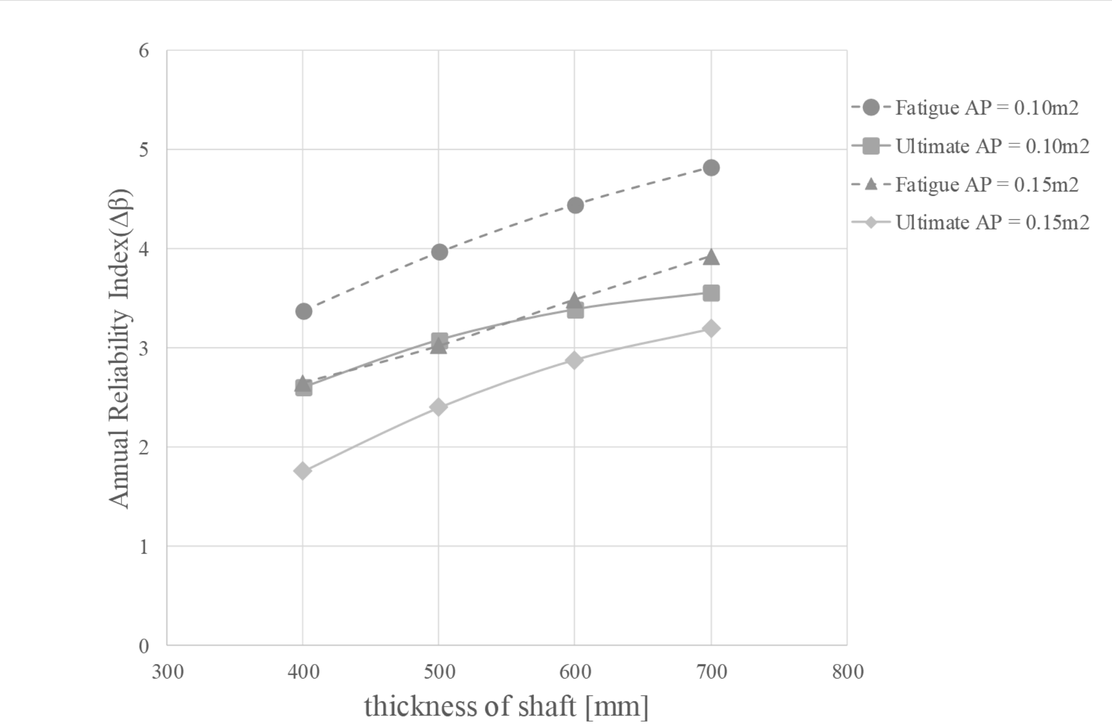

Figure 4: Sensitivity of reliability index to area of pre-stressing $A_R = 0.2\ \mathrm{m}^2$.

4. CONCLUSIONS AND FUTURE WORK

Probabilistic design of wind turbines has the potential to contribute significantly to reduction of the Levelized Cost of Energy and increased sustainability of wind turbines. The overall approach is presented in this paper and illustrated for offshore wind turbine tower and foundation made of concrete. The probabilistic design approach requires formulations of stochastic models for all uncertain parameters related to loads, strength and models, and development of limit state equation for the relevant design load cases. This paper only considers two of these limit states, but in future work stochastic models and limit state equations can be developed using the same principles for the remaining design load cases to be considered for design of wind turbines.

ACKNOWLEDGEMENTS

Current work is carried out under the project INFRASTAR (infrastar.eu), which has received funding from the European Union's Horizon 2020 research and innovation programme under the Marie Skłodowska-Curie grant agreement No 676139. The grant is gratefully acknowledged.

5. REFERENCES

[1] IEC 61400-1, Wind turbine generator systems – Part 1: Safety requirements, 4th edition ed., Geneva: International Electrotechnical Commission, 2019.

[2] fib MC2010, "FIB Model Code for concrete structures 2010," Ernst & Sohn, Berlin Germany, 2013.

[3] P. J. Tanver, J. Xiang and F. Spinato, "Reliability analysis for wind turbines," *Wind Energy,* vol. 10, pp. 1-18, 2007.

[4] P. Tanver, "Offshore Wind Turbines: Reliability, Availability and Maintenance," Institution of Engineering and Technology, 2012.

[5] W. Dong, T. Moan and Z. Gao, "Reliability-based gear contact fatigue analysis for wind turbines under stochastic dynamic conditions," in *ICOSSAR 2013*, New York, 2013.

[6] H. O. Madsen, S. Krenk and N. C. Lind, Methods of Structural Safety, New York: Dover Publications, 2006.

[7] JCSS, "JCSS PROBABILISTIC MODEL CODE," JCSS, 2002.

[8] J. D. Sørensen and H. S. Toft, "Safety Factors IEC 61400-1 background document," DTU Wind Energy, Denmark, 2014.

[9] J. D. Sørensen and H. S. Toft, "Probabilistic Design of Wind Turbines," *Energies,* vol. 3(2), pp. 241-257, 2006.

[10] J. D. Sørensen, "Reliability-based calibration of fatigue safety factors for offshore wind turbines," *International Journal of Offshore and Polar Engineering,* vol. 22, no. 3, pp. 234-241, 2012.

[11] H. S. Toft and , "Probabilistic Design of Wind Turbines," PhD thesis, Aalborg University, 2010.

[12] D. Veldkamp, "Chances in Wind Energy - A Probabilistic Approach to Wind Turbine Fatigue Design," PhD thesis, DUWIND Delft University, 2006.

[13] J. Velarde, A. Mankar, C. Kramhøft and J. D. Sørensen, "Uncertainty Modeling and Fatigue Reliability Assessment of Offshore Wind Turbine Concrete Structure," *IJOPE,* 2018.

[14] A. Mankar, S. Rastayesh and J. D. Sørensen, "Sensitivity and Identifiability Study for Uncertainty Analysis of Material Model for Concrete Fatigue". Proc. *IRSEC 2018,* Shiraj, 2018.

[15] A. Mankar, I. Bayane, J. D. Sørensen and E. Brühwiler, "Probabilistic reliability framework for assessment of existing reinforced concrete bridge structures," *Engineering Structures*. Submitted, 2018.

[16] A. Mankar and J. D. Sørensen, "Probabilistic fatigue design of reinforced-concrete wind turbine foundations". Submitted for *ICASP-13,* Seoul, South Korea, 2019.

[17] S. Márquez-Domínguez and J. D. Sørensen, "Probabilistic Fatigue Model for Reinforced Concrete Onshore Wind Turbine Foundations," in *Safety, Reliability and Risk Anaysis: Beyond the Horizon ESREL 2013,* Amsterdam, 2013.

[18] J. Velarde, C. Kramhøft and J. D. Sørensen, "Reliability-based Design Optimization of Offshore Wind Turbine Concrete Structures". Submitted for *ICASP-13,* Seoul, 2019.

[19] J. D. Sørensen, Notes in Structural Reliability Theory and Risk Analysis, Aalborg University, 2011.

SIMPLIFICATION OF CALCULATION OF WIND ACTION ON PIERS WITH ROUNDED CORNERS CROSS SECTION

Ivana Štimac Grandić and Davor Grandić

Faculty of Civil Engineering, University of Rijeka, Croatia

Abstract

The piers make up between 20% and 50% of the total cost of the viaduct depending on pier heights and foundation conditions. Therefore, the design of bridge piers is crucial for the design of prestressed concrete viaducts.

By rounding the corners of rectangular cross section of pier, the total wind force on pier can be drastically reduced in comparison to total wind force on pier with sharp corners with small reducing in load bearing properties of the pier.

Calculation of total wind force on bridge piers according to EN 1991-4 is quite complicated and time consuming. Even more complicated is calculation in case of rectangular cross section with rounded corners in comparison to rectangular cross section with sharp corners. Therefore, the main goal of this paper is to investigate the influence of taking into account geometrical properties (i.e. area and moment of inertia) of simplified cross sections (with sharp corners) instead of real geometrical properties of cross sections with rounded corners in calculation of the total wind force on piers.

Keywords: wind action, rounded corners, bridge pier

1. INTRODUCTION

Continuous bridges with high piers are commonly used to span deep valleys or rivers due to their economics [1]. According to research conducted in the USA, Canada and Japan by Hasrak et al. [2] continuous precast prestressed concrete bridges are commonly used bridge type on interstates and high volume urban highways, as well as on low volume urban and high or low volume rural highways. Continuous concrete beam structures are widely used for bridges on highways in Croatia, Italy, France, Holland and Germany [3].

The design of bridge piers is crucial for the design of prestressed concrete viaducts. The piers make up between 20% and 50% of the total cost of the viaduct depending on pier heights and foundation conditions [4].

High piers are especially sensitive to wind in free standing erection phase [5,6]. According to Han et al. [6] the contribution of wind on piers in total wind force during the erection stage is between 13% and 46%, depending on loading case.

Having in mind the above mentioned facts it is easy to conclude that reducing of the wind force on piers will reduce the bridge construction costs.

Wind action on piers of rectangular cross section with rounded corners is much smaller than wind action on piers with rectangular cross section with sharp corners while reducing in load bearing properties of the rounded-corner pier in comparison to sharp-corner piers are quite small. [7]

Calculation of total wind force on bridge piers according to EN 1991-4 [8] is quite complicated and time consuming. Even more complicated is calculation in case of rectangular cross section with rounded corners in comparison to sharp corner rectangular cross section. Therefore, the main goal of this paper is to investigate the influence of taking into account geometrical properties (i.e. area and moment of inertia) of simplified cross sections (with sharp corners) instead of real geometrical properties of cross sections with rounded corners in calculation of the total wind force on piers. In the paper the comparison of the total wind force calculated using exact geometrical properties of rectangular cross section with round corners and the total wind force calculated using simplified geometrical properties (for rectangular cross section with sharp corners) will be done.

2. THE WIND FORCE CALCULATION PROCEDURE

The wind force on structural elements F_w, according to EN 1991-1-4 [8], is defined as:

$$F_w = q_p(z) \cdot c_f \cdot c_s c_d \cdot A_{ref} \tag{1}$$

where $q_p(z)$ is the peak velocity pressure at reference height z, c_f is the force coefficient for the structural element defined according to the structural element cross section and $c_s c_d$ is the structural factor. The reference area A_{ref} of the structural element is product of height of the structure or structural member h and width of the structure perpendicular to the wind b.

In the following sections the procedure for calculation of $q_p(z)$, c_f and $c_s c_d$ is shown.

The peak velocity pressure $q_p(z)$ at reference height z includes mean and short-term velocity fluctuations and it is defined by

$$q_p(z) = [1 + 7 \cdot I_v(z)] \cdot ½ \cdot \rho \cdot v_m^2(z) \tag{2}$$

where ρ is the air density, $I_v(z)$ is the turbulence intensity at height z and $v_m(z)$ is the mean wind velocity at a height z above the terrain.

$$v_m(z) = c_r(z) \cdot c_0(z) \cdot v_b \tag{3}$$

$c_r(z)$ is the roughness factor, $c_0(z)$ is the orography factor and v_b is the basic wind velocity. If we take recommended values of the direction factor and season factor equal to 1 [8] the basic wind velocity v_b is equal to the fundamental value of the basic wind velocity v_{b0}.

The recommended value for orography factor $c_0(z)$ is equal to 1 [8].

Determination of the roughness factor $c_r(z)$ at height z is given as:

$$c_r(z) = k_r \cdot \ln\left(z/z_0\right) \quad \text{for} \quad z_{min} \le z \le z_{max} \tag{4}$$

$$c_r(z) = c_r(z_{min}) \quad \text{for} \quad z \le z_{min} \tag{5}$$

$$k_r = 0{,}19 \cdot \left(z_0 / z_{0,II} \right)^{0,07} \tag{6}$$

The values of z_{min} and z_0 can be found in Table 1 ($z_{0,II}$ =0,05), while z_{max}=200 m.

Table 1: Terrain categories and terrain parameters [8]

Terrain category		z_0 [m]	z_{min} [m]
0	Sea or coastal area exposed to the open sea	0,003	1
I	Lakes or flat and horizontal area with negligible vegetation and without obstacles	0,01	1
II	Area with low vegetation such as grass and isolated obstacles (trees, buildings) with separations of at least 20 obstacle heights	0,05	2
III	Area with regular cover of vegetation or buildings or with isolated obstacles with separations of maximum 20 obstacle heights (such as villages, suburban terrain, permanent forest)	0,3	5
IV	Area in which at least 15 % of the surface is covered with buildings and their average height exceeds 15 m	1,0	10

The turbulence intensity $I_v(z)$ may be determined according to equations (7) and (8). Recommended value for the turbulence factor k_l is 1. [8].

$$I_v(z) = \frac{k_l}{c_0(z) \cdot \ln z/z_0} \qquad \text{for} \qquad z_{min} \le z \le z_{max} \tag{7}$$

$$I_v(z) = I_v(z_{min}) \qquad \text{for} \qquad z \le z_{min} \tag{8}$$

The force coefficient c_f is defined according to the structural element cross section. The force coefficient for rectangular cross section can be calculated using eq. (10)

$$c_f = c_{f,0} \cdot \psi_r \cdot \psi_\chi \tag{9}$$

The force coefficient of rectangular sections with sharp corners and without free-end flow $c_{f,0}$ is defined in diagram in Figure 1(a).

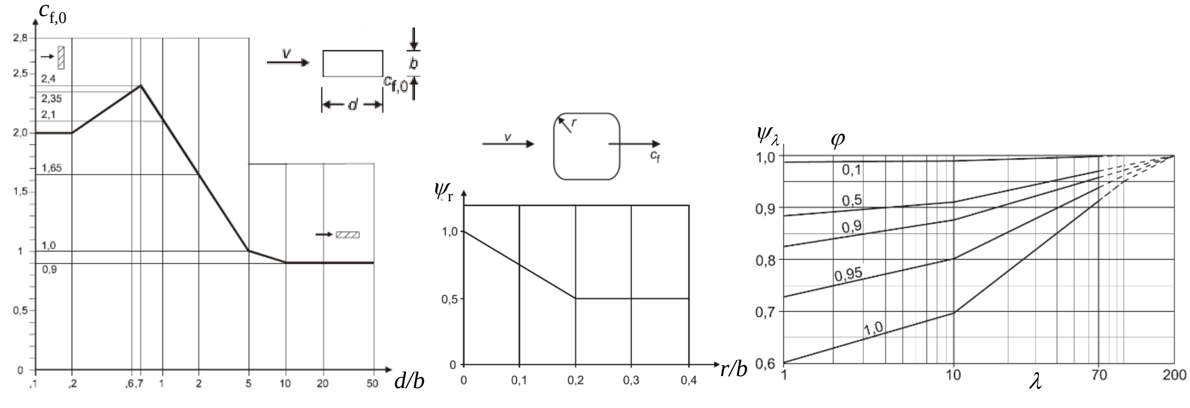

(a) (b) (c)

Figure 1: (a) the force coefficient, (b) the reduction factor, (c) the end-effect factor [8]

The reduction factors ψ_r for square sections with rounded corners is shown in Figure 1(b).

The end-effect factor ψ_λ should be determined using graph in Figure 1(c) as a function of the slenderness ratio λ and the solidity ratio φ. For rectangular cross section of the bridge piers the slenderness ratio λ may be determined as follows:

$$h \geq 50 \text{ m} \quad \lambda = 1{,}4 \cdot h/b \ \ or\ \ \lambda = 70 \ \ \text{whichever is smaller} \tag{10}$$

$$h < 15 \text{ m} \quad \lambda = 2 \cdot h/b \ \ or\ \ \lambda = 70 \ \ \text{whichever is smaller} \tag{11}$$

The structural factor $c_s c_d$ is defined as

$$c_s c_d = \frac{1 + 2 \cdot k_p \cdot I_v(z_s) \cdot \sqrt{B^2 + R^2}}{1 + 7 \cdot I_v(z_s)} \tag{12}$$

where z_s is the reference height for determining the structural factor, k_p is the peak factor, $I_v(z_s)$ is the turbulence intensity at the height z_s, B^2 is the background factor, R^2 is the resonance response factor. According to Annex B of EN 1991-1-4 [8]

$$z_s = 0{,}6 \cdot h \geq z_{min}\,. \tag{13}$$

$$k_p = \sqrt{2 \cdot \ln(v \cdot T)} + \frac{0{,}6}{2 \cdot \ln(v \cdot T)} \qquad \text{or} \qquad k_p = 3\,, \ \text{whichever is greater} \tag{14}$$

$$I_v(z_s) = \frac{k_1}{c_0(z) \cdot \ln\left(\frac{z_s}{z_0}\right)} \tag{15}$$

$$B^2 = \frac{1}{1 + 0{,}9\left(\frac{b+h}{L(z_s)}\right)^{0{,}63}} \tag{16}$$

$$R^2 = \frac{\pi^2}{2 \cdot \delta} \cdot S_L(z_s, n_{1,x}) \cdot R_h(\mu_h) \cdot R_b(\mu_b) \tag{17}$$

The mean wind velocity T in eq. (14) is equal to 600 seconds [8] and the up-crossing frequency v is defined as $v = n \cdot \sqrt{\frac{R^2}{B^2 + R^2}}$.

The turbulent length scale $L(z_s)$ in Eq. (16), for heights z_s above ground below 200 m, may be calculated as follows:

$$L(z_s) = L_t \cdot \left(\frac{z_s}{z_t}\right)^{\alpha} \quad \text{for} \quad z_{min} \leq z_s \leq z_{max} \tag{18}$$

$$L(z_s) = L(z_{min}) \qquad \text{for} \quad z_s < z_{min} \tag{19}$$

where $\alpha = 0{,}67 + 0{,}07 \cdot \ln(z_0)$, $z_t = 200$ m and $L_t = 300$ m.

The total logarithmic decrement of damping δ (eq. 17) can be determined according to Annex F of EN 1991-1-4 [17] as:

$$\delta = \delta_s + \delta_a + \delta_d \tag{20}$$

where δ_s is the logarithmic decrement of structural damping (defined according to structural type in [8]), δ_d is the logarithmic decrement due to special devices.
δ_a is the logarithmic decrement of aerodynamic damping defined as:

$$\delta_a = \frac{c_f \cdot \rho \cdot v_m(z_s)}{2 \cdot n \cdot m_e}. \tag{21}$$

m_e is the mass of the structure per unit length; n is the natural frequency of the structure.
The power spectral density function $S(z_s, n)$, in eq. (17) is defined as

$$S_L(z_s, n) = \frac{6{,}8 \cdot f_L(z_s, n)}{\left(1 + 10{,}2 \cdot f_L(z_s, n)\right)^{5/3}} \tag{22}$$

where a non-dimensional frequency $f_L(z_s, n) = \frac{n \cdot L(z_s)}{v_m(z_s)}$ is determined by the natural frequency of the structure n, by the mean velocity $v_m(z_s)$ and the turbulence length scale $L(z_s)$.
A fundamental mode shapes $R_h(\eta_h)$ and $R_b(\eta_b)$ are:

$$R_h(\eta_h) = \frac{1}{\eta_h} - \frac{1}{2 \cdot \eta_h^2} \cdot (1 - e^{-2 \cdot \eta_h}) \tag{23}$$

$$R_b(\eta_b) = \frac{1}{\eta_b} - \frac{1}{2 \cdot \eta_b^2} \cdot (1 - e^{-2 \cdot \eta_b}) \tag{24}$$

where $\eta_h = \frac{4{,}6 \cdot h}{L(s_z)} \cdot f_L(z_s, n)$ and $\mu_b = \frac{4{,}6 \cdot b}{L(s_z)} \cdot f_L(z_s, n)$.

3. CALCULATION OF THE TOTAL WIND FORCE

The total wind forces on reinforce concrete piers of different rounded corners cross sectional design (Figure 2) in free standing phase are calculated in two ways: (i) the real cross sectional properties (area and moment of inertia) of rounded corners cross sections and (ii) the sectional properties of simplified (sharp edge) cross sections (Figure 2) are taken into account in determination of structural factor (Equation (12)). In both cases, (i) and (ii), the reduction factors in Equation (9) are determined for cross sections with rounded corners.

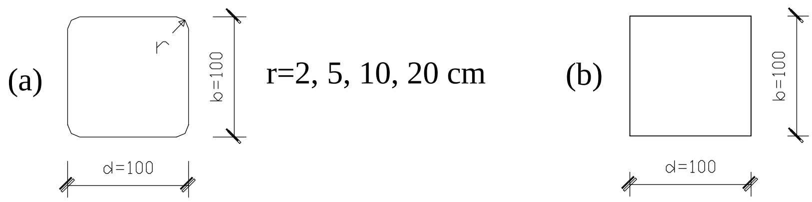

Figure 2: (a) The real pier cross sections, (b) the simplified pier cross section

The structural system of piers in free standing phase is taken as cantilever (fixed in foundations and free at the top).

Module of elasticity and specific weigh of reinforced concrete are taken as E=3,2·10^{10} N/m^2, $\gamma_c = 2500$ kg/m^3, respectively. The values of natural frequency n for each pier structure are determined according to [9].

Following pier and environmental characteristic are varied: pier height (h=20 m and h=10 m), fundamental values of the basic wind velocity (20 m/s, 30 m/s, 40 m/s and 50 m/s), terrain categories (TC 0, TC I, TC II, TC III and TC IV according to [8]).

For determination of velocity pressure of the structures where $h>2b$ the structure has to be divided in multiple parts as shown in Figure 3.

The velocity pressure should be assumed to be uniform over each horizontal part or strip. In equation (4), (5), (7) and (8) $z=z_e$ (Figure 3).

The total wind force on pier $F_{w,\mathrm{tot}}$ is the sum of wind forces acting in each part or strip $F_w(z)$

$$F_{w,\mathrm{tot}} = \sum F_w(z) = \sum q_w(z) \cdot h_z \cdot b \tag{25}$$

where h_z is the height of each part (b) or strip (h_{strip}) according to Figure 3.

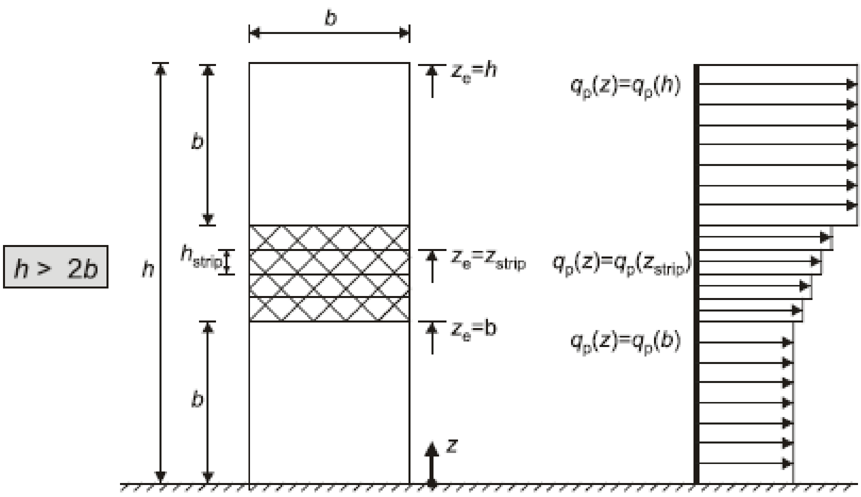

Figure 3: Reference height z_e and corresponding velocity pressure profile [8]

The bridge pier of height of 20 m and width of 1 m is divided as: the lower part extending from the ground up to 1 m; the upper part extending from top down to 1 m, the middle part of structure, between the upper and lower parts, divided into horizontal strips of 3 m height. The bridge pier of height of 10 m and width of 1 m is divided as follows: the lower part extending from the ground up to 1 m; the upper part extending from top down to 1 m, the middle part is divided into horizontal strips of 2 m height.

Following values are taken into calculations of the total wind force on piers:

- the turbulence factor k_l is taken with recommended value of 1,0 [8]
- the solidity ratio φ for non-hollow structures in the direction of wind action is equal to 1 [8]
- the air density ρ =1,25 kg/m^3
- the logarithmic decrement of structural damping δ_s is taken as 0,03 [8],
- the logarithmic decrement due to special devices $\delta_d = 0$

The total wind forces on piers of different heights, placed in different terrain category (TC) and exposed to different fundamental value of the basic wind velocity are calculated according to previous procedure taking into account real (Figure 2a) and simplified (Figure 2b) cross sectional properties in calculation of the structural factors.

The difference in total wind force taking into account real and simplified cross sectional properties ΔF is defined in Equation (26).

$$\Delta F = \frac{F^{R}_{w,\mathrm{tot}} - F^{S}_{w,\mathrm{tot}}}{F^{R}_{w,\mathrm{tot}}} \cdot 100 \; [\%] \tag{26}$$

where $F^{R}_{w,\mathrm{tot}}$ and $F^{S}_{w,\mathrm{tot}}$ are the total wind forces calculated considering the real and simplified cross sectional properties in calculation of the structural factors, respectively.

The values of difference ΔF are shown in Table 2.

Table 2. The difference ΔF in %

ΔF [%]		*h*=20 m					*h*=10 m				
		r=2 cm	*r*=5 cm	*r*=10 cm	*r*=15 cm	*r*=20 cm	*r*=2 cm	*r*=5 cm	*r*=10 cm	*r*=15 cm	*r*=20 cm
TC 0	$v_{b,0}$=20 m/s	0,0	0,0	0,1	0,2	0,4	0,0	0,0	0,0	0,0	0,2
	$v_{b,0}$=30 m/s	0,0	0,0	0,1	0,3	0,5	0,0	0,1	0,1	0,1	0,2
	$v_{b,0}$=40 m/s	0,0	0,0	0,1	0,3	0,5	0,0	0,0	0,1	0,2	0,3
	$v_{b,0}$=50 m/s	0,0	0,0	0,1	0,3	0,5	0,0	0,0	0,1	0,2	0,4
TC I	$v_{b,0}$=20 m/s	0,0	0,0	0,1	0,3	0,5	0,0	0,1	0,0	0,2	0,2
	$v_{b,0}$=30 m/s	0,0	0,1	0,1	0,3	0,6	0,0	0,0	0,1	0,2	0,3
	$v_{b,0}$=40 m/s	0,0	0,0	0,1	0,3	0,6	0,0	0,0	0,1	0,2	0,4
	$v_{b,0}$=50 m/s	0,0	0,0	0,1	0,3	0,6	0,0	0,0	0,1	0,3	0,5
TC II	$v_{b,0}$=20 m/s	0,1	0,1	0,1	0,4	0,7	0,0	0,0	0,0	0,0	0,3
	$v_{b,0}$=30 m/s	0,0	0,0	0,2	0,4	0,7	0,0	0,0	0,1	0,2	0,4
	$v_{b,0}$=40 m/s	0,0	0,1	0,2	0,4	0,7	0,0	0,0	0,1	0,2	0,5
	$v_{b,0}$=50 m/s	0,0	0,0	0,2	0,4	0,7	0,0	0,0	0,2	0,3	0,6
TC III	$v_{b,0}$=20 m/s	0,1	0,1	0,2	0,3	0,7	0,0	0,0	0,3	0,0	0,4
	$v_{b,0}$=30 m/s	0,0	0,1	0,2	0,5	0,9	0,0	0,0	0,0	0,1	0,4
	$v_{b,0}$=40 m/s	0,0	0,1	0,2	0,5	0,9	0,0	0,1	0,1	0,3	0,5
	$v_{b,0}$=50 m/s	0,0	0,1	0,2	0,5	0,9	0,0	0,0	0,1	0,4	0,6
TC IV	$v_{b,0}$=20 m/s	0,0	0,0	0,1	0,4	0,7	0,0	0,0	0,0	0,0	0,0
	$v_{b,0}$=30 m/s	0,0	0,0	0,2	0,5	0,9	0,0	0,0	0,2	0,2	0,2
	$v_{b,0}$=40 m/s	0,0	0,1	0,3	0,6	1,0	0,0	0,0	0,2	0,2	0,2
	$v_{b,0}$=50 m/s	0,0	0,1	0,3	0,6	1,0	0,0	0,0	0,1	0,3	0,5

4. CONCLUSIONS

As it can be seen from Table 2, the differences ΔF are between 0 and 1%.

The greatest difference is 1%, in cases of piers of 20 m height, placed in TC IV exposed to fundamental values of the basic wind velocity of 40 and 50 m/s. Almost no difference is for piers with r/b=0,2.

In general, the differences in calculated total wind force taking into account real and simplified cross sectional properties for determination of the structural factor

- are greater for taller piers
- increase with increasing of fundamental values of the basic wind velocity
- increase with increasing in radius of rounded corner.

From above discussion it is clear that the differences in calculated total wind force taking into account real and simplified cross sectional properties for determination of the structural factor are negligible for engineering purposes. Thus, calculating the wind action on non-hollow rectangular piers with rounded corners can be done by using the sectional properties of simplified cross section (rectangular with sharp corners) when calculate the structural factor.

ACKNOWLEDGEMENTS

This paper is a part of research supported by University of Rijeka through Grant No. 13.05.1.1.01. and Grant No. uniri-tehnic-18-127. The authors are grateful for this support.

REFERENCES

[1] Han, Y., Chen, Z-Q., Hua, X-G., Feng, Z-Q. and Xu, GJ, 'Wind loads and effects on rigid frame bridges with twin-legged high piers at erection stages', *Advances in Structural Engineering*, **20** (10) (2017) 1586-1598. https://doi.org/10.1177/1369433216684350

[2] Hastak, M., Mirmiran, A., Miller, R., Shah, R. and Castrodale, R., 'State of Practice for Positive Moment Connections in Prestressed Concrete Girders Made Continuous', *Journal of Bridge Engineering*, **8** (5) (2003) 267-272.

[3] Sesar, P., 'Optimizing of Continuous Bridge Connections', Doctoral Thesis, Faculty of Civil Engineering, J. J. Strossmayer University of Osijek, (Osijek, 2005). (in Croatian)

[4] Martínez, F. J., González-Vidosa, F., Hospitaler, A. and Yepes, V., 'Heuristic optimization of RC bridge piers with rectangular hollow sections', *Computers and Structures* **88** (5-6) (2010) 375–386, https://doi.org/10.1016/j.compstruc.2009.11.009

[5] Wardlaw, R. L., 'Wind effects on bridges', *Journal of Wind Engineering and Industrial Aerodynamics*, **33** (1-3) (1990) 301-312. https://doi.org/10.1016/0167-6105(90)90045-E

[6] Hjorth-Hansen, E., Jakobsen, A. and Strømmen, E., 'Wind buffeting of a rectangular box girder bridge', *Journal of Wind Engineering and Industrial Aerodynamics*, **42** (1-3) (1992) 1215-1226. http://dx.doi.org/10.1016/0167-6105(92)90128-W

[7] Štimac Grandić, I., Ferenčić, D., Grandić, D. and Šculac, P., 'Utjecaj oblikovanja stupova mostova na njihovo vjetrovno opterećenje' Zbornik radova: Graditeljstvo - poluga razvoja, Cavtat, Hrvatksa 2012 (Hrvatski savez građevinskih inženjera, Zagreb, 2012.) 299-310.

[8] EN 1991-1-4 Eurocode 1: 'Actions on structures - Part 1-4: General actions - Wind actions (EN 1991-1-4:2005+AC:2010+A1:2010)' (CEN, Brussels 2010)

[9] Hurty, W. C. and Rubinstein M. F., 'Dynamics of Structures' (Prentice-Hall, New Delhi,1967.)

OPTIMIZED DESIGN OF FLAT SLABS WITH DIFFERENT NOVEL TYPE OF PUNCHING REINFORCEMENT

Jakub Mečár (1), Petra Bujňáková (2) and Vladimír Sobek (2)

(1) Peikko Group Corporation, Žilina, Slovakia

(2) Faculty of Civil Engineering, University of Žilina, Žilina, Slovakia

Abstract

Nowadays, reinforced concrete flat slabs are a competitive system for structural frames of administrative and residential buildings. Optimized design of the flat slab thickness can lead to reduction of concrete consumption and weight of the building. The minimal required thickness of the flat slab is typically governed by the resistance against punching shear failure of the slab in the column area. The punching shear resistance can be increased by using punching shear reinforcement. Currently, stirrups and double-headed studs are the most common types of punching shear reinforcement used in Europe. A novel type of punching shear reinforcement has recently been developed and marketed by the company Peikko Group. Extensive experimental research of this novel type of reinforcement demonstrates that the novel punching reinforcement allows to enhance the superior resistance of concrete flat slabs in comparison to the resistance achieved by using conventional punching reinforcement system. This paper presents some practical benefits yielding from the superior structural performance of innovative punching shear reinforcement

Keywords: Punching failure, stud, maximum resistance

1. INTRODUCTION

Double headed studs are nowadays a common solution for increasing the maximum resistance against punching failure of flat slabs.

Figure 1. PSB Studs

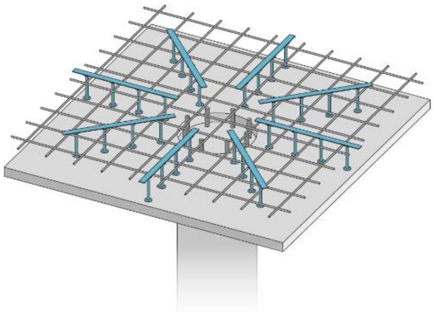

Figure 2. Flat slab reinforced with PSB studs

The use of double-headed studs as reinforcement against punching failure is currently not regulated by EN 1992-1-1. Therefore, the performance of studs placed on the European market must be assessed by European Technical Assessment. The structural performance of PSB studs produced by company Peikko have been assessed based on extensive experimental research executed in cooperation between company Peikko and EPFL in Lausanne [3]; [4]. This research allowed among others to demonstrate that the studs allow slabs to reach resistance superior to those that can be reach by using conventional reinforcement such as stirrups [7].

2. NOVEL TYPE OF PUNCHING REINFORCEMENT

A novel reinforcement system called PSB PLUS has been developed by the company Peikko Group to further increase the maximum resistance of slab against punching failure in situations, where resistance provided by PSB studs in not sufficient. PSB PLUS system combines vertical double headed PSB studs with horizontal studs. Horizontal studs are placed above column in the shape of cross and parallel to the bottom bending reinforcement.

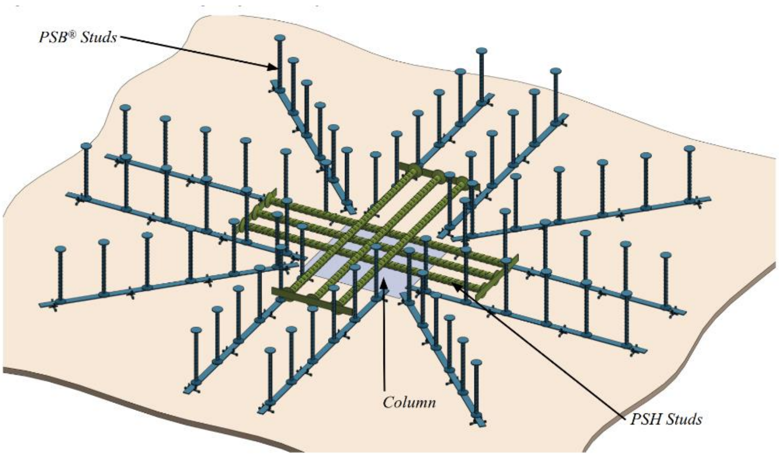

Figure 3. PSB PLUS System

A comprehensive experimental research has been performed in co-operation between Peikko Group and EPFL Lausanne in order to study the structural performance of slabs reinforced by the system PSB PLUS. The research allowed to develop a comprehensive design method to assess the structural performance of slabs reinforced with PSB PLUS. Within this method, the maximum resistance of a slab reinforced with PSB PLUS is determined as:

$$V_{Rd,max,PLUS} = V_{Rd,max,ETA} + \frac{\sum V_{Rd,PLUS}}{2} \quad (1)$$

where $V_{Rd,max,ETA}$ is maximum resistance of slab reinforced with vertical PSB studs only and $V_{Rd,PLUS}$ is the sum of resistances of horizontal headed studs (see

Table 1).

Table 1. Single resistance of horizontal PSH stud

Diameter of horizontal PSH studs	**Concrete cover of PSH studs**	**Design value of shear resistance for one PSH studs for one shear section.**
$Ø_{PSH}$ [mm]	**c_d [mm]**	**$V_{Rd,PLUS}$ [kN]**
25	46.5	24.5
32	50	40
40	54	56.8

The detailing rules for installation of PSB PLUS system are presented in Figure 4.

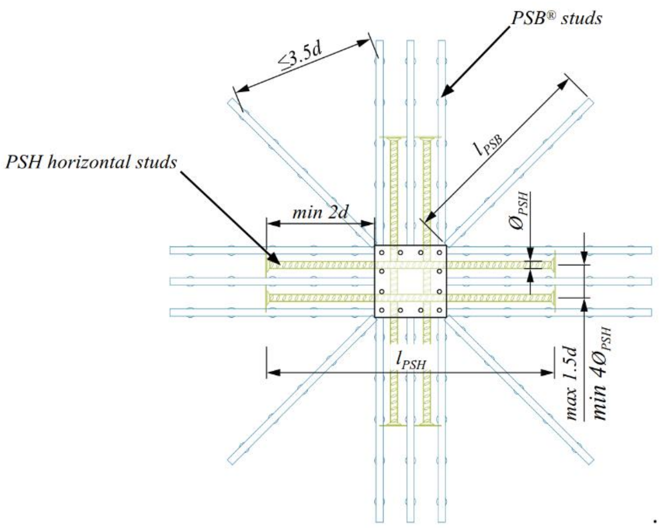

Figure 4. Installation instruction for PSB PLUS

3. PARAMETRIC STUDY

The practical benefits that are now offered by the PSB PLUS system have been demonstrated by a parametric study [6] where an administrative building illustrated on Figure 5 has been designed considering the following alternatives for the design of punching reinforcement in flat slabs:

- Stirrups
- PSB studs

- PSB PLUS

The aim of the study was to determine minimum thickness of flat slab with regards to punching failure for different punching reinforcement systems. Besides punching failure, the thickness of the slabs was also limited by a maximum deformation of the slab at mid span limited to L/250 to the span of slabs in both directions was 9600mm and concrete grade was C30/37 (Figure 5).

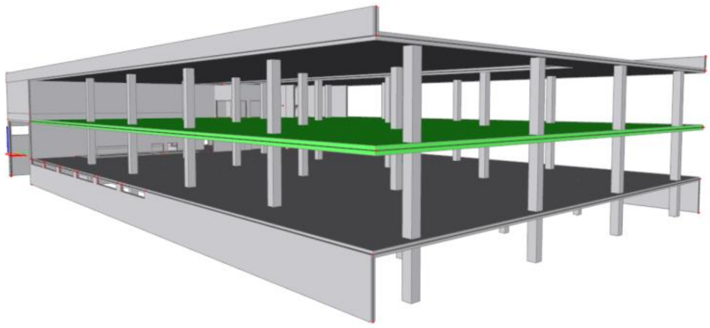

Figure 5. Selected slab for parametric study

Besides the type of reinforcement, the thickness of the flat slab and related self-weight was the only variable. Within this study, parameters like dimensions of the columns, spacing of the columns or concrete grade have been fixed to eliminate number of combinations.
The maximum punching resistance of flat slab calculated in parametric has been determined as:

$$V_{Rd,max} = k_{max} \cdot V_{Rd,c} \qquad (2)$$

where k_{max} is magnification factor depending on type of punching reinforcement and $V_{Rd,c}$ is resistance of flat slab without any punching reinforcement. The value k_{max}=1,5 was used for slabs reinforced by stirrups in accordance with EN 1992-1-1, the value k_{max}=1,96 was used for slabs reinforced with PSB studs in accordance with the ETA 13-0151.

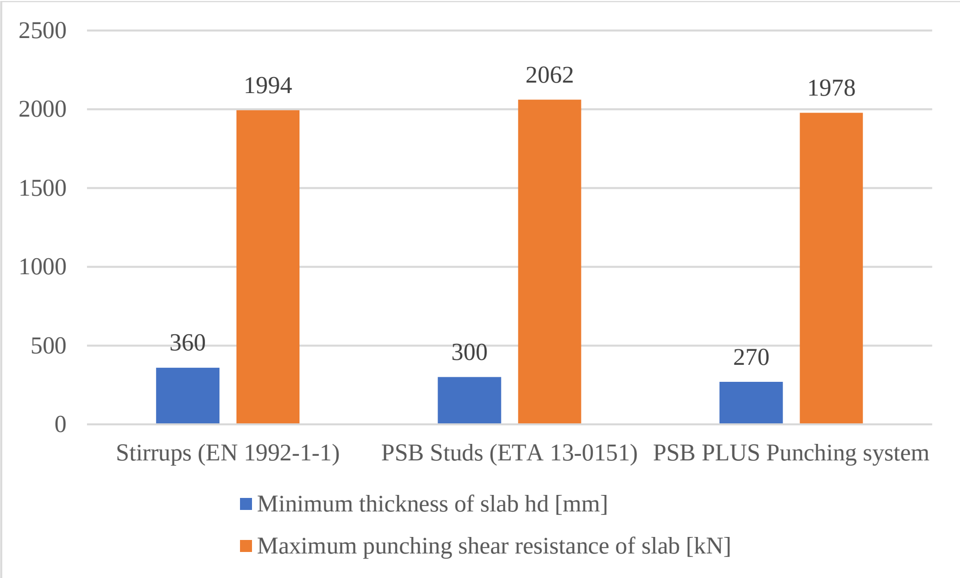

Figure 6. Comparison of minimum slab thicknesses and maxumum punching shear resistances for various systems

The novel type of punching reinforcement in form of PSB PLUS can increase maximum resistance of the slab reinforced only by PSB studs, as it is shown in equation (1). With the PSB PLUS Punching system maximum punching resistance of the slab can be reached up to $2.2{*}V_{Rd,c}$, for the situation presented in parametric study. This superior performance of the punching reinforcement allows to optimize the thickness of the slab even in comparison to slabs reinforced by PSB double-headed studs.

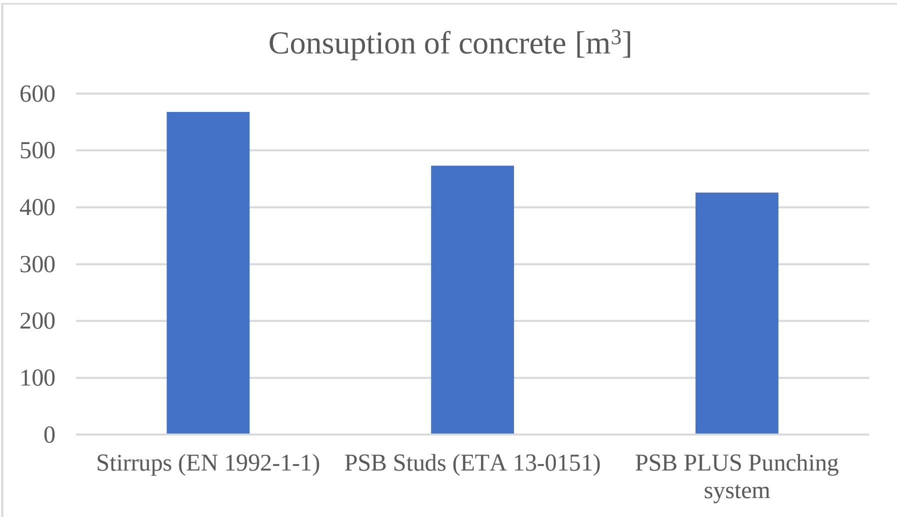

Figure 7. Comparison on consuption of concrete for one floor slab

Results presented in Figure 6 and Figure 7 have been determined for slab without considering shrinkage and creeping effect at slab which will be included in next studies.

4. CONCLUSION

The paper presents a novel punching reinforcement system named PSB PLUS. This system has been developed to reinforce flat slabs against punching shear failure. The structural performance of the system has been assessed by extensive research which allowed to developed design recommendations briefly summarized in the paper. Benefits provided by PSB PLUS have been illustrated by a parametric study. The study shows that using PSB PLUS system leads to optimization of the reinforced concrete flat slab if the punching failure is limiting design of slab thickness.

REFERENCES

[1] EN 1992-1-1: *Eurocode 2: Design of concrete structures. Part 1-1: General rules and rules for buildings* (2014)

[2] ETA-13/0151: PEIKKO *PSB Punching Reinforcement: Double headed studs as punching reinforcemen*t. Berlin: Deutsches Institut für Bautechnik, June 2013

[3] Einpaul J.; Bujnak J.; Fernandez Ruiz M.; Muttoni A.: *Study on Influence of Column Size and Slab Slenderness on Punching Strength*. In: ACI Structural Journal, 113 (2016), Farmington Hills, USA, S. 135-145.

[4] Simoes J.; Bujnak J.; Fernandez Ruiz M.; Muttoni A.: *Punching shear tests on compact footings with uniform soil pressure*. In: Structural Concrete, 17 (2014), S. 603-617.

[5] Muttoni A.; Fernandez M.: *Report MFIC 17-A18-R2: Design of Peikko PSB PLUS® punching shear system*, Lausanne (2018)

[6] Sobek V.: *Design of point-supported reinforced concrete slab*. Diploma Thesis, University of Zilina (2018)

[7] Einpaul, Jürgen, et al.: *Performance of Punching Shear Reinforcement under Gravity Loading: Influence of Type and Detailing*. ACI Structural Journal 113.4 (2016).

[8] Lips S.; Fernandez Ruiz M.; Muttoni A.: *Experimental Investigation on Punching Strength and Deformation Capacity of Shear-Reinforced Slab*, In: ACI Structural Journal,109, No. 6, Nov.-Dec. (2012), pp. 889-900

International Conference on Sustainable Materials, Systems and Structures (SMSS 2019)
Challenges in Design and Management of Structures
20-22 March 2019 – Rovinj, Croatia

LIGHT FORMWORK FOR EARTHEN MONOLITHIC SHELLS

Elizabeta Šamec (1), Akash Srivastava (2) and Stephanie Chaltiel (3)

(1) Faculty of Civil Engineering, University of Zagreb, Croatia

(2) Indian Fellow, Domaine de Boisbuchet, Lessac France

(3) ETSAB UPC, Barcelona, Spain

Abstract

The ongoing research in project *Small scale robotic manufacturing for large scale buildings,* developed through the *Innochain* network by Stephanie Chaltiel, is investigating how robotic fabrication enables construction of earthen monolithic shells in near future context. Introduction of small-scale robots (drones) in to the building process revives building of earthen shells in general by minimising labour intensive tasks, leaving more time and budget for skilled work.

By describing two case studies, paper sheds light on robotic fabrication process and timeline of the construction, as well as constraints related to architectural and structural requirements according to usage of different lightweight formworks and drone deposition techniques. The paper discusses role of pneumatic and wooden formwork, since the replacement of conventional scaffolding by use of flexible formwork is very interesting research subject [6, 7 and 8], enabling additional savings regarding the material, cost and time necessary for the construction. According to results of case studies the paper highlights key inferences to govern future physical experiments towards successful development of Bioshotcrete construction technique for earthen shells.

Keywords: light formwork, pneumatics, earthen shells, drones, digital fabrication

1. INTRODUCTION

Raw earthen structures are recognized by literature as traditional structures made from the mix of natural soft materials (clay, sand, marble powder, fibres, etc.). Although large scale inhabitable unbaked pottery is long known, for example the Musgum domes in Cameroun, due to intensive manual work it still has non-legitimate status in some European countries. Today when sustainability in construction becomes crucial, earthen architecture is being reconsidered, due to its little ecological footprint; both during construction and period of use.

The paper aligns to the research [1] carried out by Stephanie Chaltiel in the project *Small scale robotic manufacturing for large scale buildings*, a part of the *InnoChain* network. The project develops Bioshotcrete construction technique [2] that consist from the sequential layering of different types of mixes of clay and fibres over the temporary lightweight formwork using drone spraying technology, consequently leading to building a self-standing shell.

With aim to revive building of earthen architecture in modern context, this research imposes few objectives [3]. Firstly, to use non-cement based mortar, enabling construction with natural material that has unique combination of thermal insulation and heat storage properties. Clay is the most widely available primary material and it can be used in geographically diverse locations, making it extremely suitable to build temporary shelters (refugee camps and disaster zones). The traditional way of applying clay on formwork is relatively non-uniform, laborious and time-intensive process. Therefore, second objective is to minimize intense manual labour. This can be achieved by implementing robotic fabrication processes i.e. developing on-site digital fabrication strategies using small-scale robots. The last objective is to minimize formwork – the objective that this paper shall deal with elaborately.

2. BIOSHOTCRETE TECHNIQUE

The wattle and daub is a traditional earthen architecture technique consisting of coating layers on both sides of the lost formwork (made out of flexible intertwined branches) until sturdy envelopes are reached at the end of the curing time. The technique is applicable but contains very labour intensive manual tasks. For other materials, like concrete, more sustainable solutions are developed through the past, like shotcrete. Therefore, team of robotic experts, architects, engineers and drone specialists explores how to use the robotic techniques for digital fabrication in order to combine traditional procedures of building with earth and modern needs for efficient and fast construction. The research resulted in development of Bioshotcrete technique for building large scale monolithic earthen shells [2].

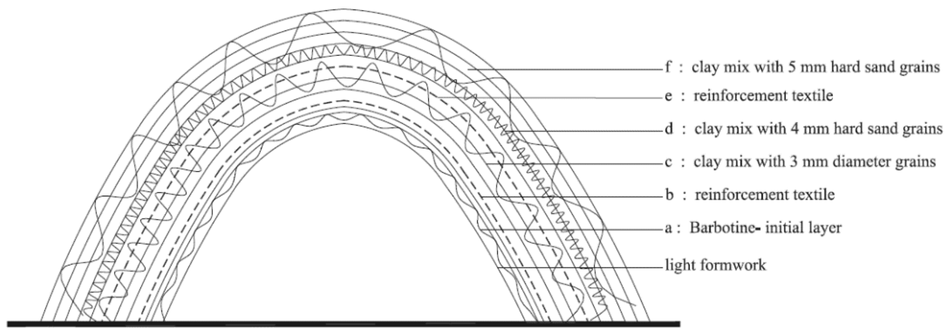

Figure 1: Cross section – succession of applied layers (based on [3])

The technique consists in projecting paste-like matter, composed of carefully formulated different clay mixes, following precise and customised deposition sequences over a temporary formwork. By modifying the proportion of each ingredient in the mix (grains, fibres, clay, water, etc.) different consistencies, levels of viscosity, elasticity and stickiness are obtained [3]. The protocol of clay mixes deposition is heavily dependent on the formwork provided, the deposition apparatus and the robotic actions. Three main layers [3] can be identified as seen from the Figure 1:

i. Liquid layer for the initial spray – contains high percentage of plaster to form a thin solid crust to replace formwork action and enables its easy removal

ii. Viscous and fibre layers – high in sands and fibres to gain thickness without overloading the delicate formwork and to absorb moisture
iii. Dry layers – contain increasing sand diameter and grain size to provide volume and thickness to gain stability and ensure structural performance

The integration between matter and robotic actions depends on spraying device, material container and process of feeding the deposition apparatus until self-standing shell is completed [3]. Monolithic shells are chosen as structural system for this application, due to their ability to exhibit advantageous load-bearing behaviour resulting in spanning a large footprint with least possible material. Since the flights taken by the drone spraying matter need to be optimised, enabling the structure to be erected in least possible time span; the smaller cross section of the structure is thus a crucial parameter.

3. FLEXIBLE FORMWORK FOR THIN SHELLS

In last years, huge carbon footprint caused by concrete industry (31,654 million tons of concrete produced per year according to [4]) is forcing us to reconsider building shell structures as possible way to use concrete properties to their advantage, reducing the needed cross section. However, producing a formwork and scaffolding for such geometry specific structures is very material and labour intensive. Replacement of classical wooden formwork with different types of flexible formworks (fabric, pneumatics, etc.), has a history in concrete construction [4, 5]. New types of flexible formworks, like cables in combination with membranes or knitted material, are recently the research topic of great interest [6, 7]. Today, development of digital fabrication technology can help expand and transform existing construction methods for shells, and potentially offer more sustainable building solutions and usage of different materials [8].

In this research a series of experiments with flexible formwork were conducted. On the beginning a robotic arm fitted with a mortar hand sprayer (8L capacity) connected to air compressor was used to deposit a variety of clay mixes [1, 3 and 9]. As formwork, fabric stretched between compression elements was used until the structure reached self-standing condition and formwork was removed. Due to restrictions of a robotic arm [3], like reaching capacity of the arm, the cost, size and impossibility to bring such heavy apparatus in remote sites, further experiments were concentrated on using drone for spraying matter. With introduction of drones in to the building process necessity for scaffolding or any height limit of the structure (up to 25 m) disappeared, enabling further cost and time benefits for the project. Two real scale case studies using drone spraying for building earthen domes were conducted in 2018. Case studies will be presented and compared, with emphasis on used formwork and matter deposition techniques.

4. CASE STUDY 1 – LARGE SCALE TEST DRONE SPRAY OVER PNEUMATIC FORMWORK

In Drone Centre Barcelona, large scale outdoor experiment was conducted by depositing clay mixes on to the pneumatic formwork [2]. Deposition was made with custom made drone, that has 4 engines (each 20hp), carrying container of 5 to 35 kg capacity. It was piloted by automated flights using GPS systems, with 1 cm precision. As formwork, affordable prefabricated 4m inflatable dome was used (Fig 2A). Pneumatics bring following benefits in to the building process of earthen monolithic shells: reduced time for the montage, lesser "skilled" manpower deployment on site, negligible transportation, price reduction by multiple usage with ability to gain different shapes and textures, etc.

Except from beneficial properties, many of the existing pneumatic formwork systems struggle with process-related inaccuracies with respect to the reference geometry and the thickness of the final structure [5]. Behaviour of pneumatic structures is inherently nonlinear. They acquire their primary load bearing capacity after undergoing deformation which, even under small pressures, may be very large [10].

Figure 2: Tests made on pneumatic formwork (from [2]) - A) installation of pneumatic formwork B) matter deposition C) deformation under matter weight and deposition pressure

Regarding this case, pneumatics bring problems related to deposition of the material during the drone spraying. The membrane, becomes deformed when material with a comparatively high density is applied. With the drone carrying large amount of material and depositing it at once (Fig. 2B, 3A) the deflection from excessive pressure present during this non-constant deposition is very large (Fig. 2C). The weight of the material and pressure under which it touches the flexible surfaces cause hard control of shell geometry, resulting in deviations from the designed structure and variable shell thickness. The accurate geometry for such a shape dependent structure is highly important especially if small thickness of the shell is desired due to lesser number of spraying flights needed.

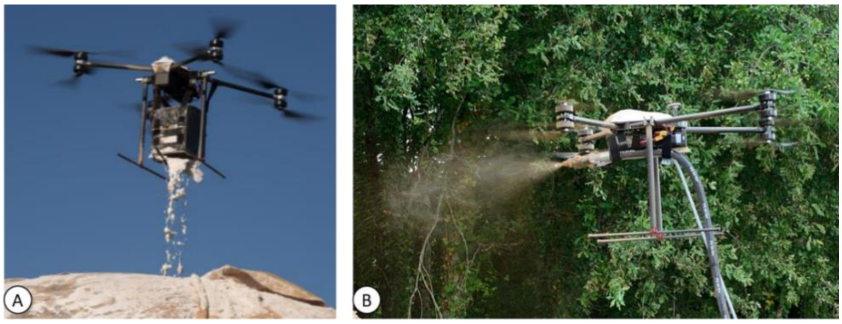

Figure 3: A) Drone carrying container with clay mix (from [2]) B) Drone with pipe connected to matter mixer and water

Therefore, the challenge is to achieve a very gentle and continuous deposition to avoid sagging and deformations. In order to accomplish that, research was concentrated on the development of the drone with ability to carry supply pipe, design and production of customised spraying devices and fitting options on the drone, allowing to vary pressure and other drone spraying parameter [2]. Drone was modified to carry pipe connected to a matter mixer with water on the ground (Fig 3B), enabling constant material feed, and helping to efficiently coat large surfaces with more homogenous coating of clay mix. After being tested indoors [10], new available spraying technology was tested for the first time on a real scale structure during the second case study.

5. CASE STUDY 2 – LARGE SCALE TEST DRONE SPRAY OVER LOST LIGHT WOODEN FORMWORK

The goal of the case study was to build in 5 days, a permanent inhabitable monolithic earthen shell in real size. The location set for the case study was a bucolic farm in south west of France. The weather conditions (min./max. temperature: 11/33 degrees, avg. rainfall 11 mm [11]) remained varied during the entire duration of study. Due to short duration of workshop, the Bioshotcrete technique had to be adopted and instead of numerous clay layers necessary to build the body of the structure, cross section was achieved by using small jute bags filled with hay, then sprayed by 5 layers of clay. The construction was divided into two parts (Figure 5) i.e. manual construction of formwork and body of the structure (3 days) and application of clay layers using drone spraying (2 days).

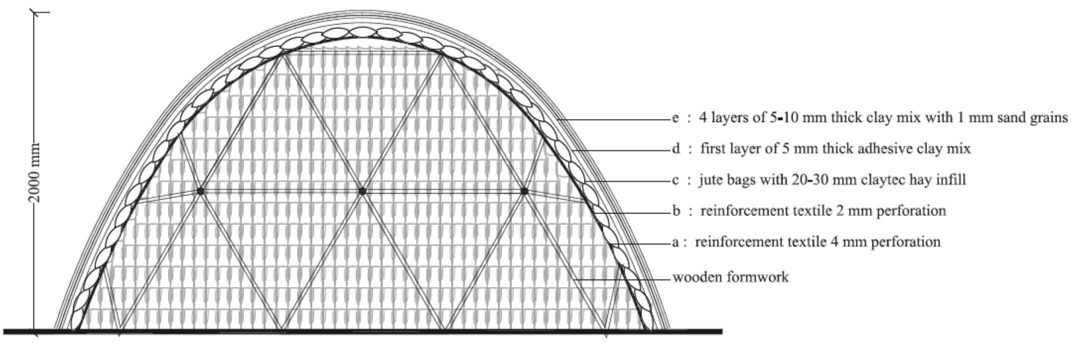

Figure 4: Cross section of the CS2 dome –modified layers for faster thickness gaining

The formwork was built as the 2m radius wooden geodesic dome anchored to the concrete ring of one feet cross section. The wooden members were joined with simple snap-together connectors, made of UV resistant plastic, manufactured by *Hubs* [12]. On to the wood, jute fabric was fixed acting as a surface to attach around 1800 jute bags filled with hay. The bags are connected to fabric in two points on the top of the bag using zip ties. The bags are laid out like tiles, with 1/3 overlap necessary to transmit the load from top to the bottom of the dome. Overlap was also preventing potential movement of the bags caused by wind generated by the drone. The jute bags were selected as easy to use prefabricated elements, and hay as the natural filling material with low mass and characteristics necessary to preserve benefits of earthen architecture. The size of the hay is 2 to 3 cm, the hey is then big enough not to drop out of the bag's perforations, and small enough to stuff the bag with right compaction. However, the first ring laid on the bottom of the dome was filled with coarse sand and aggregate (1-2 cm) to avoid moist and water suction from the ground and to provide a solid base to the dome. Although bags enabled fast generation of cross section thickness, the attachment process became the most intense manual process of this building procedure. The wooden formwork subsequently stayed as a lost formwork, due to reasons explained further in this chapter. The application of clay on to the build structure was done in 5 layers – the first more viscous layer and 4 layers containing clay with small grain size sand of less than 1 mm and linen fibres. Each clay mix deposition corresponded to mix of 8 bags of 8 kg of clay with water (a proportion of 12 l of water per bag), corresponding to 1 cm thickness to cover 25 m^2. The application method using drone enabled work in the regions unapproachable to the team otherwise, without extensive scaffolding on site. The process was spread over 36 hours with intervals of drying between each spray of the next layer. Additional two layers of special paint containing sealant are applied on the end to make the dome waterproof but still "breathable".

Figure 5: CS2: A) installation of wooden formwork, B) attachment of hay bags, C) formwork detail, D) drone spraying

Upon the successful construction of the dome in 5 days (Fig. 6A), the dome unfortunately collapsed after four weeks. Detecting possible reasons of the collapse is critical for future experiments. Initial assessments upon inspection concluded on particularly three main reasons for the failure of the structure. Firstly, the prefabricated PVC hub failed, the wooden element connected by plastic hinge (ball) to the hub (socket) snapped out (Fig. 6C). The reason is probably the working principle of joint for fast fabrication (snap together ball and socket) that is not solid enough. New version of 3D printed hubs with a locking cap is now available and should be used in further experiments with light wooden formwork. More importantly, the joint has failed because the earthen structure itself did not start to work in compression, since thickness of projected matter should have been at least 25 cm and cover all the bags. With time to apply more layers, thickens of structures cross section would enable to sustain structures own weight independently from the wooden skeleton. Lastly, it was not possible to provide 1 month of rain protection for the dome, and the weather conditions altered the curing time needed for this technique to work. Since curing was interrupted and the thickness was not sufficient to cover the bags; textile and hay have a tendency of holding on water, thus the dead load may have increased due to the pouring rains.

All these factors were taken into consideration for the subsequent case study carried out in London [13] (Fig. 6C). At first, the weight at the top of the dome (top 5 triangles) was reduced by replacing all hay bags with a plastic sheet. The sheet allowed enough daylight within the dome, while also eliminating any possibility of water entering from the top. Thereafter, the entrance to the dome was kept smaller while also providing additional poles as support frames. Thirdly, the hubs in this case were 3D printed, functioning much better with a locking cap. This resulted in a stronger skeleton and thus giving a longer life to structure.

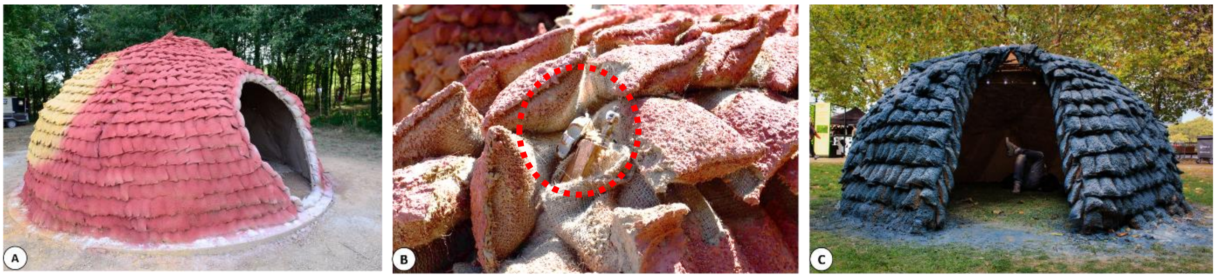

Figure 6: A) Finished dome sprayed with paint for waterproofness, B) Failure of prefabricated hub, C) London dome

6. CONCLUSIONS

The Bioshotcrete aims to incorporate alternate bio materials, advanced digital fabrication techniques and drone automated fights within the construction industry in the upcoming years.

The CS1 showed us that usage of pneumatic formwork for such future construction process is worth investigating, but due to used deposition technique emphasis is still on the large deflection problem. There are several insights gained in the CS2 that could help in dealing with mentioned problem in future experiments. By using the latest drone spraying technology, for the first time more pressure control and consequently thickness control is gained. This is very important for any light formwork used, but especially relevant for potential decreasing of currently problematic large deflections of pneumatics. By enabling the pilot to control pressure and angle of spraying in future experiments, even more thickness control can be gained, important for further improvement of the method.

Through CS2 it is confirmed that the minimal thickness of layer applied on the formwork is 0.5 cm and maximum 2 cm. Therefore, for the 3 m high dome, build using original Bioshotcrete procedure and by using pneumatic formwork, expected thickness of the cross section would be 10 cm. In that case, additional jute between clay layers needs to be added serving as reinforcement. This conclusion will be confirmed true next physical experiments.

In both case studies it is proved that the drone spraying technique allows to reach and coat different parts of the structure without the need for a scaffolding or a crane, as a huge benefit for cost and timeline of the project. New spraying technology even enables efficient spraying of lower parts of the dome, where spray angle is almost 90 degrees.

Further exploration of geometry and structural analysis are necessary to derive future full scale tests for shells with optimal structural performance. Monitoring formwork’s displacements (wooden or pneumatic) is regarded as necessary to gain more inside on formwork behaviour during the construction process. For the overall understanding of pneumatic formwork’s behaviour, development of numerical model that would consider air and load pressure as nonlinear influence would be beneficial. The climatic conditions while spraying clay over the pneumatic formwork can play a critical role in its overall construction. While the air can get cooler or warmer as the time of the day progresses, it can contract and expand the formwork, which can develop cracks on the layers applied.

As in former case studies [9], iterative geometry analysis of the constructed shell would enable more control over degree of deformation. Numerical model of the shell can provide results for analysis of displacements, utilization and stress lines, enabling to evaluate the fabrication process in terms of structural performance. Also, obtained stress lines can serve as guide lines for placement of additional reinforcement.

7. ACKNOWLEDGEMENTS

The authors would like to thank other CS2 participants, Muhammed Shameel for co-hosting the workshop and Alina Cristea for the CS2 photos.

8. REFERENCES

[1] Chaltiel, S., Bravo, M., ‘Monolithic earthen shells robotic fabrication’ in Proceedings of the ACADIA conference, Boston, November, 2017

[2] Chaltiel, S., Bravo, M., Goessens, S., Latteur, P., Mansouri, M. and Ahmad I., 'Dry and Liquid clay mix drone spraying for Bioshotcrete' in 'Creativity in Structural Design' in Proceedings of IASS Conference, Boston, July, 2018

[3] Bravo, M., Chaltiel, S., Carazas, W., ’Matter – Robotic Calibration for Bioshotcrete’ *Temes de disseny*, **34**:80-91, 2018

[4] Kromoser B., Huber P., ‘Pneumatic Formwork Systems in Structural Engineering’, *Hindawi Publishing Corporation: Advances in Material Science and Engineering*, Volume 2016, Article ID 4724036

[5] Hawkins, W.J., Herrmann, H., Ibell, T.J., Kromoser, B., Michaelski, A., Orr, J.J., Pedreschi, R., Pronk, A., Schipper, R., Shepherd, P., Veenendaal, D., Wansdronk, R. and West, M. 'Flexible formwork technologies: A state of the art review', *Structural Concrete*, **17** (6), 2016

[6] Veenendaal, D., Bakker, J. and Block, P. 'Structural design of the flexibly formed, mesh-reinforced concrete sandwich shell roof of NEST Hilo', *Journal of the International Association of Shell and Spatial Structures*, **58** (1): 23-38, 2017 (March)

[7] Popescu, M., Rippmann, M., Van Mele, T., Block, P. ‘Automated generation of knit patterns for non-developable surfaces’ in Humanizing Digital Reality - Proceedings of the Design Modelling Symposium, Paris, September, 2017

[8] Doerstelmann, M., Knippers, J., Koslowski, V., ‘ICD/ITKE Research Pavilion 2014-2015 – fibre placement on a pneumatic body based on a water spider web’, *Architectural Design*, **85** (5):60-65,2015

[9] Chaltiel, S., Bravo, M., Abdullah, I. ‘Adaptive Strategies for Mud Shell Robotic Fabrication’, International Conference on Parallelism in Architecture, Engineering & Computing Techniques – 2nd Edition, presented and accepted for publication, London, October, 2018

[10] Kubitza, W.K., Oden, J.T., ‘Numerical analysis of nonlinear pneumatic structures’, Colloquium on pneumatic structures, Stuttgart, Germany, 1967

[11] Accuwether, accessed 29th September 2018 https://www.accuweather.com/en/fr/lessac/151219/month/151219?monyr=8/01/2018#

[12] Hubs, 2017, https://buildwithhubs.co.uk/, accessed 29th September 2018

[13] Mud-spraying drones build prototype for emergency home, accessed 15th October 2018 https://www.dezeen.com/2018/10/02/stephanie-chaltiel-mud-shell-southbank-spraying-drones-emergency-homes-architecture-ldf/amp/

International Conference on Sustainable Materials, Systems and Structures (SMSS 2019)
Challenges in Design and Management of Structures
20-22 March 2019 – Rovinj, Croatia

DESIGN METHOD FOR SHRINKAGE IN LARGE-SCALE COMPOSITE CONCRETE FLOOR STRUCTURES

Thomas Cornelius Buch-Hansen

Danish building research institute, Aalborg University Copenhagen, Denmark

Abstract

Large-scale composite concrete floor are sensitive to shrinkage and need to be designed to avoid failure. In these floors, different final layers are used e.g. wooden, epoxy or acryl based final floor layer. These layers have various stiffness and strength properties, further the geometric parameters have significantly influence on the shrinkage behaviour of the composite floor. A new simplified analytical design method is developed to determine the shrinkage behaviour between the different layers in the composite floor. The model will be compared with a finite element method analysis. A case story will be analysed using the new design method. Weakness and strength of the model will be analysed and evaluated. Finally a parametric study of the model will be performed. The method reveals some interesting phenomena in large-scale composite concrete floors, built of layers with a significantly ratio of stiffness parameters, among this the influence of different geometric parameters, will be studied. It will be shown how the advantages of this new model in a simple way can predict different failure modes for concrete composite floors, to be used in design.

Keywords: Shrinkage, concrete & wood, floor structure, design method, Finite element.

1. INTRODUCTION

Connection between timber and concrete structures are usually achieved by mechanical fasteners, [1]. Nevertheless many challenges are given in using mechanical notch, screws and bolts, [2]-[4]. Mechanical connections provide sufficiently capacity in ultimate limit state, but in serviceability state adhesives have many benefits [5]. Nevertheless, some challenges still arises. The normal transformation design tools used in praxis in for instance timber concrete composite structures cannot be used due to lack of rigidity in the interlayer shear connections and the time dependent properties of the component materials, see state of the art [6].

When designing large-scale floor components where the base is concrete with a wooden or acryl based floor cover, consideration must be given to the influence of temperature and humidity on to the varies materials acting together in the structure, see also [7].

A new analytical design method will be presented, using linear elastic stress-strain conditions, [8]. The model will be compared with a finite element method analysis, [9], to validate the analytical model.

A case study of a large-scale composite concrete floor with wood as final layer, with various failure scenarios, will be presented. The design method will be used to estimate the failure.

2. CASE STORY

In 2010, a three-story high office building inclusive basement for the medical company Novo Nordisk A/S was constructed. The building should house approx. 180 employees. A total of 2700 m2 of floor space was built. On each floor is built about 900 m2 large-scale concrete slabs, having variable geometry on the loadbearing floor components on each story. The floor over the basement is built by 320 mm thick hollow core concrete elements with 200 mm top concrete. The floor over the ground floor is built by TT concrete floor elements, with 180 mm top concrete. The floor over first floor is built by TT concrete floor element, with 270 mm hard insulation and a final 180 mm top concrete. All floor is then finalised with a 10 mm alignment concrete, self-levelling, upon which a 10 mm wooden final layer is glued with step soundproofing adhesive to the alignment concrete.

The wooden layer is built up by small wooden bricks. Each brick with the size 10x20x600 mm. Shortly after finalization in October 2010 different failure scenarios occur, some places each small wood brick slipped totally, in other cases the top layer is lifted several cm as a whole section, figure 1. The wooden layer has slipped in the glue between the alignment concrete layer and the wooden layer.

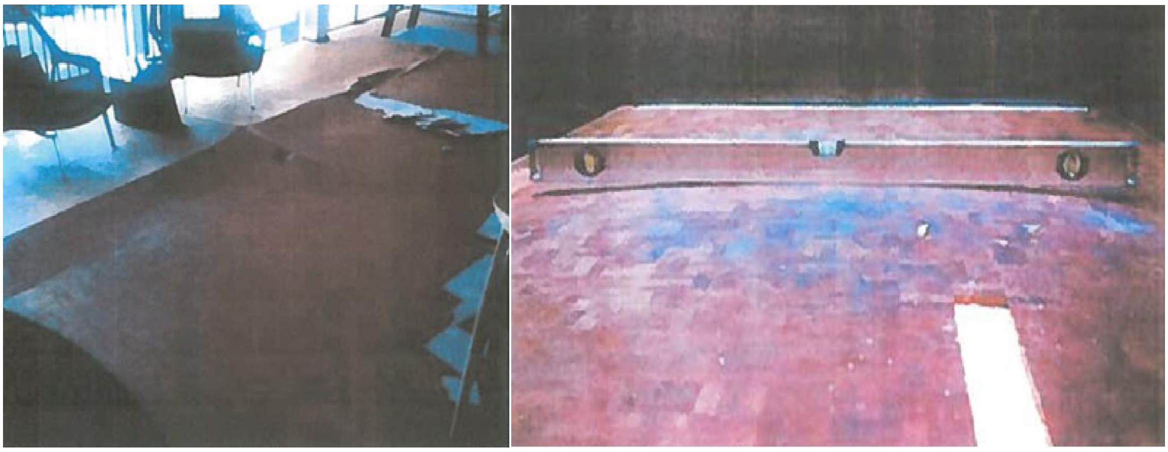

Figure 1: Different failure types in wooden floor

For comparison, some parametric studies of ceramic tile floors will also be carried out. The strength and stiffness parameters is given in the following. Modulus of Elasticity: (Oak) Wooden bricks - end-wood with E-module perpendicular to fiber direction: 600 MPa, Glue (Casco elastic) E <600 MPa, Concrete E = 30,000 - 40,000 MPa, Ceramic floor tiles E = 35 - 40,000 MPa. Poissons ratio: Wood and glue v = 0.3, Concrete v = 0.2. Strength parameters: Wood: Flexural strength $f_{k,m}$ = 30 MPa, Compression in fiber direction $f_{c,0,k}$ = 24 MPa, tensile strength in fiber direction $f_{c,0,k}$ = 19 MPa, Compression perpendicular to fiber direction $f_{c,90,k}$ = 2.7 MPa, Tensile strength perpendicular to fiber direction $f_{c,90,k}$ = 0.4 MPa, shear strength $f_{v,k}$ =

4.0 MPa. Alignment Concrete: Compression strength f_{ck} = 25 – 40 MPa, uniaxial tensile strength f_{ctk} = 1.8 – 2.5 MPa, flexural strength approx. 1.5*f_{ctk}. Glue: strength very dependent on execution condition, shear strength estimated to 0.5 MPa to 2.5 MPa.

All values are characteristic values. By estimation of actual failure strength, one may use a variation coefficient of 10% for compression and 20% for shear and tensile failure strength, and the principles in Eurocode 0 annex D, [10].

Because of the above, the actual adhesion strength in the failure interface between glue and the alignment concrete and bristle in the float concrete itself is estimated to be in the range of 1.5 to 3.0 MPa.

Swelling of concrete is disregarded, as concrete in the present case is under initial shrinkage. Wood has reversible moisture movements (swelling), which is significantly dependent on ambient moisture conditions. Initial shrinkage in concrete ε_{shrin} = 0.2 – 0.8 o/oo (mm/m)
Swelling in wood in the order of ε_{swel} = 10 o/oo (mm/m).

3. DESIGN METHOD

The following is a static model for a wooden brick loaded by side-pressure and a wooden brick without side-pressure. By 'side-pressure' is meant that the wooden bricks are located so close to each other, that a compressive stress will occur that retains the wooden bricks when swelled by the moisture effect. By 'without side pressure' is meant, that the wooden blocks are so spaced apart, that they can move freely, thus being held alone by the underlying glue/ concrete.

The glue is assumed to have roughly the same E module as or slightly less than the wood brick, which means that the glue will be deformed roughly like the wooden brick. It also means that, the biggest stresses will occur in the interface between glue and concrete. Similar is also observed in the case investigated, where failure has occurred between glue and concrete or in the concrete itself.

3.1 Design method without side-pressure

The design method "without side-pressure" is based on the assumption that, the intersection of wood, glue or concrete is fixed by a combined shear and tensile stress.

The method assumes the wooden brick is swelling and the concrete is shrinking, respectively, independently of each other, Figure 2a. Then a shear force, V, corresponding to the shear stress, τ, is applied in the cross section of both the wooden brick and the concrete part and assembles them at the intersection, Figure 2b. This will result in a bending deflection of both, which ultimately is assembled with an evenly distributed tensile stress, σ_N, between the two sub-elements, figure 2c.

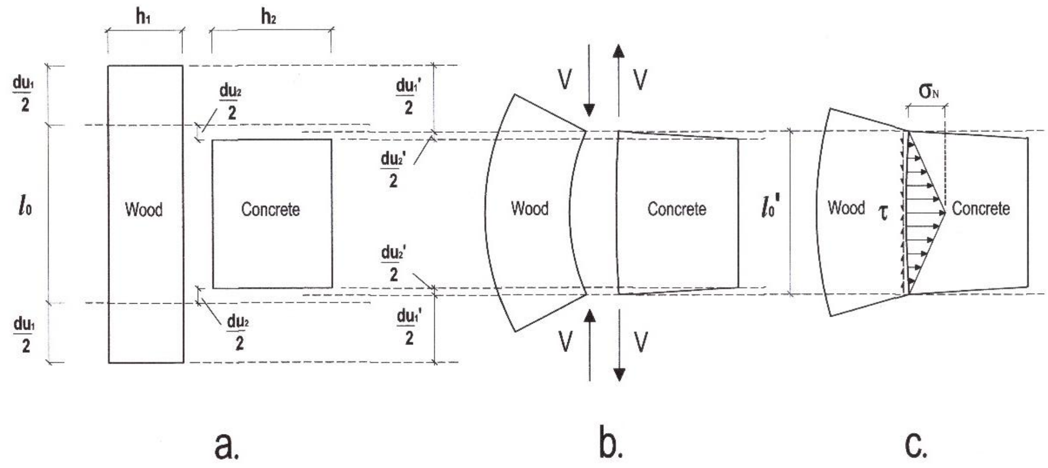

Figure 2: Principle outline of static model 'without side-pressure'.

Shear and tensile stresses will be in equilibrium. The deformation that determines the magnitude of the loads will be determined by the stiffness, S, of the two components. It will be a combination of the bending and shear stiffness that determines the deformations. For the present case, it would be sufficient to assume that the equilibrium can be determined by the bending stiffness:

$$S = Eh / L \tag{1}$$

where E is the Elasticity modulus, h the height of the components and L the length of the components.

The free deformation *du* is determined by:

$$du = \varepsilon l_0 \tag{2}$$

where ε is the differential strain and l_0 the length of the un-deformed specimen. The forced deformation du_1' of the wood (index 1) may be determined by:

$$du_1' = (du_1 + du_2) \cdot \frac{S_2}{S_1+S_2} \tag{3}$$

S being the stiffness for wood (index 1) and concrete (index 2), respectively. The forced deformation of the concrete du_2' may be determined by:

$$du_2' = (du_1 + du_2 - du_1') \tag{4}$$

The shear force *V* may then be determined by:

$$V = 1/4 \cdot hEdu'/l_0 \tag{5}$$

As it will be seen in figure 3, *V1 = V2*, expected equilibrium. The deformed length of the intersection in the final situation, see figure 2, will then be:

$$l_0' = l_0 + (du_1 - du_1') = l_0 + (du_2 - du_2') \tag{6}$$

and the stresses may be determined by:

$$\tau = 2V/l_0' \tag{7}$$

$$\sigma = Edu'/l_0' \tag{8}$$

3.2 Design method with side-pressure

When a side-pressure builds up due to swelling of the wooden brick, it will result in the build-up of a compression stress in the wooden brick. The side-pressure will maintain the brick and therefore there will be no stresses of importance in the intersection of wood brick, adhesive and concrete. The tension in the interface will in any case be significantly less than the stresses that will occur when the wooden brick can move freely, see parametric study in section 4 Evaluation of method.

The normal stress σ_N is calculated determining first the moment M_0 from bending:

$$M_0 = V \cdot h/2 \tag{9}$$

and having the Inertia I:

$$I = 1/12h^3 \tag{10}$$

and corresponding free flexural deformation in the middle u_{max}:

$$u_{max} = 1/10 M_0 l_0'^2/EI \tag{11}$$

assuming triangular stress distribution, we get:

$$\sigma_N = q = 12M_0/l_0'^2 \tag{12}$$

Thus obtaining the failure criterion using equation (7) and (12):

$$\tau_u = \sqrt{\tau^2 + \sigma_N^2} \tag{13}$$

4. EVALUATION OF METHOD

In this section parameter studies of the method 'without side-pressure' and 'with side-pressure' have been performed. The calculations are given in Table 1. Further, the method is evaluated and compared with a Finite element analysis.

4.1 Analytical design method

The Calculation in the first column 'Ref', in Table 1, is calculation with preset entry parameters.

Here it is seen, using equation (8), that the normal compression stresses in wood σ_1 are less than compression strength for wood and that normal tensile stresses in concrete σ_2 are less than tensile strength of concrete, see section 2 Case story.

Then two calculations have been made with considerably larger concrete shrinkage. It is seen that it does not have a significant influence on the failure stress τ_u, equation (12).

The next calculation shows that change in the swelling properties of the wood, on the other hand, has a significant influence on the failure stress, which almost doubles with a doubling of the swelling.

The following calculation shows the impact on the stiffness by changing the height. The same effect may be seen with a change of the modulus of Elasticity. It can again be observed that change in the stiffness of the concrete, 'Run 6' in Table 1, does not have significantly influence, opposite to the modification of the stiffness of the wooden brick, 'Run 7' in Table 1. It should be noted, that when their stiffness approaches each other, the effect would be equally great for both. This is, in principle, illustrated with the last calculation example for ceramic tiles, where a change in the stiffness has an equal influence to the two, except for the height of tile and concrete, respectively. It is also observed that there are significantly greater failure stresses.

Table 1: Parametric study of the analytical design method

MODEL 1 -without side-pressure											
		Ref	Concrete shrink		Wood swelling		Stifness (h)		Ceramic Tiles		
Term	Unit	Run 1	Run 2	Run 3	Run 4	Run 5	Run 6	Run 7	Run 8	Run 9	Run10
ε1	o/oo	10	10	10	20	5	10	10	0,2	0,2	0
ε2	o/oo	0,2	0,8	2	0,2	0,2	0,2	0,2	0,2	0	0,2
lo	mm	60	60	60	60	60	60	60	60	60	60
h1	mm	10	10	10	10	10	10	20	10	10	10
h2	mm	90	90	90	90	90	200	90	90	90	90
du1	mm	0,6	0,6	0,6	1,2	0,3	0,6	0,6	0,01	0,01	0
du2	mm	0,012	0,048	0,12	0,012	0,012	0,012	0,012	0,012	0	0,012
S1	N/mm^2	100	100	100	100	100	100	200	5500	5500	5500
S2	N/mm^2	49500	49500	49500	49500	49500	110000	49500	49500	49500	49500
du1'	mm	0,6108	0,6467	0,7185	1,2096	0,3114	0,6114	0,6095	0,0216	0,0108	0,0108
du2'	mm	0,00123	0,00131	0,00145	0,00244	0,00063	0,00056	0,00246	0,0024	0,0012	0,0012
V1	N/mm	15,3	16,2	18	30,2	7,8	15,3	30,5	29,7	14,9	14,9
V2	N/mm	15,3	16,2	18	30,2	7,8	15,3	30,5	29,7	14,9	14,9
lo'	mm	60,6	60,6	60,6	61,2	60,3	60,6	60,6	60,01	60,01	60
τ1	MPa	0,5	0,53	0,6	1	0,3	0,5	1	1	0,5	0,5
τ2	MPa	0,5	0,53	0,6	1	0,3	0,5	1	1	0,5	0,5
σ1	MPa	6,05	6,4	7,11	11,86	3,1	6,05	6,04	11,88	5,94	5,94
σ2	MPa	0,67	0,71	0,79	1,32	0,34	0,3	1,34	1,32	0,66	0,66
MODEL 2 - with side-pressure											
V	kN/m	15,3	16	18	30	8	15	30	30	15	15
Mo	kNm/m	0,0763	0,08	0,09	0,15	0,04	0,08	0,3	0,15	0,07	0,07
I	mm3	83	83	83	83	83	83	667	83	83	83
u_{max}	mm	0,56	0,59	0,66	1,13	0,28	0,56	0,28	0,02	0,01	0,01
q	MPa	0,25	0,26	0,29	0,48	0,13	0,25	1	0,49	0,25	0,25
σ_N = q	MPa	0,25	0,26	0,29	0,48	0,13	0,25	1	0,49	0,25	0,25
τ	MPa	0,5	0,5	0,6	1	0,3	0,5	1	1	0,5	0,5
τ_u	MPa	0,6	0,6	0,7	1,1	0,3	0,6	1,4	1,1	0,6	0,6

Note : index 1 corresponds to Wood brick, index 2 to Concrete.

4.2 Finite element analysis

The FEM model is constructed, with a wooden brick that is longer than the concrete element, corresponding to a swelling strain in the wood of 10 ‰. Then shear loads are applied to the nodes representing the interface between concrete and wood.

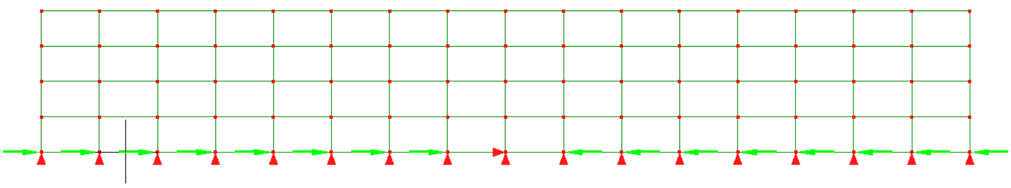

Figure 3: FEM-model wooden brick.

The shear forces are increased, until shear loads in the wood brick and the concrete element are equal. In both FEM-models, the nodes are restrained for vertical displacement.

The calculation shows that there is a triangular distribution of tensile stresses in the section, and that the equilibrium shear load, V, see equation (5), is approximately the same order of magnitude as for the analytical design method. Compared with the reference calculation, see Table 1, the FEM-analysis gives a little smaller value of the shear load of approx. 12 kN. The FEM-models show, like the analytical model, significant deformations in the wooden bricks relative to the concrete element, with a total deformation of approx. 0,6 mm in the wooden brick, see figure 4, noting that units in figure 4 are in meters.

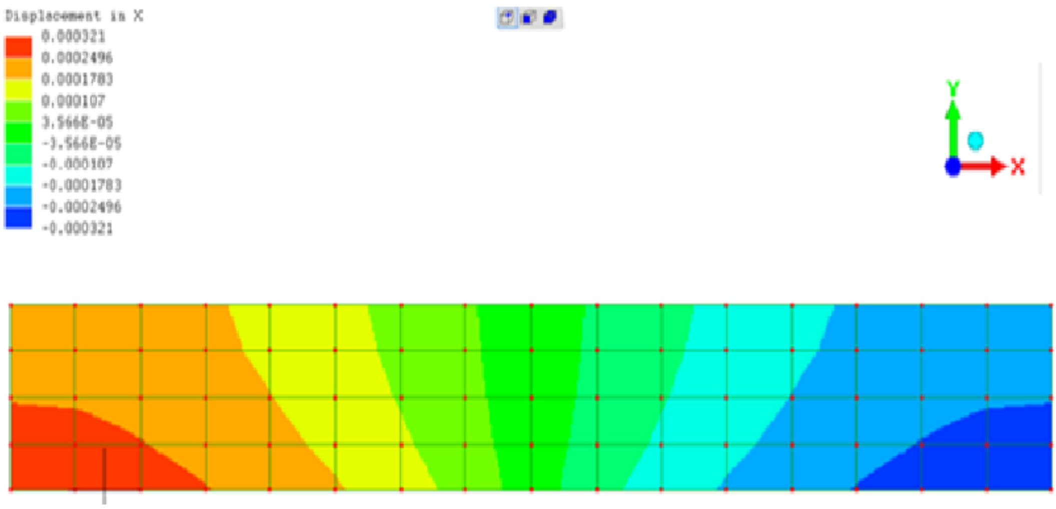

Figure 4: Horizontal displacements (X-direction) in FEM-model wooden brick.

5. DISCUSSION

One of the questions arising is, whether the deformation in the concrete would have some influence to the observed failure. The analysis shows that even if any side pressure could build up as a result of an accumulated deformation from shrinkage cracks in the concrete, the stresses in the wooden block due to the low stiffness of the wooden block would not lead to failure. The actual fracture is therefore due to the stresses that is built up because of the deformations of the wooden brick, see figure 2. After failure between the wooden bricks without side pressure and the concrete surface, moisture accumulation may continue. This will result in the lifting of the wooden blocks, as observed, see figure 1.

The composite solution: 'wood glued to concrete surface' are very dependent on the execution especially the condition of the surface before the adhesive is applied. Many methods are available to improve the adhesion effect, see e.g. [1] and [11].

In addition, consideration must be made of the shape of the stress distribution. The shear stress and tensile stresses will be somewhere between a pure plastic and an elastic triangular distribution. It is apparent that the distribution of shear stress will have the greatest impact on the failure criterion, i.e. an assumption of a parabolic distribution for the present will be reasonable. The distribution of the tensile stress does not significantly affect the result, but the FEM calculation shows that tensile stresses have the shape of a triangle distribution, which is therefore assumed in the model.

6. CONCLUSION

The adhesion strength resulting in fracture in he examined case story will be in the range of 0.5 MPa to 1.0 MPa according to the static calculations. A characteristic declared adhesion strength greater than 1.0 MPa would have been sufficient to avoid failure in the floor structure under the given material properties. The analytical design method has shown to be able to predict the stresses sufficiently accurately and thus determine the failure criterion.

The model 'with side-pressure' shows that there will be no failure, if the wood bricks are retained with side-pressure. Hence, it must be a prerequisite in the case story, that there has been sufficient distance between the wooden bricks, to achieve a displacement that results in tension in the intersection between wood/glue and concrete, leading to fracture.

The calculations 'without side-pressure' show that the stress resulting from the displacement of the concrete will not influence the failures observed. This is, because the stiffness of the wood is considerably smaller than that of the concrete.

REFERENCES

[1] Kostic, S., Merk, V., Berg, J.K., Hass, P. Burgert, I. and Cabane, E. 'Timber-mortar composites: The effect of sol-gel surface modification on the wood-adhesive interface', Composite structures, Vol 201, pp 828-833, (*Elsevier*, 2018).
[2] Fragiacomo, M. and E. Lukaszewska, 'Time-dependent behaviour of timber–concrete composite floors with prefabricated concrete slabs', Engineering Structures Vol 52, pp 687-696, (Elsevier, 2013).
[3] Taazount, M., Amziane S. and Molard, D., 'Tangential behavior of nailed composite timber–concrete floor structures', Construction and Building Materials, Vol 40, pp 506-513, (Elsevier, 2013).
[4] Lukaszeska, E., Johnsson H. and Fragiacomo M., 'Performance of connections for prefabricated timber–concrete composite floors', Materials and Structures Vol 41 pp 1533-1550. (*Rilem*, 2008).
[5] Eisenhut, L., Seim, W. and Kühlborn, S., 'Adhesive-bonded timber-concrete composites – Experimental and numerical investigation of hygrothermal effects', Engineering Structures Vol 125, pp 167-178, (Elsevier, 2018).
[6] Yeoh, D., Fragiacomo, M., De Franceschi M. and Boon K.H., 'State of the Art on Timber-Concrete Composite Structures: Literature Review', Journal of Structural engineering, Vol 137 no. 10, pp 1085-1095, (ASCE 2011).
[7] Ellis, J.L. and Ball, A., Comparison of two wood filler types with respect to relative shrinkage across variations in temperature, in humidity and within wood species', International Wood Products Journal, Vol 2:2, pp. 115-119, *Taylor&Francis*, (2011).
[8] Mase, G.T. and Mase G.E.,'Continuum Mechanics for Engineers', 2nd Edn, *Taylor&Francis, Boca Raton* (CRC Press LLC, New York 2002).
[9] LISA, 'LISA Finite element Analysis', Manual – Software Version 8.0.0, (Free Software Foundation Inc., Boston, USA, 2013).
[10] EC0. Eurocode 0 part 1, 'EN 1990 Basis of structural design', (*CEN*, Bruxelles. 2017).
[11] Lee, T., Ma, C. M., Hsu, C., Wu, H., 'Syntheses of Epoxy-Bridged Polyorganosiloxanes and the Effects of Terminated Alkoxysilanes on Cured Thermal Properties, Vol.99(6), pp.3491-3499. Journal of Applied Polymer Science, (*Ametek*, 2006).

International Conference on Sustainable Materials, Systems and Structures (SMSS 2019)
Challenges in Design and Management of Structures
20-22 March 2019 – Rovinj, Croatia

REINFORCEMENT DESIGN FOR THE COMBINED EFFECT OF RESTRAINED SHRINKAGE AND APPLIED LOADS IN SLABS: A DESIGN CHALLENGE

M. Azenha (1), C. Sousa (2), J. Granja (1), R. Faria (2) and B. Zahabizadeh (1)

(1) ISISE, Dep. Civil Engineering, University of Minho, Guimarães, Portugal

(2) CONSTRUCT, Dep. Civil Engineering, University of Porto, Porto, Portugal

Abstract

The quantification of the necessary reinforcement for crack width control in highly restrained RC slabs still remains a subject of discussion in both scientific and practitioner communities, particularly when the simultaneous effects of applied loads and restrained shrinkage deformations are considered. Indeed, different authors/designers follow distinct approaches to deal with the problem. This is however a very important matter, because in slabs, the quantity of reinforcement is frequently determined by Service Limit States (SLS) of cracking. Therefore, the use of different design criteria for SLS can bring different performance levels, and also different global costs (e.g. reinforcement can be overdesigned, or under designed and then repairs may be in order).

In such context, this paper presents and analyses the results of a design challenge launched by the research teams at UMinho and UPorto to a set of design offices. The design challenge consists in the sizing of the necessary reinforcement to satisfy adequate cracking performance in a highly restrained slab. All information about geometry, materials, loads and boundary conditions are provided in the design challenge sheet provided to participants.

A total of 7 teams have provided answers to this design challenge. Results are treated anonymously in regard to participating teams. A discussion is held with basis on common and differentiating points, and finally an analysis of the authors using non-linear finite element analysis is made, targeting to better assist interpretation of the expectable behaviour of reinforcement solutions.

Keywords: concrete cracking; imposed deformations; applied loads; design challenge

1. INTRODUCTION

In view of the open discussion, in the scientific and practitioner communities, about design procedures for quantification of the required reinforcement for crack control in restrained structures subjected to imposed deformations and external loading, a research project was recently initiated. The project is entitled "*IntegraCrete* - A comprehensive multiphysics and multiscale approach to the combined effects of applied loads and thermal/shrinkage deformations in reinforced concrete structures". One of its first tasks consists in a design challenge, launched to design offices, to access the different practices used to design such reinforcement.

This paper describes the design challenge, summarizes the responses provided by the participants, and discusses the responses through the comparison with the results of nonlinear finite element analyses (NLFEA).

2. THE DESIGN CHALLENGE

2.1 General aspects about invitation and participation

The design challenge was sent by e-mail to a number of national (Portugal) and international design offices, with a formal letter of invitation, explaining about the nature of the research project. This type of challenge is not usual in engineering practice, and for such reason, a significant part of the invitation letter is reproduced below (introduction of IntegraCrete omitted, as well as contact information for submission of responses), providing self-explanatory grounds for the relationship established with the potential participants:

> *"…We are therefore inviting some known researchers and practitioners to participate in a design challenge for a highly restrained slab, as shown in the attached file "Design challenge V1.pdf". We invite you to participate in this design challenge by responding to it and provide your best estimate of reinforcement with some background reasoning. You may just make some hand calculations and scan them, if that is the most convenient form for you. The result should be sent within 3 weeks to miguel.azenha@civil.uminho.pt, please.*
> *We want to assess the dispersion of estimates on behalf of different designers/researchers due to the absence of established standards/guidelines for this purpose. Anyway, we will not disclose the identity of any of the participants.*
> *We will prepare a report of the project that we will share with all participants and even add you as a co-author in case you wish to do so and participate actively in the discussions. Please let us know about your interest in this specific concern."*

It is noted that the design challenge did not involve any kind of funding for the participants, and hence, all work would indeed be fully voluntary. For that reason, engaging a very wide number of responses was difficult by default. Anyhow, a total of 7 participants from industry could be mobilized up to completion of the challenge. It is however noted, that deadlines needed to be extended up to more than 3 months, to make sure that all voluntary participants could afford the necessary time for this matter.

The participants were A400 (http://www.a400.pt/), AdF (http://www.adfconsultores.com/), CENOR TPF (www.tpf.pt), KPH Leipzig (http://www.khp-leipzig.de/), Mott McDonald (https://www.mottmac.com/), Newton (www.newton.pt) and Streng (www.streng.pt). A note is given to the anonymous character or responses to this challenge: responses are labelled as #1 to #7, not corresponding to the order shown above: this was not about comparing performance and finding the best answer; it was rather targeted to evaluate potential differences and common points in the adopted approaches.

2.2 The design challenge posed to participants

As mentioned above, the design challenge was proposed to participants in an attached file named "*Design challenge V1.pdf*". It was devised as to be simple from the structural layout/supports point of view, with clear hierarchy of supports, having solid slabs and supporting beams and columns. So, the challenge included a one-directional solid slab of 15cm thickness (see Fig. 1), with 5m span, supported by transverse beams (0.3m x 0.5m), which in turn also have 5m span and are supported by columns (0.3m x 0.3m). The structure is composed of 10 spans of the slab, in a total of 50m and it is longitudinally restrained by two massive extremity blocks of concrete with 5m x 5m x 3m.

The exact information provided to the participants in the design challenge is reproduced below, with particular emphasis for the existence of two levels in the design challenge is shown in the text quoted below.

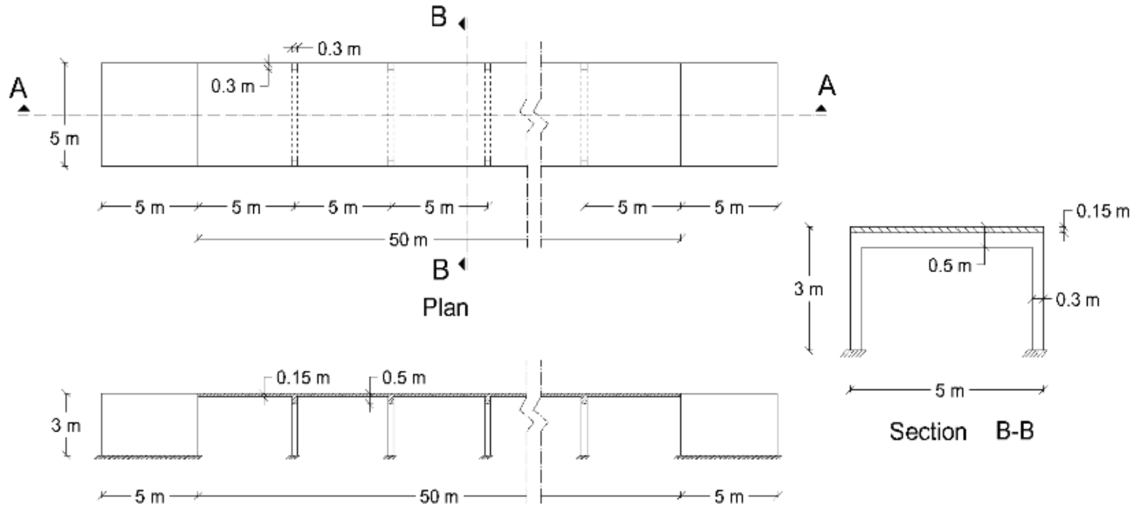

Figure 1: Relevant geometrical information for the design challenge

"Consider a restrained reinforced concrete slab, represented schematically in the figure, under the following conditions:
• Concrete class C20/25; Steel class S400C; Concrete cover 30mm
• Environment: constant temperature T=20ºC and constant humidity RH=50%
• Slab is 15cm deep, with plan dimensions of 5m × 50m
• Slab is supported in 30 × 50cm beams of the same type of concrete/steel
• The beams are supported at their extremities by 30 × 30cm columns (3m tall), which are in turn rigidly fixed at their base.
• Disregard autogenous shrinkage and consider that drying and loading both start at t=28 days.
• At the extremities, the slab is rigidly connected to two massive concrete elements of 5×5×3m. Assume that the massive elements are hardened concrete with more than 1 year old, in thermal equilibrium with the surrounding environment. The massive elements are rigidly connected to an infinitely stiff foundation.

• *Apart from self-weight, the slab has additional permanent loads g_k=2 kN/m^2 and a live load q_k=2kN/m^2 (ψ_2=0.3) - Residential building - Category A according to EC1.*

Design challenges:
1) Quantify the reinforcement necessary for an adequate control of crack widths (w_k<0.3mm) due to restrained shrinkage/temperature. In this part of the challenge, ignore the existence of applied loads and therefore disregard any bending reinforcement in the slab.
2) Considering the combined effect of applied loads and restrained shrinkage/temperature, quantify the necessary reinforcement and present the corresponding construction drawings for the slab."

3. RESPONSES TO THE DESIGN CHALLENGE

The responses are summarized by showing the reinforcement areas provided by each participant, for the two critical positions: the top surface, at the cross section over the support beam; the bottom surface, at the cross section through the mid-span, as shown in Figure 2. The structure under analysis exhibits, essentially, a unidirectional behaviour. Therefore, the discussion focuses on the longitudinal reinforcement only.

3.1 Challenge 1

All the participants adopted equal reinforcement areas at the top and bottom surfaces. This was expected in advance, because of the absence of bending moments. The results of each participant are shown in Fig. 3a. Group #5 did not provide an answer to Challenge 1. To a great extent, the responses to this first design challenge were mostly based on the equilibrium of forces at pre and post-cracking stages, as reported in equation 7.1 of EN1992-1-1:2004 [1], but with different strategies for assessment of the reduction factor associated to restraint loss due to cracking and other phenomena such as self-balanced stresses and viscoelastic effects. A significant number of participants have used the reduction factor approach devised by Luis [2]. Crack width calculations were vastly made with basis on expression 7.9 of EN1992-1-1:2004. In spite of the differences in approach, most participants reached a similar result, with an average of 5.2 cm2/m. For more details on design assumptions and results, see [3].

3.2 Challenge 2

The reinforcement calculated by each participant is shown in Fig. 2b. The methodologies applied by participants were once mostly focused on the combination of bending behaviour with the tensile force installed in the slab due to restrained shrinkage (composite bending), with the tension force being quantified with similar approaches to those exhibited in challenge 1. Then the stresses in rebars were calculated for cracked cross-sections with direct consideration of the composite bending, and then equation 7.9 of EN1992-1-1:2004 [1]. Differences arose mostly on the method to compute the reduction factor mentioned for challenge 1, and for the consideration of shrinkage in the crack width calculation expression.

It is noteworthy to mention the particular cases of Group 4, which consistently used a deformation compatibility approach devised by Dirk *et al* [4], and Group 5, which focused on the application of the recommendations of CIRIA C660 [5].

Group #1 adopted non-uniform reinforcement for the top surface at the cross section over the support beam: ϕ12//10 cm in a 1 m wide lateral band; and ϕ12//10 cm in the remaining central band. This option is motivated by the concentration of higher bending moments close to the lateral columns visible in Fig. 1. The value shown in Fig. 3 for this Group #1 is the area of reinforcement in the lateral band. All of the remaining participants assumed uniform reinforcement throughout the slab width. For the cross section through the mid-span, all the participants presented uniform constant bottom reinforcement over the slab width. Fig. 2b shows large differences in the area of reinforcement provided by the various participants, specially for the top surface.

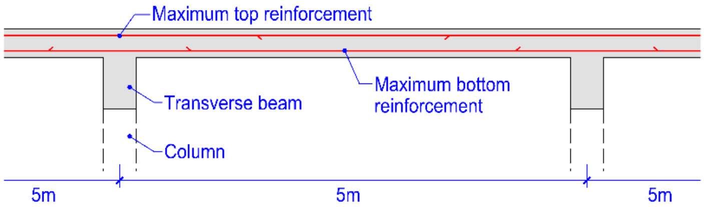

Figure 2: Critical positions for comparison of reinforcement areas provided by different teams

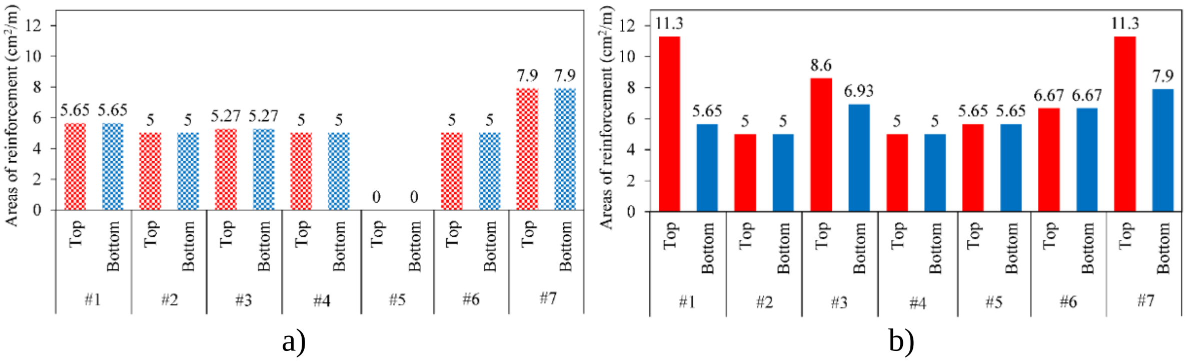

Figure 3: a) Top and bottom reinforcement areas for Challenge 1 b) Top and bottom reinforcement areas for Challenge 2

4. EVALUATING THE DESING CHALLENGE WITH NLFEA

The use of nonlinear finite element analyses (NLFEA) at the design stage is not a feasible alternative, at least for current structures. NLFEA are time consuming and require advanced software and knowledge. However, this type of analysis is a useful auxiliary to understand the behaviour of the structure of this design challenge. The internal efforts in a restrained structure subjected to imposed deformations are strongly dependent on the stiffness reduction caused by cracking. These effects can be taken into account by using constitutive models for concrete including the effects of maturity, creep, shrinkage and cracking.

4.1 FE modelling approach

The reference method for assessing the nonlinear, time-dependent, behaviour of the structure is the one shown in reference [6]. The slab is discretized by using 8-node shell finite elements, numerically integrated along the thickness, with resource to the software DIANA [7]. The concrete behaviour is simulated through a smeared cracking approach. A multiple-fixed-cracks model, with strain decomposition, is used. In this type of model, the total concrete strain is equal to the sum of: elastic instantaneous strain; creep strain; shrinkage strain; temperature induced strain; crack strain. The constitutive models to simulate the concrete behaviour are explained in reference [8].

A tension stiffening diagram is used to model the average stress in concrete, in cracked regions. Tension stiffening diagrams are suitable to simulate the concrete behaviour using coarse FE meshes, this being the approach followed in this work (see the mesh in Figure 6). One of the advantages of this modelling approach, with coarse meshes, lies on its robustness: converged results are easily reached. Another advantage is the fact that the stiffness of cracked concrete is defined in a consistent way with respect to the models proposed by design codes such as the fib Model Code [9]. The average stress in cracked concrete, owing to tension stiffening effects is, in these NLFEAs, simply taken as $k_t\ f_{ctm}$, where f_{ctm} is the average tensile strength of concrete and k_t is a tension stiffening coefficient, equal to 0.4.

It is important to understand that the crack opening is not a direct output of the NLFEA, given that a tension stiffening approach is being followed. In order to get the crack opening value, the crack strain, ε_{cr} (which is a direct output of the NLFEA) has to be integrated over a length equal to the crack spacing, $2\ l_{s,max}$. In this work, the crack spacing $2\ l_{s,max}$ is quantified based on the equation proposed by the fib Model Code [9]. A simple way to get the crack opening, w_d, consists, therefore, in averaging the ε_{cr} output values over the crack spacing length. Once the average crack strain, $\varepsilon_{cr,mean}$ is computed, the crack opening w_d is simply calculated as:

$$w_d = 2\ l_{s,max}\ \varepsilon_{cr,mean} \tag{1}$$

where $\varepsilon_{cr,mean}$ is the aforementioned average crack strain value.

The ultimate purpose of the NLFEAs is the determination of the reinforcement required to get a maximum crack width of 0.30 mm. This reinforcement has to be determined iteratively. That is, the NLFEA has to be repeated using, in each analysis, a different amount of reinforcement. An iteration is, in this context, a NLFEA using a certain amount of reinforcement. The iterations have to be continued until the specified crack opening value (0.30 mm in this case) is reached. A very small number of iterations (~4) is needed if the reinforcement adopted in iteration i+1 is quantified based on engineering calculations using the internal efforts (axial force and bending moment) obtained in iteration i. The explanation of such engineering calculations is out of the scope of this presentation.

4.2 Challenge 1

The FE model to analyse Challenge 1 consists on a single longitudinal strip of FEs, i.e., one strip taken from the model shown in Figure 5. Owing to the absence of any bending effect, the axial force in such strip is constant throughout the entire model. Therefore, the different tensile strength values have to be assigned to the various FEs. Otherwise, the entire structure would crack simultaneously, and the actual crack formation sequence would not be simulated. The adopted tensile strength values are as follows: 2.10 MPa for the FE with lowest strength; increments of 0.02 MPa for the remaining FEs. At the end of the analysis, the total number of cracked FEs was 8, i.e., the cracked region is ~ 1/3 of the total model.

After iterating to reach a maximum crack opening of 0.30 mm, the required area of reinforcement was obtained: top and bottom reinforcements equal to 7,2 cm^2/m. Figure 4 shows relevant results of the NLFEA: the restraint force (axial for in the slab due to the total end restraint) and the crack opening in the first formed crack. It interesting to note that, even though the maximum force occurs in the first ages (upon the formation of the first crack), the maximum crack opening is obtained at long term. This is due to the evolution of concrete shrinkage and its effects on the slip between concrete and steel. As mentioned in §4.1, the presented crack opening is the product of the crack strain (output of the NLFEA) and the crack spacing (equal to 349 mm, according to the fib Model Code [9], for 10 mm reinforcement bars).

As shown in Figure 4a, the axial force in the slab, at long term, is 272 kN, which is 82% of the bare concrete cracking force ($A_c\ f_{ctm}$ = 330 kN).

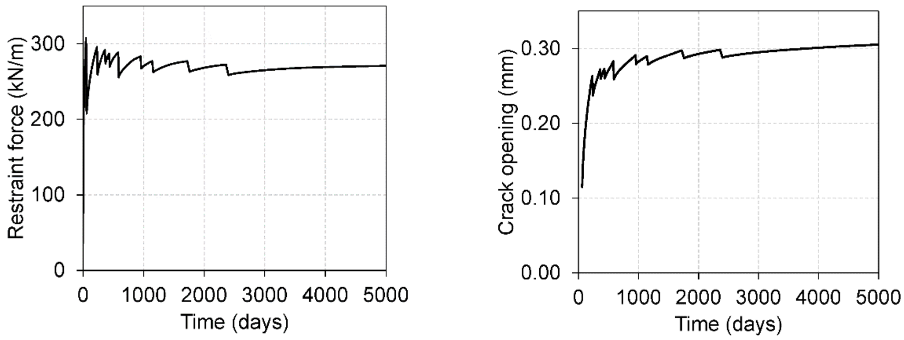

a) b)

Figure 4: Results of the NLFEA for Challenge 1: a) time variation of the restraint force (axial force in the slab); b) time variation of the crack opening for the first formed crack.

4.2 Challenge 2

Figure 5 depicts the FE model for Challenge 2. The tensile strength is uniform throughout the entire model, equal to f_{ctm} = 2.2 MPa. Unlike Challenge 1, in this case the tensile stresses are not constant, owing to bending effects. By iterating in order to reach a maximum crack opening (at the concrete surface, the control position specified in the fib Model Code [9]) of 0.30 mm, the following reinforcement quantities are reached: 11,0 cm^2/m at the top and 8.9 cm^2/m at the bottom surface. Figure 6 shows the crack patterns at long term (5000 days after casting), at the top and bottom slab surfaces. In the image, the crack strains are represented by vectors perpendicular to the crack.

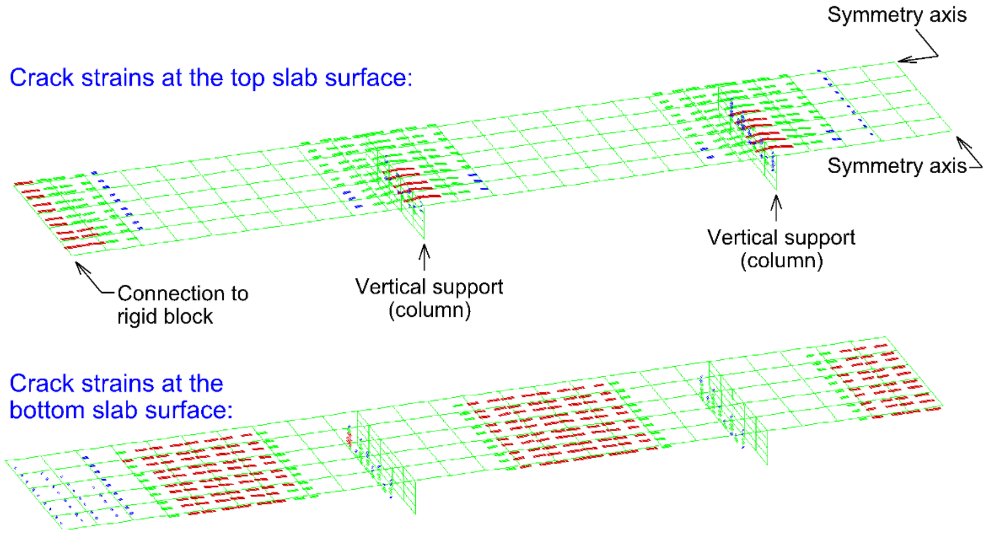

Figure 5: Crack strains, represented by a vector normal to the crack, at the end of the analysis.

As regards the restraint force, it is important to note that there is a significant decrease (owing to bending effects) with respect to the results of Challenge 1. In Challenge 2, at long term, the axial force in the slab is $\sim$ 150 kN/m (45% of $A_c\ f_{ctm}$). This value corresponds to the average over the slab width.

5. CONCLUSIONS

The design challenge, proposed to various design offices and teams, was briefly presented. It focuses on the cracking control and structural behaviour of structures submitted to restrained deformations and imposed loading. Then, nonlinear finite element analyses were used to analyse the structures' behaviour. Very important differences, in the results reached by different design teams, were observed. These differences have very important economic implications in the design of large restrained structures. This issue deserves attention by the scientific and practitioner communities, in order to improve the experimental validation of design methods and also to produce clear and feasible design procedures for restrained structures.

ACKNOWLEDGEMENTS

Funding provided by the Portuguese Foundation for Science and Technology (FCT) to the Research Projects PTDC/ECM/099250/2008, EXPL/ECM-EST/1323/2013 and PTDC/ECM-EST/1056/2014 (POCI-01-0145-FEDER-016841), as well to the Research Units ISISE (POCI-01-0145-FEDER-007633) and CONSTRUCT (POCI-01-0145-FEDER-007457) is gratefully acknowledged. A word of acknowledgment is also given to the participants in the design challenge, with fundamental importance for the discussion held herein. The authors would also like to acknowledge the benefits of cross-linking research through the network of COST Action TU1404 "Towards the next generation of standards for service life of cement-based materials and structures" (www.tu1404.eu).

REFERENCES

[1] EN 1992-1-1, 'Eurocode 2 – Design of concrete structures, Part 1-1: General rules and rules for buildings', (CEN, Brussels, 2004).
[2] Câmara, J., Luís, R., 'Imposed Deformation Effects on Slabs and Walls to Control Cracking: Non Linear Analysis and Design Criteria', European Symposium on Service Life and Serviceability of Concrete Structures, ESCS-2006, (Helsinki, 2006).
[3] Azenha, M., Sousa, C., Zahabizadeh, B., Granja, J. and Faria, R., 'Design challenge for reinforcement in a highly restrained slab', Seminar 'Design of reinforcement for RC elements under the combined effect of applied loads and restrained shrinkage', (Porto, 2017).
[4] Schlicke, D., Vie Tue, N., 'Minimum reinforcement for crack width control in restrained concrete members considering the deformation compatibility', *Structural Concrete*, **16** (2015) 221-232.
[5] Bamforth, P., 'C660D - Early-age thermal crack control in concrete', (CIRIA, London, 2007).
[6] Sousa, C., Faria, R. and Felisberto, E., 'Numerical analyses of the combined effects of external actions and restrained shrinkage deformations in slabs'. Seminar 'Design of reinforcement for RC elements under the combined effect of applied loads and restrained shrinkage', (Porto, 2017).
[7] DIANA FEA BV, 'DIANA, Finite Element Analysis', release 10.2, (Delft, 2017).
[8] Sousa, C., Leitão, M., Faria, R. and Azenha, M., 'A formulation to reduce mesh dependency in FE analyses of RC structures under imposed deformations', *Eng Struct,* **132** (2017) 443-455.
[9] *fib*, 'Model Code for Concrete Structures 2010', (Ernst & Sohn, London, 2013).

FLEXURAL BEHAVIOUR OF HYBRID STEEL FIBRE REINFORCED CONCRETE (HSFRC)

Tomislav Kišiček, Martina Carić, Marina Frančić Smrkić, Tvrtko Renić and Domagoj Damjanović

Faculty of Civil Engineering, University of Zagreb, Croatia

Abstract

Addition of steel fibres to the concrete mixture can enhance the post-cracking flexural behaviour of concrete elements because of its tension softening behaviour. As an appropriate environmental solution, recycled steel fibres obtained from waste tyres combined with manufactured fibres led to a product called hybrid steel fibres reinforced concrete (HSFRC). An experimental programme was conducted to obtain the flexural behaviour of HSFRC beams. An analytical model according to RILEM 162-TDF design recommendations considering bi-linear stress-strain diagram for steel bars and tri-linear stress-strain diagram for standard SFRC in tension was used for calculation of cracking moment, ultimate resistance and related curvature. Deflection in the middle of the span was evaluated after curvature calculation with increasing of the load. The results from analytical and experimental data are presented and compared in this paper, confirming the benefits of using fibres in the tensile behaviour of concrete.

Keywords: Hybrid SFRC, deflection, experimental analysis, analytical analysis

1. INTRODUCTION

Fibre reinforced concrete (FRC), especially, steel fibre reinforced concrete (SFRC) has gained considerable attention over recent years. FRC is a composite material made of concrete and short fibres usually with uniform distribution and random orientation. Steel fibres are the most commonly used in FRC but their wider application is limited to a certain number of structures, mainly because of their high price. Accordingly, alternative types of fibres have been a subject of recent research.

In hybrid fibre reinforced concrete (HFRC) different types of fibres (two or more), with diverse material properties, are combined to comprise prosperity of each type and their composite action. Considering a suitable ecological solution of the waste tyres disposal problem and economical savings, a combination of recycled steel fibres together with manufactured steel fibres resulted in a development of hybrid recycled steel fibre concrete (HSFRC) that will be discussed in this research.

An enhancement in concrete behaviour by the addition of fibres is reflected in the following aspects: improved post-peak response in flexure – increased capacity, tensile ductility and energy absorption, reduced initial cracks during the curing period, increased strength and integrity of concrete after the cracking. These benefits depend on the fibre type, volume content, length and shape of the fibres and properties of the matrix, as well.

FRC has application in pavements, overlays, slabs, beams, marine structures, repairing and rehabilitation projects, but mostly in non-structural or semi-structural elements, due to lack of completely developed codes or recommendations. However, numerous researches led to the publication of several instructions about design and application of FRC for structural purposes, as RILEM [1], Italian code CNR-DT 204/2006 [2], and German regulation DBV/2001 [3].

2. EXPERIMENTAL INVESTIGATIONS

The composition of the concrete mixtures used in experimental program is presented in table 1. The mix of plain concrete is marked as PC, while HSFRC mix, marked as H, contains 20 kg of manufactured fibres and 20 kg of recycled fibres per cubic meter of concrete. Manufactured steel fibres are straight with hooked ends, 35 mm in length and 0,55 mm in diameter. Shape and size of recycled fibres are irregular due to mechanical recycling process. They measure on average 20 mm in length and 0,15 mm in diameter [4]. Hardened concrete properties were determined according to European standards (compressive strength – HRN EN 12390-3 [5], modulus of elasticity – HRN EN 12390-13 [6], flexural tensile strength – HRN EN 14651 [7]).

Table 1: Mixture composition

Components [kg/m^3]	Mixture	
	PC	H
Cement	370	
Water	170	
Superplasticiser	2,22	
Aggregate	1840	1825
Manufactured steel fibres	0	20
Recycled steel fibres	0	20

Four beam types measuring 50 cm × 18,5 cm × 240 cm with effective depth of 14,9 cm and different reinforcement ratio were tested (table 2). Specimens were reinforced in longitudinal direction with steel rebars B500B, 10 mm and 12 mm in diameter. Steel rebar properties were determined according to HRN EN ISO 15630-1:2010 [8] and HRN EN ISO 6892-1:2009 [9] on three specimens for each diameter type.

Table 2: Beam types

Beam type	Concrete mix	Reinforcement	Reinforcement ratio [%]
PC	PC	5 ϕ 12	0,76
H1	H	5 ϕ 12	0,76
H2		4 ϕ 12	0,61
H3		4 ϕ 10	0,42

Beams were subjected to a four-point bending test, with supports placed 220 cm apart and with a shear span of 75 cm (figure 1 and figure 4). They were continuously supported over their width with steel rollers 40 mm in diameter. Loading was applied using the 600 kN hydraulic actuator, with the displacement control rate of 3 mm/min [10]. Vertical displacements were measured with LVDT sensors placed in the middle of the span.

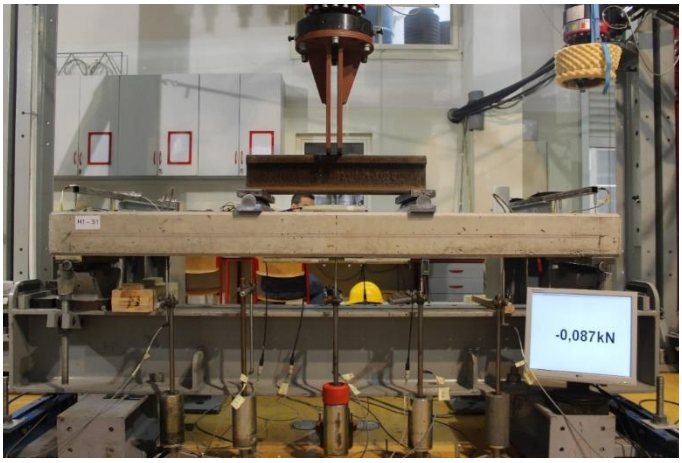

Figure 1: Test setup

3. ANALYTICAL MODEL

Within this research an analytical model of force/deflection behaviour of specimen beams was made. The idea was to calculate moment – curvature diagram of beam cross section and for numerous amounts of load to calculate mid-span deflection of specimen until failure.

3.1 Constitutive models for materials

For this analysis, following material models have been used: bi-linear behaviour of steel reinforcement as described in HRN EN 1992-1-1 [11], then parabola-rectangular behaviour of concrete in compression and finally RILEM model [1] for HSFRC in tension. The constitutive models are shown in figure 2.

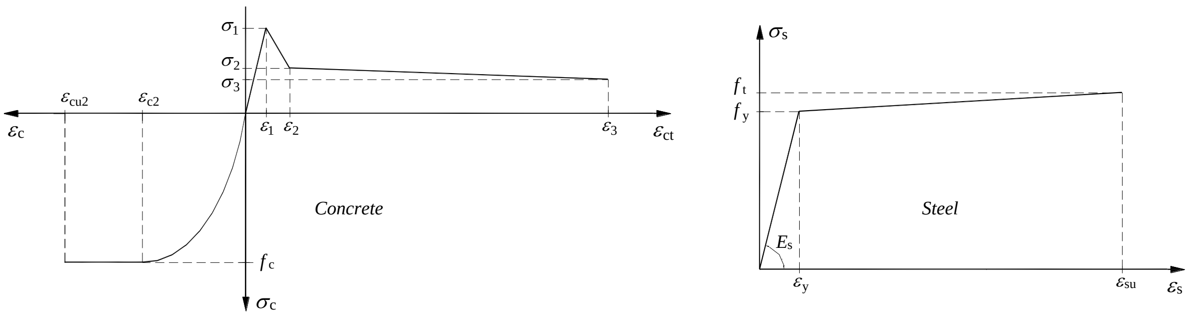

Figure 2: Constitutive models of materials

3.2 Moment – curvature diagram

The behaviour of every reinforced cross-section can be described by the moment – curvature diagram. Such diagram can be described by three characteristic points [12].

First point of the diagram determines the moment when concrete reaches its tensile strength and the first crack appears. After that point, the cross section is cracked, stiffness is smaller, tension force is carried out by tensile steel reinforcement in plain concrete, together with the additional carrying capacity of fibres in HSFRC, while compression force is carried out by concrete in compression.

The second point of the moment – curvature diagram is reached when steel reinforcement starts to yield. After the second point, stiffness decreases more, and it could happen that the diagram has a softening branch, as it can be seen in calculations. As a result of that, ultimate moment of cross-section can be smaller of yielding moment. The reason for that behaviour is the additional carrying capacity of HSFRC. The characteristic shape of the moment – curvature diagram is shown in figure 3 a).

3.3 Calculation of deflection

To carry out a deflection calculation, the model of the beam is divided into a certain number of intervals. For each amount of load, at the beginning, in the middle and at the end of each interval, bending moment distribution is calculated. For each amount of bending moment, from the moment – curvature diagram, which was calculated before, the curvature of cross section is determined. When the curvature distribution along the beam is known, the deflection line could be determined from the simple procedure [12] shown in figure 3 b), and according to equation (1):

$$v_j = \int_0^L R \cdot m \, dx = \sum_0^{\text{int}} R_i \cdot m_i \tag{1}$$

where v_j is the deflection of beam in point j, R_i is the area of curvature distribution diagram along the beam in interval i, and m_i is the value of bending moment from unit force in point j (figure 3 b)). Repeating that calculation for each position of unit force along the beam the deflection line of beam can be calculated. For each amount of load the force – mid-span deflection line is plotted.

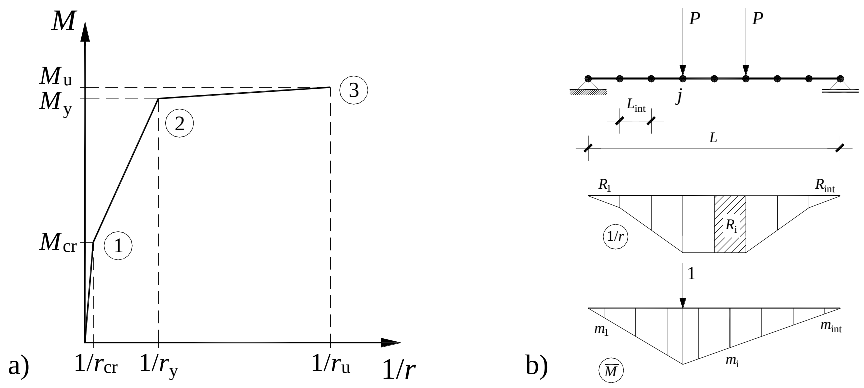

Figure 3: Calculation of deflection

The procedure can be carried out easily if there's no softening branch in the moment – curvature diagram. In the case of softening branch of the moment – curvature diagram the calculation of deflection is carried out in the manner of displacement-controlled experiment. After the second point of moment – curvature diagram, for each amount of mid-span curvature (in a softening branch of diagram) the bending moment and corresponding load are determined. In the area between the supports and forces the procedure of determination of curvatures is the same as before for that amount of load. As steel yields in the middle area (between forces) a jump discontinuity appears in curvature distribution along the beam (figure 4).

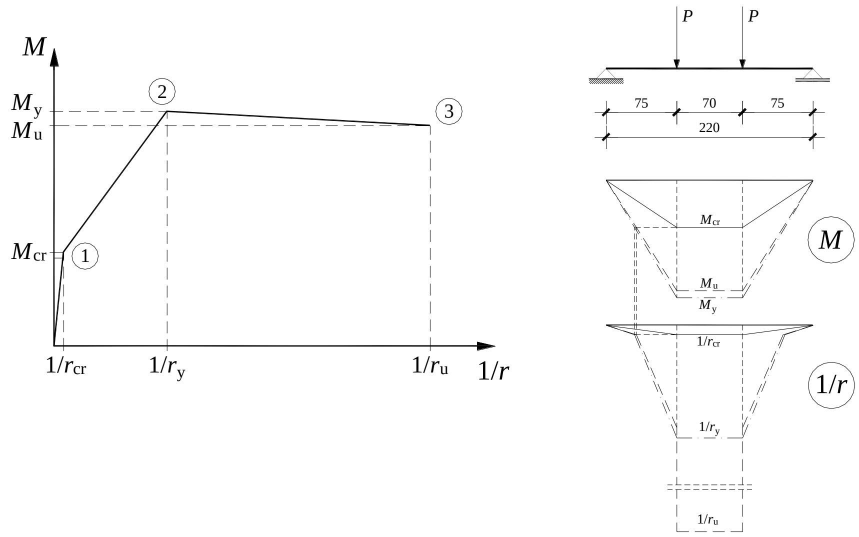

Figure 4: Moment – curvature diagram with a softening branch and corresponding curvature distribution along the beam

4. RESULTS OF ANALYTICAL CALCULATIONS AND COMPARISON WITH EXPERIMENTAL RESULTS

4.1 Moment – curvature diagrams

For each type of beam from table 2 the moment – curvature diagrams have been calculated according to described procedure. The characteristics of concrete used in calculations are given in table 3. Characteristics of steel were: $f_y = 505$ N/mm^2, $f_t = 621$ N/mm^2, $\varepsilon_{su} = 0{,}05$, $E_s = 200000$ N/mm^2. Values of characteristic points of moment – curvature diagrams are given in table 4.

The moment – curvature diagrams are shown in figure 4. From the values in table 4 and from figure 5 it can be seen that HSFRC beams have a higher value of cracking moment due to better behaviour of such concrete in tension. As the analytical model doesn't take into account a tensile reinforcement before first cracks appear, the cracking moment for all HSFRC beams is the same. Yielding moments of HSFRC beams have higher values comparing to one in PC beam. Comparing yielding moments in HSFRC beams, the higher value occurs in the beam with bigger amount of reinforcement. Ultimate moment is also higher comparing beam H1 and PC, but it decreases with decreasing amount of reinforcement (beams H2 and H3). Therefore, the beam H3 has even smaller ultimate moment than beam PC. From figure 3 the softening branch of diagrams for beams H1, H2 and H3 can be seen. This is more obvious with smaller amount of reinforcement in cross section of the beam (H1 vs. H3).

Table 3: Characteristics of concrete

	PC	H1	H2	H3
f_c (N/mm^2)	45,60	46,1	46,4	46,6
ε_{c2}	0,002	0,002	0,002	0,002
ε_{cu2}	0,0035	0,0035	0,0035	0,0035
σ_1 (N/mm^2)	4,71	6,44	6,44	6,44
ε_1	0,000139	0,00019	0,00019	0,00019
σ_2 (N/mm^2)	0,29	3,14	3,14	3,14
ε_2	0,000239	0,00029	0,00029	0,00029
σ_3 (N/mm^2)	0	1,06	1,06	1,06
ε_3	0	0,025	0,025	0,025

Table 4: Values of Moment – curvature diagrams

	PC		H1		H2		H3	
Point	1/r (1/cm)	M (kNm)	1/r (1/cm)	M (kNm)	1/r (1/cm)	M (kNm)	1/r (1/cm)	M (kNm)
1	$1{,}45\times10^{-5}$	13,43	$1{,}96\times10^{-5}$	18,37	$1{,}97\times10^{-5}$	18,37	$1{,}98\times10^{-5}$	18,37
2	$2{,}24\times10^{-4}$	39,12	$2{,}46\times10^{-4}$	58,52	$2{,}40\times10^{-4}$	51,50	$2{,}31\times10^{-4}$	42,93
3	$2{,}02\times10^{-3}$	45,19	$1{,}35\times10^{-3}$	57,26	$1{,}58\times10^{-3}$	47,75	$2{,}20\times10^{-3}$	32,59

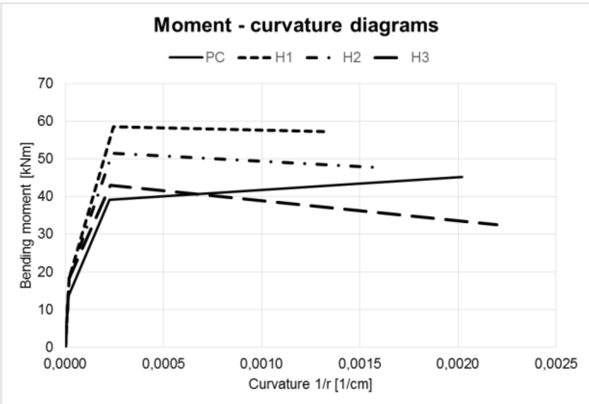

Figure 5: Moment – curvature diagrams

When the curvatures are compared, the beam PC has bigger ultimate curvature than the beam H1 (with the same reinforcement) and also bigger ductility. With decreasing amount of reinforcement, the ductility of HSFRC beams increases.

4.2 Load – deflection diagrams

Calculated moment – curvature diagrams for beams are used to calculate the load – deflection diagrams of each beam. Those diagrams are compared with experimental ones and they are shown in figures 6 and 7. It must be noted that experimental curves show smaller ultimate deflections of beams than calculated ones, for the reason that experiment had to be stopped around deflections of 4,5 cm due to danger of damaging LVDT sensors. Load – deflection diagram for beam PC shows almost the same results from calculations and experiment until the yielding of reinforcement started. After yielding of reinforcement, for the same force calculated deflections are bigger than experimental ones.

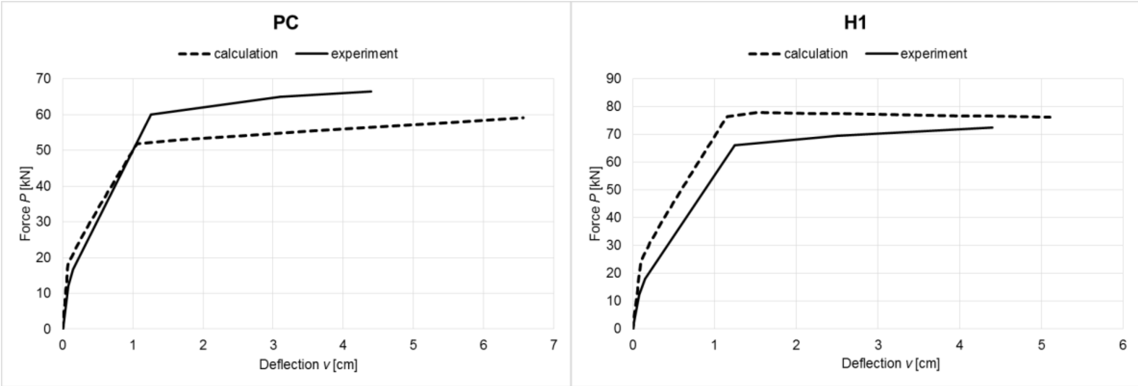

Figure 6: Load – deflection diagram of beams PC and H1

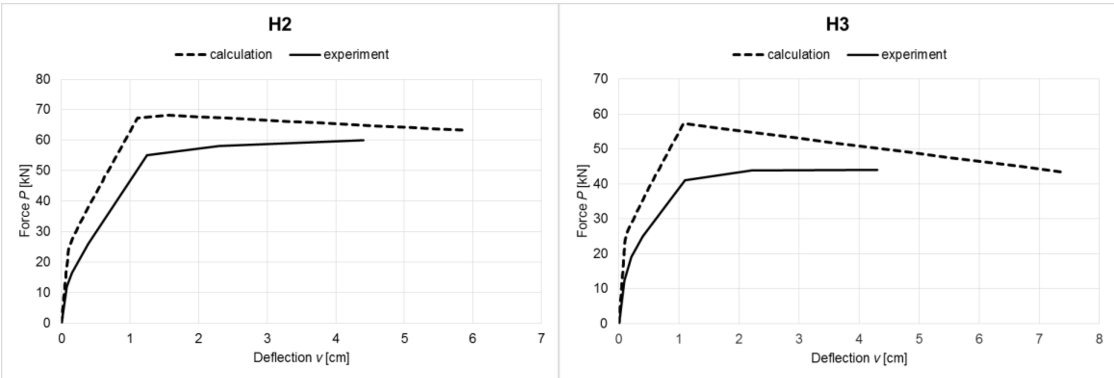

Figure 7: Load – deflection diagram of beams H2 and H3

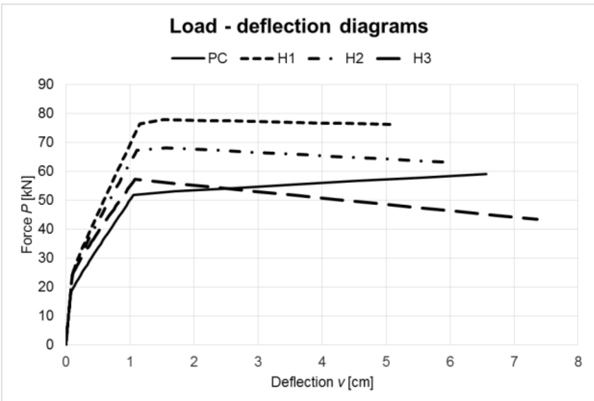

Figure 8: Calculated load – deflection diagram of all beams

That is not the case with beams H1, H2 and H2. They show smaller calculated deflections than experimental one from beginning to the end of the load – deflection curve. The experimental curves didn't show softening behaviour as the calculated curves.

Figure 8 shows a comparison of all calculated load deflection curves. The shapes of calculated load – deflection curves are expected if we compare them to the calculated moment – curvature diagrams for each beam type.

5. CONCLUSIONS

From the analysis described in this paper it can be concluded that usage of described moment – curvature diagrams in deflection estimation for HSFRC beam could lead to wrong conclusions because the calculated deflections are smaller than real ones. So, if the aim of calculation is to satisfy serviceability limit state, we should have that in mind. It can be concluded that RILEM recommendations for constitutive model of concrete in tension lead to overestimation of the performance of HSFRC elements in flexure, especially in case of elements with lower amount of conventional steel reinforcement. The described procedure can be improved with refined constitutive model of concrete in tension.

ACKNOWLEDGEMENTS

The authors wish to acknowledge financial support granted in the scope of the 7th Framework Programme of the European Community „Innovative Use of All Tyre Components in Concrete", under contract number 603722 and short-term scientific support from University of Zagreb.

REFERENCES

[1] RIILEM 162-TDF.: Test and design method for SFRC- Final Recommendation, Vol. 36. 2003
[2] CNR-DT 204/2006, Guide for the Design and Construction of Fiber-Reinforced Concrete structures, National research council advisory committee on technical recommendations for construction, Rome, 2007.
[3] DBV. 2001. DBV - Merkblatt Stahlfasserbeton. Deutscher Beton - und Bautechnik -Verein E.V. – DBV.
[4] Frančić Smrkić M.; Damjanović D.; Baričević A.: Primjena recikliranih čeličnih vlakana u betonskim elementima izloženima zamoru. Građevinar. 69. (2017), 10; 893–905.
[5] HRN EN 12390-3:2012. Ispitivanje očvrsloga betona- 3. dio: Tlačna čvrstoća ispitnih uzoraka, Hrvatski zavod za norme, 2012.
[6] HRN EN 12390-13:2013. Ispitivanje očvrsloga betona-13. dio: Određivanje sekantnog modula elastičnosti pri tlaku, Hrvatski zavod za norme, 2013.
[7] HRN EN 14651:2008 - Ispitna metoda za beton ojačan metalnim vlaknima – Mjerenje savojne čvrstoće, Hrvatski zavod za norme, 2008.
[8] HRN EN ISO 15630-1:2010 Čelik za armiranje i prednapinjanje betona - Metode ispitivanja - 1. dio: Armaturne šipke, valjana žica i žica, Hrvatski zavod za norme, 2010.
[9] HRN EN ISO 6892-1:2016 Metalni materijali -- Vlačno ispitivanje -- 1. dio: Metoda ispitivanja pri sobnoj temperaturi, Hrvatski zavod za norme, 2016.
[10] Frančić Smrkić, M.; Košćak, J.; Damjanović, D.: Primjena 2D digitalne analize slike za mjerenje pomaka i širina pukotina na AB elementima. Građevinar. 70. (2018), 9; 771-781
[11] HRN EN 1992-1-1:2013, Eurokod 2: Projektiranje betonskih konstrukcija – Dio 1-1: Opća pravila i pravila za zgrade, Eurocode 2: Design of concrete structures – Part 1-1: General rules and rules for buildings, European Committee for Standardization, Bruxelles
[12] Kišiček, T., Sorić, Z., Galić, J.: "Određivanje progiba betonskih nosača s armaturom od polimera armiranih vlaknima", Građevinar 60 (2008) 6. str. 499-511.

RESEARCH FOR RESTORATIVE INFRASTRUCTURE

Ivana Milić (1) and Jelena Bleiziffer (2)

(1) Faculty of Civil engineering, University of Zagreb, Croatia (Ph.D. student)

(2) Faculty of Civil engineering, University of Zagreb, Croatia

Abstract

Moving from sustainable to restorative approach is an important subject in current research. Restorative meaning shifting the focus from less bad in sustainability criteria to contributing to a positive outcome. It is widely recognized that developed infrastructure is vital for economic development as it facilitates manufacturing, services and trade. Infrastructure development has a strong effect on quality of life, and today the awareness that assessment of environmental, social, and economic consequences of infrastructure development needs to be an integral part in considering all stages of its life is rising. The infrastructure is very much different from buildings. It has an immense impact in terms of used resources, and the determination of user benefits is different. Over the past years some tools were developed to assess the sustainability of infrastructure, even those that differentiate the levels of achievement from conventional i.e. state of the practice, over improved (encouraging) and enhanced (on the right track), all the way to superior (remarkable performance), conserving (zero negative impact) and restorative (restoration of resources, ecological, economic and social systems). This paper aims at summarizing the current research for restorative infrastructure, and subsequently discussing challenges of application on an example of two new bridges in Croatia.

Keywords: sustainable development, restorative infrastructure, climate change, sustainable bridges

1. INTRODUCTION

Facing some significant changes globally, a proper consideration of new situations is necessary to take them into account with the correct approaches. According to [1] in 2007, for the first time in history, the global urban population exceeded the global rural population, and since then the world population has remained predominantly urban. In 2014, 54 per cent of the world's population is urban, so by 2050, it is expected that in the world will be 34 per cent of rural population and 66 per cent urban population [1]. According to [2]: „An integrated approach to urbanization will be based on a holistic view of its social development, economic development, environmental management (at the local, national and global levels) and governance components“. Wilson (1992) stated: „The raging monster upon the land is population growth, in its presence, sustainability is but a fragile theoretical construct“ [3] . Europe, with 73 per cent of its population living in urban areas [1], is expected to be over 80 per cent urban by 2050. In urban areas climate change can significantly increase risks for people, economies and ecosystems, and substantial emissions reductions in next few decades can reduce that risks in the 21st century and beyond and contribute to climate-resilient pathways for sustainable development [4]. In 2015, in Paris is reached an agreement called „The Paris Agreement“ to combat climate change, adapt to its effects and accelerate the actions and investments needed for a sustainable low carbon future [5]. The Paris Agreement tends to keep a global temperature rise this century below 2 degrees Celsius and to pursue efforts to limit the temperature increase further to 1.5 degrees Celsius [5]. According to [4]: „multiple lines of evidence indicate a strong, consistent, almost linear relationship between cumulative CO_2 emissions and projected global temperature change to the year 2100“. These changes happening on global level, are in multiple ways, directly or indirectly connected with civil engineering sector. As example, the cement sector, used for concrete as the dominant construction material is the third-largest industrial energy consumer in the world, responsible for 7% of industrial energy use, and the second industrial CO_2 emitter, with about 7% of global CO_2 emissions [6]. About half of the cumulative anthropogenic CO_2 emissions between 1750 and 2011 have occurred in the last 40 years [4]. Beginnings of the sustainable development approach can be found at The United Nations Conference on the Human Environment held in 1972. in Stockholm. That was the first major international conference to discuss environmental issues [7] and sustainability approaches on the global level. Sustainable development most common term is one in the „Our Common Future“ [8] report by the World Commission on Environment and Development (WCED) in 1987. Sustainable development is defined as follows: “Sustainable development is development which meets the needs of the present without compromising the ability of future generations to meet their own needs“ [8]. Some of the important conferences which followed are: UN Conference on Environment and Development (Rio de Janeiro, 1992), Rio + 5 (New York, 1997), UN World Summit on Sustainable Development (Johannesburg, 2002.), UN Conference on Sustainable Development also known as „Rio + 20“ (Rio de Janeiro, 2012.). In Rio de Janeiro, in 2012. it is decided to launch a process to develop a set of Sustainable Development Goals (SDGs), which will build upon the Millennium Development Goals and converge with the post 2015 development agenda. As a results of conferences a significant number of documents have been adopted. Some of important are: Agenda 21 (UN, 1992), signed in Rio de Janeiro, the Millennium Development Goals (MDGs) established in the United Nations Millennium Declaration (UN, 2000) and the Sustainable Development Goals (SDGs) adopted by the UN General Assembly in September 2015 (UN, 2015). The 2030 Agenda for Sustainable Development [9] represents the synthesis of the UN conferences on sustainable development of 1992, 2002, 2012, and the Millennium Development Goals. SDGs consist 17 Sustainable development goals, their 169 targets and are including new areas such as climate change, economic inequality, innovation, sustainable consumption [9]. Drexhage and Murphy [7] stated that in earlier days sustainable development has been primarily environmental issue but today „it is generally accepted that sustainable development calls for a convergence between the three pillars of economic development, social equity, and environmental protection“. Ololade [10] point out that „fostering interdisciplinary research will advance the goal of sustainable development“.

2. SUSTAINABILITY OF BRIDGES

Designing a sustainable infrastructure have a great impact on sustainable development. William J. Bertera stated [11]: „Recognizing that many of our resources are finite and that development has environmental, social, and economic consequences, we have come to realize that it is not enough to create infrastructure that is intelligently designed, well-engineered, and competently constructed. It must also be sustainable“. Designing a sustainable bridge can be defined according to Whittemore [12] as the one that is "conceived, designed, constructed, operated, maintained and eventually put out of service in such a fashion that these activities demand as little as possible from the natural, material and energy resources of the surrounding supporting community". Generally, various authors discuss that sustainable development must be considered as a decision – making strategy. It is usually accepted that decision-supporting systems of bridges' life-cycles can be divided on different stages: planning, design, construction, operation and maintenance.

The research project SBRI (Sustainable Steel – Composite Bridges in Built Environment) [13] points out benefits of steel-composite bridges regarding sustainability using integral holistic approach. Project SBRI [13] last in Europe in a period 2009 to 2012., while project SBRI + have as a goal valorisation, dissemination and extension of the method developed in SBRI project for advance applications. In SBRI studied and compared are different variants of three main types of bridges: A - small motorway bridges, B - crossings of motorways and C - big motorway bridges. The focus is on all stages over the complete lifecycle of the bridges [13].

Holistic approach used in this research project combine three analyses: Lifecycle Performance (LCP) analyses, Lifecycle Assessment (LCA) and Lifecycle Costs (LCC) analyses. Lifecycle Performance (LCP) **-** starts with the construction of the bridge (including the production of raw material), continue with operation of the bridge (including maintenance) and with demolition at the end-of-life. A special focus is given to inspections and maintenance because of its long lifespan so are defined three scenarios. Standard scenario for a 100-year service life, according to the normal service life of bridges, and it predicts that there will be enough money for all the necessary inspections and maintenance actions. Lack of money scenario predict that there is not enough money to the necessary maintenance actions so inspections in the early stages of the bridge will be less frequent, due to those later. In prolonged life scenario maintenance and inspection activities frequencies will be the same as for the standard scenario up to first 80 years and the decision of maintaining the bridge for an additional 30 years (130 years total) is taken around year 80 of lifecycle of the bridge. For the operation phase, it was assumed that the average service life for each structural or non-structural element of the bridge is the same for the standard, lack of money and prolonged life scenario.

Lifecycle Assessment (LCA) **-** The standards for general framework, and requirements for lifecycle environmental analysis (LCA) adopted in this project is according to ISO standards 14040 and 14044. All stages over the complete lifecycle of the bridges, from raw material extraction until end-of-life procedures, are included. Also, the transportation of materials and equipment should be included in the system boundary. The used methodology is developed by the Centre of Environmental Sciences [14] in the University of Leiden. The environmental indicators adopted in the lifecycle approach is: Abiotic depletion (ADP), Acidification (AP), Eutrophication (EP), Global warming (GWP), Ozone layer depletion steady state (ODP) and Photochemical oxidation (POCP).

Lifecycle Costs (LCC) - The total lifecycle costs include construction costs, initial costs such as design cost, operation costs (inspection and repair costs), end-of-life costs (dismantlement) and user costs. Construction cost must include all materials and work costs needed for each component. Because the costs are being incurred at varying points in time (in LCCA), there is a need to convert them into a value at a common point in time [15]. Several methods exist to lead to LCC: the payback method, the equivalent annual costs, the internal rate of return and the net present value approach. Also, inspection strategies may be different in each country based on climate conditions and prioritization strategies proper to each country [16]. There are many proposed optimal maintenance strategies for critical structural elements [17, 18, 19]. In the end-of-life stage bridge is demolished and the materials are sorted in the same place before being sent to their final destination, so cost took into account the costs of bridge dismantlement, costs of transportation and costs for deposition of materials and/or revenue due to recycling of materials. For steel-composite bridges, it is assumed that the steel structure is going to be reused and that concrete and bitumen materials, are cut down and transported to waste disposal areas. User costs are indirect and hardly measurable. In the case of highway bridges, these costs are those incurred by the users due to maintenance operations of highway structure causing congestion or disruption of the normal traffic flow. PROMETHEE – Preference Ranking Organization Methodology of Enrichment Evaluation is used in this research project for the combination of criteria. Considered scenarios are: scenario 1 - took into account equal importance for the three criteria: environmental, economic and user costs (1/1/1), scenario 2 - considered a higher importance to the environmental criterion (2/1/1), scenario 3 - considered a higher importance to the economical criterion (1/2/1) and scenario 4 - considered a higher importance to the user costs criterion (1/1/2).

3. RESTORATIVE INFRASTRUCTURE

Envision [11] is a sustainability rating system, made as a decision making guide for evaluate and give a recognition to infrastructure projects that have a significantly influence in promoting a sustainable future. Envision is oriented on non-habitable infrastructure and can be used for all types and sizes of civil infrastructure project. Envision has 60 sustainability criteria which are called credits and is organized in 5 categories and 14 subcategories. First category is *Quality of life* and is divided into 3 subcategories which are *Purpose*, *Wellbeing* and *Community*. Second category is *Leadership* and its subcategories are *Collaboration*, *Management* and *Planning*. Third category is *Resource Allocation* and is divided into three subcategory: *Materials*, *Energy* and *Water*. Four category is *Natural world* and is divided into three subcategory: *Siting*, *Land +Water* and *Biodiversity*. Last, fifth category is *Climate and Risk* and has two subcategory*: Emissions and Resilience*. Each credit contains of: intent statement and metric, levels of achievement, a description, ways to advance to higher achievement levels, evaluation criteria and documentation, sources, and related Envision credits. Five level of achievement are defined [11] as follows: Improved - *Performance that is above conventional. Slightly exceeds regulatory requirements*; Enhanced - *Sustainable performance that is on the right track*; Superior - *Sustainable performance that is noteworthy, but not conserving;* Conserving - *Performance that has achieved essentially zero negative impact*; Restorative - *Performance that restores natural or social systems*. In every credit each level of achievement has assigned a specific number of points considering estimated contribution on sustainability. Described are the evaluation criteria and documentation which is necessary to demonstrate that a level of achievement has been met and usually lower levels of achievement must be satisfied in order for the higher levels to be achieved. For projects seeking Verification and Envision Award, there is a independent third-party project verification program where a qualified expert contracted by ISI is verifying and confirms the levels of achievement, required documentation, and final score submitted by the project team. According to [20] Cost REstore, sustainability is defined as: *Limiting impact. The balance point where we give back as much as we take* and restorative is define as: *Restoring social and ecological systems to a healthy state.* According to Envision: [11] „to really contribute to sustainability, projects must do more than just make incremental improvements. These incremental improvements may have diminished negative impacts, but they do not contribute to the restoration of economic, environmental, and social conditions to sustainable levels". The last level of achievement *restorative* is not applicable on all credits and presents an explicit level of achievement [11]. Improving sustainable performance and achieving *conserving* level of achievement presents a performance which do not have negative impact. The new point of view is trying to put on that projects must do more good, and not just less bad, or not bad achieving no impact level. To point out the difference, as example, in category *Natural world*, subcategory *Biodiversity,* credit *Restore disturb soil* has only two levels of achievement. Level *conserving* considers restoring 100 % of soils disturbed during construction in the site's vegetated area and the level *restorative* considers restore 100 % of soils disturbed as a results of previous development. In the same category and subcategory credit *Control invasive species*, level *conserving* considers having a management plan for controlling invasive species and their identification while level *restorative* considers effective programs and actions established to eliminate existing invasive species from the project site. In category *Quality of life*, subcategory *Wellbeing*, credit *Encourage alternatives modes of transportations*, level *conserving* describes project which enhances public transportation facilities and encourages the use of public and nonmotorized transportation. The level *restorative* considers that project is designed and constructed in a way that rehabilitates modes of transportation that were unused or disrepair. It is interesting that subcategory *Collaboration*, *Planning* and *Materials* don't have a *restorative* level in none of theirs credits. The Envision rating system encourages innovative methods and different types of innovation and also makes a step out to a restorative approach in designing infrastructure projects.

4. FUTURE URBAN SUSTAINABLE DEVELOPMENT IN CROATIA

To go ahead with global strategies of sustainable development and country's strategic priorities, there are some projects and visions in Croatia for future urban sustainable development. According to [21]: „in order to the future of Zagreb would be in line with the fundamental provisions of planning and sustainable development, improving infrastructure for ensuring a better life of citizen at the same time, holistic approach in project planning is required". One of strategic priorities of sustainable development of Zagreb City is to balance the economic growth of the north and the south part of Zagreb City [21]. Sava River flowing in west – east direction 20 km across Zagreb and with a 100 to 105 m wide corridor divide north (old) and south (new) part of the city. In order to enhance transportation infrastructure five more bridges across Sava are planned, two of which are footbridges [21]. The City Council of Zagreb and the Croatian Society of Structural Engineers organized public competitions for the preliminary bridge designs for the two new bridges [21, 22, 23]. From available literature [21, 23] all submissions from the open design competition sought to achieve a design which respects

Zagreb and Croatian cultural heritage, ensures the functionality and quality of the roadway, railway and pedestrian traffic, and also accomplish the economic, durability, buildability and maintainability demands. According to [22] strict requirements with respect to aesthetic value and blending with natural and urban environment are required. In order to attract citizens to the banks, pedestrian approaches have been design carefully [22]. So in one bridge design, in order to not dominate views, and to minimise the visual impact of the ramp, ramp deck, pedestrian causeway deck and railings are provided to be made of glass [22]. As the most important aspect in restorative design which can be recognized in this project is development of the littoral area of the Sava River which was so far used only as a protection from floods. In development of that idea are considered many aspects that were recognized as unavoidable future demands such as growth of population, traffic congestion, economic growth of different parts of the city and moving focus from the city centre. Especially great impact this bridges will have at increasing level of quality of urban life. Some of the important aspects towards sustainable design will be enhancing mobility, stimulating sustainable growth, and encouraging alternative ways of transportation with restorative aspects in reviving transportation options. So, integrating the Sava River in the city will restore now unused parts of the city, but in not so distant future according to [23] some additional facilities will be built in this area, making this the new city centre. This is a vision of sustainable development in Zagreb based on available literature from preliminary design competitions of two bridges. Although, all projects are not finished yet as authors of this paper are familiar with, this preliminary designs are set as a very good foundation on future urban sustainable development of Zagreb as a modern and sustainable European city.

CONCLUSION

This paper tries to give attention to the importance of global strategies on sustainable development with highlights on civil engineering sector, based on designing sustainable infrastructure with a specific accent on sustainable bridges. So, the paper highlights a different approaches on defining the measurement of sustainability worldwide. Observing these approaches of measurement of sustainability of bridges, we can conclude that sustainability has its proper metric, and can be properly quantified considering holistic integrated approach, all relevant aspects and their contribution to sustainability. It is important to develop a framework (on global and national levels) with properly defined boundaries of all relevant aspects of sustainability and their criteria, set their proper metrics and guidelines how to achieve it, to help bridge engineers to plan and design bridges with clearly defined meaning of sustainability in all life cycle of a bridge. Also, this paper highlights an ambitious idea according to which projects must have positive outcome. Restorative principles take a shift up and encourage positive outcomes of projects considering the philosophy that to really contribute on sustainable development it is not enough just have no negative impact, but projects must do more good to really promote future sustainable development and participate in it.

REFERENCES

[1] UN, Department of Economic and Social Affairs, Population Division (2014). World Urbanization Prospects: The 2014 Revision, Highlights (ST/ESA/SER.A/352).
[2] UN, Department of Economic and Social Affairs, World Economic and Social Survey, Sustainable Development Challenges, Chapter III - Towards sustainable cities, (2013) 54-84. (ST/ESA/344)
[3] Edward O. Wilson, The diversity of life, 1992.

[4] IPCC, 2014: Climate Change 2014: Synthesis Report. Contribution of Working Groups I, II and III to the Fifth Assessment Report of the Intergovernmental Panel on Climate Change [Core Writing Team, R.K. Pachauri and L.A. Meyer (eds.)]. IPCC, Geneva, Switzerland, 151 pp.
[5] https://unfccc.int/process-and-meetings/the-paris-agreement/the-paris-agreement, UN Climate Change (27.09.2018.)
[6] https://www.wbcsd.org/Sector-Projects/Cement-Sustainability-Initiative World Business Council for Sustainable Development (27.09.2018.)
[7] Drexhage, J. and Murphy, D. 2010. Sustainable Development: From Brundtland to Rio 2012. New York, USA: International Institute for Sustainable Development (IISD).
[8] http://www.un-documents.net/wced-ocf.htm, Report of the WCED: Our Common Future.
[9] UN, Transforming our world: The 2030 Agenda for sustainable development,(A/RES/70/1) (2015)
[10] Olusola O. Ololade, Sustainable Development: An Overview, Environ. Sci. & Engg. Vol. 1, Sustainable Development (2017).
[11] Envision rating system for sustainable infrastructure, v2, (2015), ISI
[12] Whittemore, D., 'Sustainable Structures for the Bridge Engineer', Structure magazine, (2010)
[13] SBRI: Sustainable Steel-Composite Bridges in Built Environment, Research Programme of the Research Fund for Coal and Steel RFSR-CT-2009-00020; (2009-2012), Handbook.
[14] Jeroen B. Guinée (Ed.) Kluwer: Handbook on lifecycle assessment; Operational Guide to the ISO standards; Academic Publishers; (2002).
[15] Troive S.: Structural LCC Design of Concrete Bridges; Doctoral Thesis, Royal Institute of Technology, TRITA-BKN; Bulletin 41, ISSN 1103-4270; Stockholm, (1998).
[16] Woodward, D. G.: Lifecycle costing—Theory, information acquisition and application; International Journal of Project Management, vol. 15, no. 6, 335–344, (1997).
[17] Frangopol D. M. & Estes A.C.: Lifecycle Evaluation and Condition Assessment of Structures; Chen W.-F. &.Lui E. M.(eds); Structural Engineering Handbook, 2nd Edn CRC Press,36,(2005).
[18] Vorster, M. C., Bafna, T.&Weyers,R. E.: Model for determining the optimum rehabilitation cycle for concrete bridge decks; Journal of Structural Engineering, ASCE, vol.1319, 62–67; (1991).
[19] Markow, M., Madanat, S. & Gurenich, D.: Optimal rehabilitation times for concrete bridge decks; Transportation Research Record, vol. 1392; (1993).
[20] COST Restore: REthinking Sustainability TOwards a Regenerative Economy, CA16114
[21] Radić J., Kušter M., Kindij A., Mandić A., Two new bridges across Sava River in Zagreb, IABSE, January (2009).
[22] Radić J., Kušter M., Kindij A., Structural - Architectural Approach to Bridge Design, IABSE, 34th International symposium on bridge and structural engineering, Venice (2010).
[23] Radić J., Kindij A., Mandić A., Finding a solution for two new bridges in Zagreb, International Conference and EurekaBuild Event, Dubrovnik, Croatia, May (2008).

International Conference on Sustainable Materials, Systems and Structures (SMSS 2019)
Challenges in Design and Management of Structures
20-22 March 2019 – Rovinj, Croatia

BENEFIT OF DAMPING IN STRUCTURAL CONCRETE FOR RAILWAY STRUCTURES AND TRACK COMPONENTS

Sakdirat Kaewunruen (1), Ruilin You (2) and Keiichi Koto (3)

(1) The University of Birmingham, Birmingham, UK

(2) China Academy of Railway Sciences, Beijing, China

(3) Railway Technical Research Institute, Tokyo, Japan

Abstract

There are two types of modern railway tracks including ballasted and ballastless tracks. Ballasted tracks are optimally designed for suitability to railway operations with train speed less than 250 km/h, while ballastless tracks are more suitable for tunnelling work or higher speed trains. In both types of railway track systems, concrete is often used. However, the systems requirements for this material for real world applications are particularly demanding. Statistically, impact loading conditions comprise of nearly 25% of annual track loads. Also, abrasion from curve effects of train-track interaction causes high wear and tear. For example, railway concrete sleepers have been generally used in ballasted railway track and concrete slabs have been used for ballastless tracks around the world for over 50 years. Both safety-critical track components are commonly used to redistribute wheel forces onto track structure and to assure stable track gauge for safe passages of rolling stocks. The dynamic behaviours of concrete components are commonly well known; however, its damping characteristic is often neglected. With the increased demand for heavier and faster trains, the nature of track forces applying onto each track component is no longer static or quasi-static. The ignorance of damping can no longer be persisted as pre-mature damage or failure of track components can take place at a faster rate. A single sleeper failure may not affect open, plain track operations but it can give rise to the risks of rail breaks at rail joints, welds, bridge ends, switches and crossings, curved track, etc. Such the risks can later result in detrimental train derailments. This paper will highlight the development of high-damping concrete and the benefits of damping on the vibration mitigation of railway concrete sleepers in a track system. An established and validated finite element model of sleeper has been adopted for further studies. The model has been validated by experimental results. The insight into the vibration suppression of railway sleepers will help track engineers to decide the better choice of materials for manufacturing railway concrete sleepers.

Keywords: dynamic damping, railway tracks, track components, vibration reduction material

1. INTRODUCTION

Majority of civil infrastructures is built using concrete material, currently produced at a rate of 2 billion tonnes per year [1]. This is somehow responsible for 5% of global carbon dioxide emissions annually [2-6]. On the other hand, it is well known that concrete has several disadvantages such as low tensile strength, low ductility, brittle, low damping (low energy dissipation), and high susceptibility to cracking. This interior weakness causes concrete structures to deteriorate and lose its integrity when subjected to repeated harsh environmental conditions and dynamic loading conditions [7-10]. Thus, when exposed to these high-intensity conditions, concrete structures are at a risk of failure. In addition, the high global usage of concrete material combined with the large amount of pollution its production produces every year, is a major concern. Paris Agreement in 2016 has imposed the limit of carbon emission so that global warming can be limited to be less than 2°C in 2100 [11-12]. This implies that the use of high-carbon materials such as cement should be even more efficient and effective as much as possible. Therefore, a sustainable policy needs to be taken to discover a solution to these existing issues in material production and selection for design and manufacturing [13]. The sustainable approach within this study involves developing a method to reduce carbon emissions and to improve the resilience of concrete structures. This study comprises of novel concrete innovation incorporating waste materials (see Figure 1) for the purposes of reducing carbon emissions and also improving damping of concrete [14-16].

Figure 1: Waste car tyres

It is well known that railway sleepers (also called 'railroad tie' in North America) are a vital safety-critical component of railway track structures. Railway sleepers are the cross beam element supporting rails in order to provide load support and to secure rail gauge. Today, the most common material for manufacturing sleepers is concrete [17, 18]. The experience of design and application of railway concrete sleepers have been over 60 years around the world. Their key functions are to redistribute loads from the rails onto the underlying ballast bed, and to secure rail gauge for safe and smooth train passages. Based on the current design approach using static and quasi-static theory of solid mechanics, the design life span of the concrete sleepers is targeted at around 50 years in Australia and around 70 years in Europe [19, 20]. In design practice, dynamic problems have not fully been taken into account, giving rise to the lack of new innovation for concrete sleepers. Current industry practice is still based on the topological optimisation using static analysis and the selection of tailored or bespoke dynamic factors for quasi-static design [21-23]. This is because the current design and testing standards are rather primitive and overly simplified. Figure 2 shows a typical ballasted railway tracks. The track superstructure includes rail, rail pads, fasteners, sleepers and ballast; and the track substructure contains ballast mat, subballast (or capping layer), geosynthetics, subgrade and formation.

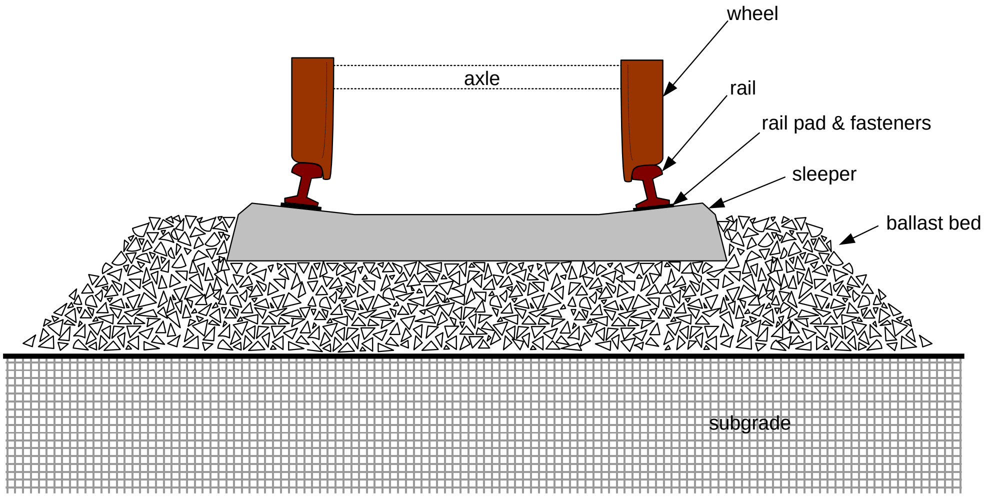

Figure 2: Typical ballasted track and its components

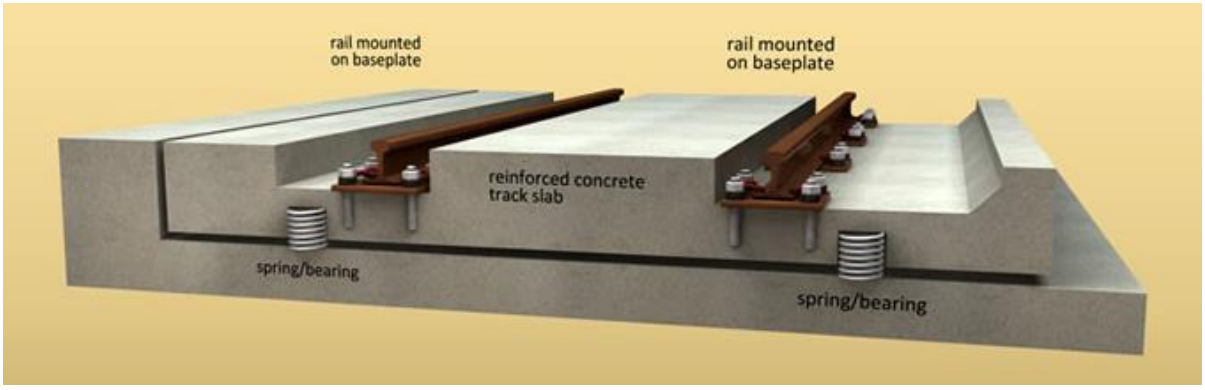

Figure 3: Typical ballastless track and its components

With concrete track slab systems as shown in Figure 3, the ballast is replaced by a rigid concrete track slab which transfers the load and provides track stability. Resilience is introduced into the track system by means of elastomeric components. These elastomeric components may be pads, bearings or springs depending on the type of slab track system. The rails are mounted on fastening systems over the concrete track slab. A resilient layer or spring system supports the slab to isolate track vibration from the ground and support structure.

Both ballasted and ballastless tracks are inevitably exposed to dynamic loading conditions [18]. However, the concrete material damping aspect has never been fully investigated. This paper is the first to present an advanced railway concrete sleeper modeling capable of analysis into the vibration attenuation effects of dynamic loading on the dynamic behaviors of railway concrete sleepers. The emphasis of this study is placed on the nonlinear dynamic design of railway concrete sleepers subjected to effective viscous damping of concrete material. It is the first time that the responses of concrete sleepers incorporating material damping have been investigated. The insight into the vibration attenuation will help structural and track engineers making a better choice in advanced material design and selection. It will also inspire materials engineers to further improve the dynamic material capabilities.

2. HIGHLY-DAMPED CONCRETE USING CRUMB RUBBER FROM RECYCLED CAR TIRES

There are 3 types of rubber, which researchers have tested so far. They are ground rubber, rubber chips and crumb rubber. Mendis [24] presented that compressive strength of concrete dramatically decreases when rubber is added inside. Compared with different types of rubber, Li et al [25] concluded that rubber chips and ground rubber reduce more compressive strength than crumb rubber. In order to reduce the effect of waste rubber, Thomas et al [26] proposed to replace a part of natural aggregate in concrete with some crumb rubber.

In this study, Ordinary Portland cement type I with characteristic strength of 52.5 MPa was selected to prepare concretes. Clean water supplied from the laboratory was used to make hydration reaction in the concrete mixtures. Natural sand and crushed gravel provided by civil engineering laboratory were used as fine and coarse aggregate. Sand has a maximum particle size of 5 mm, and crushed gravels have a maximum size of 10 mm. Before using in the mixture, moisture contents of these materials were investigated in order to adjust the proportion of concrete mix and keep water cement ratio (w/c) constant following the design [10, 27]. Table 1 shows the mixture proportion of highly damped concrete.

Table 1: Mixture proportions of concrete, Unit in kg/m^3.

No.	Mixes	Cement	Water	Gravel	Sand	Silica Fume	425 µm rubber
1.	RFC (Control)	530	233	986	630	-	-
2.	SFC (Control)	477	233	986	630	53	-
3.	SFRC-425-5	477	233	986	598.5	53	31.5
4.	SFRC-425-10	477	233	986	567	53	63

The vibration testing was conducted based on the vibration theory. The exponential curve fitting is used for the direct damping calculation method using the natural frequency and vibration response of the sample. As illustrated in Figure 4, the RFC had average damping ratio of 0.02146 at 28 days, and it improved around 21.76% when replacing cement with 10wt% of silica fume due to the large interface area between silica fume particles and cement matrix which can better dissipate vibration energy. In this study, SFRC-425-10 was the concrete mix which has the highest damping ratio (0.04128 and 0.04038 at 7 and 28 days).

3. NONLINEAR FINITE ELEMENT MODELLING

Using a general-purpose finite element package STRAND7 [28], the numerical model of railway tracks included the beam elements, which take into account shear and flexural deformations, especially for modeling a more realistic concrete sleeper as shown in Figure 5. In this study, the realistic support condition is simulated using the tensionless beam support feature in STRAND7. This attribute allows the beam to lift or hover over the support while the tensile supporting stiffness is omitted. This attribute creates nonlinear boundary conditions to the sleeper model, requiring Newton Raphson's numerical iterations to resolve the sleeper-ballast contact perimeter. The tensionless support option can correctly represent the ballast characteristics in real tracks. The geometrical and material properties of the finite element model has been validated with experimental results of a specific rail track [29, 30].

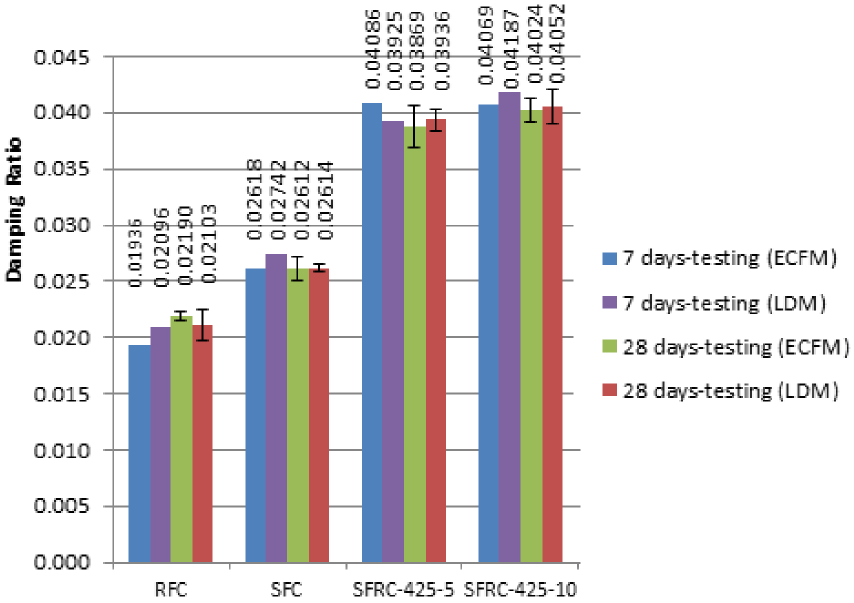

Figure 4: Damping ratio of concrete

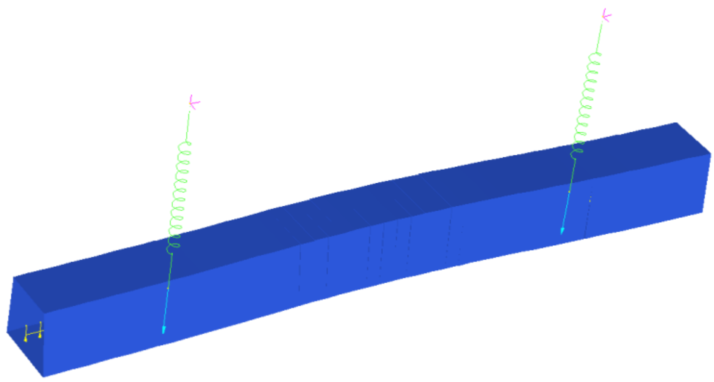

Figure 5: Highly damped concrete sleeper modelling

4. BENEFIT OF CONCRETE DAMPING IN TRACK DYNAMICS

The dual wheelset impact loads of 100 kN magnitude and 3 msec duration are applied at both railseats to stimulate impact vibrations. This impulse is equivalent to the effect of common wheel burns (e.g. 3-5mm flats) on railway tracks. The effects of material damping on the vibration loss of railway concrete sleeper at railseats in a railway track system can be illustrated in Figure 6. It is clear that material damping affects the track dynamics across the frequency span. Especially at the low frequency range associated to the crack of sleepers (<200 Hz), the higher level of vibration loss can be observed. The damping of concrete can suppress well the impact vibrations at railseats of the concrete sleeper where the structural damage often occurs. This can be implied that the improvement in material damping can considerably suppress vibrations that can cause breakage of sleeper and underlying ballast. This insight can also be observed for railway bridge viaducts [31, 32, 33]. The dynamic load effects can be suppressed, resulting in lesser dynamic defections and bending stresses. Since the concrete sleepers are generally designed to be ‘uncracked’ under serviceability limit state (i.e. dynamic impact factor of 2.0 to 2.5), the results clearly show that damping enhancement (>4% of damping ratio) can significantly improve the long-term performance and durability of the concrete sleepers. It is important to note that most of track load spectra tend to be a low frequency range (e.g. <20 Hz), it is clear that the damping improvement can yield a better life cycle of railway concrete sleepers and associated track components.

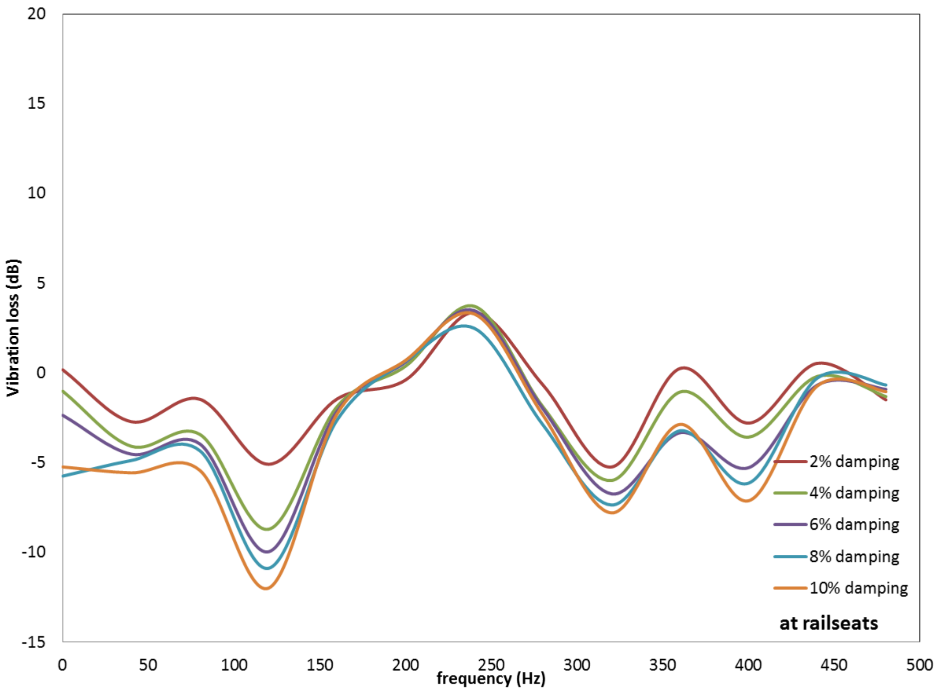

Figure 6: Vibration loss (in dB) of each railway sleeper in a track system

5. CONCLUSION

The insight into vibration attenuation of the sleeper due to the material damping is rather limited in both academic and industry. The ignorance of damping in design has resulted in very little research into advanced concrete technology for railway applications. This study is the world first to incorporate advanced knowledge of novel concrete with high damping for dynamic design of railway concrete sleepers. This paper highlights the effects of concrete damping on the vibration attenuation of railway concrete sleepers in a track system. Using an established and validated finite element model of concrete sleepers, realistic sleeper-ballast contact conditions have been adopted for nonlinear transient analysis. This study is the first to reveal that the concrete damping can provide high level of vibration attenuation in concrete sleepers in a track system across wide range of frequencies. This insight will help structural and track engineers to make a better choice of advanced concrete and composite materials for manufacturing railway concrete sleepers.

ACKNOWLEDGEMENTS

The authors are sincerely grateful to European Commission for the financial sponsorship of the projects H2020-S2R Grant No. 730849 “Switch and Crossing Optimal Design and Evaluation”; and H2020-MSCA-RISE Grant No. 691135 “RISEN: Rail Infrastructure Systems Engineering Network,” which enables a global research network that tackles the grand challenge of railway infrastructure resilience and advanced sensing in extreme environments (www.risen2rail.eu).

REFERENCES

[1] Chung D. Strain sensors based on the electrical resistance change accompanying the reversible pull-out of conducting short fibers in a less conducting matrix. *Smart Mater. Struct*., 4(1), 59-61. (1995).
[2] Kaewunruen S, Sussman JM, Matsumoto A. Grand challenges in transportation and transit systems. *Front Built Environ* 2016; 2(4).
[3] Kaewunruen, S.; Martin, V. Life Cycle Assessment of Railway Ground-Borne Noise and Vibration Mitigation Methods Using Geosynthetics, Metamaterials and Ground Improvement. *Sustainability*, 10, 3753 (2018).
[4] Tuler, M.V.; Kaewunruen, S. Life cycle analysis of mitigation methodologies for railway rolling noise and groundbourne vibration. *J. Environ. Manag*. 191, 75–82. (2017).
[5] Ngamkhanong, C.; Kaewunruen, S. The effect of ground borne vibrations from high speed train on overhead line equipment (OHLE) structure considering soil-structure interaction. *Sci. Total Environ*. 627, 934–941 (2018).
[6] Kaewunruen, S. Monitoring of rail corrugation growth on sharp curves for track maintenance prioritization. *Int. J. Acoust. Vib.* 23, 35–43 (2018).
[7] Kaewunruen, S.; Remennikov, A.M. Current state of practice in railway track vibration isolation: An Australian overview. *Aust. J. Civ. Eng.*, 14, 63–71 (2016)
[8] Remennikov, A.M.; Kaewunruen, S. A review of loading conditions for railway track structures due to train and track vertical interaction. *Struct. Control Health Monit.* 15, 207–234. (2008).
[9] Azzoug, A.; Kaewunruen, S. RideComfort: A development of crowdsourcing smartphones in measuring train ride quality. *Front. Built Environ*. 3, 3. (2017).
[10] Meesit, R., Kaewunruen, S., Vibration characteristics of micro-engineered crumb rubber concrete for railway sleeper applications, *J. of Advanced Concrete Technology* 15 (2), 55-66, (2017).
[11] Binti Sa’adin, S.L., Kaewunruen, S., Jaroszweski, D. Risks of Climate Change with Respect to the Singapore-Malaysia High Speed Rail System. *Climate*, 4, 65. (2016). doi:10.3390/cli4040065
[12] Binti Sa’adin, S.L., Kaewunruen, S., Jaroszweski, D. Heavy rainfall and flood vulnerability of Singapore-Malaysia high speed rail system. *Australian Journal of Civil Engineering*, 14(2), 123-131. (2016). doi: 10.1080/14488353.2017.1336895
[13] Kaewunruen S. and Lee C.K., Sustainability Challenges in Managing End-of-Life Rolling Stocks. *Front. Built Environ*. 3:10. (2017). doi: 10.3389/fbuil.2017.00010
[14] Kaewunruen, S.; Wang, Y.; Ngamkhanong, C. Derailment-resistant performance of modular composite rail track slabs. *Eng. Struct.* 160, 1–11. (2018).
[15] Kaewunruen S., Remennikov A.M. and Murray M.H. Introducing a new limit states design concept to railway concrete sleepers: an Australian experience. *Front. Mater.* 1:8. (2014). doi: 10.3389/fmats.2014.00008

[16] Kaewunruen S., Rachid A. and Goto K. Damping effects on vibrations of railway prestressed concrete sleepers, *World Multidisciplinary Civil Engineering-Architecture-Urban Planning Symposium*, IOP Conference Series: Material Science and Engineering, (2018).

[17] You R., Li D., Ngamkhanong C., Janeliukstis R. and Kaewunruen S. Fatigue Life Assessment Method for Prestressed Concrete Sleepers. *Front. Built Environ.* 3:68. (2017). doi: 10.3389/fbuil.2017.00068

[18] Remennikov A.M., Murray M.H., Kaewunruen S., Reliability-based conversion of a structural design code for railway prestressed concrete sleepers. *Proceedings of the Institution of Mechanical Engineers, Part F: Journal of Rail and Rapid Transit* 226, 155-173. (2012).

[19] Standards Australia, *Australian Standard: AS1085.14-2003 Railway track material - Part 14: Prestressed concrete sleepers*, Sydney, Australia. (2003).

[20] British Standards Institute, *European Standard BS EN13230 Railway applications. Track. Concrete sleepers and bearers*, London UK. (2016).

[21] Kaewunruen S., Remennikov A.M., Influence of ballast conditions on flexural responses of railway concrete sleepers, *Concrete in Australia: J. of Conc. Inst. of Australia* 35 (4), 57-62. (2009).

[22] Wolf H.E., Edwards J.R., Dersch M.S. and Barkan C.P.L., Flexural Analysis of Prestressed Concrete Monoblock Sleepers for Heavy-haul Applications: Methodologies and Sensitivity to Support Conditions. In: *Proceedings of the 11th International Heavy Haul Association Conference*, Perth, Australia, June, 2015. (2015).

[23] Vu M., Kaewunruen S., Attard M., (2016). Chapter 6 – Nonlinear 3D finite-element modeling for structural failure analysis of concrete sleepers/bearers at an urban turnout diamond, in Handbook of Materials Failure Analysis with Case Studies from the Chemicals, Concrete and Power Industries, p.123-160, Elsevier, the Netherlands. doi:10.1016/B978-0-08-100116-5.00006-5

[24] Mendis, A.S.M., Al-Deen, S., Ashraf, M. Behaviour of similar strength crumbed rubber concrete (CRC) mixes with different mix proportions. *Construction and Building Materials*, 137, 354–366, (2017) doi:10.1016/ 2017.01.125.

[25] Li, D.; Mills, J.E.; Benn, T.; Ma, X.; Gravina, R.; Zhuge, Y. Review of the performance of high-strength rubberized concrete and its potential structural applications. *Advances in Civil Engineering Materials,* 5, 149-166. (2016).

[26] Thomas, B.S.; Kumar, S.; Mehra, P.; Gupta, R.C.; Joseph, M.; Csetenyi, L.J. Abrasion resistance of sustainable green concrete containing waste tire rubber particles. *Construction and Building Materials*, 124, 906-909 (2016).

[27] Akono AT, Chen J, Kaewunruen S, Friction and fracture characteristics of engineered crumb-rubber concrete at microscopic lengthscale, *Construction and Building Materials* 175, 735-745 (2018).

[28] G+D Computing *Using Strand7: Introduction to the Strand7 finite element analysis system*, Sydney, Australia. (2001).

[29] Kaewunruen S., Remennikov A.M., Sensitivity analysis of free vibration characteristics of an in-situ railway concrete sleeper to variations of rail pad parameters, *Journal of Sound and Vibration* 298(1): 453-461. (2006).

[30] Kaewunruen S., Remennikov A.M., Experimental simulation of the railway ballast by resilient materials and its verification by modal testing, *Experimental Techniques*, 32(4): 29-35. (2008).

[31] Malveiro, J., Sousa, C., Riberiro, D., Calcada, R., Impact of track irregularities and damping on thefatigue damage of a railway bridge deck slab, *Structure and Infrastructure Engineering*, (2018). doi: 10.1080/15732479.2017.1418010

[32] Ülker-Kaustell, M., Karoumi, R. Influence of non-linear stiffness and damping on the train-bridge resonance of a simply supported railway bridge. *Eng. Struct.*, 41, 350–355. (2012).

[33] Kaewunruen S., Kimani S. K., Damped frequencies of precast modular steel-concrete composite railway track slabs, *Steel & Composite Structures, An Int J.*, 25 (4), 427-442 (2017).

COMPARISON THE BEHAVIOUR OF RC BEAMS WITH GFRP, CFRP AND STEEL REINFORCED BARS

Naser Kabashi, Cene Krasniqi, Arber Kepuska and Besart Avdyli

University of Prishtina, Faculty of Civil Engineering and Architecture, Department of Materials, Prishtina, Kosovo

Abstract

The replacement of the conventional steel bars with the GFRP or CFRP is one of the targets of this paper, including the parameters and properties of the materials. The design procedures should account the properties and will be focused on the tensile strength, modulus of elasticity and also take in considerations the corrosion under the environmental aggressive conditions. This paper presents the experimental work on flexural behaviour of concrete beams reinforced with GFRP bars and CFRP bars. Total fifteen reinforced concrete beams were tested using the four-point loading. The geometrical parameters of tested beams are: 130×220×2200 mm, reinforced with different diameters of bars for GFRP and CFRP. Reinforcement ratio and the strength of concrete influenced the behaviour of GFRP and CFRP, RC beams and contributes to the improvement in reducing the deflections and cracks width.

Keywords: RC Beams, GFRP, CFRP, Deflection, Cracks.

1. INTRODUCTION

From years ago, researchers and civil engineers have been searching alternatives for steel bars and attempt to decrease the high costs of repair and maintenance of structures damaged by corrosion. The using of polymer materials instead of steel bars in concrete element, led to the applying of Fiber Reinforced Polymers (FRP) into field of engineering in elements of structures. The behaviour of FRP bars under environmental aggressive conditions, light weight, nonmagnetic characteristics and mechanical properties, such are tensile strength are the main parameters for replacement the conventional steel in elements of structures. But use of these materials have been limited because the modulus of elasticity, ductility, large creeps, bond between the FRP bars and concrete and high cost.

Many researchers worked in this field, reinforced elements with FRP, analyse the linear relations between stress and strain in FRP bars, positions and geometrical parameters of cracks, deflections of members and in general behaviour of members. The design of FRP reinforced concrete members are governed by serviceability limit state requirements. This is because the modulus of elasticity of FRP bars is much smaller than steel bars, therefore affects the deformation response of FRP reinforced beams.

In this paper, the effect of GFRP and CFRP on the strength, cracks, deflection, ductility and energy absorption capacity of the reinforced concrete beams versus steel bars are experimentally investigated in concrete beams analysing with different cods.

2. EXPERIMENTAL WORK

Fifteen reinforced beams were prepared for testing, five sets with three beams, from which twelve are reinforced with GFRP and CFRP bars and three with conventional steel bars with cross section: 22 cm/13 cm and span 200 cm, shown in fig. 1

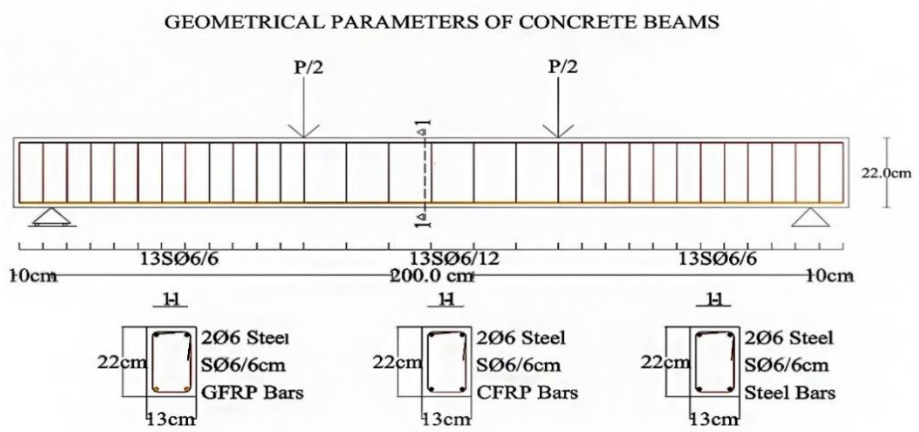

Figure 1: Geometrical parameters of concrete beams for testing

The reinforced of concrete beams is done with different FRP reinforced bars, GFRP, CFRP, and conventional steel bars, shown in table 1.

Table 1: Characteristics of reinforced concrete beams

Set-beams	Reinforcement in upper zone	Reinforcement in down zone	Bending Moment M_{max} [kNm]	Percent of reinforcement ρ_b [%]
“1”	Ø6	Ø6 GFRP	8.60	0.501
“2”	Ø6	Ø8 GFRP	16.34	0.415
“3”	Ø6	Ø10 GFRP	27.00	0.353
“4”	Ø6	Ø8 CFRP	37.90	0.737
“5”	Ø6	Ø10 CFRP	42.88	0.329
“6”	Ø6	Ø6 steel	4.48	1.59
“7”	Ø6	Ø8 steel	8.37	2.10
“8”	Ø6	Ø10 steel	12.68	1.59

2.1 Materials

The different types of reinforcement bars were used in our research in first step was focused in determinations the mechanical properties of FRP bars. The results are presented in Table 2, based on the testing process according the Standard ASTM D 7205. In the edges of the bars were set metallic shells in order to avoid constriction of the FRP bars shown in Figure 2. The properties of conventional steel bars were used from known parameters based on the previous research works. FRP bars used in our research were two types: GFRP (helically grooved) and CFRP (sand-coated), shown in figure 2. The mechanical properties of testing GFRP and CFRP are presented in table 2.

Figure 2: Testing the mechanical properties of Reinforced bars (GFRP CFRP)

Table 2: Mechanical properties of used GFRP and CFRP bars

	GFRP			CFRP	
Strain ε^*_{frp}	Ø6	Ø8	Ø10	Ø8	Ø10
	0.0204	0.0234	0.0256	0.0095	0.015
Tensile strength [MPa]	1022.10	1108.2	1194.3	1265.4	1420
Elas.Mod. [GPa]	55			155	

2.2 Preparing the tests beams

The concrete beams were reinforced in down zone using the GFRP, CFRP and conventional steel, and in upper zone the conventional steel bars presented in fig.1. Concrete mixes design was prepared with requested class of concrete C 30/37 in this study case.

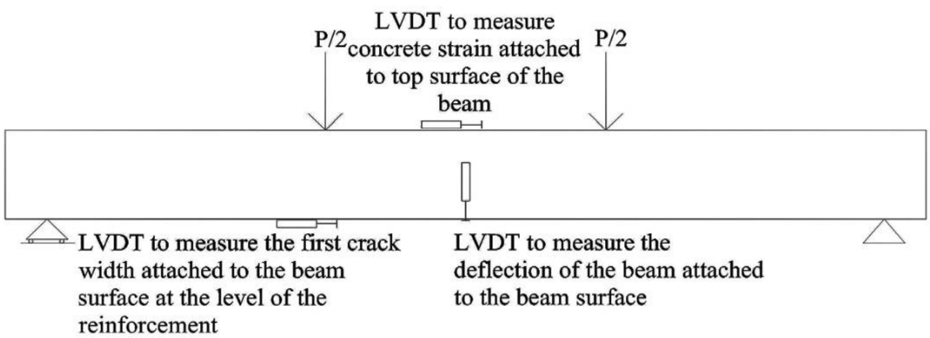

Figure 3: Testing set up and positions of the measurements

The beams were observed during the test under load applying process. Testing equipment MCC8 Controls were used during the testing, presented in fig.3.

During the test, crack formation on the side of each beam was marked and the corresponding loads were recorded. LVDT was used to measure the width of the first flexural crack right under the concentrated force. Also, compression concrete zone was instrumented with LVDT to measure the strain of concrete, and another LVDT was in mid-span of the beam to measure the deflection, presented in fig.4.

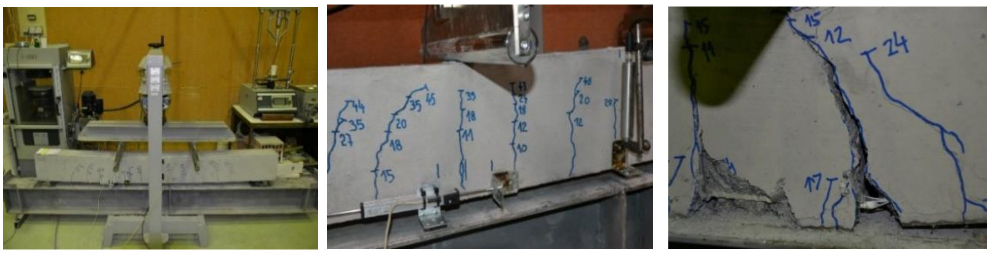

Figure 4: Cracks in longitudinal span of testing beam

3. TEST RESULTS

3.1 Crack pattern and mode of failure

Due to the brittle nature of concrete and because of changing loading conditions and other factors which are not considered in the design (such as internal stresses resulting from casting), the design Codes give guidelines for checking the amount of reinforcement that is required in a structure to keep the crack-width limited to a certain value at specified load-levels. Checks in design codes are mainly based on the forces and bending moments in the cross-section of the structure. Presented in Table 3.

Table 3: Equations for calculations using the different actual codes.

Expression	Procedure
Cracking	
$w = 2.2k_b \dfrac{M}{j \cdot d \cdot E_f \cdot A_f} \cdot \dfrac{h_2}{h_1} \sqrt[3]{d_c \cdot A}$	ACI & CSA.
$w = \beta \cdot s_{rf} \sigma_f \left[1 - \beta_1 \beta_2 \left(\sigma_{sr}/\sigma_f\right)^2\right] / E_f$	EC 2
Deflection	
$\Delta = \dfrac{P \cdot a}{24 E I_e}(3L^2 - 4a^2)$	ACI 318
$\Delta = \frac{P \cdot a}{24 E I_{cr}} \cdot \left[3L^2 - 4a^2 - 8\left(1 - \frac{I_{cr}}{I_g}\right)\left(\frac{M_{cr}}{M_a}\right)^3 \cdot a^2\right]$	CSA A23.3-05
$\Delta = \left[1 - \left(\frac{M_{cr}}{M_a}\right)^2\right] \Delta_g + \left[1 - \left(1 - \left(\frac{M_{cr}}{M_a}\right)^2\right)\right] \Delta_{cr}$	EC 2

3.2 Cracks and Deflection parameters in testing beams

The balanced reinforcement ratio and the nominal flexural strength defined in the presented sections can be obtained by using a sectional analysis in different stages of SLS theory, including the percent of ratio "Moment-M/Mu" analysing with different Codes and Experimental results in this case study, Table 4 and Fig 6a and Fig 6b.

Table 4: Deflections (*Defl.) and Cracks (*Cr) for different analysing sets

Beams		Code	SLS %	"SLS"		75%-Ratio		100%-Ratio	
				Crack	Defl.	Crack	Defl.	Crack	Defl.
"1"	Ø6 GFRP	ACI	27.4	0.89	8.68	2.44	38.13	3.25	51.76
		CSA		0.89	11.16	2.44	38.17	3.25	51.58
		EC2		1.33	6.12	4.06	35.86	5.45	49.82
		Exp.		0.73	7.57	2.91	44.8	3.81	48.50
"2"	Ø8 GFRP	ACI	24.5	0.89	5.28	2.44	27.25	3.25	36.87
		CSA		0.89	7.4	2.44	27.38	3.25	36.84
		EC2		0.69	4.5	2.33	26.22	3.12	35.96
		Exp.		0.71	8.29	2.91	43.25	3.81	48.31
	Ø8 CFRP	ACI	31.3	0.38	6.64	0.92	15.78	1.23	21.04
		CSA		0.38	6.23	0.92	15.63	1.23	20.92
		EC2		0.49	5.52	1.20	15.31	1.61	20.68
		Exp.		0.38	8.30	0.60	18.50	0.79	28.43
"4"	Ø8 steel	ACI	75.0	0.26	6.04	0.32	7.16	0.35	7.91
		CSA		0.26	5.60	0.32	6.81	0.35	7.62
		EC2		0.27	5.05	0.32	6.35	0.36	7.19
		Exp.		0.24	6.50	0.26	8.30	2.14	18.65

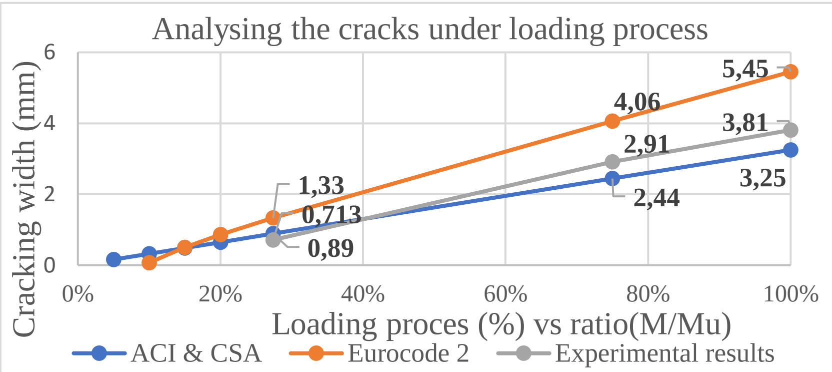

Figure 6a: Cracks analyse using the different Codes for -Ø6 GFRP

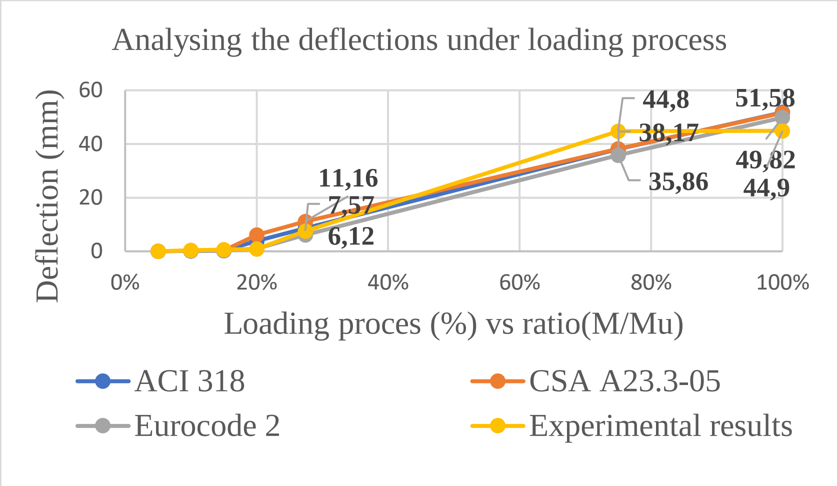

Figure 6b: Deflections analyse using the different Codes for Ø6 GFRP

3.3. Failure mode compared between theoretical and experimental study

The flexural capacity of FRP reinforced flexural member is dependent on whether the failure is governed by concrete crushing or FRP rupture. The failure mode can be determined by comparing the FRP reinforcement ratio to the balanced reinforcement ratio (that is, a ratio where concrete crushing and FRP rupture occur simultaneously). Because FRP does not yield, the balanced ratio of FRP reinforcement is computed using its design tensile strength. However, once the beam cracked, the stiffness of the GFRP reinforced concrete beam decreased at a faster rate compared with the control beam. This lead in a larger deflection of the GFRP reinforced concrete beams. Crack propagations were observed during the tests and the serviceability limit state for all testing beams is presented in table 5.

Table 5: Behaviour the testing beams for different type of reinforcement

Type of bars	Bar diameter (mm)	Maximum load in “SLS” [kN]	Maximum load [kN]	Serviceability limit state [%]
GFRP	8	10.0	40.10	24.9
CFRP	8	22.70	69.10	32.8
Steel	8	27.40	31.70	86.4

3. CONCLUSIONS

- Reinforced beams with GFRP and CFRP bars behaved linearly up to failure based on the linear characteristics of FRP bars and low modulus of elasticity of FRP bars than conventional steel bars.
- The serviceability limit state (SLS) for FRP bars and conventional steel bars results with lower percent of usage the FRP materials (24.9%⇒32.8%⇒86.4%) (GFRP⇒CFRP⇒Steel) based on the mechanical properties.
- The cracks and deflection for the beams under the loading 75%, reinforced with GFRP, CFRP and conventional steel bars evaluated by experimental analysis, behaved the differently: cracks (2.91⇒0.60⇒0.26) ;(diameter Ø8 mm - GFRP⇒CFRP⇒Steel)

- The use of GFRP and CFRP bars as replacement of steel reinforcement bars in concrete beams result with reducing the stiffness but increasing the max. loading, from 31.7kN⇒40.10kN⇒69.10kN (Ø8 mm)
- Results of experimental analysis in this case Study for deflections and cracks of concrete beams analysing show closer behaviour with ACI 318 than other Codes.

REFERENCES

[1] ACI 440.1R-06; Guide for the Design and Construction od Concrete Reinforced with FRP Bars", ACI Committee, 2006
[2] L.C.Bank;Composites for Constructions: Structural Design with FRP Materials", John Willey &Sons, New York, 2006
[3] N.Kabashi,at.al; Flexural Behaviour and Cracks in Concrete beams reinforced with GFRP bars, ICPIC 2018, Washington DC, 2018
[4] Alsayed, SH.;Flexural Behaviour of Concrete Beams Reinforced with FRP Bars, Journal :Cement and Concrete Composites, nr.20.pp.1-11, 1998
[5] CNR-DT 2032006; Guide for Design and Construction of Concrete Structures Reinforced with Fiber-Reinforced Polymer Bars" National Research Council, Rome; Italy,2006
[6] CSA-S806-02; Design and Construction of Building Components with Fibre Reinforced Polymers" Canadian Standards Association, Ontario, 2002.
[8] Arduini, M., & Nanni, A. (1997). Parametric study of beams with externally bonded PRP reinforcement. AC'I Structural Journal, 94(5), 493—501. 79 Flexural Behaviour and Cracks in Concrete Beams Reinforced with GFRP
[9] CEB-FIB, Bulletin 40

MATERIALS FOR INFRASTRUCTURE PROJECTS BASED ON DURABILITY AND SUSTAINABILITY ISSUES

I. Papayianni, E. Anastasiou, M. Papachristoforou and A. Liapis

Laboratory of Building Materials, School of Civil Engineering, Aristotle University of Thessaloniki, Greece

Abstract

Infrastructure projects such as dams, roads, docks or airfield pavements have a great impact to economy. Extending their lifespan as well as reducing the footprint of the total life cycle of these projects is of major importance. The selection of the materials for their construction should not only fulfill the specific design criteria, but also those of general economy in terms of cost, saving natural resources, reducing emissions and prolonging service life without often repair works. The infrastructure projects are usually sponsored and managed by State agencies and serve as prototype constructions since their long-term behavior is de facto monitored for safety and good operation reasons. Therefore, their materials' performance is also checked and evaluated. In our period of decarbonization and alternative energy sources, new pavements and pump-storage systems are needed for exploitation and transferring energy. If conventional concrete will be used, the advantages of CO_2 reduction are partially devaluated.

Therefore, an effort has to be made to upgrade locally available materials such as supplementary cementing ones and recycled aggregates by testifying properly their potential, focusing on testing durability aspects.

It must be taken into account that most of the aforementioned materials are not covered by regulative frames and the management of the whole procedure up to the end use should be thoroughly described.

In the paper, two examples of selecting materials and designing the concrete mixtures for the construction of road pavements and pump-storage systems are given. Local raw materials such as fly ash, steel slags and excavated rock have been used. Test recommended by the relevant EN standards were applied to check the suitability of the alternative raw materials. The designed concrete mixtures were tested to meet the predefined durability requirements. The CO_2 footprint and environmental profile of the proposed mixtures for these infrastructure projects have also been estimated by the Life Cycle Assessment methodology, to testify the benefits of the alternative materials' solution for these infrastructure projects.

Keywords: infrastructure, durability, sustainability, local materials

1. INTRODUCTION

The contribution of infrastructural projects to a country's economy is indisputable. New jobs and opportunities for several product and service suppliers come along with the construction as well as the use phase of an infrastructure work. Moreover, compared to a private project (e.g. residence building), it serves a much wider group of individuals, contributing to the improvement of a community's standard of living. Therefore, infrastructure projects are usually sponsored and managed by State agencies and serve as prototype constructions since their long-term behavior is de facto monitored for safety and good operation reasons.

For the above-mentioned reasons, it is important to incorporate the concepts of durability and sustainability in the design and construction of an infrastructure work. Durability, which is indeed another aspect of sustainability, should be considered in a construction that requires a long service life, without often repair works (that would obstruct its public use). This long service life is translated into reduced emissions and resources' usage (due to maintenance/reconstruction) and consecutively reduced costs. Thus, the three-fold character of sustainability (social, environmental and economic efficiency [1]) could be fulfilled and constantly monitored on an infrastructural work.

2. MATERIALS

In this paper, two projects are being studied. The first is a pilot construction of a road pavement, made from Roller Compacted Concrete (RCC). The second one, which is in the design phase, is a pump-storage system that consists of two reservoirs, bordered by hard-core dams. The common ground between these two cases is the effort to utilize locally available materials, in order to reduce emissions and costs from the avoided transportations, as well as to contribute to local economy.

2.1 Road pavement materials

The pilot construction of the RCC road pavement was implemented in a rural road next to the National Road of Thessaloniki-Serres (E65), near Liti, in the area of Northern Greece. The total length of the pavement is 1000 m, 500 m of which were constructed with concrete that incorporates limestone aggregates, and the other 500m with aggregates from Electric Arc Furnace (EAF) slags. Slags are the industrial by-products of the steel production process. Depending on the production method, slag accounts for 7.5-15% of the total steel produced [2], and the total annual world production is estimated at 170-250 million tons for 2017 [3]. Annual slag production in Greece is about 250,000 tons and consists only of EAF steel slag. Table 1 shows the physical properties of both limestone and slag aggregates and the standards according to which, these properties were measured.

Table 1: Physical properties of used aggregates

Property	Test method	Crushed Limestone	EAF slag
App. specific density (kg/m^3)	EN 1097-6	2680	3330
Loose bulk density (kg/m^3)	EN 1097-3	1385	1482
Percentage of voids (%)	EN 1097-3	48.3	55.5
Water absorption (%)	EN 1097-6	0.75	2.50

Resistance to fragmentation (%)	AASHTO T96	24.1	13.9
Flakiness index (%)	EN 933-3	38.4	8.0
Freeze-thaw resistance (1% NaCl) (%)	EN 1367-6	0.87	0.81
Magnesium sulphate soundness (%)	EN 1367-2	21.4	23.6
Steel slag expansion (%)	EN 1744-1	-	0.14
Aggregate abrasion value AAV (%)	EN 1097-8	-	3
Polished stone value PSV (%)	EN 1097-8	-	64

As a binder for these two types of concrete a mixed type binding system based on fly ash was used instead of Portland cement, for environmental and cost reasons. Fly ash in Greece is a by-product of lignite-fired power plants and despite the abundant quantities produced annually, only a small percentage is utilized and the rest is landfilled, causing serious environmental problems. The use of fly ash or slags in RCC road pavements is common practice in many countries such as USA, Austria, Australia and many relevant technical guidelines exist [4-6]. The characteristics of the constituents of the mixed-type hydraulic binder are given in Table 2.

Table 2: Chemical analysis and characteristics of the constituents of the hydraulic binder

Content/ Property	Cement clinker	Calcareous fly ash	Limestone filler	Natural pozzolan
SiO_2 (%)	21.35	34.40	0.20	63.80
Al_2O_3 (%)	5.40	13.60	0.20	18.10
Fe_2O_3 (%)	3.40	6.10	0.05	4.10
CaO (%)	65.75	32.80	55.00	2.80
MgO (%)	1.60	3.80	0.60	1.00
CaO_{free} (%)	1.30	6.40	n/a	n/a
$SiO_{2\text{-reactive}}$ (%)	n/a*	n/a	n/a	35.00
SO_3 (%)	1.20	6.78	0.00	0.00
L.O.I. (%)	0.00	3.26	44.10	3.20
Insoluble residue (%)	0.00	23.80	0.00	82.80

*not measured

The final composition of the binder (comprised of 50% calcareous fly ash, 25% clinker, 12.5% natural pozzolan and 12.5% limestone filler) and its characteristics are given in Table 3.

Table 3: Properties of the produced mixed type hydraulic binder

Physical properties	
Blaine (cm^2/g)	9550
Fineness (retained at 45 μm)	0.4
Water requirement (%)	41.5
Initial setting time (min)	210
Le Chatelier dilation (mm)	0.0
2-day compressive strength (MPa)	15.9
7-day compressive strength (MPa)	26.3
28-day compressive strength (MPa)	40.1
Chemical properties	

L.O.I. (%)	8.40
SO_3 (%)	3.20
Insoluble residue (%)	26.40
CaO_{free} (%)	4.80
Chemical analysis	
SiO_2 (%)	29.90
Al_2O_3 (%)	12.65
Fe_2O_3 (%)	3.80
CaO (%)	42.90
MgO (%)	2.20

2.2 Hard-core dam materials

The construction of the hard-fill dams will take place in Amphilochia, in Western Greece, bordering the Ionian Sea and the Gulf of Patras. The area, being very rich in water resources such as rivers and lakes, makes for an optimum location for the construction of hydraulic projects. The geotechnical study of the region showed that the rocky material of the area consists of siltstone and sandstone rocks. After extensive tests at the Laboratory of Building Materials (AUTH) for their suitability (separately and in combination) for the dam construction, the sandstone was found to perform better than siltstone. The properties of crushed sandstone aggregates are shown in Table 4.

Table 4: Properties of crushed sandstone aggregates

Properties' Standards	ASTM C131 Los Angeles (%)	EN 933-3 Flakiness index (%)	EN 1367-2 Soundness (%)	ASTM C1260-01 Alkali aggregate expansion (%)
Properties' values	31.26	29.83	20.51	20.6
Category according to Standards	LA35	FI35	MS25	-

Considering previous experience in using the local calcareous fly ash (CFA) in stabilizing earthen materials [7] as well as the low heat evolution potential of CFA [8] it was decided to use CFA for hydraulically bound mixtures with crushed sandstone for the construction of the dam. The fly ash will be acquired from Ptolemaida basin, 250 km far from Amfilochia. The characteristics of the CFA are shown in Table 5.

Table 5: Characteristics of CFA used as hydraulic binder

Constituents	% by mass
CaO_{free}	4.96
SiO_2	34.8
Al_2O_3	14.83
Fe_2O_3	2.40
CaO	31.34
MgO	1.39
SO_3	2.37
Na_2O	4.95
K_2O	2.88
Loss of Ignition	4.55

Moisture content %	0.24
App. Specific gravity	2.38
Fineness Retained on 45μm sieve	0.43

3. LABORATORY AND ON-SITE TESTING

For both projects, laboratory tests were conducted in order to design the final concrete mixtures. The road pavement was also monitored several months after its construction, for its mechanical and durability behaviour.

3.1 Road pavement

After several trial mixtures in the Laboratory, the ones that are being shown in Table 6 are those that were implemented on-site. The mixture named LMR refers to the section with lime aggregates' concrete, while the SGR refers to slag aggregates' concrete. The average width of the road was 6.25 m and the desired thickness 20 cm. It should also be noted that ordinary equipment was used, similar to that of asphalt concrete pavement construction.

Table 6: Concrete mixtures for the 2-section road pavement

Section	LMR	SGR
unit	kg/m^3	kg/m^3
CEM I 42.5	-	-
Hydraulic road binder	280	280
Water	148,4	162,2
Limestone aggregates (fine)	985	1111
Limestone aggregates (coarse)	985	-
EAF Slag aggregates (coarse)	-	1090
Superplasticizer (%wt. of binder)	0,60%	0,60%

At 28 and 180 days after the construction of the RCC road pavement, a survey was carried out and cores were obtained by drilling in order to test mechanical and durability properties. The compressive strength was measured according to EN 12390-3 and the static modulus of elasticity according to ASTM C469. The resistance of the concrete to Chloride Ion penetration was measured according to ASTM C1202. Frost resistance was also measured by freeze-thaw cycle testing, according to ASTM C666. The abrasion resistance of the pavement's surface was measured on-site, according to EN 13892-4. The results of the above-mentioned tests are given in Table 7.

Table 7: Mechanical and durability properties of the 2-section road pavement

Section	LMR	SGR
28d Compressive strength (MPa)	29.61	28.76
28d Modulus of Elasticity (GPa)	21.70	21.46
180d Compressive strength (MPa)	27.60	26.20
180d Modulus of Elasticity (GPa)	25.30	17.00
Chloride penetration (Coulombs/Category)	1749 (Low)	2556 (Medium)
Mass loss after 10 freeze-thaw cycles (%)	0.23	0.48
Mass loss after 56 freeze-thaw cycles (%)	0.66	4.66
Abrasion resistance (depth of channel, mm)	6.77	4.49

3.2 Hard-core dam

In order to improve the properties of the crushed sandstone filling, it was decided to add CFA at ratios of 10 and 15% by mass. The optimum moisture and max dry density according to modified Proctor method ASTM D1557 were measured and the California Bearing Capacity Ratio (CBR) was determined, following ASTM D1883-99 method. Expansion under confined immersion of CBR samples was also measured. A compilation of the results is shown in Table 8.

Table 8: Results of Proctor and CBR tests concerning mixtures of siltstone with CFA

Mixtures	Sandstone – 10% CFA	Sandstone – 15% CFA
Optimal moisture (%)	31.26	29.83
Maximum dry density Proctor (g/cm^3)	2.13	2.12
CBR (%)	160	310
Expansion at 10/30/65 drops (mm)	0.05 / 0.05 / 0.05	0.05 / 0.05 / 0

4. SUSTAINABILITY ASSESSMENT

The Life Cycle Assessment methodology is used to evaluate and compare the environmental impact of the studied projects, as it is described in the International Standards ISO14040 and ISO 14044. The assessment is based on correlating all the inputs and outputs of the studied system (resources and energy consumption, air/water/soil emissions etc.) with certain environmental impact categories, through models (characterization models) that summarize and express the results into one single measurement unit. For this paper the “IPCC 2007 GWP 100a” characterization model was used, which describes the contribution of the assessed projects to climate change (Intergovernmental Panel on Climate Change – IPCC), and the unit in which the results are presented is the results is kilograms of CO_2 equivalent (kg CO_2 eq) per functional unit. The data for the assessment have been taken mainly from industries in Greece, as well as literature.

4.1 Road pavement assessment

For the assessment of the two-section road pavement, the boundaries that were chosen are characterized as “Cradle to Grave” meaning that the whole life cycle of the pavement is considered, from the raw materials acquisition, to the construction, to the use of the pavement (along with maintenance works when they were needed) and finally to its decommission (part of it was suitable for recycling in order to produce materials that can be used for other purposes or reconstruction of the pavement). The whole life cycle of the construction was chosen at 54 years, which was defined from existing experience and according to expectations for the slag concrete section. A third pavement scenario was also introduced (APR), that refers to a common Asphalt pavement, in order to have a better comparison of the studied cases with the existing practice. In Figure 6 the results are shown, for the 3 different cases. The results are presented in kg CO_2 eq, per km of constructed pavement.

To evaluate the economic impact of the compared cases, the methodology of the Net Present Value (NPV)is being used, with which all future expenses and incomes that derive from the life cycle of the constructed pavements are expressed in economic terms of the time of the assessment, in our case the present time (time point = 0). The assessment period was chosen as 40 years, mainly because the methodology states that after that time frame the financial rates are not accurately predictable and this may lead to inaccuracies in the assessment. The results of the economic assessment are also shown in Table 9.

Table 9: Environmental and economical assessment of the road pavement

Section	LMR	SGR	APR
Life Cycle Assessment			
unit	kg CO_2 eq/km	kg CO_2 eq/km	kg CO_2 eq/km
Initial Construction	1,71E+05	1,71E+05	1,21E+05
Maintenance	-	-	9,92E+04
Reconstruction	5,43E+04	-	2,04E+05
Recycling	1,56E+04	1,70E+04	1,43E+04
Total	2,41E+05	1,88E+05	4,38E+05
Life Cycle Cost Analaysis			
unit	€/km	€/km	€/km
Total	30.96	29.96	56.03

4.2 Hard-core dam assessment

Since the project is still in design, it would be difficult to conduct a comprehensive assessment for the complete construction. For this reason, a mix design process was conducted in the Laboratory of Building Materials, according to existing experience on similar constructions' requirements. The process showcased that there was a need for slight alterations to the initial mixtures; ratios, in order to construct the lean concrete dam. In Table 10 four different mixtures are compared, one with cement binder and limestone aggregates (LD1), one with cement binder and a combination of limestone and sandstone aggregates (LD2) making use of the abundance of the area, one with cement and CFA binder with limestone aggregates and the last one with cement and CFA binder along with a combination of limestone and sandstone aggregates. The designing of the mixtures was In Table 10 there is also been given an economical assessment of the four studied scenarios.

Table 10: Environmental and economical assessment of the lean concrete dam

Scenario	LD1	LD2	LD3	LD4
Concrete mixtures				
unit	kg/m^3	kg/m^3	kg/m^3	kg/m^3
CEM II 32.5	100	100	60	60
Fly ash	-	-	60	60
Water	176.5	176.5	197	197
Limestone aggregates	1988	-	1953	-
Sandstone	-	1988		1953
Life Cycle Assessment				
unit	kg CO_2 eq/m^3	kg CO_2 eq/m^3	kg CO_2 eq/m^3	kg CO_2 eq/m^3
Materials	101.31	101.75	66.42	67.08
Transportation	2.36	1.92	5.85	5.39
Production	2.33	2.33	2.33	2.33
Total	106.00	106.00	74.60	74.80
Economical Assessment				

unit	€/m^3	€/m^3	€/m^3	€/m^3
Materials	19.3	9.33	16.50	6.69
Transportation	0.93	0.79	2.37	2.23
Production	0.36	0.36	0.36	0.36
Total	20.59	10.48	19.23	9.28

5. DISCUSSION - CONCLUSIONS

The use of large amounts of raw materials for infrastructure projects make their impact to cost and environmental footprint more obvious. Since they are often monitored for safety and good serviceability reasons, their performance may be recorded, as well as the frequency and cost of maintenance work needed. From this point of view, infrastructure projects with alternative and local materials could help as prototypes, in pushing circular economy into practice. A strategy of adopting sustainability indices for the approval of an infrastructure project, could be a great impetus in the construction sector. Social, economic and environmental issues should be communicated and promoted to local society, in order to persuade for their equal importance to the realization of an infrastructure project.

ACKNOWLEDGEMENTS

Part of this research work was developed in the frame of the TEFRODOS Project 2011-2014, funded by the General Secretary of Research and Technology in Greece. In addition, part of the research was developed within a scholarship, funded by the Act “Support of research manpower, through the development of PhD research”, coming from resources of the OP “Human Resources Development, Education and Lifelong Learning”, 2014-2020 with support from the European Social Fund and the Greek Government.

REFERENCES

[1] World Commission on Environment and Development, 'Our common future', (Oxford University Press, Oxford, 1987).
[2] National Slag Association, 'Steel slag – a premier construction aggregate', (Accessed February 12th, 2010 at http://www.nationalslag.org, 2001).
[3] U.S. Geological Survey, 'Mineral Commodity Summaries', (USGS, 2017).
[4] National Concrete Pavement Technology Center, 'Guide for Roller-Compacted Concrete Pavements', (Iowa State University and Portland Cement Association, USA, 2010).
[5] ACI, 'ACI 325.10R-95: State-of-the-art report on roller-compacted concrete pavements. ACI Manual of Concrete Practice', (American Concrete Institute, USA, 2001)
[6] PCA, 'Guide Specification for Construction of Roller-Compacted Concrete Pavements', (Portland Cement Association, Illinois, USA, 2004).
[7] Papayianni I., Papachristoforou M., Stavridakis E., 'Use of calcareous fly ash for improving mechanical and physical characteristics of soils', in 'EUROCOALASH 2012', Proceedings of an International Conference, Thessaloniki, September, 2012 (available at http://www.evipar.org/innet/files/EUROCOALASH2012/Docs/default.htm).
[8] Stefanakos I., Tsiknakou P., 'Technical, Economic and Environmental experiences and conclusions from the use Processed fly ash for the construction of Platanovrisi Dam on the River Nestos', in 'EVIPAR 1st Hellenic Conference', Proceedings of a National Conference, Thessaloniki, November 2005, (available at http://www.evipar.org/Category.asp?cat=79&lang=gr&sub=139).

ADHESION PARAMETER "k_b" OF RC BEAMS WITH GFRP AND CFRP BARS UNDER THE FLEXURAL LOADS

Naser Kabashi (1), Cene Krasniqi (1), Besart Avdyli (1), Arbër Këpuska(1) and Drilona Disha (2)

(1) University of Prishtina, Faculty of Civil Engineering and Architecture, Department of Materials, Prishtina, Kosovo

(2) Polytechnic University of Tirana, Faculty of Civil Engineering, Tirana Albania

Abstract

The adhesion parameter "k_b" of RC beams with GFRP and CFRP reinforced bars under the applied loads is one of the targets of this paper. The design procedures should account the behavior of the RC beams and all parameters focused on the adhesion parameter "k_b".

The experimental work in this paper compare with analytical calculations will present the difference or probably improvement or detail analysis of effect the "k_b" value in completing the behavior of the RC beams.

The design of RC beams with FRP bars is typically governed by serviceability state rather than ultimate state. This required verifying of crack width in RC beams with FRP bars, members at service load.

This study purpose is to investigate the "k_b" values and verifying the dependency of the "k_b" values on GFRP and CFRP bars, diameter and strength limited to the critical flexural crack width. The investigation included 12 beams, using the four-point load test. The geometrical parameters of tested beams with dimensions: 130×220×2200 mm, reinforced with different diameters, helically-grooved GFRP, and sand-coated CFRP bars. The measured of cracks were used to assess the current "k_b" values recommended in FRP design codes and guides.

Keywords: RC Beams, GFRP, CFRP, "k_b" values, cracks.

1. INTRODUCTION

Steel bars have been traditionally used in reinforced concrete structures but from time to time in these structures were detect several problems related with durably corrosion, cover splitting and deboning between the concrete and reinforcement. The using of Polymer Materials instead of steel in concrete structures, led to the entry of Fiber Reinforcement Polymer (FRP) into field structures and constructions. The alternative reinforcement such Fiber Reinforced

Polymers (FRP) is focused on corrosion resistant by nature and they are becoming more common reinforcing materials in concrete elements of structures and bridges in protection the damages parameters. The reinforcement of structural elements using the GFRP and CFRP in general is focused in bond behavior such mutual adhesion between concrete and reinforced bars interfaces. Bond mechanism is based on the transfers of effort between the bars and concrete occur three mechanisms: (1) Chemical adhesion between bars and concrete; (2) Mechanical interlocking arising from the textures on the bar surface and (3) Frictional forces arising from the roughness of the interface between the bar and surrounded concrete. Due to a lower modulus of elasticity of FRP bars, the design of FRP reinforced concrete members is governed by serviceability state rather than ultimate state. Crack width calculations include the effect of bond between FRP bars and surrounding concrete. This is considered in FRP design code and guides through the so-called bond depend coefficient (k_b). The different products of FRP bars with different surface configurations and mechanical properties (such as sand-coated, helically-grooved, deformed etc.) present the differences influenced in bond performance. The bond between concrete and FRP bars depends on many factors such are bar surface, bar diameter, concrete class, etc. It was noticed that there has been a tendency for FRP bars of larger diameter to show lower bond strength. Thus, the variations of surface configuration, bar diameter and concrete strength are expected to affect the bond depend coefficient kb. This article presents an investigation of determine bond-depend coefficient kb of different types and diameter of FRP bars with different surface configuration, moreover it compares current kb values recommended by FRP design codes and experimental results.

2. EXPERIMENTAL WORK

Fifteen reinforced beams were prepared for testing, with dimensions:

220×130 mm and span 2000 mm. Five sets with three samples, from which twelve are reinforced with GFRP and CFRP bars and three with conventional steel bars. The concrete beams are reinforced in down layer using the GFRP, CFRP and conventional steel, and in upper zone the conventional steel bars and in all beams were applied steel stirrups presented in fig.1. Concrete mixes design was prepared with requested class of concrete C30/37. Testing set up of beams is done based on the procedure and measurements used in this case, LVDT in critical positions for analyzing the cracks, deflections and displacements, a LVDT was used to measure the width of the first flexural crack in the beam right under the concentrated force. The beam was observed during the test until the first flexural crack appeared. As soon as it appeared, the load was paused until the initial crack width was measured on the beam's side surface. Also, compression concrete zone was instrumented with LVDT to measure the strain of concrete, and another LVDT was positioned in the mid spam of beam to measure the deflection presented in fig.1.

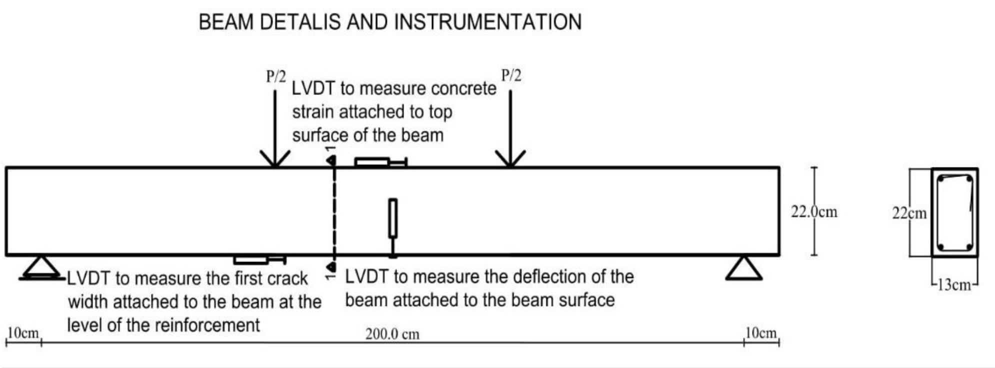

Figure 1: Beam details and instrumentation and geometrical parameters of concrete beams

According the Standard ASTM D 7205 first are determinate the mechanical properties of reinforced FRP bars. In the edges of the bars were set metallic shells in order to avoid constriction of the FRP bars shown in Figure 2. The properties of conventional steel are used from known parameters based on the previous research works for S500. FRP bars used in our research were two types: GFRP (helically grooved) and CFRP (sand-coated).

Figure 2: Determination of mechanical properties of reinforced bars (GFRP & CFRP)

Table 1: Mechanical properties of used GFRP and CFRP bars

	GFRP			CFRP	
d (mm)	Ø6	Ø8	Ø10	Ø8	Ø10
Strain ε^*_{frp}	0.0204	0.0234	0.0256	0.0095	0.015
Tensile strength [MPa]	1022.10	1108.2	1194.3	1265.4	2000
Elasticity modulus [GPa]	55			155	

2.1 Prediction of Adhesion coefficient k_b

The determination of kb, based on the ACI derived by cracks, using modifying the Gergely–Lutz equation (1). Some typical kb predicted values for deformed GFRP bars cited in ACI are between 0.8 and 1.80. But the ACI Codes and Manuals suggested that designers assume a value of 1.2 for deformed GFRP bars unless more specific information were available for a particular bar.

$$w = 2.20 \frac{f_{frp}}{E_f} \cdot \beta \cdot k_b \cdot \sqrt[3]{d_c \cdot A} \tag{1}$$

w - cracks

It should be mentioned that the recommended kb values provided by design codes and guides in the absence of experimental test data depend only on the surface configurations of the FRP bars. According to CSA, kb should be determined from the measured crack widths and strains in the FRP bars at the service stage. The value of kb, according to experimental data can determine with the following equation (2). This equation includes the measured value of cracks.

$$k_b = \frac{E_f \cdot w}{2.20 \cdot \beta \cdot f_f \cdot \sqrt[3]{d_c \cdot A}} \tag{2}$$

3. TEST RESULTS AND DISCCUSION

As we can see in the figure 3, except vertical cracks also was appeared horizontal cracks, which is an indication of failure of bond mechanism between concrete and FRP bars. The GFRP bar exhibits a stiff behavior at the beginning of loading. At increased loads, the bar, in comparison with the other bars, shows a considerable slip with a ductile behavior.

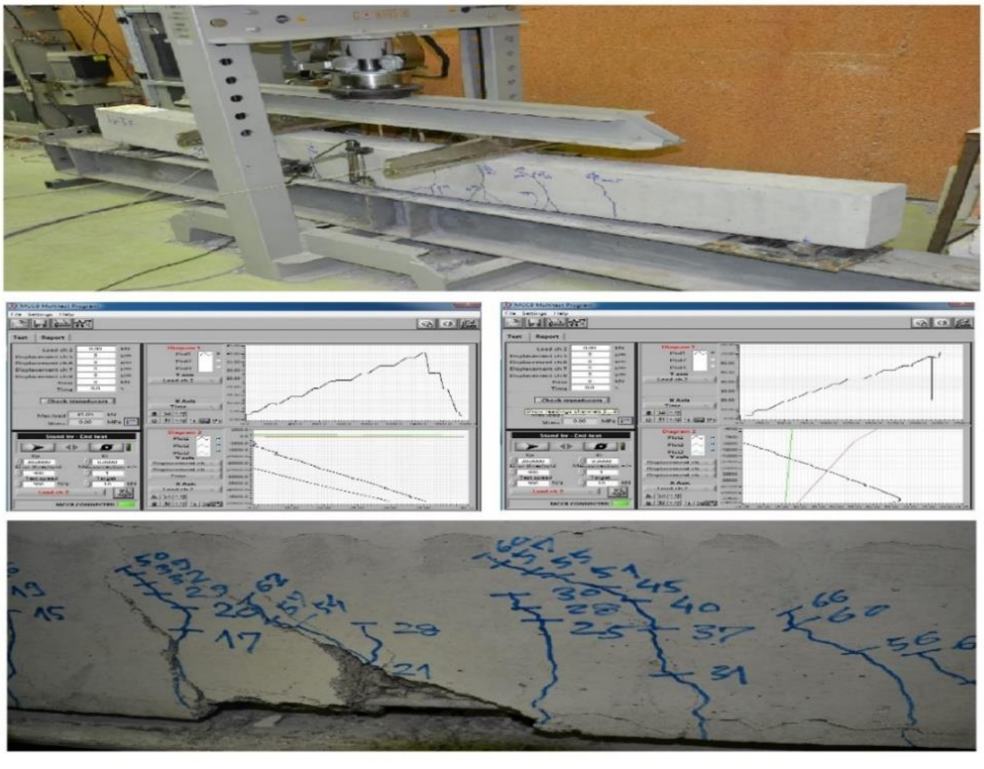

Figure 3: Cracks in longitudinal span of testing beam

The adhesion parameter values (bonding effect) based in our experimental data are present in following table 2, and average value from three beams of sets and presented in figure 4.

Table 2: Adhesion values: two stages: under SLS and 75 % of apply loading

Set	Bar diameter (mm)	Bar type	k_b "SLS"	k_b (M/Mu - 75%)
S_1B_1	6	GFRP	1.09	1.33
S_2B_2	8	GFRP	1.40	1.68
S_3B_3	10	GFRP	0.70	1.04
S_4B_2	8	CFRP	1.04	0.88
S_5B_3	10	CFRP	1.03	1.05
S_5B_1	6	Steel	1.74	/
S_7B_2	8	Steel	0.78	/
S_8B_3	10	Steel	1.0	/

*Notes SiBi- Set i and Beam i

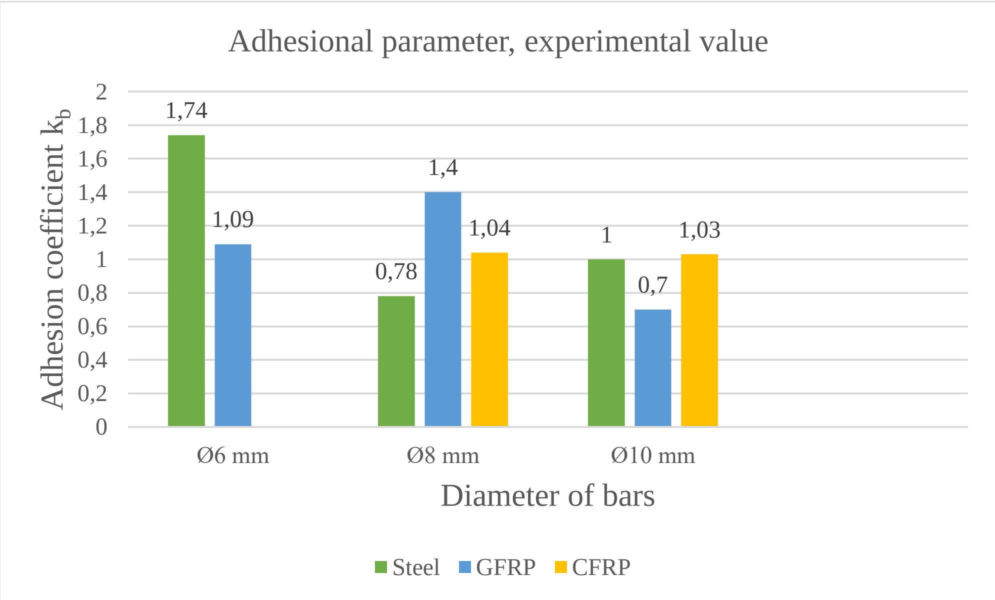

Figure 4: Difference between theoretical and experimental values of adhesion parameter "k_b"

3.1 Analyzing and compare the results between theoretical and experimental data

The predicted section, predicted crack width of FRP-RC beams using the $\mathbf{k_b}$ values recommended by different FRP manuals and Codes is not available, yielded differenced in most cases, and using the same value for different FRP bars with the same surface configurations. The interference of the width of cracks is directly in relation with "$\mathbf{k_b}$" and for width less than 1.0 mm, in our case analyzing with SLS. The analytical using value of "$\mathbf{k_b}$" has the different compare with the experimental results in different type of bars, presented in fig.4. As we could see from the results the beams reinforced with CFRP have shown better behavior than beams reinforced with GFRP. This is because GFRP bars have lower modulus of elasticity than CFRP bars. The failure of beams reinforced with GFRP occurred because of GFRP bars rupture or concrete rupture, while failure of beams reinforced with CFRP bars occurred because of sliding of CFRP rebars.

4. CONCLUSIONS

The aim of this study is focused in investigation the $\mathbf{k_b}$ value depends of the FRP type bars, bars diameter and for typical concrete compression strength.
Based on the experimental results we provide the following results:

- Effect of the bars diameter of FRP influenced in bond coefficient ($\mathbf{k_b}$) value is not linear but is different comparing the analytical and experimental results, focused in GFRP, based on the surrounding surface contact with concrete.
- The calculated strains using cracked section analysis and calculations the k_b is recommended by CSA, which is closer with experimental results.
- Generally, the average k_b of CFRP bars were smaller than the GFRP bars with same diameter.
- The research predicts using the value of k_b but just in case of absence of experimental results, because in many cases will be different and non-applicable.

REFERENCES

[1] ACI 440.1R-06; Guide for the Design and Construction of Concrete Reinforced with FRP Bars", ACI Committee, 2006
[2] L.C.Bank; Composites for Constructions: Structural Design with FRP Materials", John Willey &Sons, New York, 2006
[3] N.Kabashi, at.al; Flexural Behavior and Cracks in Concrete beams reinforced with GFRP bars, ICPIC 2018, Washington DC, 2018
[4] Baena, M., Torres,.Turon,A. and Barris,C.: Experimental Study of bond behavior between concrete and FRP bars using pull-out test, Journalof Composites, Engineering Part B, 2009
[5] CNR-DT 2032006; Guide for Design and Construction of Concrete Structures Reinforced with Fiber-Reinforced Polymer Bars" National Research Council, Rome; Italy,2006
[6] CSA-S806-02; Design and Construction of Building Components with Fiber Reinforced Polymers" Canadian Standards Association, Ontario, 2002.
[8] R.Tepfers,L.De Lorenzis; Bond pf FRP Reinforcement in Concrete-A challenge; Mechanics of Composite Materials, Vol. 39, No. 4, 2003
[9] McCallum, B.E.C., and Newhook, J.P. (2012). Evaluation of the bond dependent coefficient and parameters which influence crack width in GFRP reinforced concrete. Proceedings of the Sixth International Conference on Advanced Composite Materials in Bridges and Structures. ACMBS VI, Kingston, Ontario, Canada, May 22–25,8 p.
[10] CEB-FIB, Bulletin 40

EXPERIMENTAL STUDY ON FLEXURAL DAMAGE OF RC PIERS HAVING CUT-OFF REBARS

Hisako KOBAYASHI (1) and Kaoru KOBAYASHI (2)

(1) East Japan Railway Company, Japan

(2) JR East Consultants Company, Japan

Abstract

Many reinforced concrete (RC) piers have cut-offs where the number of rebars in the longitudinal direction are reduced according to the cross-sectional force.

Usually RC piers receive damage at their bases. Thus, for RC piers set in a river, it is expected that recovery work after an earthquake would require huge temporary construction facilities and result in large expenses and work time.

If damage occurs above the water surface where recovery work can be easily done, more reasonable seismic design of RC piers including recoverability can be achieved (Figure 1).

In this research, we carried out cyclic loading tests using specimens where flexural damage is predominant at an intermediate section of the pier frame.

In this report, we studied deformation performance based on the cyclic loading tests.

Specimens had no hoop rebar around the cut-offs section and had the spiral rebar on the core concrete in the same section.

As a result, in the specimens in which the spiral rebar spacing was changed, in the load-displacement relationship after the load was lowered, the load drop of the specimen with the smallest spiral rebar spacing was gentle.

And the angle of rotation was 1/10 of specimen with half of the yield loading.

Keywords: cut-off point, Cyclic loading test, Flexural damage, ductility factor

1. INTRODUCTION

On October 23, 2004, the Niigataken-chuetsu earthquake, with a magnitude of Mj=6.8, occurred in Japan. Figure 2 shows the cover concrete can spall in the Niigataken-chuetsu earthquake. This damage was showed in the Higashi-nihon-taiheiyo-oki earthquake on March 11, 2011.

With a design that prevents damage at cut-offs, however, damage can occur at the pier bases, making it difficult to find damage of RC piers that are set in rivers or underground.

We have been studying a structure that can make flexural damage occur at the cut-off point of RC piers excellent in elastoplastic energy absorptivity. The aim of intentionally allowing damage in the intermediate section of a pier frame is to facilitate easier checking and detection of damage and thus earlier recovery.

In this basic study, we conducted cyclic loading tests using specimens with different pitches of the inner spiral reinforcement as parameters to check the deformational characteristics of RC piers having cut-off rebars.

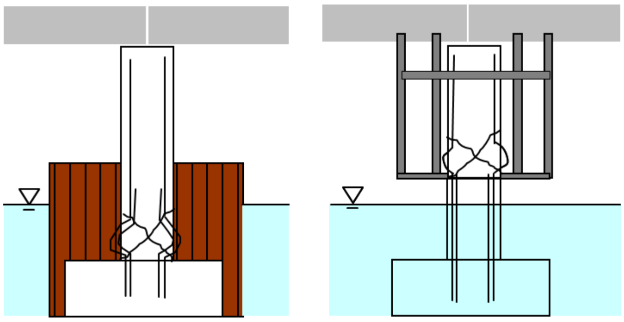

Figure 1: Images of RC piers repairing

Figure 2: Damage of RC piers after the earthquake

2. EXPERIMENTAL PROGRAMS

2.1 Outline

The specimens and parameters used in the experiments are given in Table 1. Table 2 is a material specification, and Figure 3 shows a reinforcement arrangement and a shape of the specimens.

Assuming RC piers of common railway structures, we used model specimens of approx. one-third scale. The longitudinal rebar had cut-offs, the rebar diameter was D10, and the thickness of the cover concrete was 35 mm. The diameter of the inner spiral reinforcement was 180mm. As shown in Figure 3, the length of the area provided with inner spiral reinforcement was 1D (350 mm) + 100 mm above and below that (550 mm total), with the cut-off at the middle. In order to more clearly identify the effect of inner spiral reinforcement, we used easily removable D6 tie hoops of right-angled hooks at 150 mm pitch.

Table 1: Specimens and parameters for experiment

Specimen No.	B*H	a (Sheer span)	d (effective-depth)	co (height of cut-off)	Longitudinal rebar arrangement		Inner spiral reinforcement			axial force
	mm	mm	mm	mm	cut-off	base	φ	pitch(mm)	number	Mpa
No.1	1050*350	2200	315	1000	D10*13	D10*24* 2layers	9	20	4	0.60
No.2	1050*350	2200	315	1000	D10*13	D10*24* 2layers	9	40	4	0.60
No.3	1050*350	2200	315	1000	D10*13	D10*24* 2layers	9	60	4	0.60

Table 2: Material specifications

Specimen No.	Compressive strength of concrete (Mpa)		Yield strength of steel bar (Mpa)	
	Pier	footing	longitudinal rebar	Inner spiral reinforcement
No.1	27.2	32.4	387	336
No.2	21.8	27.7	414	336
No.3	20.9	21.6	387	339

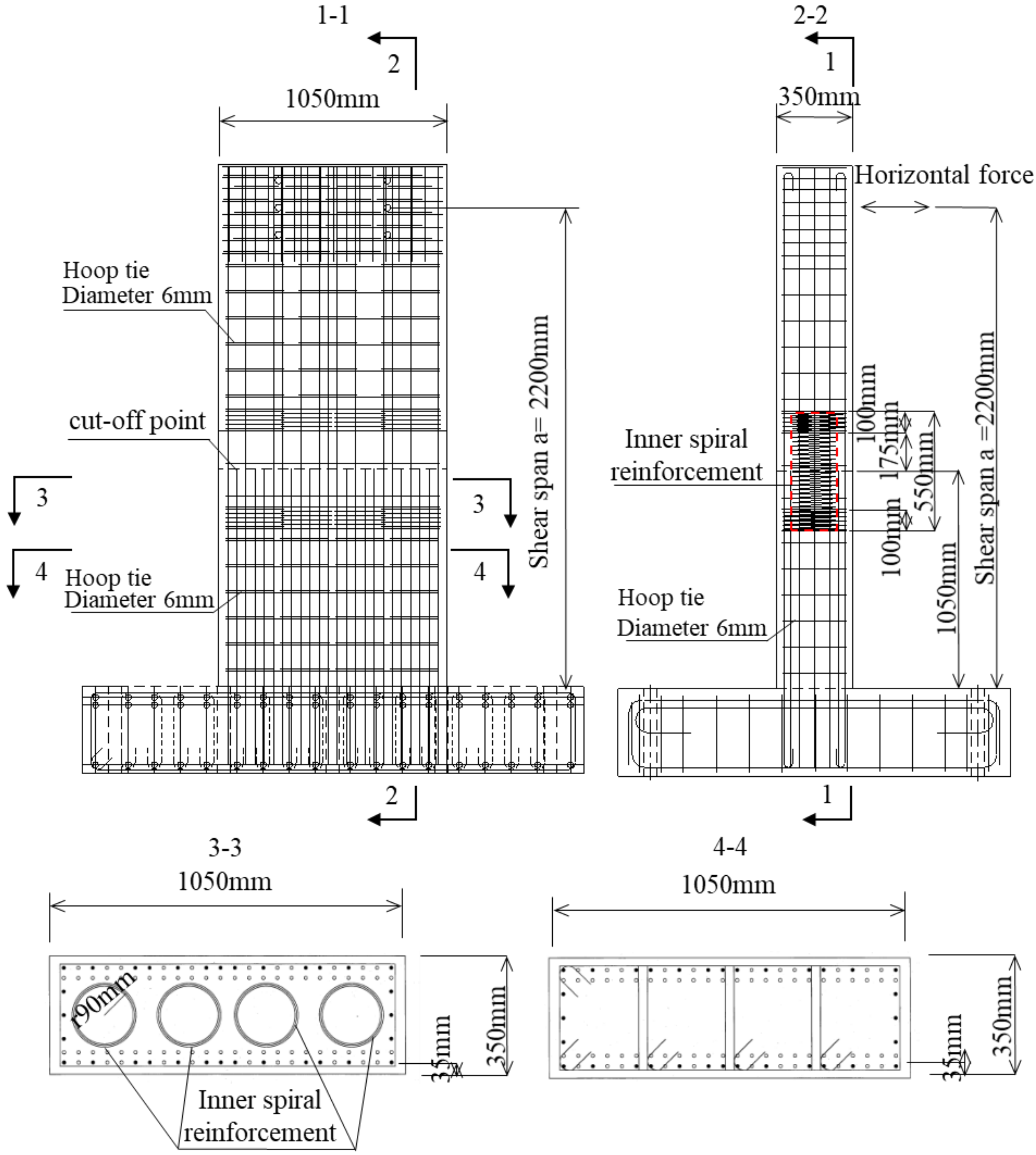

Figure 3: Reinforcement arrangement and a shape of the specimens

Table 3 shows calculated result of specimens. The ratio of calculated shear capacity to flexural capacity of the specimens is between 2.81 and 3.14 under the rebar cut-off point and between 2.81 and 3.06 above the rebar cut-off point. We avoided remarkable shear damage, based on the past studies[1][2]. The flexural performance ratio at the rebar cut-off point at the bending yield is between 0.75 and 0.76.

Table 3: Calculated result of specimens

Specimen No.	Vmy[1] (kN)	Vmu[2] (kN)	Vmyc[3] (kN)	Vmuc[4] (kN)	Vyc[5] (kN)	Vy /Vmy	Vyc /Vmyc	My (kN・m)	Myc (kN・m)	Myc /Mxyc[6]
No.1	166	193	126	145	386	3.14	3.06	366	152	0.76
No.2	175	202	132	151	370	2.81	2.81	386	158	0.75
No.3	161	187	123	141	369	3.04	3.01	355	147	0.76

1)Vmy=My/a
2)Vmu=Mu/a
3)Vmyc=Myc/(a-co), Myc: Yield bearing capacity at cut-off point
4)Vmuc=Muc/(a-co), Muc: Ultimate bearing capacity at cut-off point
5)Vyc: Yield sheer strength at cut-off point
6)Mxyc=My*(a-co)/a

2.2 Loading test method

Figure 4 shows the specimen overview.

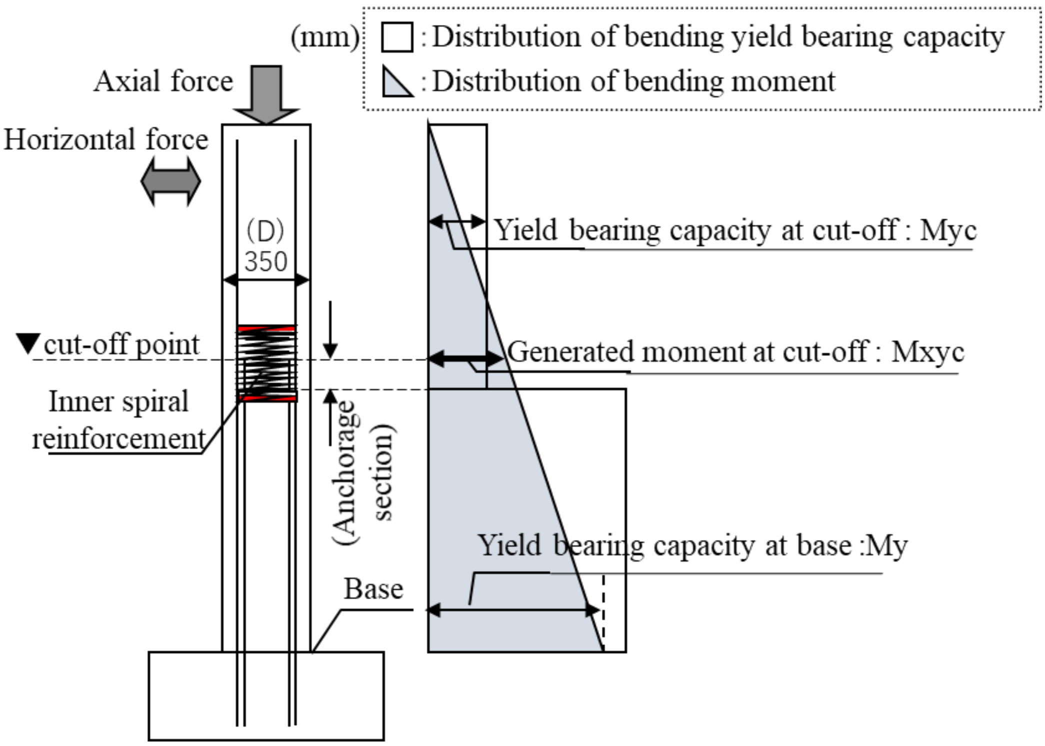

Figure 4: Specimen Overview

In the cyclic loading test, we defined as "yield displacement δy " the horizontal displacement of the load point at the point when the strain of the main reinforcement of the specimen base on the outermost edge in the loading direction reached the yield strain. We applied loads, sequentially increasing the displacement amplitude by the integral multiple of horizontal displacement n *δy (n=1,2,3…,12,14,16 δy after 10 δy). No.2 and No.3 were loaded by the integral multiple of horizontal displacement n *δy (n=1,2,4,6,8,10,12,14 δy) to prevent rebars from fatigue damage by loading cycle.

3. EXPERIMENTAL RESULTS

3.1 Load-displacement relationship and Strain of steel bar

Figure 5 compare the experimental load-displacement relationships.

In specimen No.1, the cover concrete spalled at 5 δy, and the longitudinal rebar started to bulge around the cut-off point at 6 δy, the load fell to 50% of the yield load at 12 δy, (82.19kN). The Inner spirals reinforcement exposed at 14 δy.

This load-displacement behaviour of specimen was observed other specimens. Three specimens were similar classification of damage modes with which the longitudinal rebars yielded and failed near the rebar cut-off point.

No.1, No.2, and No.3 has different pitches of inner spiral reinforcement at 20 mm, 40 mm, and 60 mm respectively. As the pitch larger, the load becomes large and the maximum load is maintained up to approx. 6δy (displacement of 100 mm), while the load tends to drop in the area of large deformation after around 10 δy (displacement of 165mm).

In Figure 5, the shapes of the envelope curves are the same to 8 δy. With No.2 and No.3, the envelope curve that shows mild load drop unique to inner spiral reinforcement was not seen after around 8 δy (displacement of 133mm), while the load mildly drops with No.1.

And Figure 6 shows strain of longitudinal rebar at yield and ultimate. The load dropped to approximately under yield load is regarded as the ultimate load.

In Figure 6, the yield strain of longitudinal rebar is the same. But, the ultimate strain of it

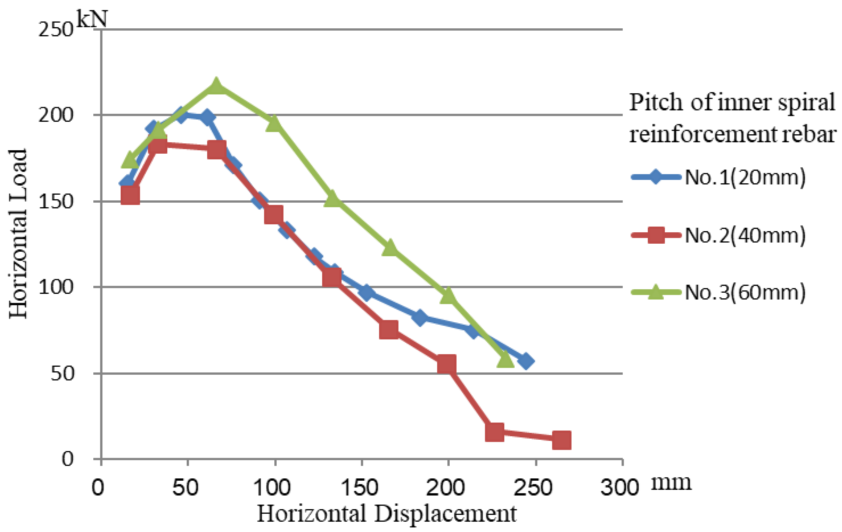

Figure 5: Load-displacement relationships

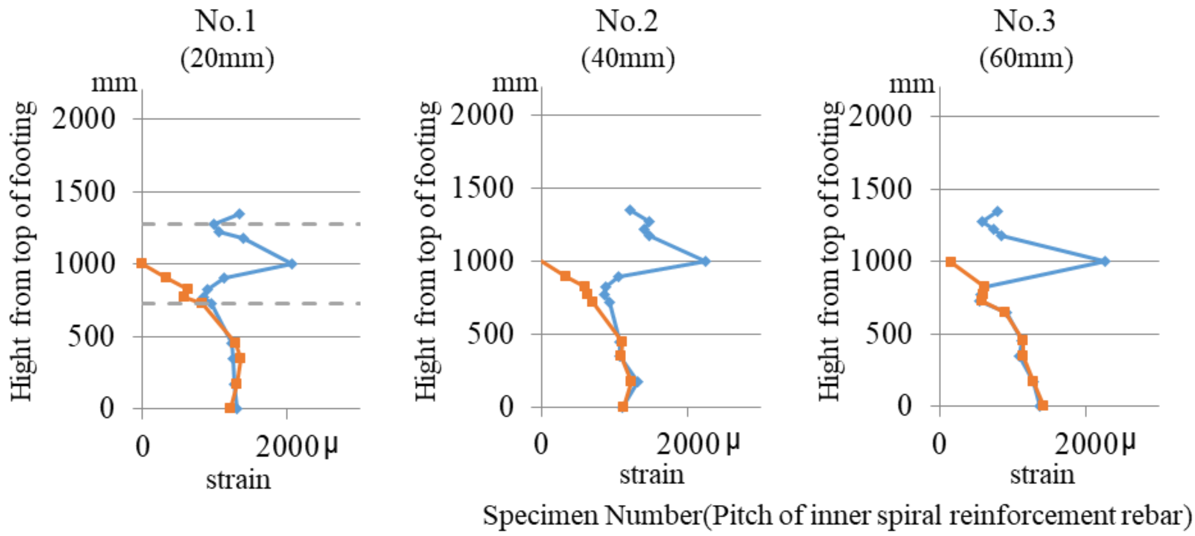

Yield strain of longitudinal rebar

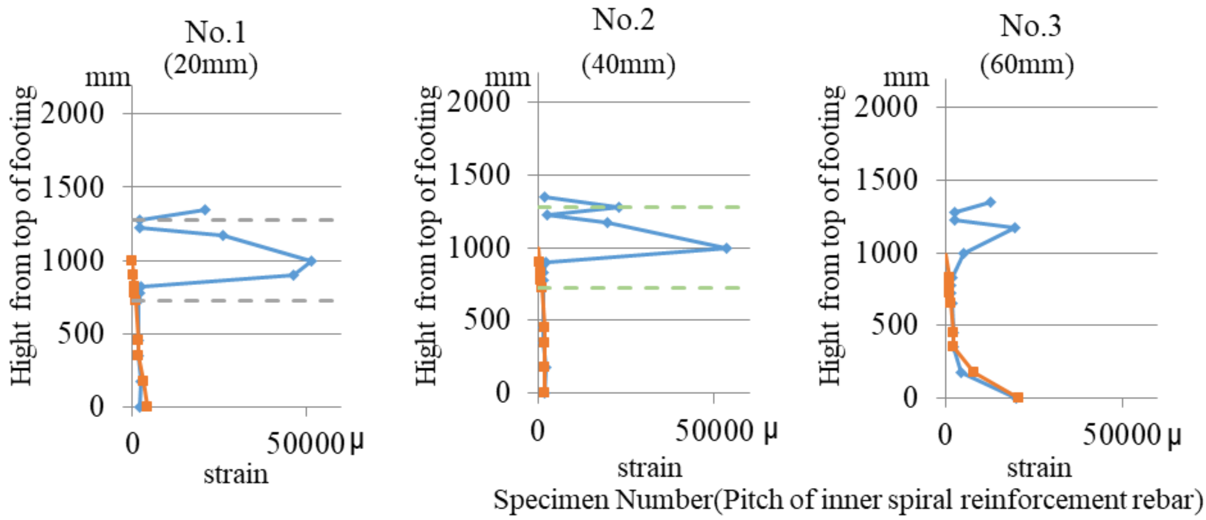

Ultimate strain of longitudinal rebar

Figure 6: Strain of longitudinal rebar at yield and ultimate.

are different. The difference is showed in specimens No.3, the strain around the cut-off point are smaller than No.1 and No.2. From this also, No.3 was damaged relatively slight of other specimens at ultimate of specimens.

Figure 7 shows the failure properties when exposing inner spiral reinforcement. We had checked the level of soundness of the core concrete in the inner spiral reinforcement after the tests, we found no crushing.

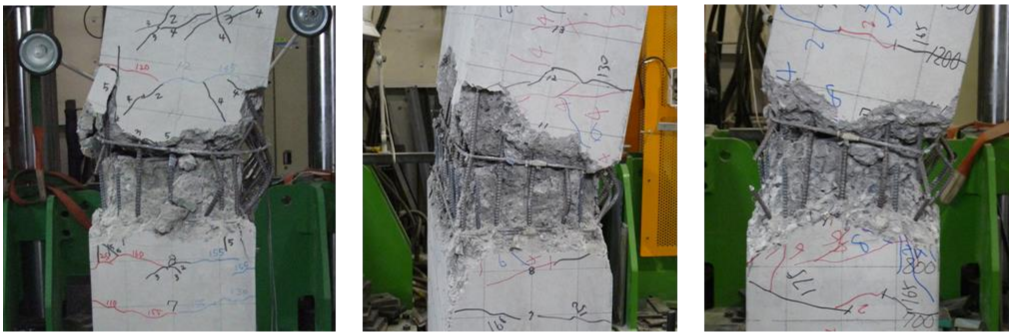

Figure 7: Comparison of failure around the cut-off point

3.2 Ductility factor and Angle of rotation

Yielding of a member, the yield load, and the yield displacement were each assumed to be the state when the cross section of the pier bottom reaches yield, the calculated load at the time of yield, and the measured displacement under the yield load.

Table 4 shows the yield load (Py), the maximum load (Pmax), yield deformation (δy), ultimate deformation (δu), ductility factor (δu/δy) of each specimen. The yield load, the maximum load and ductility factor were largest with No.3.

Table 5 shows the angle of rotation. θsp is the angle of rotation when exposing inner spiral reinforcement. A roughly similar trend as ductility factor is found. It is seen that the angle of rotation θu increases from 0.0380 to 0.0526 with pitch of inner spiral reinforcement, indicating that a longer pitch of inner spiral reinforcement is an effective way to increase ductility factor. The angle of rotation θsp were approx 1/10 of all specimens with between 55 kN to 75 kN loading. Especially, the angle of rotation was 0.0971 with No.1 which maintained 75kN loading. After entering the area of large deformation, load bearing ability drops more with larger pitch.

Table 4: Ductility factor

Specimen No.	Py(kN)	Pmax(kN)	δy(mm)	δu(mm)	δu/δy
No.1	161	200	15	84	5.48
No.2	154	183	17	89	5.32
No.3	174	218	17	116	6.97

Table 5: Angle of rotation

			(rad)
Specimen No.	Angle of rotation θy	Angle of rotation θu	Angle of rotation θsp
No.1	0.0069	0.0380	0.0971
No.2	0.0076	0.0404	0.0900
No.3	0.0075	0.0526	0.1054

4. CONCLUSIONS

From the cyclic loading tests using RC pier model specimens of 20 mm to 60 mm inner spiral reinforcement rebar pitch, we obtained the following results related to cut-off damage.

- Load bearing ability according to the pitch of the inner spiral reinforcement is the same until the load dropped to under yield load.
- After entering the area of large deformation, load bearing ability drops more with larger pitch.
- Inner spiral reinforcement rebars were effective to confine core concrete under the area of large deformation.

REFERENCES

[1] Tadayoshi Ishibashi, Takeshi Tsuyoshi, Kaoru Kobayashi, Masashi Kobayashi, "An Experimental Study on Damage Levels and Repairing Effects of Reinforced Concrete Columns Subjected to Reversal Cyclic Loading with Large Deformation" Japan Society of Civil Engineers, *Journal of Materials, Concrete Structure and Pavements*, Vol.47, No.648(May 2000):55-69

[2] Railway Technical Research Institute, comp. Railway Bureau, Ministry of Land Infrastructure, Transport and Tourism edit., *Design Standards for Railway Structures and Commentary (Concrete Structure)*, Maruzen Company Limited (April 2004)

CORROSION INITIATION ASSESSMENT OF CONCRETE COMPONENTS OF WIND TURBINES: OVERVIEW AND CHALLENGES

Emilio Bastidas-Arteaga (1), Syed Y. Alam (1), Xiao-Hui Wang (2) and Yue Li (3)

(1) University of Nantes, Centrale Nantes, Institute for Research in Civil and Mechanical Engineering, CNRS UMR 6183, France

(2) College of Ocean Science and Engineering, Shanghai Maritime University, China

(3) Department of Civil Engineering, Case Western Reserve University, USA

Abstract

Reinforced or prestressed concrete components are to be placed in a severe marine environment for floating wind turbine (FWT), resulting in increasing reinforcement corrosion risks and reducing durability. Therefore, a comprehensive corrosion initiation assessment becomes crucial to optimize the service capacity and safety of the wind turbine to reduce the cost associated with construction, inspection, repair and loss of power generation. In this context, the first part of this paper provides an overview of the key factors for corrosion initiation assessment and existing assessment approaches. The second part of the paper focuses on the different challenges that should be addressed to provide a comprehensive corrosion initiation assessment. It was found that further research is required to perform a lifetime assessment that combines the effects of chloride ingress and cyclic load in a stochastic framework. One of the major challenges will be to deal with non-linearities of deterioration models and the higher dimension of the stochastic problem.

Keywords: Reinforced Concrete, Chloride ingress, Corrosion, Fatigue load, Wind turbine, Reliability

1. INTRODUCTION

Wind is a renewable energy source that can help to reduce future carbon emissions and meet the increasing demand for energy for a growing world population. Currently, most of the wind energy generation is located onshore. By the end of 2016, the worldwide wind capacity had reached 486 GW with onshore capacity accounting for around 97% of it [1]. However, space limitation, visual impact, and noise generated by onshore wind turbines led to a shift to offshore windfarms [2]. Without the issues of visual impact and noise, design of wind turbines can focus on efficiency. In addition, offshore locations provide higher and steadier wind speeds [3] and the possibility of using larger turbines. Currently, majority of global offshore wind farms are located in Europe [3]. There are 81 offshore wind farms in 10 European countries with a cumulative installed capacity of 12,631 MW [4]. Offshore wind farms are more expensive (1.5 – 2 times [5]) relative to onshore farms due to the cost of the towers, foundations, underwater cabling, installation and maintenance [6]. However, higher winds offshore implies greater productivity that may offset some of the costs. In addition, proper reliability-based design, lifetime assessment and optimal maintenance planning of offshore wind farms will result in great reduction of costs, making them more economically competitive and removing the main obstacles of its deployment.

France aims to install 6000 MW of floating offshore wind farms in the horizon 2030 in areas where water depths are greater than 40 m. Some floating wind turbine (FWT) are constituted by reinforced or prestressed concrete (RC) components, e.g. XCF-CETEAL, IDEOL (France, Figure 1) and Windcrete (Spain). FWT will be placed in a severe environment characterised by complex mechanical actions (cyclic loading) and mechanisms of degradation (corrosion, fatigue, bio colonisation, etc.), which significantly affect their durability and increases reinforcement corrosion initiation risks [7]. The corrosion can affect the service capacity and safety of FWT resulting in significant inspection, repair and loss of production costs [8].

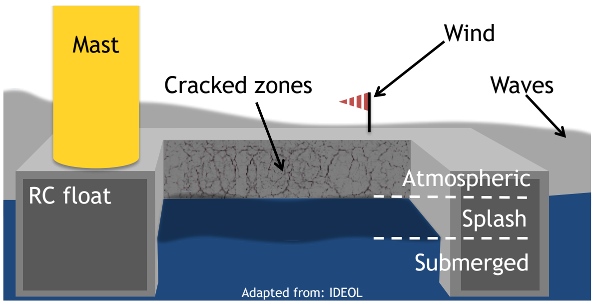

Figure 1: Interaction between metocean conditions (fatigue loading), concrete cracking and chloride ingress for a RC float

In this context, a comprehensive lifetime assessment of corrosion initiation risks will be therefore crucial to optimise the durability performance of FWT. Thus, the objective of this paper is to provide an overview of the current practices and further challenges that should be addressed to improve the corrosion initiation assessment of RC components of FWT.

2. CORROSION INITIATION LIFETIME ASSESSMENT

Under service conditions, the RC components of FWT will be subjected to complex cyclic mechanical loading generating multiaxial stresses of varying amplitude and with various stress ratios. These stresses will be characterised by very high load frequencies (Figure 2 [9,10]) and produce concrete cracking. In parallel, chloride ingress from the surrounding environment leads to corrosion initiation when a significant amount of chlorides reaches the reinforcing bars or tendons [11–14] (Figure 3). Chloride ingress could be accelerated in a cracked concrete [15] and therefore produce premature corrosion initiation. Corrosion will generate a significant reduction of structural lifetime, increase maintenance costs and compromise structural serviceability and safety [8,16]. The following sections will describe the single and combined deterioration mechanisms affecting corrosion initiation.

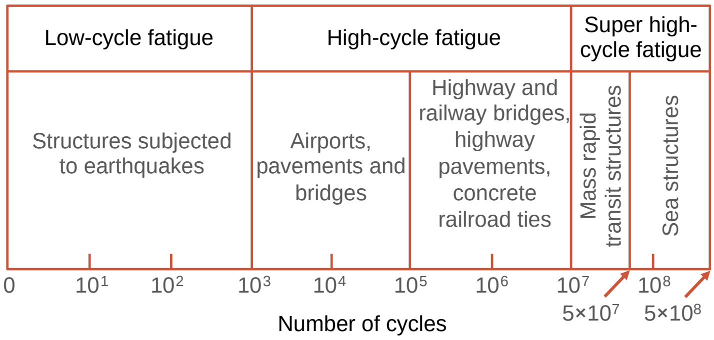

Figure 2: Fatigue loading spectrum for infrastructure (Adapted from [10])

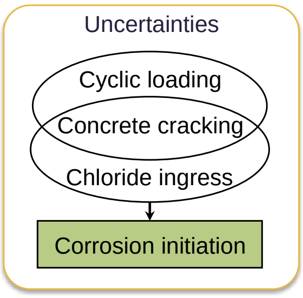

Figure 3: Deterioration processes leading to corrosion initiation

2.1 Chloride ingress

Chloride ingress into RC (or chlorination) is the main mechanism leading to corrosion initiation for coastal and offshore RC structures. To simulate chloride ingress into concrete, Fick's diffusion law [17] has been widely used and considered as an acceptable approach with more or less complex analytical [18,19] and numerical [20–25] solutions. The numerical solutions can be used to model chloride ingress at given exposure zones: submerged, splash and atmospheric [20–22]. These models provide the evolution in time of the concentration of chlorides inside the concrete that is used to estimate the time to corrosion initiation. The more advanced models are able to account for realistic environmental conditions (temperature, relative humidity, etc.), several chloride ingress mechanisms (diffusion, convection, capillarity, etc.), interaction between chlorides and other ions, concrete cracking and boundary conditions (saturation, wetting-drying cycles, etc.). Most part of these models are based on numerical methods and require solving in time non-linear and coupled partial differential equations.

2.2 Concrete cracking under cyclic loading

Several studies have been conducted to study fatigue of concrete under uni- and multiaxial loads. Most part of experimental works focused on uniaxial compression loads because it is very difficult from a technical point of view to set up multiaxial fatigue tests. Multiaxial fatigue studies mainly consider bi or triaxial loading. Some studies focused on the fatigue behaviour of concrete subjected to biaxial stresses [26,27]. These studies found that the damage is reflected by the appearance of cracks during the first cycles and that the fatigue behaviour was subsequently governed by the propagation of these cracks. For triaxial fatigue tests, other studies [28–30] found that the fatigue resistance depends on the magnitude and amplitude of the applied stresses. On the basis of the cyclic stress-strain curve, they defined a strain modulus in fatigue and established damage models based on the relation between the fatigue strain modulus and the number of cycles. More recently, Zhao et al. [31] performed triaxial tests with constant and variable amplitude. Experimental results have shown that for variable amplitude fatigue loads, the residual fatigue stress is related to the relative fatigue cycle and the lateral compression stress rate, but has little relation to the loading process. Previous works illustrated the complexity of the multiaxial fatigue problem in concrete. It should be noted that the fatigue behaviour will be influenced by several factors. For example, the type of stress (traction, compression), level of confinement, magnitude and speed of application of the loads, and concrete formulation [32].

Modelling the behaviour of concrete under cyclic loading is not an easy task. Classical approaches to model fatigue are: (1) Wöhler curve or total fatigue life approach; (2) Linear Elastic Fracture Mechanics (LEFM); and (3) Continuum damage mechanics.

The Wöhler approach estimates total fatigue life without distinction between the number of cycles required to initiate fatigue cracks and propagate it up to a critical size. Fatigue life curves for concrete could be found in different standards (e.g. [33]) and could be used to estimate the total fatigue life of a RC component under a given number of cycles and stresses level. However, with this approach it is difficult to consider that one structure will be subjected to loads with different levels of intensity and frequency as well as the accumulation of damage.

LEFM focuses on estimation of the number of cycles required to propagate a crack up to a critical size from an existing crack. This approach has been used for several studies to predict the propagation of cracks in concrete [34,35]. Nevertheless, it is difficult to implement it to study the nucleation and propagation of several cracks in a whole beam.

Continuum damage mechanics (e.g., Mazars formulation [36]) represents a more comprehensive way the behaviour of concrete under cyclic loads. Similarly to comprehensive chloride ingress models, continuum damage approaches require finite elements analysis.

2.3 Combined effects

Quantifying the effects and modelling the combined action of chloride ingress and fatigue-induced concrete cracking for RC structures are very difficult tasks. Experimental research work dealing with chloride ion penetration in cracked concrete considered several techniques for generating cracks [37–39]. Although the above-mentioned research works highlighted the importance of considering cracks as a major influencing factor for chloride ingress processes, most of the tests were realised in concrete specimens without reinforcing bars. On the other hand, field surveys have reported the significant influence of concrete cracking on the chlorination mechanism and then on the corrosion initiation time of reinforcing bars. For example, a field survey of 57 bridges in Kansas, USA, has indicated that the chloride concentration at a depth of 76 mm from the location of a surface crack exceeded the corrosion threshold of conventional reinforcement within the first year [40]. Another survey of 219 marine structures along the Norwegian coastline showed that the signs of corrosion could be seen as early as 5-10 years for cracked concrete [41]. This early time for corrosion initiation greatly influences the whole lifetime assessment of the RC structures; especially for RC components of FWT whose design lifetime varies between 20 and 30 years.

Experimental studies involving chlorination in cracked concrete are very useful for improving the understanding of the deterioration process as well as modelling and lifetime purposes. For example, some authors [37,38] identified functions and factors to account for the effects of concrete cracking on the chloride diffusion coefficient. Such functions and factors are introduced in chloride ingress models to estimate the time to corrosion initiation by considering cracking effects. Numerical solutions comprehensively account for the complex interactions among physical and chemical mechanisms, which are inherent to chloride ingress.

2.4 Uncertainties and spatial variability

An accurate assessment of the time to corrosion initiation for RC floats also requires taking into account the various sources of uncertainty and spatial variability related to the problem: material, construction, inspection, cyclic loading, models, etc. Evaluating the reliability of structures subjected to deterioration processes and fatigue is a very complicated task. It involves the interaction of different scientific domains such as deterioration, damage continuum mechanics, nonlinear analysis and reliability approaches. Petryna et al. [42] evaluated the reliability of RC structures under fatigue loading. They considered a two-scale mechanical model coupled with a probabilistic approach (response surface) and validated with experimental results. They compared their results with those obtained by local and linear fatigue models and found that the latter cannot be applied at the scale of the structure. Concerning chlorination, there are also significant uncertainties and spatial variability mainly related to material properties and environmental exposure conditions [18,19,43–45]. Bastidas-Arteaga et al. [7] proposed a probabilistic approach to estimate the service life of reinforced concrete structures subjected to corrosion and fatigue of reinforcement. This work has shown that environmental conditions and loading have a great influence on the service life of the structure; however, they have not considered the effect of concrete cracking. More recently, Wang et al [15] performed accelerated chlorination tests on cracked RC beams to characterise the effect of pre-exposure loading on the probabilistic assessment of the corrosion initiation time. They found that considering pre-exposure loading conditions that generate cracks has an important effect on the assessment of the time to corrosion initiation (Figure 4). It is therefore observed in Figure 4 that a threshold probability of corrosion initiation of 0.5 occurs at 20 yr (unloaded condition) but it could take place early at 13 and 10 yr for static and fatigue loading conditions, respectively.

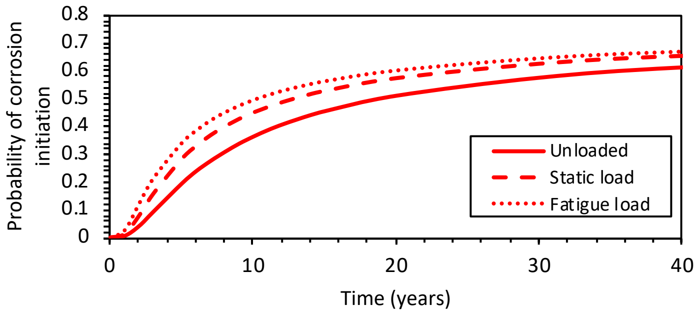

Figure 4: Probability of corrosion initiation for several load conditions.

Concerning spatial variability, Stewart [45] found that there is an appreciable increase in probabilities of failure when spatial variability of deterioration process is included in the analysis in comparison with probabilities of failure based on the mid-span limit states only. This finding strongly suggests that as well as uncertainties, considering spatial variability would lead to significant decreases in structural reliability of deteriorating RC members. Thus, previous works indicated that quantifying and propagating uncertainties and spatial variability in coupled chlorination and fatigue processes becomes crucial for improving its design and lifetime assessment.

3. CHALLENGES

Improving the corrosion initiation assessment of RC components of FWT requires significant model improvements on existing deterministic and probabilistic frameworks. The efforts carried out during the last decades to improve the assessment of corrosion initiation for RC structures placed in coastal and offshore locations provided numerical models that are able to account for realistic exposure conditions. However, these models require a significant number of input parameters and a certain degree of expertise to be used correctly. Taking into account the computational cost, most part of studies and applications focused on corrosion initiation assessment considering one-dimensional chloride ingress for particular exposure zones (submerged, splash and atmospheric). However, RC floats will be exposed simultaneously to all these zones (Figure 1), and therefore, chloride ingress in the bounds between these zones becomes a very complex process. For example, chlorides from the submerged zone could migrate to the splash zone increasing corrosion initiation risks. In addition, considering the specific geometry of the structural components could increase corrosion initiation risks when the reinforcing bars are subjected to chlorides coming from several sides of the structural components (e.g., external corners in Figure 1). Taking into account the above-mentioned considerations on the corrosion initiation assessment is necessary to optimise its durability performance during the design of RC floats.

Concerning concrete cracking due to fatigue loading, existing approaches based in continuum damage mechanics could be useful to determine the degree of cracking of RC components during the time. These results could be incorporated in the chloride ingress models by integrating the effect of concrete cracking on concrete diffusivity by using for example the relations given in [37]. However, one major challenge in combining cracking and chlorination processes is to account for the effect of cyclic loading in time that will open and close cracks influencing the chloride ingress processes. The extent of this effect will vary in the structural component depending on the geometry of the float, its reinforcement, and its loading conditions and will result on more or less exposed zones. To the authors' best knowledge, this kind of modelling has not been carried out and would require significant computational efforts.

Dealing with the uncertainties and spatial variability involved in the problem is also a very challenging issue. Metocean databases are necessary to quantify the uncertainties related with wind, waves and current actions. A comprehensive experimental campaign should be carried out to well characterise the uncertainties and spatial variability related with the used materials (concrete, steel, tendons) as well as construction processes. This comprehensive database will be useful to propose appropriate models to represent uncertainties and spatial variability (e.g., random variables and/or fields). Once these random variables and fields are identified, its propagation into the combined models of chloride ingress and concrete cracking under cyclic loading becomes a very hard task because it will produce high dimensional and multiscale stochastic problems. Using traditional methods to propagate uncertainty becomes therefore computationally intractable and new options should be explored to deal with this problem.

4. CONCLUSIONS

The challenges mentioned previously highlight the need to propose a comprehensive methodology for corrosion initiation assessment of RC components of FWT by considering the interactions between RC chlorination and fatigue mechanisms in a stochastic framework. Towards this aim, further research needed to conduct to provide:

- well-established physics-based concrete deterioration models that will be coupled to assess combined effects of chlorination and fatigue in a widespread way;
- a comprehensive methodology to take into account hydrodynamic loads induced by metocean conditions;
- a methodology to combine the phenomena of chlorination under different exposure zones and concrete cracking under cyclic load; and
- a framework to quantify and propagate the main sources of uncertainty in the problem.

ACKNOWLEDGEMENTS

The support of the Regional Council of ‘Pays de la Loire’ throughout the BUENO 2018-2021 project (Durable Concrete for Offshore Wind Turbines) is gratefully acknowledged.

REFERENCES

[1] GWEC. Wind in numbers. 2017;

[2] Lozano-Minguez E, Kolios AJ, Brennan FP. Multi-criteria assessment of offshore wind turbine support structures. Renew. Energy 2011;36:2831–2837.

[3] Kaldellis JK, Kapsali M. Shifting towards offshore wind energy—Recent activity and future development. Energy Policy 2013;53:136–148.

[4] Pineda I, Tardieu P. The European offshore wind industry - key trends and statistics 2016. 2017.

[5] OWCOG. A framework for offshore wind energy development in the US. 2005.

[6] Breton S-P, Moe G. Status, plans and technologies for offshore wind turbines in Europe and North America. Renew. Energy 2009;34:646–654.

[7] Bastidas-Arteaga E, Bressolette P, Chateauneuf A, Sánchez-Silva M. Probabilistic lifetime assessment of RC structures under coupled corrosion-fatigue processes. Struct. Saf. 2009;31:84–96.

[8] Bastidas-Arteaga E, Schoefs F. Sustainable maintenance and repair of RC coastal structures. Proc. Inst. Civ. Eng. - Marit. Eng. 2015;168:162–173.

[9] Jonkman JM. Dynamics modelling and loads analysis of an offshore floating wind turbine. National Renewable Energy Laboratory; Technical report NREL/TP-500-41958; November: 2007.

[10] Hsu TTC. Fatigue of Plain Concrete. ACI J. Proc. 1981;78:292–305.

[11] Wang L, Zhang X, Zhang J, Dai L, Liu Y. Failure analysis of corroded PC beams under flexural load considering bond degradation. Eng. Fail. Anal. 2017;73:11–24.

[12] Wang L, Zhang X, Zhang J, Yi J, Liu Y. Simplified Model for Corrosion-Induced Bond Degradation between Steel Strand and Concrete. J. Mater. Civ. Eng. 2017;29:04016257.

[13] Du X, Jin L. Meso-scale numerical investigation on cracking of cover concrete induced by corrosion of reinforcing steel. Eng. Fail. Anal. 2014;39:21–33.

[14] Dai L, Wang L, Zhang J, Zhang X. A global model for corrosion-induced cracking in prestressed concrete structures. Eng. Fail. Anal. 2016;62:263–275.

[15] Wang X-H, Bastidas-Arteaga E, Gao Y. Probabilistic analysis of chloride penetration in reinforced concrete subjected to pre-exposure static and fatigue loading and wetting-drying cycles. Eng. Fail. Anal. 2018;84:205–219.

[16] Saad L, Aissani A, Chateauneuf A, Raphael W. Reliability-based optimization of direct and indirect LCC of RC bridge elements under coupled fatigue-corrosion deterioration processes. Eng. Fail. Anal. 2016;59:570–587.

[17] Tuutti K. Corrosion of steel in concrete. Swedish Cem. Concr. Inst. 1982;

[18] Vu KAT, Stewart MG. Structural reliability of concrete bridges including improved chloride-induced corrosion. Struct. Saf. 2000;22:313–333.

[19] Val DV, Stewart MG. Life-cycle analysis of reinforced concrete structures in marine environments. Struct. Saf. 2003;25:343–362.

[20] Saetta A, Scotta R, Vitaliani R. Analysis of chloride diffusion into partially saturated concrete. ACI Mater. J. 1993;90:441–451.

[21] Martín-Pérez B. Service life modelling of {RC} higway structures exposed to chlorides, University of Toronto, 1999.

[22] Nguyen P-T, Bastidas-Arteaga E, Amiri O, El Soueidy C-P. An efficient chloride ingress model for long-term lifetime assessment of reinforced concrete structures under realistic climate and exposure conditions. Int. J. Concr. Struct. Mater. 2017;11:199–213.

[23] Flint M, Michel A, Billington SL, Geiker MR. Influence of temporal resolution and processing of

exposure data on modeling of chloride ingress and reinforcement corrosion in concrete. Mater. Struct. 2013;47:729–748.
[24] Geiker M, Michel A, Lepech MD, Wu J, Stang H. Multi-scale and multi-physics deterioration modelling for design and assessment of reinforced concrete structures. RILEM Tech. Lett. 2017;2:119.
[25] Ožbolt J, Kušter M, Balabanić G, Oršanić F. Numerical Modelling of Degradation of Reinforced Concrete Structures Exposed to Cracking and Chlorides, in: IABSE Symp. Rep., Rotterdam: 2013: pp. 546–553.
[26] Subramaniam K V., Popovics JS, Shah SP. Fatigue response of concrete subjected to biaxial stresses in the compression-tension region. ACI Mater. J. 1999;96:663–669.
[27] Shiming S, Yupu S. Dynamic biaxial tensile?compressive strength and failure criterion of plain concrete. Constr. Build. Mater. 2013;40:322–329.
[28] Shi L, Wang L, Song Y, Shen L. Dynamic properties of large aggregate concrete under triaxial loading. Mag. Concr. Res. 2015;67:282–293.
[29] Yan D, Lin G, Chen G. Dynamic properties of plain concrete in triaxial stress state. , (1), 89. ACI Mater. J. 2009;106:89–94.
[30] Yang JH, Zhao DF, Song YP. A study on variable-amplitude fatigue test and damage of concrete in tension and under multi-lateral pressures. China Civ. Eng. J. 2005;38:37–44.
[31] Zhao D, Gao H, Liu H, Jia P, Yang J. Fatigue Properties of Plain Concrete under Triaxial Tension-Compression-Compression Cyclic Loading. Shock Vib. 2017;2017:1–10.
[32] He Z, Zhang J. Strength characteristics and failure criterion of plain recycled aggregate concrete under triaxial stress states. Constr. Build. Mater. 2014;54:354–362.
[33] Fédération internationale du béton. fib model code for concrete structures 2010. Ernst & Sohn: 2012.
[34] Ohtsu M. Crack propagation in concrete: Linear elastic fracture mechanics and boundary element method. Theor. Appl. Fract. Mech. 1988;9:55–60.
[35] Bhowmik S, Ray S. An improved crack propagation model for plain concrete under fatigue loading. Eng. Fract. Mech. 2018;191:365–382.
[36] Mazars J, Hamon F, Grange S. A new 3D damage model for concrete under monotonic, cyclic and dynamic loadings. Mater. Struct. 2015;48:3779–3793.
[37] Djerbi A, Bonnet S, Khelidj A, Baroghel-bouny V. Influence of traversing crack on chloride diffusion into concrete. Cem. Concr. Res. 2008;38:877–883.
[38] Jang SY, Kim BS, Oh BH. Effect of crack width on chloride diffusion coefficients of concrete by steady-state migration tests. Cem. Concr. Res. 2011;41:9–19.
[39] Gowripalan N, Sirivivatnanon V, Lim CCC. Chloride diffusivity of concrete cracked in flexure. Cem. Concr. Res. 2000;30:725–730.
[40] Lindquist WD, Darwin D, Browning J, Miller GG. Effect of Cracking on Chloride Content in Concrete Bridge Decks. 2006;
[41] Gjørv OE. Durability of reinforced concrete wharves in Norwegian harbours. Matériaux Constr. 1969;2:467–476.
[42] Petryna Y., Pfanner D, Stangenberg F, Kr?tzig W. Reliability of reinforced concrete structures under fatigue. Reliab. Eng. Syst. Saf. 2002;77:253–261.
[43] Bastidas-Arteaga E, Chateauneuf A, Sánchez-Silva M, Bressolette P, Schoefs F. A comprehensive probabilistic model of chloride ingress in unsaturated concrete. Eng. Struct. 2011;33:720–730.
[44] Schoefs F, Bastidas-Arteaga E, Tran TV, Villain G, Derobert X. Characterization of random fields from NDT measurements: A two stages procedure. Eng. Struct. 2016;111:312–322.
[45] Stewart MG. Spatial variability of pitting corrosion and its influence on structural fragility and reliability of RC beams in flexure. Struct. Saf. 2004;26:453–470.

BENCHMARKING CHLORIDE INGRESS MODELS ON REAL-LIFE CASE STUDIES: KRK BRIDGE AND MASLENICA BRIDGE STRUCTURES

Marija Kušter Marić (1), Joško Ožbolt (2) and Gojko Balabanić (3)

(1) Faculty of Civil Engineering, University of Zagreb, Croatia

(2) Institute for construction materials, University of Stuttgart, Germany

(3) Faculty of Civil Engineering, University of Rijeka, Croatia

Abstract

Many chloride ingress models for service life prediction of concrete structures have been developed in the last three decades, but their application in management of existing and design of new bridges is still not on the satisfactory level, due to complexity of transport and corrosion processes, but also due to difficulty in quantifying the material, structural, environmental and corrosion related parameters and their interactions.

Two chloride ingress models, recently developed 3D chemo-hygro-thermo mechanical model implemented into finite element code MASA and well-known Life-365, are used for two real life case studies: Maslenica Bridge and Krk Bridges, located in very aggressive maritime environment on the Adriatic coast. Both models are capable to predict the chloride content in concrete after 13 and 20 years of sea exposure with satisfactory accuracy. However, presence of cracks in concrete significantly decreases reinforcement depassivation time. Influence of crack width and depth, but also distance between cracks on chloride ingress in concrete should be considered to predict initiation phase of reinforcement corrosion more realistically.

Keywords: chloride, numerical model, cracks, case study

1. INTRODUCTION

The main cause of degradation of reinforced concrete bridges is chloride-induced corrosion of steel reinforcement in concrete leading to service life reduction and maintenance costs increase. In order to implement sustainable bridge management, it is necessary to determine service life of structures using numerical models. Many chloride ingress models for service life prediction of structure have been developed in the last three decades, but their application in management of existing and design of new bridges are still not on the satisfactory level, due to complexity of transport and corrosion processes in reinforced concrete structures, but also due to difficulty in quantifying the material, structural, environmental and corrosion related parameters and their interaction.

Two chloride ingress models, the 3D chemo-hygro-thermo mechanical (3D CHTM) model and Life-365, are used for two real life case studies: Maslenica Bridge and Krk Bridges, located in very aggressive maritime environment on the Adriatic coast.

2. 3D CHEMO-HYGRO-THERMO MECHANICAL MODEL

The recently developed 3D CHTM model [1-3], implemented into the MASA finite element code, is one of the most comprehensive models for service life prediction of concrete structures exposed to mechanical and non-mechanical loads.

The modelling of corrosion induced damage of concrete includes the following physical, electrochemical and mechanical processes: (i) transport of capillary water, heat, oxygen and chloride through the concrete cover; (ii) immobilization of chloride in the concrete; (iii) drying and wetting of concrete and related hysteretic property of transport of water through concrete; (iv) transport of OH- ions through electrolyte in concrete pores; (v) cathodic and anodic polarisation and mass sinks of oxygen on steel surface due to cathodic and anodic reaction; (vi) distribution of electrical potential and current density; (vii) transport of corrosion products through concrete pores and cracks; (viii) concrete cracking due to mechanical and non-mechanical actions and its interaction with non-mechanical processes. Since the chloride ingress models are in focus in this paper, only processes related to the transport of chlorides before depassivation of steel reinforcement will be explained in detail.

Transport of capillary water is described in terms of volume fraction of pore water in concrete by Richard's equation [1,4], based on the assumption that transport processes take place in aged concrete, i.e., the hydration of cement paste is completed:

$$\frac{\partial \theta_w}{\partial t} = \nabla \cdot \left[D_w(\theta_w) \nabla \theta_w \right] \tag{1}$$

where θ_w is volume fraction of pore water (m^3 of water / m^3 of concrete) and $D_w(\theta_w)$ is capillary water diffusion coefficient (m^2/s) described as a strongly non-linear function of moisture content [1].

Transport of chloride ions through a non-saturated concrete occurs as a result of convection, diffusion and physically and chemically binding by cement hydration product [1,4]:

$$\theta_w \frac{\partial C_c}{\partial t} = \nabla \cdot \left[\theta_w D_c(\theta_w, T) \nabla C_c \right] + D_w(\theta_w) \nabla \theta_w \nabla C_c - \frac{\partial C_{cb}}{\partial t} \tag{2a}$$

$$\frac{\partial C_{cb}}{\partial t} = k_r \left(\alpha C_c - C_{cb} \right) \tag{2b}$$

where C_c is concentration of free chloride dissolved in pore water (kg_{Cl^-}/m^3 pore solution), $D_c(\theta_w,T)$ is the effective chloride diffusion coefficient (m^2/s) expressed as a function of water content and concrete temperature T, C_{cb} is concentration of bound chloride (kg_{Cl^-}/m^3 of concrete), k_r is binding rate coefficient, α = 0.7 is constant [1].

The mechanical part of the model is based on the micro-plane model for concrete with relaxed kinematic constraint [5]. In the finite element analysis cracks are treated in a smeared way, i.e. smeared crack approach is employed. To assure the objectivity of the results with respect to the size of the finite elements, the crack band method is used [6].

The governing equation for the mechanical behaviour of a continuous body in the case of static loading condition reads:

$$\nabla[D_m(u, \theta_w, T)\nabla u] + \rho b = 0 \tag{3}$$

in which D_m is material stiffness tensor, ρb is specific volume load, T is temperature and u is displacement field. In the mechanical part of the model the total strain tensor is decomposed into mechanical strain, thermal strain, hygro strain (swelling–shrinking) and strain due to expansion of corrosion products.

The transport processes in concrete depend on the damage (crack) in concrete. Hence, the water and chloride diffusivity, as the relevant parameters for transport processes, are employed in the model as function of crack width based on the experimental results for permeability in cracked and fully saturated concrete (Figure 1) [1].

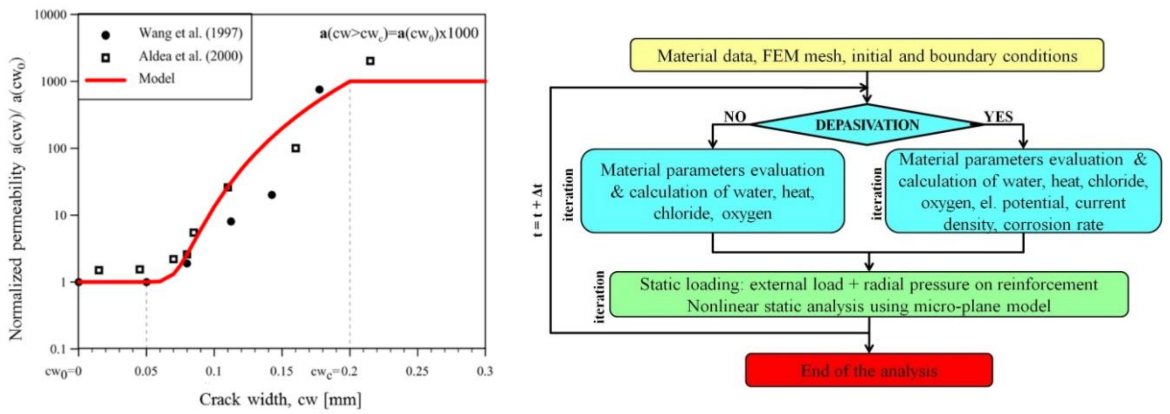

Figure 1: Normalized concrete permeability as a function of a crack width (left) and 3D CHTM model algorithm (right)

3. LIFE 365

The Life-365 model calculates chloride ingress in un-cracked concrete according to the Fick's second law, assuming diffusion as dominant transport processes [7]:

$$\frac{dC}{dt} = D\frac{d^2C}{dx^2} \tag{4}$$

where C is chloride content, D is apparent diffusion coefficient, x is depth from the exposed surface and t is time.

The chloride diffusion coefficient is a function of time:

$$D_{ref} = D_{28} = 1 \cdot 10^{(-12.06+2.40w/c)} \tag{5a}$$

$$D(t) = D_{ref}\left(\frac{t_{ref}}{t}\right)^m \tag{5b}$$

$$m = 0.2 + 0.4\left(\frac{\%FA}{50} - \frac{\%SG}{70}\right) \tag{5c}$$

where D_{ref} is diffusion coefficient at time t_{ref} = 28 days and temperature T_{ref} = 293K (20°C), *w/c* is water-to-cement ratio, *m* is constant depending on concrete mixture based on the level of fly ash (%FA) or slag (%SG) in concrete.

3. APPLICATION OF CHLORIDE INGRESS MODELS ON CASE STUDIES

3.1 Case studies

Krk Bridge, built in 1980, and Maslenica Motorway Bridge, built in 1997, are long span reinforced concrete arches located in extremely aggressive maritime environment on the Adriatic coast in Croatia [8,9]. High sea salinity with average value of 38.5 ‰ and strong Bora wind make those bridges very vulnerable to chloride induced corrosion. Namely, the Bora wind blows from north and north-east, causes salt spray and deposits chlorides on all structural elements [8, 10-12]. The Bora is a dry wind, occurring without precipitation. Hence, there is no flushing of chloride from the concrete surfaces during rain, while the layer of salt on the exposed surface of the concrete structures is constantly being renewed.

Although, both bridges have good quality concrete (Table 1), first signs of reinforcement corrosion appeared early, already after few years of services due to combination of aggressive

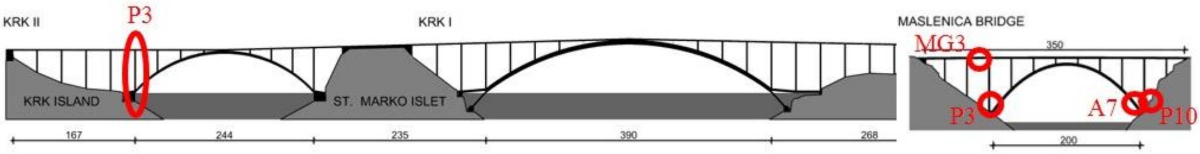

Figure 2: Layouts of the Krk Bridge (left) and Maslenica Bridge (right) with marked position where chloride content is determined and compared with numerical results

Table 1: Concrete mix design for Krk Bridge and Maslenica Bridge [10,13]

Component	Krk Bridge		Maslenica Bridge	
	Type	Mass [kg/m^3]	Type	Mass [kg/m^3]
Cement	CEM II/A-S 42.5 20% slag	450	CEM II/A-S 42.5 R 12% slag, 18% fly ash, 5% lime	400
Aggregate	D_{max} =16 mm Alluvial crashed carbonate gravel	1854 1869	D_{max} =16 mm Quarry Vrsi	1854
w/c	0.36		0.40	
Admixture I	Superplasticizer	0.890	Superplasticizer	7.40
Admixture II	Air-entraining agent	0.667	Air-entraining agent	0.08
Admixture III	-	-	Retarder	0.80

environment and errors during design or construction, e.g. not sufficient depth of concrete cover, cracks and damage of concrete cover, etc. In the first two decades of service, comprehensive investigation and repair works were provided for each bridge.

3.2 Numerical modelling

The analyses are carried out for two environmental exposure conditions XS1 and XS3, according to the European Standard EN 206:2013. Applied diffusivities for both numerical models are shown in Table 2, while initial and boundary conditions for both exposure conditions and both numerical models are listed in Table 3.

Two different approaches are applied for numerical modelling using 3D CHTM model. For calculation of chloride content in concrete of the Krk Bridge, segment of structural element is modelled with an assumed parallel-face crack of constant width, ranging from 0.0 mm for un-cracked concrete to 0.2 mm presenting an open crack.

For the Maslenica Bridge case study, "V" shaped cracks are generated by four-points bending, with maximal crack width on concrete surface of 0.2 mm or larger (Figure 3 a-b). Comparing the distribution of chlorides at different times in cracked concrete (Figure 3c), it can be seen that chlorides penetrate along the crack immediately after crack opening, and after 1 year chloride content in crack decreases, because chlorides penetrate in the horizontal direction, in the region between the cracks. Therefore, there is a slight decrease of their concentration in the crack, i.e. with increase of time chlorides tend to be smeared-out into the horizontal direction. Contrary to cracked concrete, the chloride concentration in un-cracked concrete cover increases gradually by time (Figure 3 c).

Table 2: Applied diffusivities in numerical models

Model	Parameter	Krk Bridge	Maslenica Bridge
3D CHTM	Chloride diffusion coefficient in un-cracked concrete, $D_{c,0}$ (m^2/s)	$1.00x10^{-12}$	$5.50x10^{-12}$
	Capillary water diffusion coefficient in un-cracked concrete, $D_{w,0}$ (m^2/s)	$2.20x10^{-10}$	$2.20x10^{-10}$
Life-365	Chloride diffusion coefficient in t_{ref}= 28 days *Dref* (m^2/s)	$6.37x10^{-12}$	$7.94x10^{-12}$
	Chloride diffusion coefficient *D(t)* (m^2/s)	$1.11x10^{-12}$ t=20 years	$0.96x10^{-12}$ t=13 years

Table 3: Initial and boundary conditions

Exposure class		Condition	3D CHTM model	Life-365 model
XS1, XS3	Capillary water	Initial	$\theta_{wi}=0.010$	-
		Boundary	$\theta_{wi}=0.050$	-
XS1	Chlorides	Initial	C_c=0 kg/m$^3_{por.sol.}$	C_s=0 % $m_{con..}$
		Boundary	C_c=8.5 kg/m$^3_{por.sol.}$	Krk Bridge: C_s=0.25% m_{con} Maslenica Bridge: C_s=0.27 % m_{con}
XS3		Initial	C_c=0 kg/m$^3_{por.sol.}$	C_s=0 % $m_{con..}$
		Boundary	C_c=20 kg/m$^3_{por.sol.}$	Krk Bridge: C_s=0.6% m_{con} Maslenica Bridge: C_s=0.64 % m_{con}

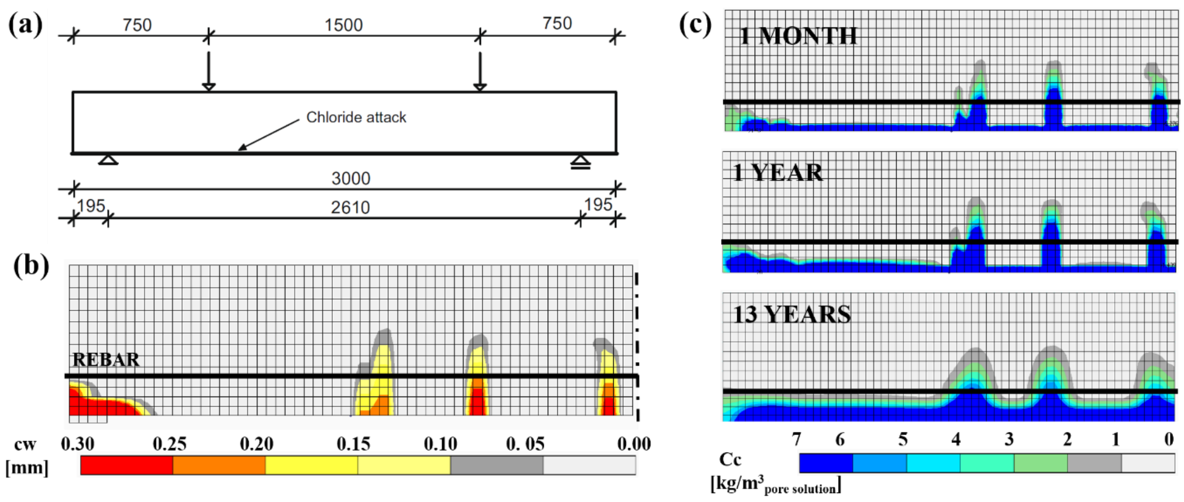

Figure 3: Numerical modelling for the Maslenica Bridge case study: a) geometry of numerical model, b) V-shaped cracks development due to 4-points bending and c) transport of free chlorides through concrete after 1 month, 1 year and 13 years

3.3 Comparison of numerical and measured chloride values

In order to compare numerical results with measured values, the total amount of chlorides, in numerical simulation provided by 3D CHTM model are expressed as percentage of concrete mass:

$$\frac{m_{free+bound\ chlorides}}{m_{concrete}} = \frac{C_c \cdot p \cdot S + C_{cb}}{\rho} \tag{6}$$

where p is porosity, S is saturation and ρ is density of concrete.

Comparisons of numerical results, calculated by 3D CHTM model and Life-365, and measured values on the Krk Bridge and Maslenica bridge are shown on Figures 4 and 5, respectively.

Values obtained on the Krk and Maslenica bridges are within the range of numerical results calculated by two different numerical models leading to the conclusion that boundary conditions for the numerical models (exposure classes XS1 and XS3) are well assumed and the both models are capable to predict the chloride content in concrete after 13 and 20 years of sea exposure with satisfactory accuracy.

However, early presence of cracks in concrete can caused reinforcement depassivation already during the first year of service (Figure 3c). This phenomenon is confirmed on the analysed bridge case studies: during the concrete samples taking, obvious signs of reinforcement corrosions, in form of brown spots and concrete cover delamination, were detected although the chloride content at the reinforcement level did not achieve the threshold value.

Moreover, it is important to model chloride ingress in 3D domain, since chloride penetrate fast into the crack and after certain time chlorides penetrate in the region between the cracks. Hence, not only crack width, length and depth, but also distance between cracks has significant impact on prediction of depassivation time.

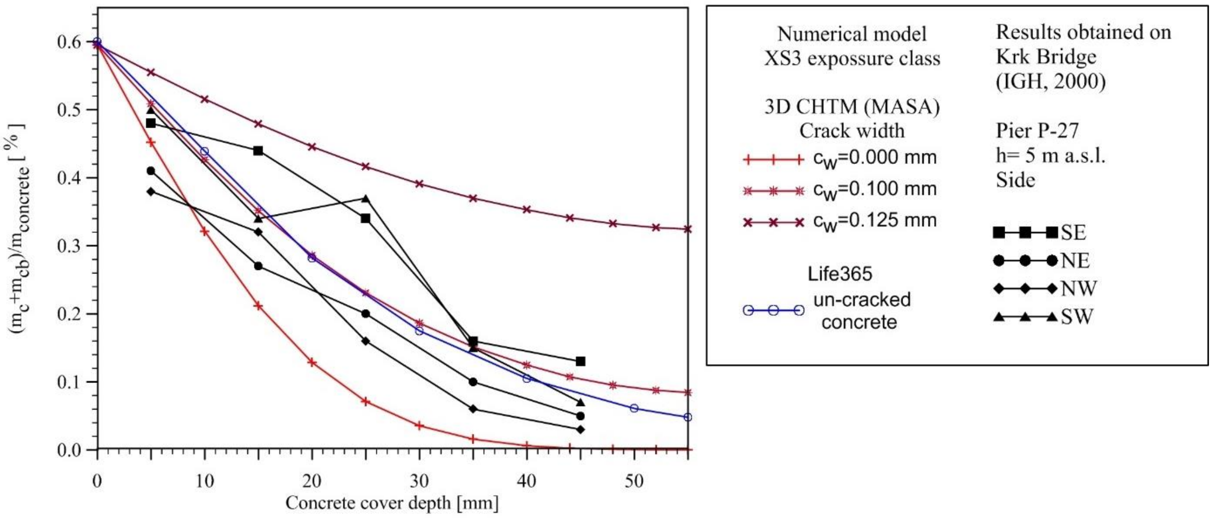

Figure 4: Total chloride content after 20 years of sea exposure: comparison of the numerical results and measured values on the Krk Bridge

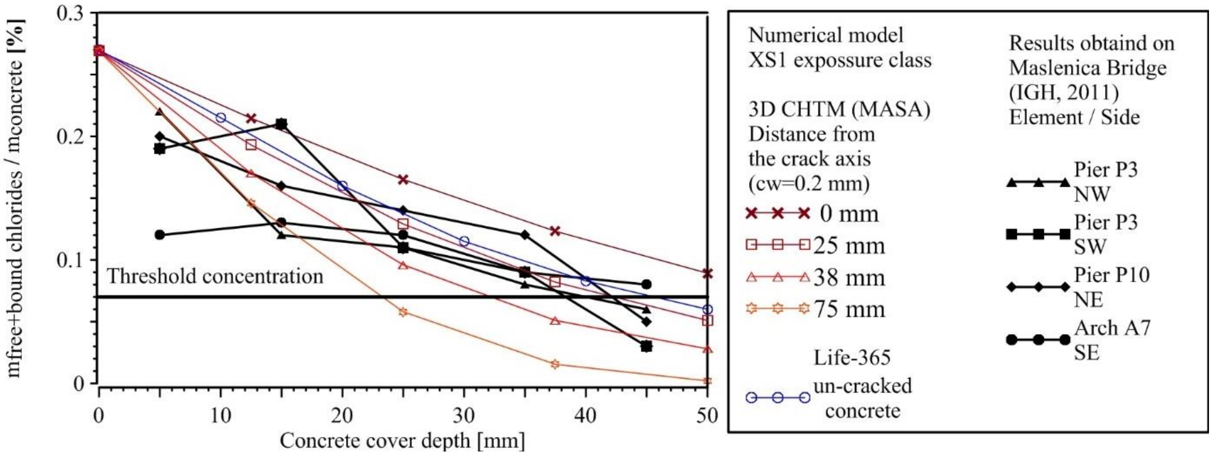

Figure 5: Total chloride content after 13 years of sea exposure: comparison of the numerical results and measured values on the Maslenica Bridge

4. CONCLUSIONS

Two chloride ingress models, recently developed 3D chemo-hygro-thermo mechanical model implemented into finite element code MASA and well-known Life-365, are used for two real life case studies: Maslenica Bridge and Krk Bridges located in very aggressive maritime environment on the Adriatic coast. Both models are capable to predict the chloride content in concrete after 13 and 20 years of sea exposure. However, presence of cracks in concrete significantly decreases reinforcement depassivation time. Influence of crack width and depth, but also distance between cracks on chloride ingress in concrete should be considered to predict depassivation time more realistically.

ACKNOWLEDGEMENTS

This research was carried out in the framework of the UKF project 04/17 "Influence of concrete damage on reinforcement corrosion - computer simulation and in-service performance of bridges (CODEbridges)" [14] supported by Unity through Knowledge Fund.

REFERENCES

[1] Ožbolt J, Balabanić G, Periškić G, Kušter M (2010) Modelling the effect of damage on transport processes in concrete. Constr Build Mater 24:1638-1648.
[2] Ožbolt J, Balabanić G, Kušter M (2011) 3D numerical modelling of steel corrosion in concrete structures. Corros Sci 53:4166-4177.
[3] Ožbolt J, Oršanić F, Balabanić G (2016) Modeling influence of hysteretic moisture behavior on distribution of chlorides in concrete. Cem Concr Compos 67:73-84.
[4] Bear J, Bachmat Y (1991) Introduction to modeling of transport phenomena in porous media. Kluwer Academic Publishers, Boston
[5] Ožbolt, J. et al.; Microplane model for concrete with relaxed kinematic constraint, *Int J Solids Struct*, 38 (16) 2001, pp. 2683–2711
[6] Bažant, Z. P. & Oh, B. H. (1983) Crack band theory for fracture of concrete. *Rilem*, 93 (16), , pp. 155-177
[7] Thomas MDA, Bentz EC (2018) Life-365™ Service Life Prediction Model™ and Computer Program for Predicting the Service Life and Life-Cycle Cost of Reinforced Concrete Exposed to Chlorides Version 2.2.3 September 28, 2018. University of Toronto
[8] Radić J, Šavor Z, Puž G (2003) Extreme Wind and Salt Influence on Adriatic Bridges. Struct Eng Int 13:242-245.
[9] Radić, J. Šavor Z, Mandić A (2010) Two Notable Arch Bridges on The Croatian Adriatic Highway, *Structural engineering international*, 20 (2010) 1, pp. 36-40
[10] Stipanović Oslaković I, Bjegović D, Mikulić D (2010) Evaluation of service life design models on concrete structures exposed to marine environment. Mater Struct 43:1397-1412.
[11] Kušter Marić, M. et al. (2016) Analysis on durability of reinforced concrete bridges in maritime environment. *Annual 2015 of the Croatian Academy of Engineering*: 57-78. Zagreb: Croatian Academy of Engineering.
[12] Kušter Marić, M. et al. (2017) Service life prediction of concrete structures in maritime environment – case study: Maslenica Motorway Bridge. *Proceedings of the 1st International Conference on Construction Materials for Sustainable Future (CoMS_2017),* Zagreb: Faculty of Civil Engineering, University of Zagreb.
[13] Stipanović, I. et al. (2007) Time dependent changes of durability properties of concrete from Maslenica Bridge at the Adriatic Coast. Integral Service Life Modeling of Concrete Structures, Bagneux: RILEM Publications S.A.RL, 87-95
[14] Influence of concrete damage on reinforcement corrosion - computer simulation and in service performance of bridges (CODEbridges), www.grad.unizg.hr/codebridges , 01.10.2018

MODELING CORROSION OF STEEL REINFORCEMENT IN CONCRETE

Joško Ožbolt (1), Gojko Balabanić (2) and Filip Oršanić (1)

(1) Institute of Construction Materials, University of Stuttgart, Germany

(2) Faculty of Civil Engineering Rijeka, University of Rijeka, Croatia

Abstract

Aggressive environmental conditions, such as exposure to the sea climate or use of de-icing salts, have considerable influence on durability of reinforced concrete structures due to the reinforcement corrosion induced damage. In the present paper recently developed coupled 3D chemo-hygro-thermo-mechanical (CHTM) model for concrete is discussed. The model takes into account the interaction between non-mechanical processes and mechanical properties of concrete (damage). The mechanical part of the model is based on the microplane model. It is validated through a 3D transient FE analysis of a pull-out of corroded steel reinforcement from a concrete beam-end specimen, which was exposed to aggressive environmental conditions. For the corrosion phase the influence of the anode and cathode position on the electric potential, current density, corrosion rate and corrosion induced damage is investigated. Moreover, the effect of corrosion on the pull-out capacity of reinforcement and the influence of transport of corrosion products through cracks are studied.

Keywords: Reinforced concrete, corrosion, CHTM model, finite elements

1. INTRODUCTION

Durability of reinforced concrete structures is mainly influenced by the corrosion of steel reinforcement. Especially vulnerable are structures exposed to harsh sea climate conditions or highways and garages treated with de-icing salts during winter seasons [1]. Reinforcement corrosion can be initiated by: (i) the carbonation of the concrete and (ii) the penetration of chlorides from de-icing or sea salts. Both processes can destroy the inherent, thin, corrosion-protective oxide layer of the steel embedded in the concrete. After destruction of this oxide layer (depassivation), the so-called active corrosion phase, in which the steel is gradually converted into corrosion products (rust), initiates. The resulting consequences are: (i) reduction of the steel cross section by conversion of iron into iron oxides, (ii) cracking and possibly spalling of concrete cover due to the increasing volume of the corrosion products in relation to the steel and (iii) reduction of the bond strength between reinforcement bar and concrete. Consequently, the durability, failure capacity and ductility of concrete structure can be significantly reduced. In addition to the macro-cell corrosion of the steel reinforcement, in the case of chloride-induced corrosion the local (pitting) corrosion also occurs [2]. This type of corrosion is particularly dangerous as it causes local damage resulting in a large decrease in ductility and reduction of the cross-section of the reinforcing steel bar.

According to current research status, there is only one coupled 3D CHTM model capable of simulating all relevant non-mechanical and mechanical processes and their interaction. This model was developed at the Institute of Construction Materials, University of Stuttgart, and implemented into the 3D FE code [3] [4]. Over the past years, the model has been calibrated, verified and further improved based on the extensive experimental tests [5]. In the following its theoretical background and application is presented.

2. CHEMO-HYGRO-THERMO-MECHANICAL MODEL FOR CONCRETE

The recently developed 3D chemo-hygro-thermo-mechanical model couples the above mentioned physical and electrochemical processes with the mechanical behavior of concrete (damage). In the model the transport of capillary water is described in terms of volume fraction of pore water in concrete by Richard's equation [6], based on the assumption that transport processes take place in aged concrete, i.e., the hydration of cement paste is completed:

$$\frac{\partial \theta_w}{\partial t} = \nabla \cdot \left[D_w(\theta_w) \nabla \theta_w \right] \tag{1}$$

where θ_w is volume fraction of pore water (m^3 of water/m^3 of concrete) and $D_w(\theta_w)$ is capillary water diffusion coefficient (m^2/s) described as a strongly non-linear function of moisture content. Transport of chloride ions through a non-saturated concrete occurs as a result of convection, diffusion and physically and chemically binding by cement hydration product [4]:

$$\theta_w \frac{\partial C_c}{\partial t} = \nabla \cdot \left[\theta_w D_c(\theta_w, T) \nabla C_c \right] + D_w(\theta_w) \nabla \theta_w \nabla C_c - \frac{\partial C_{cb}}{\partial t} \tag{2a}$$

$$\frac{\partial C_{cb}}{\partial t} = k_r \left(\alpha C_c - C_{cb} \right) \tag{2b}$$

where C_c is concentration of free chloride dissolved in pore water (kgCl-/m^3 pore solution), $D_c(\theta_w,T)$ is the effective chloride diffusion coefficient (m^2/s) expressed as a function of water content and concrete temperature T, C_{cb} is concentration of bound chloride (kgCl-/m^3 of concrete), k_r is binding rate coefficient, $\alpha = 0.7$ is constant [3].

Assuming that oxygen does not participate in any chemical reaction before depassivation of steel, transport of oxygen through concrete is considered as a convective diffusion problem:

$$\theta_w \frac{\partial C_o}{\partial t} = \nabla \cdot \left[\theta_w D_o(\theta_w) \nabla C_o \right] + D_w(\theta_w) \nabla \theta_w \nabla C_o \tag{3}$$

where C_o is oxygen concentration in pore solution (kg of oxygen/m^3 of pore solution) and $D_o(\theta_w)$ is the effective oxygen diffusion coefficient [3], dependent on concrete porosity p_{con} and water saturation of concrete Sw.

Based on the constitutive law for heat flow and conservation of energy, the equation which describes temperature distribution in continuum reads:

$$\lambda \Delta T + W(T) - c\rho \frac{\partial T}{\partial t} = 0 \tag{4}$$

where λ is thermal conductivity (W/(m K)), c is heat capacity per unit mass of concrete (J/(K kg)), ρ is mass density of concrete (kg/m^3) and W is internal source of heating (W/m^3). More detail related to the strong and weak formulations of the processes up to the depassivation of reinforcement can be found in Ožbolt et al. [3].

The corrosion of steel is activated with the depassivation of the steel reinforcement in concrete. The non-mechanical processes important for the propagation stage of steel corrosion in concrete are: (1) Mass sinks of oxygen at steel surface due to cathodic and anodic reaction, (2) The flow of electric current through pore solution and (3) The cathodic and anodic potential.

The oxygen consumption at the cathodic and anodic surfaces is a result of the following reactions of dissolved oxygen in the pore water with the electrons on the cathode:

$$2H_2O + O_2 + 4e^- \rightarrow 4OH^- \tag{5}$$

The transport of hydroxyl ions to the anode, where corrosion products forms:

$$Fe^{2+} + 2OH^- \rightarrow Fe(OH)_2 \tag{6}$$

$$4Fe(OH)_2 + O_2 + 2H_2O \rightarrow 4Fe(OH)_3 \tag{7}$$

It can be calculated as:

$$D_o(S_w, p_{con}) \left.\frac{\partial C_o}{\partial n}\right|_{cathode} = -k_c i_c \qquad k_c = 8.29 \times 10^{-8} \frac{\mathrm{kg}}{\mathrm{C}} \tag{8a}$$

$$D_o(S_w, p_{con}) \left.\frac{\partial C_o}{\partial n}\right|_{anode} = -k_a i_a \qquad k_a = 4.14 \times 10^{-8} \frac{\mathrm{kg}}{\mathrm{C}} \tag{8b}$$

where n is outward normal to the steel bar surface and i_c and i_a are cathodic and anodic current density (A/m^2), respectively. The constants k_c and k_a are calculated using the stoichiometry of chemical reactions (Eqs. 5-7) and Faraday's law.

According to Butler – Volmer kinetics, in the present model kinetics of reaction at the cathodic and anodic surface can be estimated from:

$$i_c = i_{0c} \frac{C_o}{C_{ob}} e^{2.3(\Phi_{0c} - \Phi)/\beta_c} \qquad i_a = i_{0a} e^{2.3(\Phi - \Phi_{0a})/\beta_a} \tag{9}$$

where C_{ob} is oxygen concentration at surface of concrete element exposed to sea water (kg/m^3), Φ is electric potential in pore solution near reinforcement surface (V), i_{0c} and i_{0a} are the exchange current density of the cathodic and anodic reaction (A/m^2), Φ_{0c} and Φ_{0a} are the cathodic and anodic equilibrium potential (V), β_c and β_a are the Tafel slope for cathodic and anodic reaction (V/dec), respectively.

The electric current through the electrolyte is a result of motion of charged particles and, if the electrical neutrality of the system and the uniform ions concentration are assumed, can be written as:

$$\mathbf{i} = -\sigma(S_{w,} p_{con}) \nabla \Phi \tag{10}$$

where σ is electrical conductivity of concrete. The equation of electrical charge conservation, if the electrical neutrality is accounted for and the electrical conductivity of concrete is assumed as uniformly distributed, reads:

$$\nabla^2 \Phi = 0 \tag{11}$$

Rate of rust production J_r (kg/m^{2}s) and mass of hydrated red rust per related surface (A_r) of rebar m_r (kg), respectively, are calculated as:

$$\begin{aligned} J_r &= 5.536 \times 10^{-7} \, i_a \\ m_r &= J_r \Delta t A_r \end{aligned} \tag{12}$$

where Δt is time interval in which the corrosion is taking place. The coefficient of proportionality between the anodic current density i_r and rate of rust production J_r is calculated using the stoichiometry of chemical reactions and Faraday's law [4].

The distribution of corrosion product (red rust) R (kg/m^3 of pore solution) into the pores and through the cracks in concrete has been mathematically formulated as a convective diffusion problem:

$$\theta_w \frac{\partial R}{\partial t} = \nabla \cdot \left[\theta_w D_r \nabla R \right] + D_w(\theta_w) \nabla \theta_w \nabla R \tag{13}$$

in which D_r is the diffusion coefficient (m^2/s) of corrosion product. It is important to note that the Eq. (13) does not directly describe the transport of the red rust, but rather the distribution of the rust formed in the concrete pores and cracks as a consequence of soluble species, which can dissolve in concrete pore solution and subsequently migrate in pores and cracks, reacting with oxygen in the pore water [7]. Detailed experimental and numerical investigations have been carried out recently in order to calibrate the present model with this respect [5].

The microplane model for concrete with relaxed kinematic constraints [4] is applied in the mechanical part of the model. One-dimensional corrosion contact elements are employed in the model to account for the inelastic strains due to the expansion of corrosion products. They are placed radially around the bar surface and their main function is to simulate the contact between reinforcement and the surrounding concrete. These contact elements can take up only shear forces in direction parallel to reinforcement axis and compressive forces perpendicular to the adjacent surface of the reinforcement. The inelastic radial expansion due to corrosion Δl_r is calculated as:

$$\Delta l_r = \frac{m_r}{A_r} \left(\frac{1}{\rho_r} - \frac{0.523}{\rho_s} \right) \tag{14}$$

where $\rho_r = 1.96 \times 103$ (kg/m^3) and $\rho_s = 7.89 \times 103$ (kg/m^3) are densities of rust and steel, respectively, 0.523 is the ratio between the mass of steel (m_s) and the corresponding mass of rust (m_r) over the related surface of reinforcement A_r that corresponds to the contact element. For more detail see [3] [4].

3. NUMERICAL CASE STUDY

The application of the presented 3D CHTM model is here demonstrated through numerical study of the pull-out of the reinforcement bar from the beam-end specimen. The specimen is first exposed to aggressive environmental conditions, which caused corrosion of embedded reinforcement bar. Subsequently the bar is pulled out from the specimen and for the different levels of corrosion the numerical results are compared with the test results obtained by Fischer at al. [8]. The experiments were carried out under accelerated corrosion, which approximately corresponds to the severe splash natural conditions. Only two specimen types with four bars arranged in corners are studied. In the first specimen type, the diameter of the reinforcement bar is 12 mm with a concrete cover of 20 mm (ϕ12/20 mm) and in the second, the bar diameter of 16 mm with a cover of 35 mm (ϕ16/35 mm) is used. The total embedment length of the reinforcement in both cases is 180 mm, whereas the rest of the length is isolated with a plastic sleeve (Fig. 1). For more detail see [4] [8].

(a)

(b)

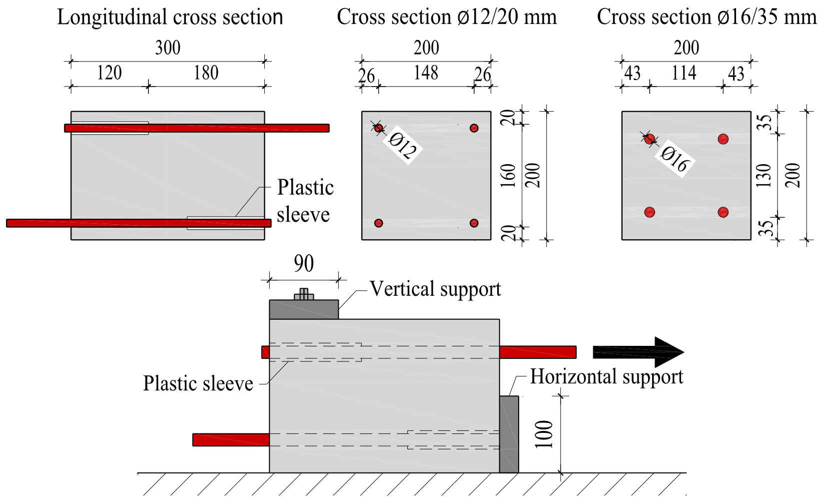

Figure 1: Geometry of the beam-end specimen (a) and pull-out loading condition (b) (Fischer et al. 2012)

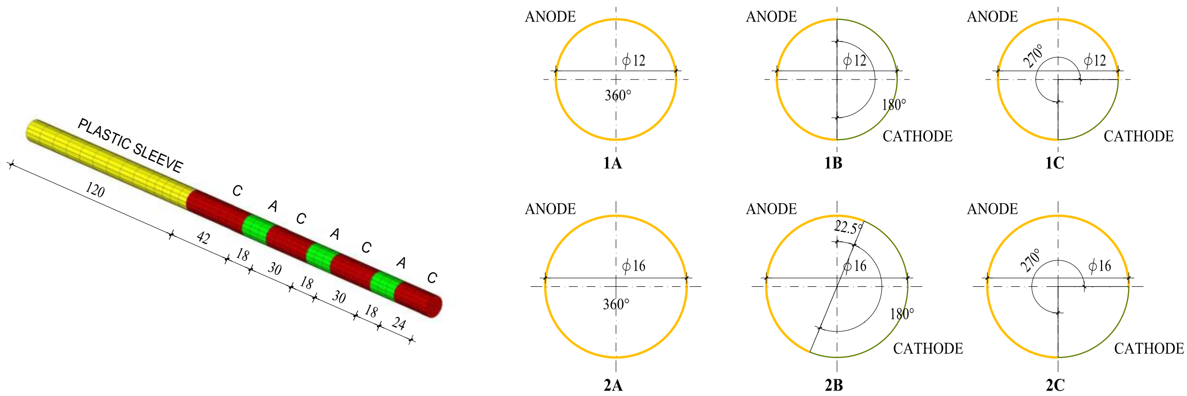

(a) (b)

Figure 2: Assumed anodic and cathodic regions: (a) along the length and (b) along the cross-section of the reinforcement bar

In the analysis is assumed that certain length sections of the bar are activated as anode (depassivated) at the start of the analysis, i.e. the processes before depassivation of reinforcement are not computed. This predefined position of anode and cathode (Fig. 2a), assuming initially un-cracked concrete, is kept unchanged during the computation. In this way after depassivation only the electric potential, current density, distribution of oxygen and cracking of concrete are calculated. More detail related to the position and size of anodic and cathodic areas can be found in [9]. One of the aims of the study was to investigate the influence of the position of anode along the cross-section of the bar reinforcement. Therefore, for each specimen (reinforcement diameter) three configurations of the anodic surface over the circumference are assumed (see Fig. 2b).

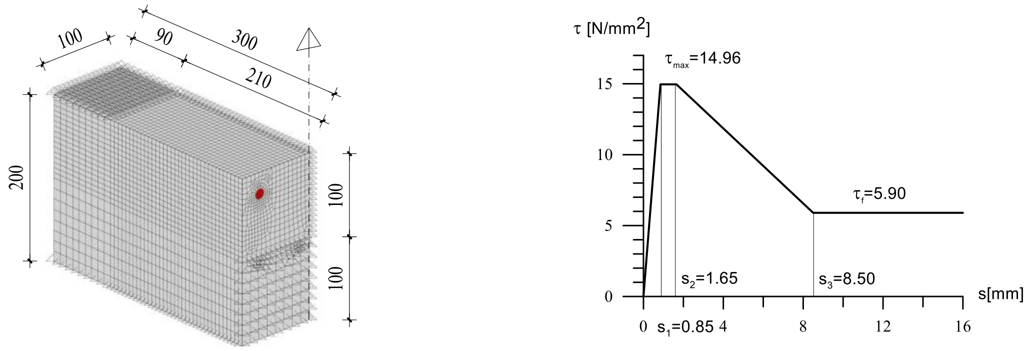

(a) (b)

Figure 3: Model geometry (all in mm) in the case of the first (a) and (b) the second specimen

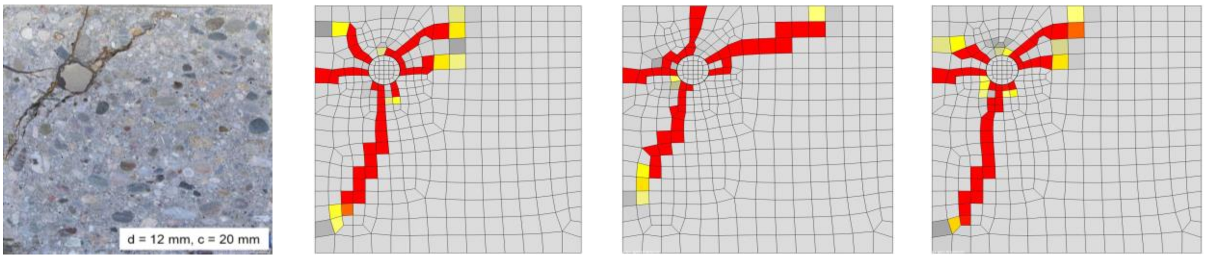

Fischer [5] 1A 1B 1C

Figure 4: Comparison of the crack patterns in the cross section at the beam's mid-span for the cases 1A-C with the experimental results

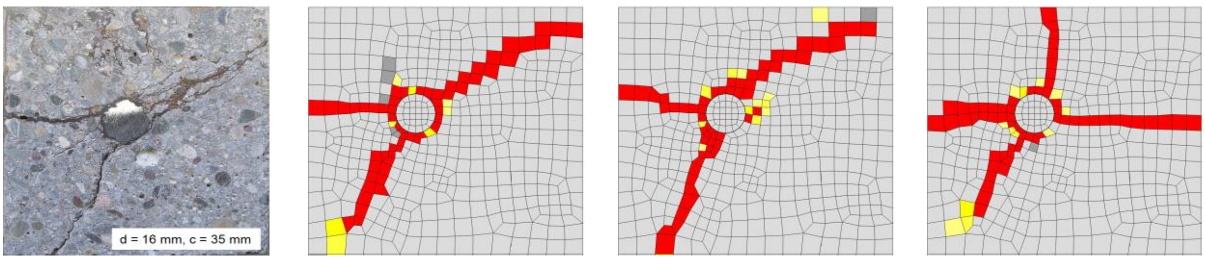

Fischer et al. (2012) 2A 2B 2C

Figure 5: Comparison of the crack patterns in the cross section at the beam's mid-span for the cases 2A-C with the experimental results

Because of the complexity of the model and in order to reduce the computational time only half of the specimen is modeled (Fig. 3a). Eight-node solid 3D finite elements are used to model the concrete and the reinforcement bar. To simulate the expansion due to the formation of corrosion products, 1D radially oriented corrosion contact finite elements are used with a length of 0.1 mm. These elements can take up radial forces (only compressive) and shear forces in direction of reinforcement axis (see Fig. 3b). Experimentally observed and numerically predicted crack patterns in the mid cross section of the specimen, 7 years after depassivation of reinforcement, are shown in Fig. 4 and Fig. 5. For the first specimen (ϕ12 / 20 mm) the position of anode 1A and 1C leads to a similar crack formation around the reinforcement bar, whereas type 1B gives better agreement with the experimental crack pattern. For the type 2, the case 2B leads to the best agreement with the test data. The above presented results show that the position of cathode and anode in the case 1B for the first specimen (ϕ12 / 20 mm) gives the best agreement with the experimental results. Therefore, this case is chosen to demonstrate the effect of distribution of corrosion products over the cracks. Two cases are considered: (a) transport of rust is neglected and (b) transport is accounted for. The same as before, for each case the beams are exposed to the corrosion processes over the period of 7 years. The damage (cracking) due to the expansion of corrosion products after 1 and 7 years, respectively, for the type 1B is shown in Fig. 6. The numerical results indicate a significant influence of the rust distribution on the corrosion induced damage for the here-studied type of chloride induced corrosion, with relatively high saturation.

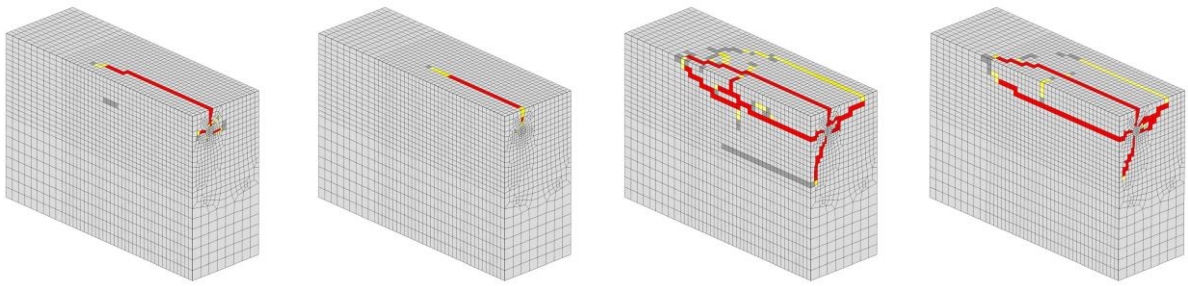

Figure 6: Predicted crack patterns due to corrosion induced damage after 1 and 7 years for specimen type 1B

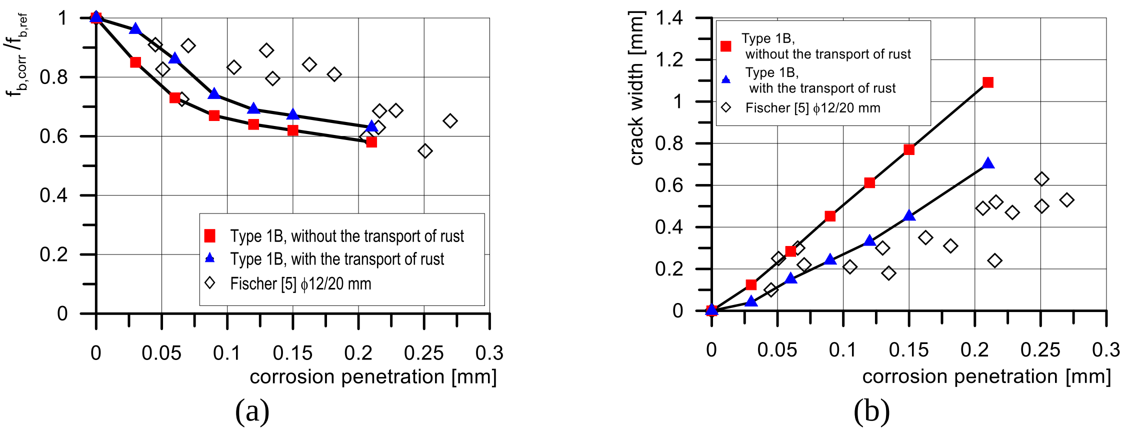

Figure 7: Predicted and measured results for specimen 1B: (a) The relative pull-out capacity as a function of the average corrosion penetration and (b) average crack width as a function of the average corrosion penetration

To demonstrate the influence of corrosion products transport through cracks on bond resistance, the reinforcement bar is pulled out from the concrete specimens (type 1B) at t =0 (reference), 1, 2, 3, 4, 5 and 7 years, respectively. The predicted and experimentally measured (average) pull-out capacities and average crack widths are shown in Fig. 7 as a function average corrosion penetration. In spite of high complexity of the problem, it can be seen that for both specimen types the numerical prediction, for the case where the transport of corrosion products is accounted for, exhibits nice agreement with the experimental data.

4. CONCLUSIONS

- The coupled 3D CHTM model for analysis of non-mechanical and mechanical processes related to the corrosion of steel reinforcement in concrete is briefly discussed. The model is employed in the transient 3D finite element analysis of the corrosion induced damage of steel reinforcement that is pulled out from the concrete beam-end specimen.
- For the assumed environmental conditions and material properties it turns out that the predicted corrosion induced crack pattern depends on the geometry (bar diameter and concrete cover), position of anode and cathode and on the transport of corrosion products through cracks.
- As the results of numerical analysis show, corrosion induced damage significantly reduces the pull-out capacity. The predicted and experimentally measured pull-out capacity show very good agreement.

ACKNOWLEDGEMENTS

The authors gratefully acknowledge the financial support provided by Deutsche Forschungsgemeinschaft (DFG) and by the National Foundation Science, Higher Education and Technological Development of the Republic of Croatia.

REFERENCES

[1] Tutti, K., ‘Corrosion of steel in concrete’, Technical report, Stockholm, (1993).
[2] Oldham, K.B., Myland, J.C., Bond, M., ‘Electrochemical Science and Technology - Fundamentals and Applications’, John Wiley & Sons, Ltd., 2012.
[3] Ožbolt, J., Balabanić, G., Periškić, G., Kušter, M., ‘Modelling the effect of damage on transport processes in concrete’, *Constr. Build. Mater.* **24** (9) (2010), 1638–1648.
[4] Ožbolt, J., Oršanić, F., Balabanić, G., ‘Modeling pull-out resistance of corroded reinforcement in concrete: Coupled three-dimensional finite element model’, *Cement and Concrete Composites* **46**, (2014), 41–55.
[5] Sola, E., ‘Experimental and numerical study of chloride induced corrosion in reinforced concrete’, Ph.D. Thesis, University of Stuttgart, Germany, 2017.
[6] Bear, J., Bachmat, Y., ‘Introduction to modeling of transport phenomena in porous media’, Boston: Kluwer Academic Publishers, 1991.
[7] Wong, H.S., Zhao, Y.X., Karimi, A.R., Buenfeld, N.R., Jin, W.L., ‘On the penetration of corrosion products from reinforcing steel into concrete due to chloride-induced corrosion’, Corros. Sci. **2**(7) (2010), 2469–2480.
[8] Fischer, C., Ožbolt, J. and Gehlen, C., ‘Verbundfestigkeit von korrodierter Bewehrung, in: Dauerhaftigkeitsbemessung von Stahlbetonbauteilen auf Bewehrungskorrosion’, Teil 2: Dauerhaftigkeitsbemessung. Berlin: Beuth (Deutscher Ausschuss für Stahlbeton 602), S. 47-88.
[9] Ožbolt, J., Balabanić, G., Sola, E., ’Determination of critical anodic and chathodic areas in corrosion processes of steel reinforcement in concrete’, *Materials and Corrosion* **68** (6), (2017).

International Conference on Sustainable Materials, Systems and Structures (SMSS 2019)
Challenges in Design and Management of Structures
20-22 March 2019 – Rovinj, Croatia

COMPARISON OF THE BEHAVIOR OF CRACK WIDTH-GOVERNING PARAMETERS WITH EXISTING MODELS

Chavin N. Naotunna, S.M Samindi, M.K Samarakoon and Kjell T. Fosså

Department of Mechanical and Structural engineering and Material science, Faculty of Science and Technology, University of Stavanger, Stavanger, Norway

Abstract

Cracking has both short- and long-term effect on reinforced concrete structures' durability, aesthetic view and liquid/gas tightness. The tensile stress induced by loads is one of the main reasons, among many, for cracking during the service life of a structure. To minimize the adverse effect of cracking due to service load, the crack width is controlled at the structural design stage. Euro Code 2 (EC2) and Model Code 2010 (MC2010) are widely used in Europe to control cracks in concrete structures. However, the existing methods used in EC2 and MC2010 have many limitations, and the predicted values still do not tally with the experimental results. Further, today's some clients (e.g. road authorities) demand high covers that exceed the limitations given in the existing crack control methods. As the first step to improving the existing models, the effects of many crack width-governing parameters are studied from previous literature. Next, a parametric study has been carried out to compare the actual behavior of most governing parameters with the predictions of the existing models.

Keywords: crack width, crack spacing, service load, parametric study

1. INTRODUCTION

Cracking has a significant short-term and long-term impact on the durability of reinforced concrete structures [1], causing a high level of intervention and repair costs [2]. Tensile stresses induced by loads (i.e. axial load, bending moments, shear, torsion), imposed deformations (i.e. differential settlements, shrinkage/creep, and temperature differences) and environmental induced loads (i.e. frost action, carbonation and chloride penetration) can lead to cracks over concrete structures. The results discussed in [1] of experiments on 16-year-old loaded cracked and un-cracked specimens and the results from experiments with 4-year-old and 10-year-old loaded specimens conducted at the Technical University of Munich [3, 4] prove that the load induced cracks cause the initiation of corrosion, which leads to reduced durability. There is a consensus that the appeared concrete cracks in reinforced concrete structures leads to penetrate CO_2, chloride and other corrosive agents to the rebar and can initiate steel corrosion [3, 5].

Therefore, controlling the cracks during a structure's service life is a main concern of the construction industry.

The existing method used to reduce the adverse effects from cracks in reinforced concrete structures due to service load is to control the width of the crack. Generally, crack width is controlled while designing the structure, to control rebar corrosion, for better appearance and to control leakages in liquid- or gas-retaining structures. For non-experts in the field, the adverse effects of cracks can be very great; therefore, to avoid unnecessary concern about cracks, it is recommended to limit the crack width to 0.25 mm [6]. When designing a liquid-retaining structure, the crucial concern is the maximum allowable crack width and that is to avoid leakages during its service life [7]. The most widely used structural design codes in Europe are Eurocode 2 (EC2) and Model code 2010 (MC2010). A structural member is designed in such a way that the calculated crack width is less than the maximum allowable crack width prescribed in each design code.

The existing crack control methods have many limitations, and one of the most demanding improvements required is the concrete cover. MC 2010 is not applicable for concrete covers higher than 75 mm, while EC2 is limited to 70-mm concrete covers. Moreover, the predicted crack widths do not match the experimental readings. However, as the first step to improve the existing codes, a study has been conducted to examine the degree of effect of the main governing parameters on crack width. Next, the code-predicted crack widths have been compared with the experimental results of previous researchers.

2. INFLUENCING FACTORS ON CRACK WIDTH DISCUSSED IN MC2010 AND EC2

To discuss the cracking phenomenon in the above-mentioned codes, a reinforced concrete tie was studied in pure tension, as it can represent the tensile side of a bending member with or without any axial force [8]. When a reinforced tie is axially tensioned from the rebar, the force in rebar is transmitted to the surrounding concrete, due to the bond stress between rebar and concrete. Cracking occurs when the transmitted force in concrete reaches its tensile strength [9, 10], and the length required to transmit the relevant force is the transfer length. In general, both codes calculate the crack width by multiplying the maximum crack spacing with the mean strain difference. Table 1 shows the crack-width calculation models in both codes.

Table 1: Crack-width calculation models in EC2 and MC2010

Eurocode 2	Model Code 2010
Crack Width	
$w_k = s_{r,max}(\xi_{sm} - \xi_{cm})$ $s_{r,max}$ Maximum crack spacing ξ_{sm} Mean strain of rebar between cracks ξ_{cm} Mean strain of concrete between cracks	$w_d = 2\, l_{s,max}(\varepsilon_{sm} - \varepsilon_{cm} - \varepsilon_{cs})$ $l_{s,max}$ Effective length ε_{sm} Average steel strain over the $l_{s,max}$ ε_{cm} Average concrete strain over the $l_{s,max}$ ε_{cs} Shrinkage strain of concrete
Crack Spacing	
$s_{r,max} = k_3 c + k_1 k_2 k_4 \varphi / \rho_{p,eff}$ φ Bar diameter $\rho_{s,ef}$ Effective steel ratio c Cover k_1 Factor for bond properties k_2 Factor for distribution of strain	$l_{s,max} = k\, c + (1/4)(f_{ctm}/\tau_{bms})(\varphi_s / \rho_{s,ef})$ $l_{s,max}$ Effective length k Empirical parameter considering cover c Cover τ_{bms} Mean bond strength (steel-concrete) φ_s Bar diameter

k_3 Use 3.4; Norwegian Standards [11] k_4 Use 0.425; Norwegian Standards [11]	$\rho_{s,ef}$ Effective steel ratio f_{ctm} The tensile strength of concrete
Mean Strain differences	
Crack Formation Stage $\xi_{sm} - \xi_{cm} \geq 0.6\ (\sigma_s / E_s)$ Stabilized cracking stage, $\xi_{sm} - \xi_{cm} = \dfrac{\sigma_s - k_t\,(f_{ct,eff} / \rho_{p,eff})\,(1+\alpha_e\,\rho_{p,eff})}{E_s}$ σ_s Stress of steel at the cracked section k_t Factor on the loading duration $\rho_{p,eff}$ $= (A_s + \xi_1^2\,A_p') / A_{c,eff}$ A_s Reinforcement area A_p' Area of post tension tendons $A_{c,eff}$ Effective area of concrete in tension α_e $= E_s/E_c$	Crack Formation Stage, $\varepsilon_{sm} - \varepsilon_{cm} = \sigma_{sr} / E_s * (1-\beta) - \eta_r\,\varepsilon_{sh}$ Stabilized cracking stage, $\varepsilon_{sm} - \varepsilon_{cm} = (\sigma_s - \beta\,.\sigma_{sr}) / E_s - \eta_r\,\varepsilon_{sh}$ σ_{sr} Max. steel stress at crack formation stage σ_s Stress of steel at the cracked section β Factor on the duration of load η_r Coefficient for shrinkage strain ε_{sh} Shrinkage strain

Many previous studies have been conducted to identify the influencing factors on crack widths in reinforced concrete structures due to service load. Table 2 shows some of the parameters and the discussed literature.

Table 2: Factors influencing the crack width

Affecting Parameter	Related Literature	Influence
Concrete cover	[12, 13]	Crack Spacing
φ / $\rho_{p,eff}$ (diameter to the ratio of area of steel in tensile bars to the effective area of concrete)	[12, 14]	
Tensile strength of concrete	[9]	
Bond stress between steel and concrete,		
re bar surface type	[15]	
Maximum to minimum crack spacing	[10]	
Loading condition (axial tension or bending)	[16, 17]	
Stirrups position	[2, 12]	
Duration of loads (short- or long-term)	[16, 17]	Strain Difference
Applied steel stress	[2, 12, 13, 18]	
Shrinkage	[11]	
Tensile strength of concrete	[9]	
Young's modulus of steel and concrete		
Crack width measuring point to the nearest bar	[17], [14, 19]	

It has been experimentally proved that the bond stress increases with an increase in the tensile strength of concrete [10]. Therefore, as per the crack spacing models, the transfer length remains unchanged, even if the concrete strength is increased. On the other hand, concrete tensile strength governs the maximum steel stress at the crack formation stage (σ_{sr}), which is a parameter of mean strain difference. When a crack occurs, the tensile stress in the concrete at the crack becomes zero, and the stress will be transferred to the rebar. Therefore, the mean strain difference in the 'crack formation stage' would increase with the increase in concrete tensile strength, and, in the 'stabilized cracking stage', the strain difference reduces with the increase in concrete strength. This scenario is represented in the mean strain difference calculation model in both MC2010 and EC2. Radnic and Markota [15] proved that the deformed bars cause smaller crack widths, compared to the smooth surface bars, in both bending and axial tension loading cases. That can be due to the fact that higher bond stress requires lower transfer length and, therefore, lower crack spacing leads to lower crack widths. This effect is represented in the EC 2 crack spacing model by a factor of 0.8 for high bond bars and 1.6 for plain surface bars. Caldentey [20] describes the tensile force required to crack the concrete in bending as half of the force required in axial tension, as per the difference in strain distribution of the member. Therefore, to represent this effect, EC2 considers a factor of 1.0 for axial tension and 0.5 for bending, to reduce the crack spacing. In axial tension, the effective tension area of concrete would be the full cross-section area of the member, and this would reduce in bending. Therefore, in both EC2 and MC2010, "the effective tension area of concrete" parameter also represents the variation of transfer length due to the loading method. It has been proved that the crack widths at the concrete surface increase with the increase in applied steel stress [2, 12, 13, 18] and concrete cover [12, 13]. The parameter φ / $\rho_{p,eff}$ (diameter to the ratio of area of steel in tensile bars to the effective area of concrete) has appeared in the crack spacing models in EC2 and MC2010, when considering the equilibrium of a section of transfer length. The effect of steel stress, concrete cover and φ / $\rho_{p,eff}$ will be considered in detail in the discussion of the parametric study in this paper. The experimental results in [2, 12] show that stirrups have an effect on inducing concrete cracks; nevertheless, they do not influence the maximum crack spacing and, hence, the maximum crack width. When the cover is low (i.e. 20 mm in [12]), the authors have witnessed many cracks corresponding with the stirrup location and, in larger covers (i.e. 70 mm in [12]), crack positions deviate with the stirrup position. Therefore, the effect of transfer length is still more dominant than the stirrup position [12], in finding the maximum crack width. The duration of loading is considered as an effect for the mean steel and concrete strain (represented as β factor in MC2010 and k_t in EC2). However, for the crack width considered in the maximum crack spacing, the mean strain in concrete is assumed as 'β' times the maximum concrete strain. The mean steel strain in crack formation stage is assumed as the maximum strain in the crack formation stage reduced by β times the difference of the maximum and minimum strain of steel. In the stabilized cracking stage, the concrete mean strain remains the same and the mean steel strain is assumed as applied steel strain reduced by β times the difference of the maximum and minimum strain of steel. The empirical parameter β is defined, in the stabilized cracking stage, as 0.6 for short-term loading and 0.4 for long-term loading and, in the crack formation stage, as 0.6 for both loading cases. The width of the same crack does not remain the same from the starting point to the end point. Therefore, the exact position of the crack width measurement or the exact position where the calculated crack width is represented is one of the main considerations. This effect is discussed in [14, 19] and it has been proved that, when the 'distance where the crack width being considered to the nearest bar' increases, the measured crack width also increase. The minimum crack width is considered at the concrete surface propagated above the rebar. Therefore, the crack width readings were considered only above the rebar in the experiment conducted by Tan et al. in [13] for the comparison with the calculated crack widths. Furthermore, EC2 also considers this effect and recommends using a separate equation when the spacing of the bonded re bars exceeds $5(c+\emptyset/2)$.

3. PARAMETRIC STUDY

A parametric study was carried out to identify a more reliable crack width calculation model between EC2 and MC2010. Further, the parametric study helps to compare the actual effect of a parameter on the crack width with the codes' predicted behavior. The most governing parameters of crack width prediction models discussed in this paper are concrete cover, $Ø/\rho_{p,ef}$ and applied stress. After examining various experimental data conducted by many previous researchers, data from Tan et al. [13] and Caldentey [12] were used to study the crack widths on axial tensile and bending loading cases, respectively.

The effect of applied steel stress and cover in axial tension

Experimental results from [13] were used to study the applied steel stress and cover in axial tension loading. The behavior of two specimens with similar $Ø/\rho_{p,ef}$ and covers of 40 mm and 90 mm were compared. As per the reinforcement arrangement of the specimens, each side of the specimen was subjected to three readings, corresponding to the three rebars close to each side of the specimen. Due to the inhomogeneous propagation of cracks, each reading was taken as the average crack width within a 40-mm section at the concrete surface just above a rebar. Afterwards, a 95%-fractile of the readings was considered, to compare the values with the calculated values from the codes.

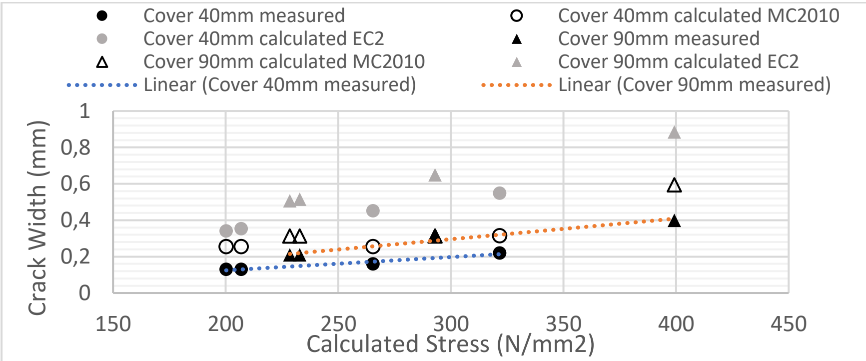

Figure 1: Crack widths of specimens with different concrete covers in axial tension [13]

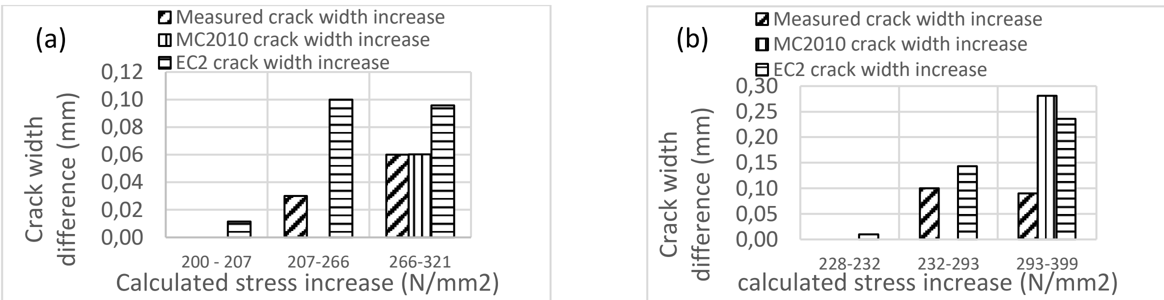

Figure 2: The crack width difference of (a) 40 mm cover and (b) 90 mm cover in Figure 1

When comparing the axial tensile loading case as per Figure 1, it is clear that the crack width increases with the applied steel stress. Further, the results prove that the crack width increases with the increase in concrete cover. This increase in measured crack width with the applied steel stress and the concrete cover matches both EC2 and MC2010 predictions. For these two test specimens, both EC2's and MC2010's predicted values are more conservative. However, as per Figure 1, the predicted values from codes seem to highly overestimate the effect from the concrete cover. Further, the effect of crack width from the increase in applied stresses' prediction can be examined by studying Figure 2 (a) and (b).

According to MC2010, at the crack formation stage, the crack width does not increase with the increase in applied load, because it predicts the maximum possible crack width at crack formation for every applied load. This assumption tallies with the simplified load-strain behavior considered in MC 2010, where the curve behaves in a parallel way to the strain axis, in the crack formation stage. However, as per the Figure 2 (a), when the cover is 40 mm, in the stabilized cracking stage, MC2010 assumes a similar increase in crack width to that of the experiment for the third stress increment. This behavior changes when the cover is 90 mm, and it can be justified, as the MC2010 is valid for concrete covers lower than 75 mm. However, according to Figure 2 (a) and (b), EC2 has overestimated the effect of steel stress on crack width in both loading stages.

The effect of applied steel stress and cover in bending

The results from the four-point bending experiment conducted in [12] are used in this parametric study. The behavior of two specimens with similar $Ø/\rho_{p,ef}$ and covers of 32 mm and 82 mm were compared in this case. In the experiment, Extensometer Measurement Points (EMP) were placed in 200-mm gaps on sides of the specimens in the constant bending zone. The maximum crack width is considered by multiplying the maximum observed strain from EMP and the gap of 200 mm. Experimental data is compared with the calculated values, which represent the maximum crack width that can occur due to maximum crack spacing.

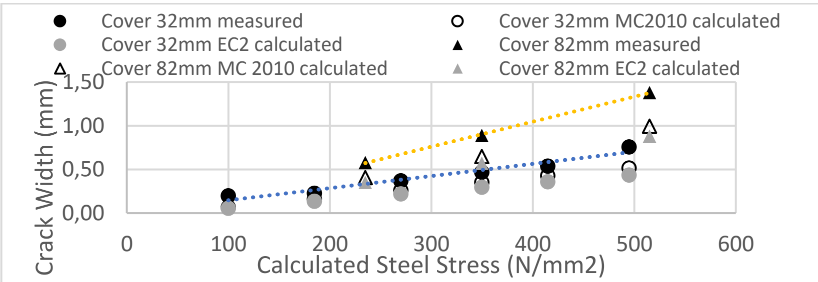

Figure 3: Crack width variation of specimens with different concrete covers in bending [12]

Similar to the axial tensile loading, the crack width increases with the increase in both applied stress and concrete cover. Further, both codes predict similar behavior when increasing the steel stress and concrete cover. However, for both specimens, the code predictions have underestimated the experimental crack widths. This could be mainly due to the method of experimental crack width measurement. When measuring the crack width, the researcher has assumed that the crack spacing is always 200 mm at the same place where the maximum strain of the specimen is recorded.

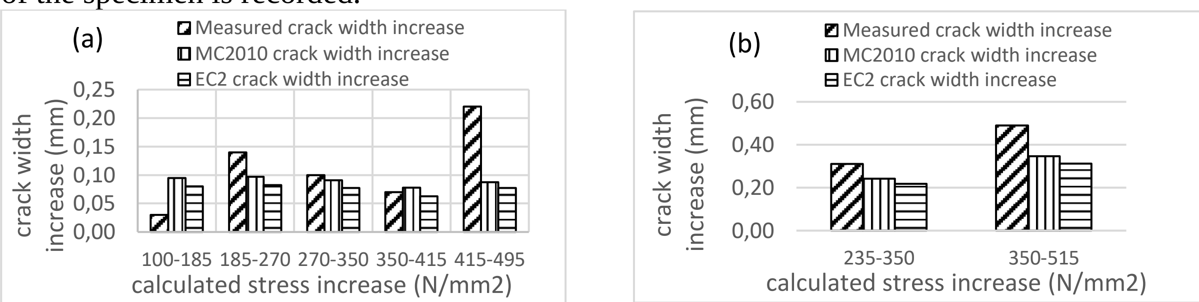

Figure 4: Crack width in specimens with (a) 32-mm and (b) 82-mm cover in Figure 3

The use of k_2 factor as 0.5 in EC2 and the effect of curvature considered in MC2010 have caused there to be higher calculated crack widths in MC 2010, compared to EC2. The crack width increments for each loading step are represented in Figure 4 (a) and (b). The effect of steel stress considered in MC2010 is more or less similar to that of EC2 in both covers. With respect to the experimental results, both codes have underestimated the effect of the steel stress on the crack width, except in two loading steps.

The effect of $\emptyset/\rho_{p,ef}$ on crack width

The parameter $\emptyset/\rho_{p,ef}$ appears in the crack spacing calculation, through consideration of the dispersion of stress from the rebar to the concrete surface, due to the bond stress in the steel/ concrete interphase within the crack and the zero slip section. This parameter depends on the rebar diameter, steel area and the effective tensile area of the concrete. In pure tension, the effective tensile area of the concrete is similar to the cross-section area of the specimen, and this would vary in the case of bending, depending on the effective tensile height. The results of the experiment conducted in [12] were used to compare the effect of $\emptyset/\rho_{p,ef}$ on the maximum crack spacing of specimens with similar cover and similar specimen sizes in bending load. As the crack spacing in the 'stabilized cracking stage' does not vary with the applied stress and the applied stress is not a function of crack spacing, the effect of applied stress is therefore negligible, when comparing the effect of $\emptyset/\rho_{p,ef}$ on crack spacing in the 'stabilized cracking stage'.

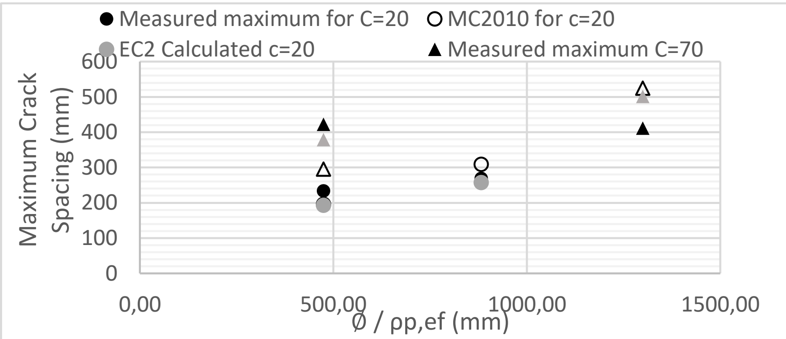

Figure 5: The behavior of "Ø/ρp,ef" parameter on crack spacing

According to Figure 5, it can be seen that the maximum crack spacing slightly increases with the increase of $\emptyset/\rho_{p,ef}$ in the smaller covers; however, this behavior cannot be observed in the large covers. When the behavior of code predictions from a lower to a higher $\emptyset/\rho_{p,ef}$ value is considered, both codes seem to have overestimated the effect of the $\emptyset/\rho_{p,ef}$ parameter. This is similar to Beeby's [14] conclusion, which states that the concrete cover has a greater influence on crack width than the $\emptyset/\rho_{p,ef}$ parameter.

4. CONCLUSIONS

The first step to improving the existing crack width calculation models due to service load influencing parameters is described in this paper. Further, the influence of each parameter on the crack width calculation models is clarified, as per the findings of previous studies. The increase in the surface crack widths with the increase in concrete cover and the applied steel stress in experiments is discussed in detail, with a comparison of EC2 and MC2010 predictions.

Moreover, it has been shown that the effect of the $\varphi/\rho_{s,ef}$ parameter on crack width decreases when the concrete cover becomes larger. From the results of the parametric study, it can be identified that the calculated values of crack widths do not match the experimental values. Further, some experimental results could not be compared with the characteristic values, due to the limitations of the codes. Therefore, the existing codes must be improved, to predict more reliable values for the crack widths.

REFERENCES

1. Francois, R. and A. Castel, *Influences of bending crack and water-cement ratio on chloride-induced corrosion of main reinforcing bars and stirrups. Discussion and Closure.* ACI Materials Journal, 2001. **98**(3).
2. Makhlouf, H.M. and F.A. Malhas, *The effect of thick concrete cover on the maximum flexural crack width under service load.* Structural Journal, 1996. **93**(3): p. 257-265.
3. Beeby, A., *Concrete in the Oceans Technical Report No. 1.* Cement and Concrete Association, Slough, UK, 1978.
4. Schiessl, P., *Admissible crack width in reinforced concrete structures. Contribution II, 3-17.* In: Preliminary reports Vol. II, Inter-association colloquium on the behaviour of in service of concrete structures. 1975.
5. Hornbostel, K. and M. Geiker, *Influence of cracking on reinforcement corrosion.* Workshop proceedings from a Nordic seminar, Crack Width Calculation Methods for Large Concrete Structures, Oslo, Norway, 2017: p. 53.
6. Beeby, A., *Cracking: what are crack width limits for?* Concrete, 1978. **12**(7).
7. Shende, S.S., S. Bhadke, and A.R. Khedikar, *Comparative study of design of water tank with new provisions.* International Journal of Current Trends in Engineering and Research (IJCTER), 2016. **2**(4): p. 481-485.
8. Debernardi, P.G., M. Guiglia, and M. Taliano, *Effect of secondary cracks for cracking analysis of reinforced concrete tie.* ACI Materials Journal, 2013. **110**(2): p. 207.
9. Leonhardt, F., *Cracks and crack control in concrete structures.* PCI Journal, 1988. **33**(4): p.124-145.
10. Beeby, A., *Crack control provisions in the new Eurocode for the design of concrete structures.* Special Publication, 2001. **204**: p. 57-84.
11. Standard Norge, *NS-EN 1992-1-1: 2004+ NA: 2008.* Eurokode, 2008. **2**: p. 1-1.
12. Caldentey, P.A., et al., *Cracking of RC members revisited: influence of cover, $\phi/\rho s$, ef and stirrup spacing–an experimental and theoretical study.* Structural Concrete, 2013. **14**(1): p. 69-78.
13. Tan, R., et al., *Experimental and theoretical investigation of crack width calculation methods for RC ties.* Structural Concrete2018.
14. Beeby, A.W., *The influence of the parameter ϕ/ρ eff on crack widths.* Structural Concrete, 2004. **5**(2): p.71-83.
15. Radnić, J., L. Markota, *Experimental verification of engineering procedures for calculation of crack width in concrete elements.* International Journal for Engineering Modelling, 2003. **16**: p.63-69.
16. Code, M., *fib model code for concrete structures.* Structural Concrete, 2010. **14**.
17. *1–1: Eurocode 2: Design of concrete structures*,1992.
18. Gergely, P. and L.A. Lutz, *Maximum crack width in reinforced concrete flexural members.* Special Publication, 1968. **20**: p. 87-117.
19. Beeby, A., *The prediction and control of flexural cracking in reinforced concrete members.* Special Publication, 1971. **30**: p. 55-76.
20. Caldentey, A.P., *Proposal of new crack width formulas in the Eurocode 2, background, experiments, etc.* Workshop proceedings from a Nordic seminar, Crack Width Calculation Methods for Large Concrete Structures, Oslo, Norway, 2017: p. 17. The Nordic Concrete Federation.

CRACK ANALYSIS OF CONCRETE BENDING MEMBERS BASED ON REINFORCEMENT STRAIN PROFILE BETWEEN PRIMARY CRACKS

Gintaris Kaklauskas (1) and Aleksandr Sokolov (2)

(1) Department of Reinforced Concrete Structures and Geotechnical Engineering, Vilnius Gediminas Technical University, Vilnius, Lithuania

(2) Laboratory of Innovative Building Structures, Vilnius Gediminas Technical University, Vilnius, Lithuania

Abstract

Cracking models of reinforced concrete (RC) applied in practice heavily rely on empiricism. The models suggested by Eurocode 2 and Model Code are based on the empirically established effective concrete area. The authors have recently proposed a new concept of crack analysis based on the compatibility of the stress transfer and mean deformation approaches. Mean spacing between the primary cracks is obtained from the equality of mean strains of the tensile reinforcement assessed by the two concepts. The current paper is dedicated to quantification the constitutive parameters and validation of the model. A comparative analysis has demonstrated that the predictions of mean crack distance by the proposed model agree well with the tests of RC beams.

Keywords: Crack spacing, mean strain, primary cracks, reinforced concrete beam, strain compatibility

1. INTRODUCTION

Cracking is one of the most complicated phenomena of the behaviour of concrete structures. Multiple theoretical models have been proposed to predict cracking characteristics, but most of them rely on empiricism. Recently the authors (Kaklauskas 2017) have suggested a new concept of crack analysis of RC members at the stage of stabilized cracking. The philosophy behind the proposed methodology is to define the mean spacing between primary cracks through compatibility of the stress-transfer and mean deformation approaches, which, respectively, represent the discrete and smeared cracking concepts. Based on the principles of the stress-transfer approach, a strain profile of the tensile reinforcement is defined within the distance between consecutive primary cracks. Three zones with different bond characteristics and strain behavior are established in the strain profile. Parameters of crack spacing are obtained by equating mean strains of the tensile reinforcement defined by the two approaches. The bond stress-transfer approach governs the character of strain distribution of the reinforcement between adjacent cracks, whereas involvement of the mean strain approach allows the cracking spacing to be quantified. Crack spacing is defined as the sum of lengths of these zones within the length of the block.

The current paper is dedicated to quantification of the constitutive parameters and validation of the model based on a limited experimental data of mean crack spacings of RC beams reported in the literature.

2. MEAN CRACK SPACING MODEL

The current study is based on the model of mean crack spacing proposed in (Kaklauskas 2017). The model considers the primary crack pattern with secondary cracks neglected. The characteristic feature of the primary crack is its height reaching the neutral axis defined as for a fully cracked section using elastic material properties. In the current context, all other normal cracks are attributed to the category of secondary cracks. The proposed approach considers a single RC block of a length of the mean crack distance, s_{rm}, assuming that it represents the averaged deformation behavior of the cracked member. Based on the experimental evidence, reinforcement strain within the block is characterized by a strain profile consisting of straight lines shown in Fig. 1. Three zones with different bond characteristics are identified in the strain profile:

1. The *effective* zone with length l_{ef}. This zone, being responsible for the tension stiffening effect, is defined by the effective transmission of the bond stresses from the reinforcement to concrete. In (Kaklauskas 2017) following the suggestion by Marti et al. (1998), constant bond stress $\tau = 2f_{ct}$ was assumed. Linear strain variation (see Fig. 1) results in this effective length l_{ef} (see Fig. 1):

$$\varepsilon_s(x) = \varepsilon_{si} - A \cdot x \tag{1}$$

$$A = (4 \cdot \tau)/(E_s \cdot \emptyset_s) \tag{2}$$

$$l_{ef} = (\varepsilon_{si} - \varepsilon_{s0})/A \tag{3}$$

where ε_{si} is the reinforcement strain at the crack; ε_{s0} is the minimum strain in the reinforcement strain profile; A is the slope of the linear strain function; E_s is the modulus of elasticity of reinforcement; $\emptyset_s$ is the bar diameter.

2. The *debonding zone* with length l_d. In the vicinity of crack, the bond between concrete and reinforcement bar is damaged due to the local effects in the concrete surrounding the reinforcement bar. It was suggested in (Kaklauskas et al. 2017) to relate the constitutive parameter l_d to bar diameter and reinforcement strain in the cracked section:

$$l_d = (1000/3) \cdot \varepsilon_{si} \cdot \emptyset_s \tag{4}$$

3. The *central* zone with length l_c (see Fig. 1). It characterizes another area *with negligible* bond stress. The assumption of the bond damage in the *central* zone captures the influence of secondary cracks on the tension stiffening effect. The study (Kaklauskas 2017) proposed the following formula for the *central* zone length:

$$l_c = 0.44 \cdot (d - y_0) \tag{5}$$

where d is the effective depth of section; y_0 is the depth of the compressive zone in the cracked section assessed by the standard elastic theory.

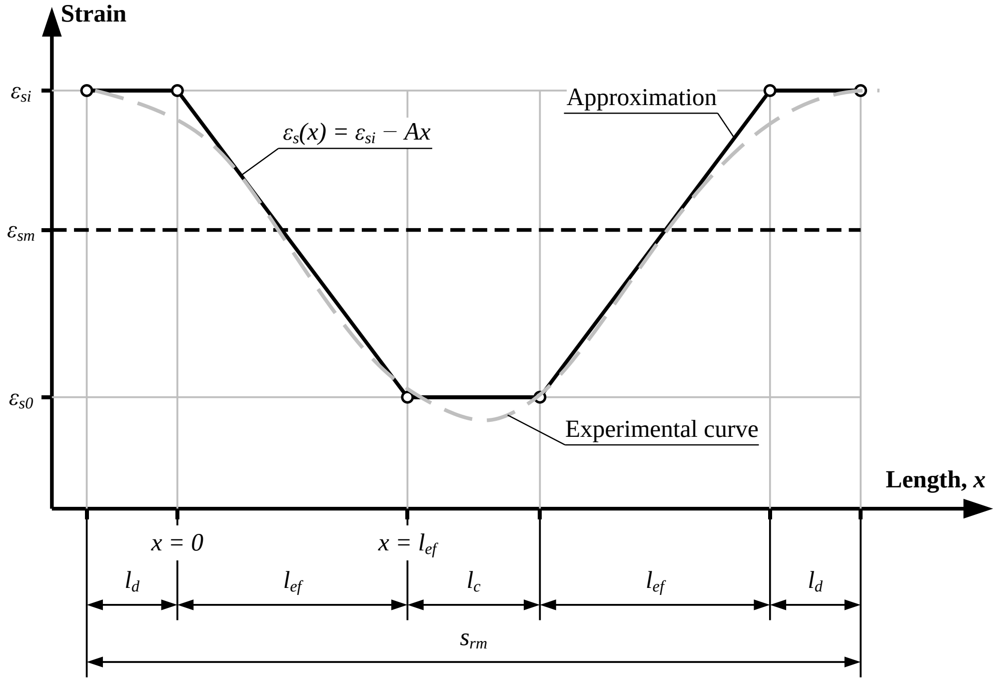

Figure 1: Reinforcement strain profile

Mean crack spacing is then expressed as the sum of lengths of different zones of the reinforcement strain profile as shown in Fig. 1:

$$s_{rm} = l_c + 2 \cdot l_{ef} + 2 \cdot l_d \tag{6}$$

To consider the equivalent loading level for different members, a unified value of reinforcement strain in the cracked section ε_{si} = 0.0015 is assumed. The respective bending moment can be assessed by this formula:

$$M = \varepsilon_{si} \cdot E_c \cdot I_{tr}/(d - y_0) \geq c \cdot M_{cr} \tag{7}$$

where E_c is the modulus of elasticity of concrete; I_{tr} is the second moment of area of the transformed section; M_{cr} is the cracking bending moment; the present study takes $c = 2.5$.

The condition of equality of mean strains defined by the mean strain approach and the adopted shape function (see Fig. 1) can be written as follows:

$$\varepsilon_{s0} \cdot l_c + 2 \cdot (\varepsilon_{si} - 0.5 \cdot A \cdot l_{ef}) \cdot l_{ef} + 2 \cdot \varepsilon_{si} \cdot l_d = \varepsilon_{sm} \cdot (l_c + 2 \cdot l_{ef} + 2 \cdot l_d) \tag{8}$$

Herein, strain ε_{sm} is calculated by the Eurocode 2 (CEN 2004) technique. Equation 8 can be expressed as the second order equation:

$$A \cdot l_{ef}^2 + B \cdot l_{ef} + C = 0 \tag{9}$$

With the solution as:

$$l_{ef} = \left(-B + \sqrt{B^2 - 4 \cdot A \cdot C}\right)/(2 \cdot A) \tag{10}$$

$$B = l_c \cdot A - 2 \cdot (\varepsilon_{si} - \varepsilon_{sm}) \tag{11}$$

$$C = (\varepsilon_{si} - \varepsilon_{sm}) \cdot (l_c + 2 \cdot l_d) \tag{12}$$

3. CONSTITUTIVE MODELLING

The suggested model has introduced three constitutive parameters, each characterising different zones of the reinforcement strain profile. These parameters that in essence govern the results of analysis of mean crack spacing are: bond stress, τ, in the effective zone, length of the debonding zone, l_d, and length of the central zone, l_c. The last two parameters were quantified earlier (Kaklauskas 2017), thus, the current study discusses the remaining parameter, namely, bond stress, τ.

The Equation 8 of strain compliance is rearranged to include bond stress τ:

$$\varepsilon_{s0} \cdot l_c + 2 \cdot \left(\varepsilon_{si} \cdot l_{ef} - 0.5 \cdot (4 \cdot \tau/(E_s \cdot \emptyset_s)) \cdot l_{ef}^2\right) + 2 \cdot \varepsilon_{si} \cdot l_d = \varepsilon_{sm} \cdot s_{rm} \tag{13}$$

From Equation 13 assuming $s_{rm} = s_{rm,exp}$ and $l_{eff} = (s_{rm,exp} - 2\ l_d - l_c) / 2$, bond stress, τ can be expressed as:

$$\tau = (E_s \cdot \emptyset_s/4) \cdot (\varepsilon_{si} - \varepsilon_{sm}) \cdot s_{rm,exp}/\left(l_c \cdot l_{ef} + l_{ef}^2\right) \tag{14}$$

Using Equation 14, bond stress was calculated for a number of bending RC members. The members with large reinforcement ratio have small lengths of the effective zone meaning that bond stress has no effect on crack spacing in such members. For that reason, members with smaller amounts of reinforcement were used to investigate bond characteristics. 28 bending members with reinforcement ratio below 1% were collected from the tests reported in the literature. The calculated values of bond stress normalised with tensile strength of concrete, f_{ct}, are presented in Fig. 2 within the range of reinforcement ratio. Fitting of the test data results in the following formula:

$$\tau = (2.8 - 50 \cdot \rho) \cdot f_{ct} \tag{15}$$

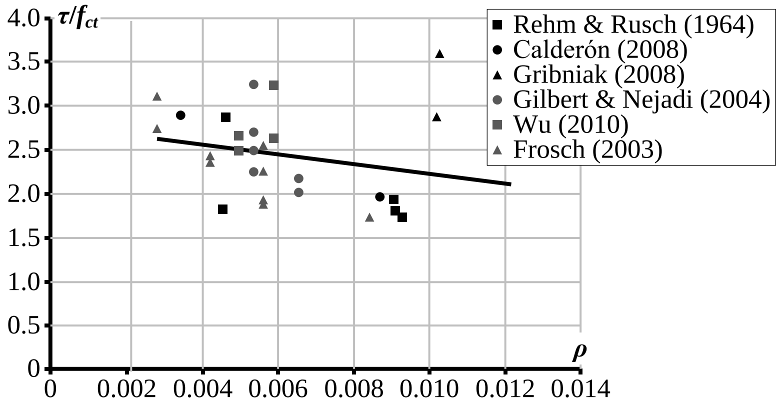

Figure 2: The effect of reinforcement ratio on bond stress

According to Equation 15, bond stress reduces with growing reinforcement ratio being 2.6 f_{ct} for ρ = 0.2% and 1.8 f_{ct} for ρ = 2%. The latter value of τ equals to the bond stress taken in the Model Code (*fib* 2013) and Eurocode 2 (CEN 2004).

4. PREDICTION OF MEAN CRACK SPACING

To check the accuracy of the proposed technique, predicted mean crack spacings s_{rm} were checked against the test data reported in the literature. Table 1 presents main characteristics of flexural RC members employed in the analysis. The predicted results are shown in Fig. 3 in terms of normalized mean crack spacing ($s_{rm,th}$ / $s_{rm,exp}$) where the horizontal axis refers to the numbering of the beams in accordance to Table 1.

Table 1: Main characteristics of test data employed in the analysis

Author	No	***h*, m**	***b*, m**	**∅s, mm**	***ρ*, %**	**f_{cyl}, MPa**
Rehm & Rusch (1964)	1 – 2	1.20	0.30 – 0.45	10 – 32	0.46 – 1.22	13 – 43
	3 – 30	0.62				
Calderón (2008)	31 – 44	0.50	0.25	10 – 25	0.34 – 2.34	22 – 28
Hognestad (1962)	45 – 49	0.41	0.20	13 – 25	1.34 – 1.44	18 – 39
Wu (2010)	50 – 52	0.40	0.20 – 0.80	12 – 16	0.50 – 0.88	26– 40
	102 – 103	0.14				
Beeby (1966)	53 – 80	0.39	0.18	19	0.93	22 – 27
Gilbert & Nejadi (2004)	81 – 84	0.34	0.25 – 0.40	12 – 16	0.54 – 0.65	37 – 39
	100 – 101	0.16				
Gribniak et.al (2008)	85 – 89	0.30	0.27 – 0.28	8 – 22	0.61 – 1.03	43 – 50
Frosch (2003)	90 – 99	0.20	0.91	16	0.28 – 0.84	44 – 47

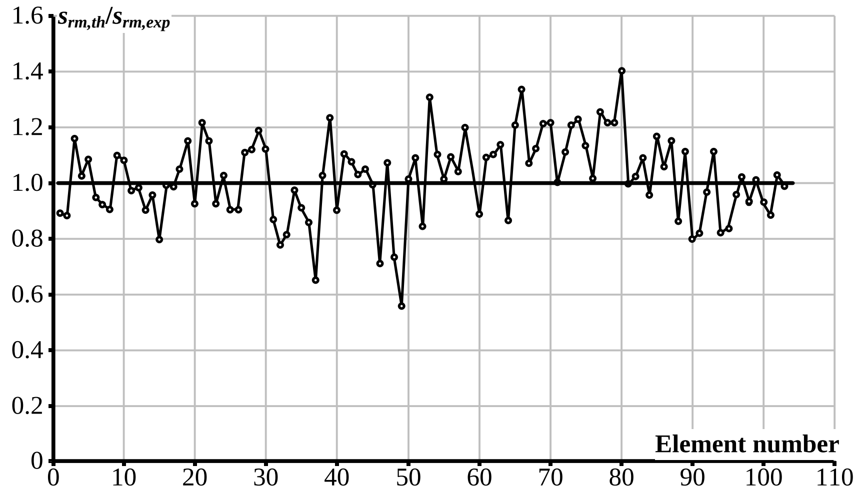

Figure 3: Prediction of crack spacing

The results obtained are discussed below:

- Mean value of the predicted normalized mean spacing between primary cracks was close to one ($s_{rm,th}$ / $s_{rm,exp}$ = 1.02).
- The accuracy was not affected by such parameters as section height, reinforcement ratio, bar diameter or concrete compressive strength giving rather consistent results within the set of test data. The coefficient of variation CV = 14.6% demonstrates adequate prediction accuracy of mean spacing between primary cracks by the proposed approach.

5. CONCLUSIONS

- The suggested method based on the strain profile of the tensile reinforcement between primary cracks is shown to be a simple and mechanically sound tool to predict mean crack spacing of RC elements.
- Good agreement of predicted and experimental mean crack spacing in terms of normalized mean value ($s_{rm,th}$ / $s_{rm,exp}$ = 1.02) and coefficient of variation (14.6%) was achieved for the data set of 104 beams.
- The accuracy of the predictions does not seem to be affected by such parameters as section height, reinforcement ratio, bar diameter or concrete compressive strength.

ACKNOWLEDGEMENTS

This research was funded by the European Social Fund according to the activity ‘Improvement of researchers’ qualification by implementing world-class R&D projects’ of Measure No. 09.3.3-LMT-K-712

REFERENCES

[1] Kaklauskas, G., 'Crack model for RC members based on compatibility of stress-transfer and mean-strain approaches', *J. Struct. Eng., ASCE.* **143** (9) (2017) 1-12.
[2] Kaklauskas, G., Ramanauskas, R. and Jakubovskis, R., 'Mean crack spacing modelling for RC tension elements', *Eng. Struct.* **150** (2017) 843-851.
[3] CEN (European Committee for Standardization), 'Design of concrete structures: Part 1-1: General rules and rules for buildings', Eurocode 2 (Brussels, Belgium. 2004).
[4] *fib* (International Federation for Structural Concrete), 'Model code for concrete structures 2010', (Wiley, Berlin 2013) 434.
[5] Rehm, G. and Rüsch, H., 'Versuche mit betonformstahlen, deutscher ausschuss fur stahlbcton', Berlin (1964).
[6] Calder´on, B. E., 'Estudio experimental de la fisuraci´on en piezas de hormig´on armado sometidas a flexi´on pura', Ph.D. thesis, Universidad Politécnica de Madrid, Madrid, Spain (2008).
[7] Hognestad, E., 'High strength bars as concrete reinforcement Part 2. Control of flexural cracking', *Journal of the PCA Research and Development Laboratories.* **4** (1) (1962) 46-63.
[8] Wu, H. Q., 'Tension stiffening in reinforced concrete – instantaneous and time-dependent behaviour', Ph.D. thesis, the university of New South Wales, Sydney, Australia (2010).
[9] Beeby, A. W., Base, G. D., Read, J. B. and Taylor, H. P. J., 'An investigation of the crack control characteristics of various types of bar in reinforced concrete beams', Research report 18, (1966).
[10] Gilbert, R. I. and Nejadi, S., 'An experimental study of flexural cracking in reinforced concrete members under short term loads', Univ. of New South Wales, School of Civil and Environmental Engineering, Sydney, Australia. (2004).
[11] Kaklauskas, G., Christiansen, M. B., Bacinskas, D. and Gribniak, V., 'Constitutive model for reinforced concrete members taking into account concrete creep and shrinkage at pre-loading stage (Gelžbetoninių elementų deformacijų modelis, įvertinantis betono susitraukimą ir valkšnumą ikieksplotacinėje stadijoje)',Technical Report NR. T-08024. Vilnius, VGTU. (2008) 46 p.
[12] Frosch, R., Blackman, D. and Radabaugh, R., 'Investigation of bridge deck cracking in various bridge superstructure systems', FHWA/IN/JTRP report no. C-36-56YY, File No. 7-4-50. West Lafayette, IN: School of Civil Engineering, Purdue University. (2003). p. 286.

International Conference on Sustainable Materials, Systems and Structures (SMSS 2019)
Challenges in Design and Management of Structures
20-22 March 2019 – Rovinj, Croatia

RESTRAINT-INDUCED CRACK FORMATION AND CRACK WIDTHS IN THICK WALLS

Dirk Schlicke (1), Katrin Hofer (1, 2) and Nguyen Viet Tue (1)

(1) Institute of Structural Concrete, Graz University of Technology, Austria

(2) Federal Waterways Engineering and Research Institute (BAW), Karlsruhe, Germany

Abstract

The present paper presents a method for the determination of the crack width of the primary crack in thick concrete members with conventional reinforcement near the surface. In contrast to the common theory for crack width calculation on basis of the successive cracking of a reinforced concrete tie, this approach is based on the deformation compatibility and distinguishes between primary cracks and secondary cracks for adequate consideration of the finding that the force in the reinforcement decreases from primary crack to first secondary crack to second secondary crack and so on.

Contrarily to the common case, in which the designer aims at the determination of required reinforcement, the present paper applies the theory for the determination of the crack width of the primary crack in order to enable the assessment of existing structures or the analysis of experiments.

Keywords: thick concrete walls, imposed deformations, restraint-induced cracking, crack width control, minimum reinforcement

1. INTRODUCTION

Concrete shows distinct volume changes due to hydration, drying, creep and thermal dilation. Under restrained conditions, in which concrete members cannot deform freely, restraint stresses occur. Temporal occurrence of herewith caused cracking is subject to a complex interplay of thermal, hygric and mechanical behaviour of the concrete as well as the structural conditions in terms of member dimensions, restraining situation, exposure and ambient conditions, etc. A profound overview on the state-of-the-art can be found in the Report of RILEM TC 254-CMS [1].

Altogether, the assessment of restrained-induced cracking requires an interdisciplinary assessment with adequate consideration of the deformation behaviour of concrete as well as the structural behaviour of the member itself.

The available methods for crack width estimation of relevant standards, such as [2] or [3], are based on the successive cracking of a reinforced concrete tie. However, the behaviour of thick concrete walls restrained at the bottom and reinforced with ordinary reinforcement near the surface is not adequately represented by this theory. This paper presents a method for the determination of the crack width in thick walls with respect to the compatibility of deformations as well as the particular mode of cracking in thick concrete members with ordinary reinforcement near the surface.

2. CRACKING PATTERNS IN BOTTOM-RESTRAINED WALLS

The stress distribution due to stress resultants (without Eigenstresses) in bottom-restrained walls depends strongly on the length-to-height-ratio (*L*/*H*) of the wall, whereby the stress maximum occurs always at the bottom, [4], [5] and [6]. This stressing causes a geometrically set cracking pattern in which primary cracks are caused systematically according to the restraining condition and the stress distribution. The distance between the primary cracks depends strongly on the height of the primary crack and is rather big compared to the crack spacing due to the reinforcement in the concrete tie. Figure 1 illustrates this context schematically.

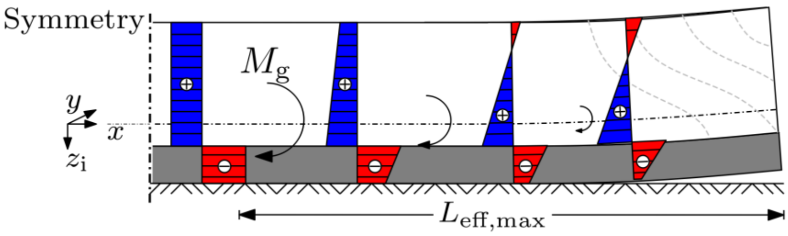

a) stress distribution over the height according to the Length-to-Height ratio (L/H)

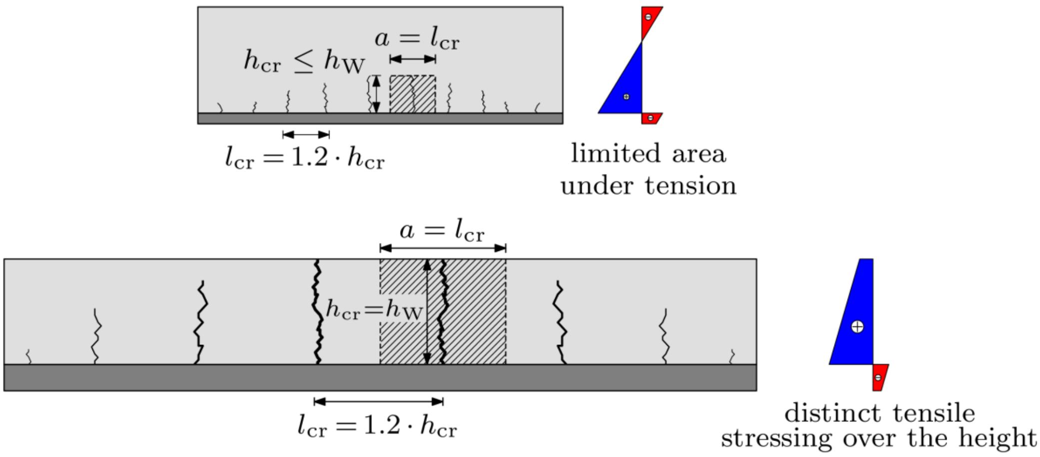

b) primary cracking according to the stress distribution over the height

Figure 1: Distribution of restraint stresses in bottom-restrained walls (a) and herewith caused geometrically set primary cracks (b) according to [4] and [5]

After primary cracking, the reinforcement is activated in the primary crack and can create additional cracks behind the transfer length. However, in the common case that the reinforcement in the thick wall is located near the surface, the new cracks caused by the anchorage of the reinforcement affect solely the effective concrete area (so called secondary cracks). Although, these secondary cracks will not proceed over the whole cross section, as illustrated in Figure 2, they still contribute to the deformation compatibility and the crack width at the surface.

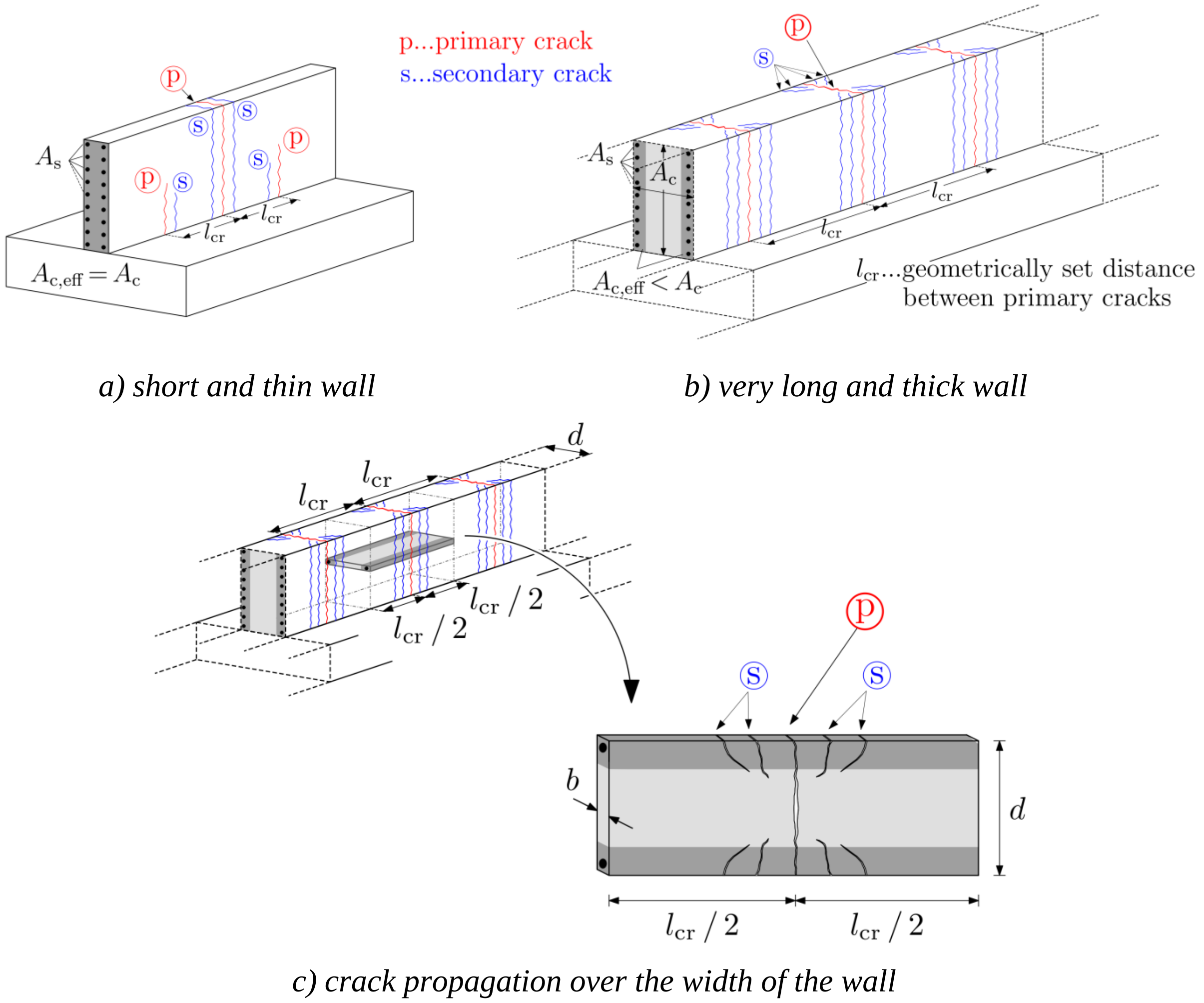

Figure 2: Schematic illustration of geometrically set primary cracks in bottom-restrained walls and secondary cracks due to reinforcement in the vicinity of the primary cracks

The outlined cracking process consisting of a primary crack and secondary cracks is characterized by the particularity that the force in the reinforcement decreases from primary crack to first secondary crack to second secondary crack and so on. This means, the crack width estimation must distinguish between primary cracks and secondary cracks.

3. WIDTH OF THE PRIMARY CRACK IN THICK CONCRETE MEMBERS

The potential to open the primary crack (w_{rest}) can generally be quantified with Eq. (1) taking into account the imposed deformation derived from the present restraint stresses, the distance of the primary cracks and the change of the member stiffness due to cracking.

$$w_{\text{rest}} = \frac{\sigma_{\text{c}}^{\text{I}}}{E_{\text{c}}} \cdot l_{\text{cr}} \cdot \frac{a^{\text{II}}}{a} \tag{1}$$

with:

$\sigma_{\text{c}}^{\text{I}}$ – restraint stresses in the uncracked state due to imposed deformations
E_{c} – Elastic modulus of the concrete
l_{cr} – geometrically set distance between primary cracks
a^{II} – degree of restraint in the cracked state
a – degree of restraint in the uncracked state

Besides the general effect of reinforcement on the limitation of the crack width in the primary crack, the reinforcement will also create secondary cracks in the vicinity of the primary cracks, whereby the crack opening of the secondary cracks will contribute to the absorption of the imposed deformations. According to [9], the sum of crack widths can be quantified with Eq. (2).

$$\sum w = w^{\text{P}} \cdot (1 + 0.9 \cdot n) \tag{2}$$

with:

w^{P} – width of the primary crack
n – number of secondary cracks

The factor 0.9 in Eq. (2) reflects the consideration, that the primary crack has the biggest width whereby the crack width of every new secondary crack decreases. This assumption was derived from non-linear FE studies and analytical considerations in [8]. A fundamental principle is hereby, that always 30 % of the steel stresses remain in the concrete between two cracks, e.g. the steel stress in the first secondary crack σ_s^1 has a size of 70 % of the steel stress in the primary crack σ_s^{P}. Figure 3 illustrates this consideration schematically.

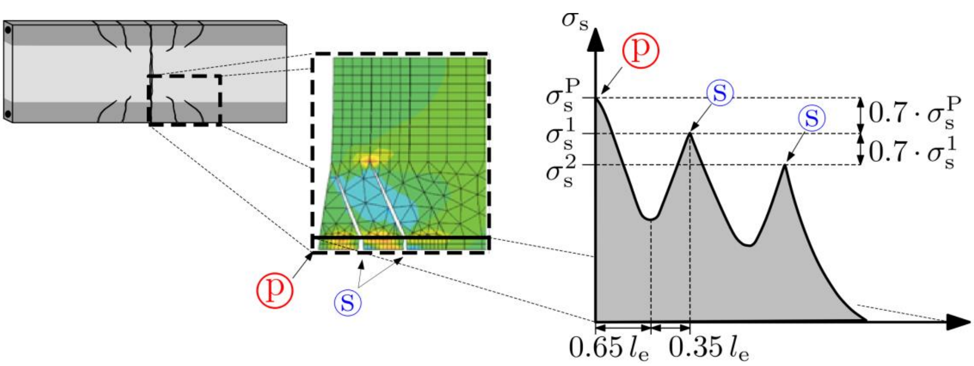

Figure 3: Distribution of steel stresses in one crack system according to [8]

Another influencing parameter of the width of the primary crack is the contribution of the concrete stresses after cracking which are still present in the uncracked area between two primary cracks. The stresses itself can easily be derived from the force equilibrium along the member with Eq. (3).

$$\sigma_c^{II} = \sigma_s^P \cdot \rho_s \tag{3}$$

with:

σ_c^{II} – restraint stresses in the uncracked state due to imposed deformations
ρ_s – reinforcement ratio with regard to the whole concrete area ($\rho_s = A_s/A_c$)

The quantification of the resulting deformation from σ_c^{II} requires also the definition of the length in which these stresses act. On the one hand, this length depends of the distance between the geometrically set primary cracks l_{cr} but also on the number of secondary cracks, which decreases the length in which σ_c^{II} appears. Figure 4 illustrates this consideration schematically.

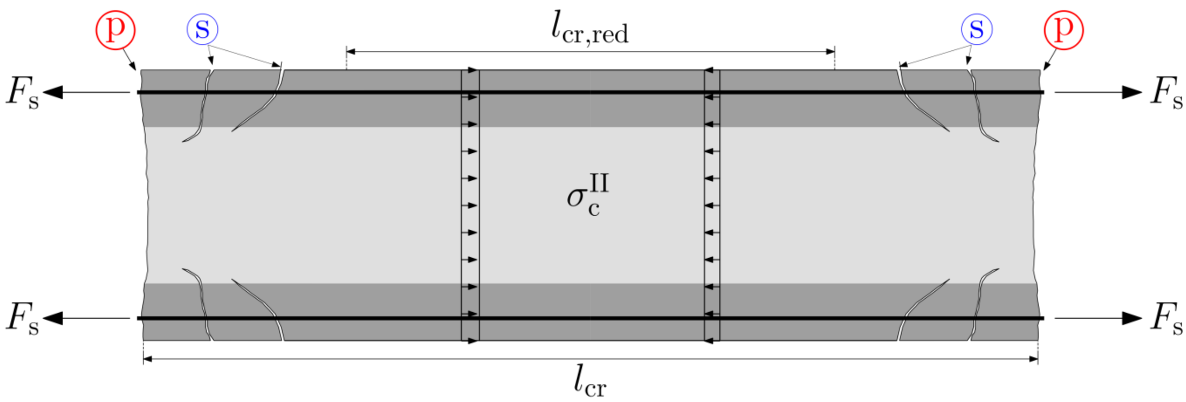

Figure 4: Force equilibrium between two primary cracks and length with concrete stresses between two primary cracks in a thick member with reinforcement near the surface

Altogether, the width of the primary crack can be derived from equating Eq. (1), (2) and (3) with regard to the contribution of the deformation of concrete in the uncracked area between two primary cracks ($\sigma_c^{II} \cdot l_{cr,red}$). It reads:

$$w^P = \left(\frac{\sigma_c^I}{E_c} \cdot l_{cr} \cdot \frac{a^{II}}{a} - (\sigma_s^P \cdot \rho_s) \cdot l_{cr,red}\right) \cdot \frac{1}{(1 + 0.9 \cdot n)} \tag{4}$$

The solution of Eq. (4) is not trivial since the parameters involved are connected to each other. For example, the number of secondary cracks n strongly affects a^{II} and $l_{cr,red}$. And this affects the steel stress in the primary crack σ_s^P which in turn affects n.

Aiming at practical applications, this interplay was investigated in [7] by means of comprehensive parametric studies. Finally, the following simplification was proposed:

$$\frac{\sigma_c^I}{E_c} \cdot l_{cr} \cdot \frac{a^{II}}{a} - (\sigma_s^P \cdot \rho_s) \cdot l_{cr,red} = \frac{\sigma_c^I}{E_c} \cdot l_{cr} \cdot \frac{k_{mod}}{a^{0.6}} \quad (5)$$

with:

k_{mod} – factor for consideration of the contribution of elastic concrete strains in the area between primary cracks; the strong influence of the number of secondary cracks is regarded implicitly with a distinction between low or high stressing by comparing concrete stresses σ_c^I with the present tensile strength $f_{ct,eff}$

Intensity of stressing	requirements on tightness	
	high	low
$\sigma_c^I < 2 \cdot f_{ct,eff}$	0.75	0.6
$\sigma_c^I \geq 2 \cdot f_{ct,eff}$	0.85	0.65

Applying this simplification in Eq. (4) leads to a solution, which still depends on one unknown, namely the number of secondary cracks n. However, if the present reinforcement $a_{s,min}$ is known, n can be determined by inverting the equation for determination of required reinforcement for crack width control in [7], see Eq. (6).

$$a_{s,min} = \sqrt{\frac{d_s \cdot d_1^2 \cdot b^2 \cdot f_{ct,eff}}{w_k \cdot E_s} \cdot (0.5 + 0.34 \cdot n)} \quad (6)$$

with:

d_s – reinforcement diameter
d_1 – distance from the centre of gravity of the reinforcement to the surface, e.g. for one reinforcement layer: $d_1 = c_{nom} + d_s/2$ with c_{nom} = concrete cover
b – linear metre
w_k – crack width criteria
E_s – Elastic modulus of the reinforcement
n – required number of secondary cracks, which is determined from the equilibrium between Eq. (1) and (2)

Altogether, the width of the primary crack can finally be determined with Eq. (7):

$$w^P = 0.01 \cdot \frac{f_{ct,eff} \cdot d_s}{\rho_{eff}^2 \cdot E_s} \cdot \left(1 + \sqrt{1 + 639 \cdot \frac{\sigma_c^I}{E_c} \cdot l_{cr} \cdot \frac{k_{mod}}{a^{0.6}} \cdot \frac{\rho_{eff}^2 \cdot E_s}{f_{ct,eff} \cdot d_s}}\right) \quad (7)$$

with:

ρ_{eff} – reinforcement ratio with regard to effective concrete area $A_{c,eff} = 2.5 \cdot d_1 \cdot b$

4. SUMMARY

The present paper presents a method for the determination of the crack width of the primary crack in thick concrete members with conventional reinforcement near the surface. The particularity of this approach is the distinction between primary cracks and secondary cracks for adequate consideration of the finding that the force in the reinforcement decreases from primary crack to first secondary crack to second secondary crack and so on.

The underlying theory was developed by [4], [7] and [8] and is applied in a guideline for the design of reinforcement for crack width control in thick hydraulic structures [9]. Contrarily to the common case, in which the designer aims at the determination of required reinforcement, the present paper applies the theory for the determination of the crack width of the primary crack in order to enable the assessment of existing structures or the analysis of experiments.

ACKNOWLEDGEMENTS

The cooperation with the Federal Waterways Engineering and Research Institute (BAW) in Karlsruhe, Germany was scientifically and financially significant for the project's success and we thank Dipl.-Ing. Rainer Ehmann and Dr.-Ing. Jörg Bödefeld for the prosperous collaboration. The authors would also like to thank the team of the Laboratory for Structural Engineering at Graz University of Technology (LKI) for their great support.

REFERENCES

[1] E. M. R. Fairbairn and M. A. D. Azenha, eds., Thermal cracking of massive concrete structures. State-of-the-art report of the RILEM Technical Committee 254-CMS. 2019.

[2] EN 1992-1-1:2015: EUROCODE 2: Design of concrete structures - Part 1-1: General rules and rules for buildings. (2015)

[3] fib Model Code 2010: fib Model Code for Concrete Structures 2010 (2013)

[4] Schlicke D., 'Mindestbewehrung für zwangbeanspruchten Beton', *PhD thesis* 2nd Ed., (Graz University of Technology, 2014, in German)

[5] Schlicke, D. and Tue, N. V., 'Minimum reinforcement for crack width control in restrained concrete members considering the deformation compatibility', *Struct. Conc.* **16** (2015) 221–232.

[6] Schlicke, D., Matiašková, L. and J. Šoltész, 'Effect of partial restraining conditions and Poisson's ratio in bottom-restrained walls', *Proc. of Int. Conf. SynerCrete'18*, (RILEM Publications, Paris, France, 2018), pp. 573–578

[7] Turner, K., 'Ganzheitliche Betrachtung zur Ermittlung der Mindestbewehrung für fugenlose Wasserbauwerke', *PhD thesis* (Graz University of Technology, 2017, in German)

[8] Bödefeld, J., 'Rissmechanik in dicken Stahlbetonbauteilen bei abfließender Hydratationswärme', *PhD thesis* (University of Leipzig, 2010, in German)

[9] BAW-Merkblatt (2010), Merkblatt früher Zwang – Rissbreitenbegrenzung für frühen Zwang in massiven Wasserbauwerken. Referat Massivbau der BAW, Karlsruhe.

International Conference on Sustainable Materials, Systems and Structures (SMSS 2019)
Challenges in Design and Management of Structures
20-22 March 2019 – Rovinj, Croatia

QUANTIFYING DYNAMIC PROPERTIES OF BRIDGES FOR BRIDGE-VEHICLE INTERACTION MODELLING

Maja Kreslin, Peter Češarek, Jan Kalin, Andrej Anžlin and Aleš Žnidarič

Slovenian National Building and Civil Engineering Institute

Abstract

Bridge weigh-in-motion systems measure axle loads and spacings of all vehicles in the traffic flow and have as such an important role in the field of traffic and road infrastructure management. They require a existing bridge, which is often sensitive to environmental influences. Consequently, accuracy of the weighing results depends on various factors. One of the key ones is the unevenness of road surface that causes unpredictable dynamic vehicle-bridge interaction. This problem was investigated within the research project that dealt with influence of the road surface unevenness on accuracy of bridge weigh-in-motion results.

This paper presents the experimental part of the project which dealt with the spatial numerical model for simulating the response of a bridge with uneven road surface during crossing of a vehicle. The comparison of the numerical results with the results of extensive field tests, primarily strains and displacements of the bridge due to the crossings of selected vehicles, shows that the mathematical model in Abaqus software is well able to reproduce the measured response of bridge-vehicle interaction.

Keywords: bridge-vehicle interaction, road surface unevenness, bridge weigh-in-motion system

1 INTRODUCTION

Bridge weigh-in-motion (B-WIM) technology [1, 2], used to measure axle loads and spacings of all vehicles in the traffic flow, requires a bridge which may have uneven road surface that causes unpredictable dynamic vehicle-bridge interaction [3]. Numerous studies have shown that such interaction is a complex problem. It depends on [4]: characteristics of the bridge (bridge geometry, support conditions, bridge stiffness, damping characteristics, etc.), characteristics of the vehicle (axle spacing, weight distribution, stiffness and damping characteristics of the suspension system), characteristics of the loading (vehicle velocity, position of load, number of vehicles contributing to the loading case, etc.) and road surface condition (road profile of the bridge deck and the approaches to the bridge, presence of bumps, ruts, potholes, etc.). Various ways of modelling bridge-vehicle interactions exist. The choice of a particular model depends on the complexity of the problem and the required accuracy. The simplest approach is to model the bridge as an Euler-Bernoulli beam and the vehicle as a moving force/mass [4, 5]. More realistic vehicle models include spring and dashpot systems [6]. In the case of 3D approaches, the bridge can be modelled as a plate [7] or by 3D finite elements [5, 8, 9]. For such cases the 3D vehicle models with many degrees of freedom were developed [10].

Incorporating suitable, site-specific road profile into a vehicle-bridge interaction model remains a challenge. Uneven road surface (settlements, potholes, ruts…) increases the level of dynamic interaction between the vehicle and the bridge, and the dynamic excitation varies not only with respect to the type of the vehicle and its suspension but also related to the transverse location of the crossing vehicle. The studies have shown [11] that an uneven road profile can increase the dynamic amplification factor beyond the values from the codes. Ideally, for road-vehicle interaction modelling, the profile of the road surface should be measured. Unfortunately, it is in most cases numerically generated [12]. The problems of presence of bumps or potholes on road surfaces are described in [13]. In the case of spatial description of bridge-vehicle interaction, the information longitudinal and transverse road profile is required.

This paper describes outcomes of a study that validated the results of a simulated spatial numerical model with the measured response of a vehicle that was crossing a bridge with uneven road surface. The model is based on [14, 15, 16], which is often used in various studies. Different numerical results (i.e. frequencies of the bridge, frequencies of the vehicle, deformations of bridge) are compared with the results of extensive field measurements on the selected bridge, which included measurements of dynamic properties of the bridge and the vehicle, as well as strain recordings on the bridge during crossings of selected vehicles.

2 FIELD MEASUREMENTS

2.1 Description of the bridge

The test bridge was an existing 16-m long structure located near Ljubljana, Slovenia (Figure 1). Views from the side and from the top are shown in Figure 2.

The structural system consists of reinforced concrete slab and two reinforced concrete piers. It was designed in 1945 and later partly reconstructed. Details about the works are not available in the archives. The exact dimensions of the bridge were obtained from field measurements. Figure 2 displays the cross section and elevation of the bridge. The thickness of the asphalt layer amounts to 16 cm. Material characteristics, i.e. E = elastic modulus and ν = Poisson's ratio, were assumed to be $E = 31\ GPa$ and $\nu = 0.2$ for concrete and $E = 5\ GPa$ and $\nu = 0.2$ for asphalt. The test bridge was subjected to loading of vehicles that crossed the structure with different velocities and at changing transverse position, as described in section 2.5.

2.2 Measurements of dynamic properties of bridge

To determine dynamic characteristics of the bridge (natural frequencies and damping), it was equipped with 6 accelerometers on the lower part of the plate (Figure 3). The locations

Figure 1: Test bridge

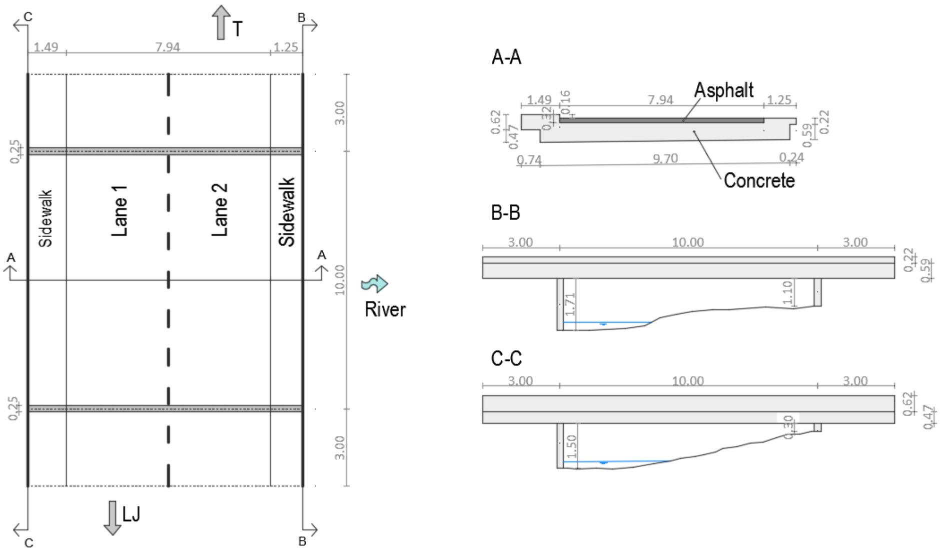

Figure 2: Dimensions of the test bridge, obtained by field measurements

were selected in such a way, that expecting vibration modes can be measured. Time histories of the accelerations during the free flow traffic were recorded at a sampling frequency 4096 Hz. Fourier Transformation was used to determine the natural frequencies and corresponding damping ratio. In the analyses only 3 seconds intervals, when vehicle left the bridge, were considered. Figure 3 shows the mean spectra of 44 intervals. The identified frequencies were 15.3 Hz and 38.3 Hz and corresponding damping ratio 5 % and 3 %. Modes shape data of identifying frequencies were obtained by filtering original signal. If compared with the numerical model, only the first and the third modes were excited with the free traffic flow.

2.3 Measurement of road profile

Measurements of road surface profile (longitudinal and transverse) were performed using terestric laser scanning (TLS). TLS represent measurement technology for a quick, detailed and precise description of the geometry. The result of that kind of technology is point cloud, which needs to be processed for further use.

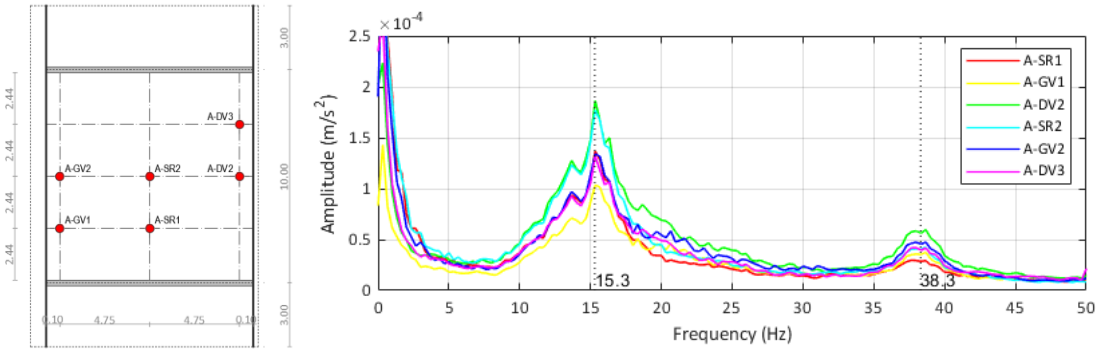

Figure 3: Locations of the accelerometers (left) and dynamic responses of the bridge in frequency domain (right)

Measurements of road surface profile of testing bridge were carried out from five stands. The selected point density was 7 mm at ten meters (this applies both for horizontal and vertical direction). The processed point cloud of the road points directly above the bridge contained about half a million points. Based on those points, the triangular network model was created (Figure 4. left). This model, which describes road surface unevenness of testing bridge, was later implemented into a detailed numerical model [17] for simulating driving vehicle over bridge with uneven surface.

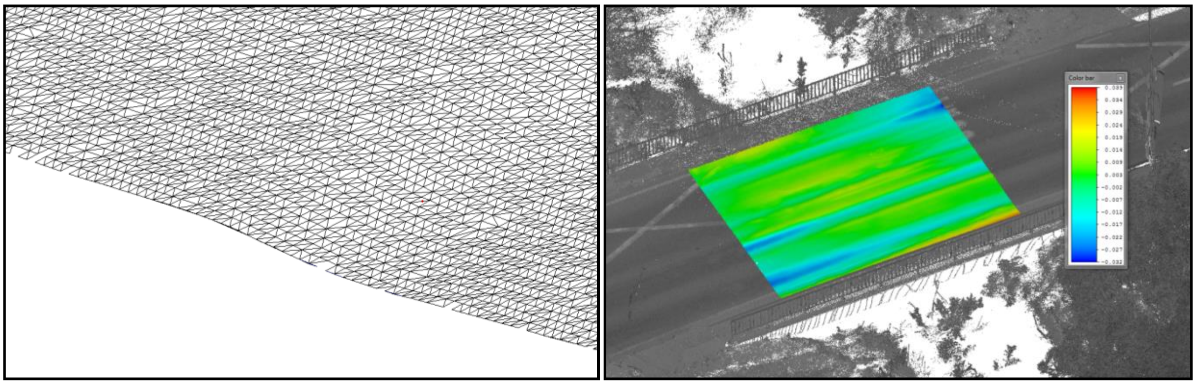

Figure 4: Results of measurements of road profile

2.4 Measurement of properties of test vehicle

A 3-axle truck (Figure 5), with known geometric characteristic and measured natural frequencies of vehicle, stiffness of suspension and weights of individual axles, was used for the test. The individual axles were statically weighed. The gross weight of the empty and fully loaded vehicle amounted to 12.0 and 23.9 tons, respectively. The stiffness of the front and rear suspension was calculated as a coefficient between ΔF and Δu. ΔF was the difference between the weight of a full and empty truck, whereas Δu was the change of vertical displacement at suspensions positions caused by ΔF.

Vibrations of the rolling vehicle were recorded with 5 transducers (Figure 5) at a sampling frequency of 512 Hz. Fast Fourier Transformation (FTT) was used to determine the natural frequencies. The identifying frequencies were 1.30 (the first mode), 1.40 – 1.50 (the second mode) and 2.90 – 3.00 Hz (the third mode), respectively.

Figure 5: Test vehicle (left) and one of vibration transducers (right)

2.5 Measurements of response of bridge in terms of deformation

The response of the bridge the crossings of the selected vehicles was measured with 14 strain gauges at locations presented in Figure 6. The test vehicle (empty and full) crossed the bridge in both lanes, at three different speeds (0, 40 and 60 km/h) and transverse positions (PP1, PP2, PP2). Altogether, 144 crosses were recorded. The strains were acquired with the B-WIM system [2]. Figure 6 shows a typical bridge response in time domain, at all 14 locations, under a fully loaded vehicle crossing in lane 2 (Figure 2), at 40 km/h and at transverse position PP2. The sensor 8 was glued over a crack; therefore, the corresponding strains are incomparably higher than the others. During the test, the bridge was closed to traffic.

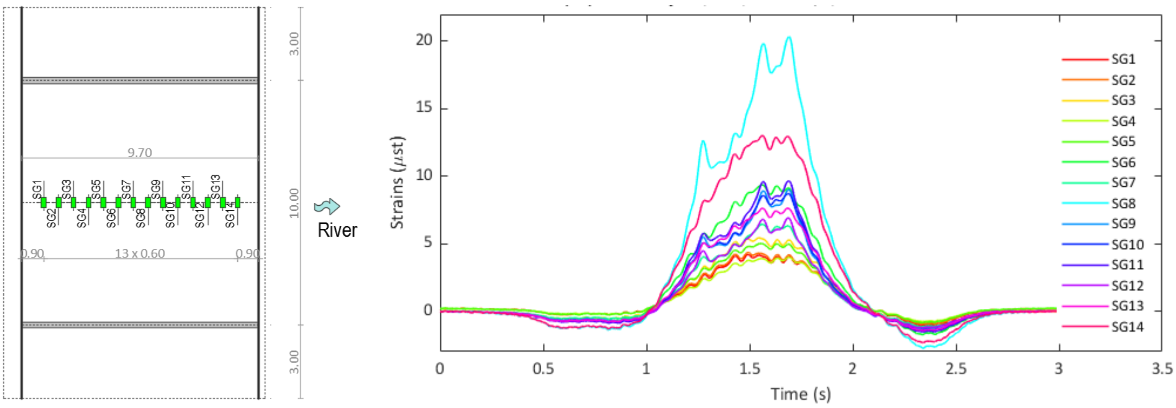

Figure 6: Locations of strain gauges (left) and results of measured deformations of bridge under a crossing vehicle at lane 2 with speed 40 km/h and at transverse position PP2 (right)

3 DEVELOPMENT AND VERIFICATION OF NUMERICAL MODEL

The numerical model for simulating the response of a vehicle crossing the bridge with an uneven road surface consisted of three parts: (1) modeling of the bridge with an uneven road surface, (2) modeling of the vehicle and (3) simulating of the vehicle crossing the bridge at different speeds and different transverse position. Individual parts of modelling were verified with results of extensive field measurements.

3.1 Vehicle model

The vehicle was modelled as a multibody system consisting of three lumped masses – one mass for the vehicle body, one for the front and one for the rear axis. The masses were connected with springs and dampers that represent vehicle suspensions. This type of vehicle model is common in literature [14, 15, 16]. It has eight degrees of freedom: one translation in driving direction, three vertical translations of the three masses, two rotations of the body mass (roll and pitch) and one (rolling) rotation for each of the axle masses (Figure 7).

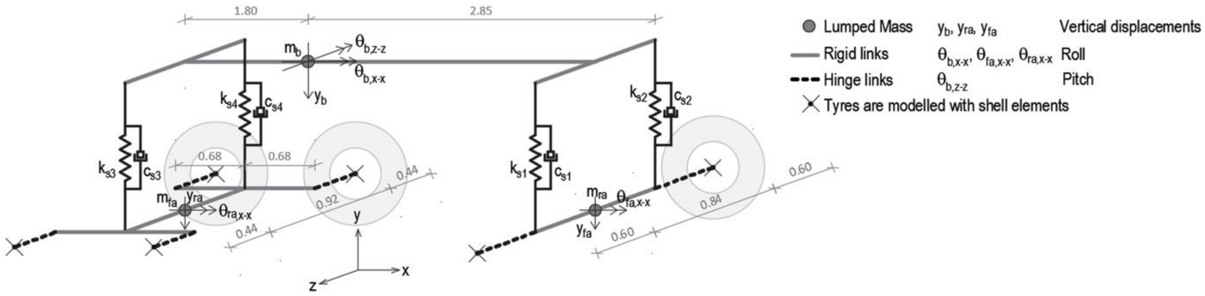

Figure 7: Numerical model of the vehicle

Special attention was given to tyres. In literature their interaction with a bridge is usually established point-wise or with a rigid surface that represents the area of the tire in contact with the bridge. These are then connected to the axes with elastic springs to represent elasticity of the tires. Thus, the tyres were modelled as elastic bodies using shell elements [18]. Their geometry and material properties were taken from the manufacturer's fact sheet and the vehicle owner provided their pressure. The reasons for choosing elastic tyre model were twofold: to model as accurately as possible (i) the tyre-bridge interaction (the contact area in particular) and (ii) not only the generalised road unevenness, but also the individual holes and bumps.

Passing of a vehicle over a hole or a bump in the road may cause numerical difficulties (time integration may require exceedingly small time steps or even diverge) if the contact is modelled point wise or with a rigid surface. If contact is modelled with two elastic bodies (pavement and tyre), such difficulties are avoided. The vehicle model was validated by comparing the eigen-frequencies of the model with the measured frequencies of the real vehicle. The first eigen-mode was the rotation of the vehicle around longitudinal axis (roll), and the second and the third the inclinations of the front and rear axles, respectively. The computed frequencies of the first three modes were 1.20 Hz, 1.74 Hz and 3.05 Hz, while the corresponding measured frequencies of the vehicle were 1.30 Hz, 1.40-1.50 Hz and 2.90 Hz. All values were in good agreement with the computed frequencies.

3.2 Bridge model

The bridge was modelled using C3D8R solid elements (8 node linear spatial elements with reduced integration). Dimensions of the bridge obtained from the field measurements were considered. The rotational boundary springs were used for modelling supports. The road surface unevenness was implemented into the model by triangular network model. The first three eigenvalues calculated by the model amount to 0.067 s, 0.032 s in 0.022 s, whereas measured frequencies of the bridge were 0.065 Hz for the first mode and 0.022 Hz for third. The second mode was not excited with the free-flow traffic.

3.3 Coupled vehicle-bridge interaction model

Coupled vehicle-bridge interaction simulation of a driving vehicle that crosses the bridge consisted of models of the bridge, of the road surface unevenness, of the vehicle and of the carriageway before and behind the bridge (Figure 8, left). The latter was modelled as a fixed supported rigid body. Standard surface-to-surface contact, implemented in the Abaqus software [17], was used to model contact of the area of the tire and the pavement construction. The simulations of the response of the bridge to the passages of selected vehicle at different speeds and different transverse position were performed by dynamic, implicit analysis. The results showed that simulated strains in Lane 2 matched well with the measured values (Figure 8, right), whereas agreement of the results in Lane 1 was less satisfactory. One of the reasons was that the bridge was rehabilitated in that part and the data taken into account in the model did not reflect the actual state of the structure.

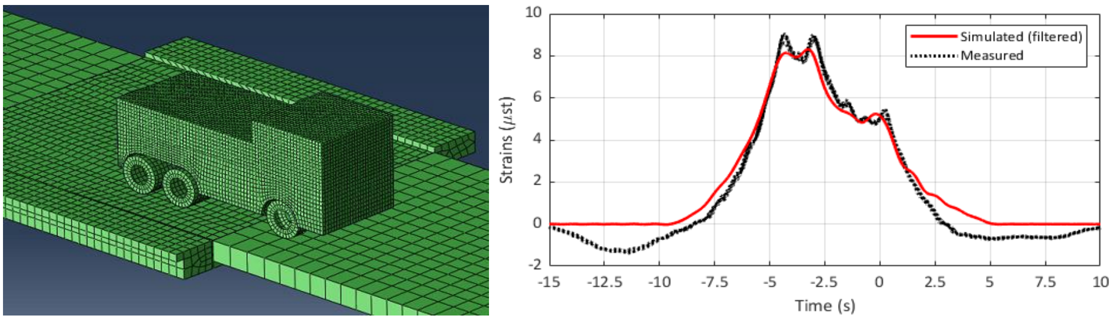

Figure 8: Coupled model (left) and comparison of experimental and simulated results (right)

4 CONCLUSIONS

This paper discusses experimental validation of detailed numerical model for simulating the response of a vehicle crossing the bridge with an uneven road surface. Extensive field measurements on a bridge (i.e. measurements of dynamic properties of bridge and vehicle, measurements of strains of the bridge due to the crossings of selected vehicles, laser scanning of the road profile) were performed and were used to validate the numerical model that simulated a vehicle crossing the bridge.

The model consisted of coupled sub-models of the bridge, the road surface unevenness, the vehicle and the carriageway before and behind the bridge. The bridge was modelled with solid elements, whereas laser scanned road surface unevenness was represented by a triangulated network model. The vehicle was modelled as a multibody system consisting of lumped masses connected with springs and dampers. Tires of the vehicle were modelled as elastic bodies using shell elements in order to model tyre-bridge interaction as accurately as possible. The comparison between the results of the numerical and measured model shows that the numerical model in well able to provide real response of bridge-vehicle interaction.

5 ACKNOWLEDGEMENTS

We acknowledge financial support from the Slovenian Research Agency through the research programme No. P2-0273 and post-doctoral project No. Z2-7431.

6 REFERENCES

[1] F. Moses, “Weigh-In-Motion system using instrumented bridges,” *ASCE Transportation Engineering Journal,* vol. 105, no. 3, pp. 233-249, 1979.

[2] A. Žnidarič, J. Kalin and M. Kreslin, “Improved accuracy and robustness of bridge weigh-in-motion systems,” *Structure and Infrastructure Engineering* , vol. doi.org/10.1080/15732479.2017.1406958, no. 1, p. 13, 2017.

[3] R. Corbally, A. Žnidarič, D. Cantero, D. Haijalizadeh, J. Kalin, M. Kreslin, C. Leahy, E. J. OBrien and E. Zupan, “Algorithms for Improved Accuracy of Static Bridge-WIM Systems,,” *D1.3 Report of Bridgemon project, Cestel,* 2014.

[4] D. Humar and A. Kashif, “Dynamic response analysis of slab-type bridges,” *Journal of Structural Enginnering,* vol. 121, no. 1, pp. 48-62, 1995.

[5] L. Frýba, Vibration of solids and structures under moving loads, Groningen, Netherlands: Noordhoff International Publishing, 1972.

[6] P. Chatterjee, T. Datta and . C. Surana, “Vibration of continuous bridges under moving vehicles,” *Journal of Sound and Vibration,* p. 169(5), 1994.

[7] Z. Q and S. Law, “Dynamic load on continuous multilane bridge deck from moving vehicles,” *Journal of Sound and Vibration,* p. 251(4), 2002.

[8] A. González, “Development of Accurate Methods of Weighing Trucks in Motion, PhD. Thesis,” Department of Civil Engineering, Trinity College Dublin, Dublin, 2001.

[9] L. Kwasniewski, J. Wekezer and J. Malachowski, “Finite element analysis of vehicle bridge interaction,” *Finite Elements in Analysis and Design,* p. 42(11), 2006.

[10] D. Huang, T. Wang and M. Shahawy, “Dynamic behavior of horizontally curved girder bridges,” *Computers & Structures,* p. 57(4), 1995.

[11] T. Wang, M. Shahawy and . D. Huang, “Dynamic response of highway trucks due to road surface roughness,” *Computers & Structures,* p. 49(6):10551068, 1993.

[12] Y. Yang and B. Lin, “Vehicle-Bridge interaction analysis by dynamic condensation method,” *ASCE Journal of Structural Engineering,* p. 21(11):16361643, 1995.

[13] G. Michaltsos and T. Konstantakopoulos, “Dynamic response of a bridge with surface deck irregularities,” *Journal of Vibration and Control,* p. 6:667689, 2000.

[14] L. Daniel and J. Kortiš, “The comparison of different approaches to model vehicle-bridge interaction,” *Procedia Engineering 190,* pp. 504-509, 2017.

[15] J. Wyss, D. Su and Y. Fujino, “Prediction of vehicle-induced local responses and application to a skewed girder bridge,” *Engineering Structures,* vol. 33, pp. 1088-1097, 2011.

[16] J. Oliva, J. Goicolea and M. Antolin, “Fully three-dimensional vehicle dynamics over rough pavement,” *Transport,* vol. 166, pp. 144-157, 2013.

[17] Dassault Systems, “ABAQUS Documentation,” Providence (RI), USA, 2019.

[18] M. Roller, P. Betsch, A. Gallrein and J. Linn, “On the Use of Geometrically Exact Shells for Dynamic Tire Simulation,” in *in: Terze Z. (eds) Multibody Dynamics. Computational Methods in Applied Sciences, vol.35,* Cham., 2014.

International Conference on Sustainable Materials, Systems and Structures (SMSS 2019)
Challenges in Design and Management of Structures
20-22 March 2019 – Rovinj, Croatia

ESTABLISHING THE EFFECT OT THE TAIL LENGTH ON EXTRAPOLATION WHEN FITTED TO WIM DATA

P.F. van der Spuy and R. Lenner

Stellenbosch University Department of Civil Engineering, South Africa

Abstract

When using the Block Maxima approach with Extreme Value Theory to extrapolated bridge live load effects to a return period, it is essential to estimate the length of the tail accurately. The main reason for using a small fraction of the sample is that the parent population generally does not follow an extreme value model.

It is typical in the development of traffic load models to fit Gumbel or Weibull distributions to the upper $2\sqrt{n}$ of block maxima data points, where n is the total number of data points in a series. The length of the upper tail is therefore assumed to be $2\sqrt{n}$ as per Castillo's recommendation and this has been followed in many bridge live load studies. Extrapolated traffic load effects have, however, been found to be highly sensitive to the assumed length of the distribution tail.

This study used Weigh in Motion data from South Africa to illustrate the sensitivity of extrapolated load effects to the assumption of the upper tail length. It shows that each load effect case should be treated individually and engineering judgement is necessary to determine the length of the tail.

Keywords: generalised extreme value, block maximum, extrapolate, tail, weigh in motion

1. INTRODUCTION

Weigh in Motion (WIM) data is typically only available for a couple of years. When determining characteristic values for bridge traffic loading it is necessary to extrapolate the load effects from measured data to some acceptable return period using some statistical distribution. Only the upper tail of a parent distribution contributes significantly to the extrapolated value at the return period [1]–[3] and it is known that the tail behaves asymptotically as one of the Extreme Value (EV) distributions [4]. In [4] the author suggests a tail length of $2\sqrt{n}$, but no details are given as to how this value was derived. Although the unsubstantiated $2\sqrt{n}$ tail length has been used extensively in studies on bridge traffic loading, various other tail lengths have also been applied, including $\sqrt{n}$, $3\sqrt{n}$ and the upper 30 % of values [2],[5]–[9]. This paper investigates the implications of these assumptions using Extreme Value Theory (EVT) with the Block Maxima (BM) method. A block size of one day is used in this study which is sufficiently small to prevent wasteful data associated with the BM method and adequate to comply with the independently and identically distributed assumption of EVT. In South Africa heavy vehicles are allowed to travel over weekends and the load effects are therefore similar throughout the week.

2. WIM DATA AND CALCULATION OF LOAD EFFECTS

2.1 Data source

Lenner et al. [10] showed that National Route 3 between Durban and Johannesburg is the heaviest freight route in South Africa. It is also the main import/export rout into and out of South Africa. Although there are many WIM stations along this route, the Roosboom station was chosen for this study as it is thought to be representative of the heaviest traffic and has been measuring since November 2000. The station is considered to be well calibrated [11]. Three years of data from 2014 to 2016 were used in this study. The time stamp of WIM data at this station is 0.01 s which is preferable [12].

2.2 Post calibration and cleaning

As a post-calibration procedure to correct recorded axle loads in retrospect, De Wet [11],[13] developed the Truck Tractor (TT) method. It was accepted by the South African National Roads Agency Limited (SANRAL) to further improve the calibration of WIM data and was used in this study.

Due to the nature of measuring equipment and installation there are often invalid records. Slavik developed a technique called Golem (unpublished) to specifically address sources of WIM error in South Africa. Golem rejects any records that meet the following criteria:

- Vehicles travelling less than 5 km/h or more than 150 km/h
- Trucks with length less than 4 m or longer than 26 m
- Vehicles with fewer than two axles
- Vehicles with Gross Vehicle Weight (GVW) smaller than 3.5 t
- Vehicles with any individual axle weighing more than 16 t
- Vehicles with axle spacings of less than 0.53 m or longer than 10 m

2.3 Calculation of load effects

WIM sensors record the dates, times, speeds, axle weights and axle spacings of vehicles. By using time differences between vehicles and their speeds it is possible to calculate the distance between them. Each day is considered individually and a daily convoy is constructed by placing the vehicles behind each other in a queue. These queues are moved across bridge spans daily to record the daily maximum load effects.

The load effects that were investigated are sagging moments and shear forces on single span structures and hogging for two span structures [14]–[16]. Daily convoys were passed over span lengths between 5 m and 30 m in 0.444 m increments which corresponds to 0.02 s intervals at 80 km/h. Characteristic load effects on longer spans tend to be governed by presence of multiple vehicles which falls outside the scope of this paper.

3. EXTREME VALUE DISTRIBUTIONS

The EV family of distributions consists of three types namely Gumbel (Type 1), Frechet (Type 2) and Weibull (Type 3). Together, these three distributions make up the Generalised Extreme Value (GEV) distribution [17].

Several studies have argued that bridge traffic load effects follow the Weibull distribution [1],[7],[18],[19]. This is logical if one considers that the Weibull distribution is bounded, hence there is some finite upper limit. It is conceivable that traffic loading must have an upper bound. The Frechet EV distribution is an unbounded distribution and bridge traffic load effects should not fall within this distribution type. It is possible for bridge traffic load effects to approach a Gumbel EV distribution and several authors have applied it for this purpose [6],[8],[18],[20]–[24].

To prevent the user from having to check for both Weibull and Gumbel, it is easier to rather fit the GEV distribution which does not require a predetermined choice of distribution, but rather uses a shape factor to distinguish between the three types [17].

$$G(z) = \exp\left\{-\left[1+\xi\left(\frac{z-\mu}{\sigma}\right)\right]^{-1/\xi}\right\} \tag{1}$$

Equation (1) shows the Cumulative Distribution Function (CDF) of the GEV distribution for a random variable Z with μ being the location parameter, σ the scale parameter and ξ the shape parameter. The shape parameter describes the tail of the underlying data set and is negative for a Weibull EVD, positive for a Frechet EVD and zero for the Gumbel EVD [17].

4. RETURN PERIOD

A 5 % probability of exceedance (p = 0.05 fractile) in a 50 year reference period, or design working life, was used in this study for characteristic values [25], similar to the Eurocode [26]. It is also the approach which has been adopted in the South African building design codes [27]. This translates to a return period of 975.3 years according to [12]. Extrapolating from three years of data to such long return periods introduces statistical uncertainty which must be addressed when a reliability analysis is performed.

5. RESULTS

The GEV distribution was fitted from the upper 3 % to the upper 30 % of daily maximum load effects and extrapolated to the return period of 975.3 years to obtain the characteristic load effects. The three years of data yielded 1088 days of actual measurements with the WIM sensors being out of operation for an additional eight days. The upper $\sqrt{n}$ of data points corresponds to the upper 33 days of measurements, or the upper 3 %. The upper $2\sqrt{n}$, which has been used most frequently, corresponds to the upper 6 % of daily maxima.

Figures 1 to 3 show that extrapolated characteristic load effects for different tail lengths. It shows that there is great variability for all load effects and that it is nearly impossible to establish some empirical rule as to how long the tail of bridge live load effects is. It is recommended that the user carefully inspects each data set individually to determine the most appropriate length of the tail for extrapolation. A possible solution to this subjectivity is to perform long run Monte Carlo simulations to increase the number of points in the tail or to simulate the entire reference period.

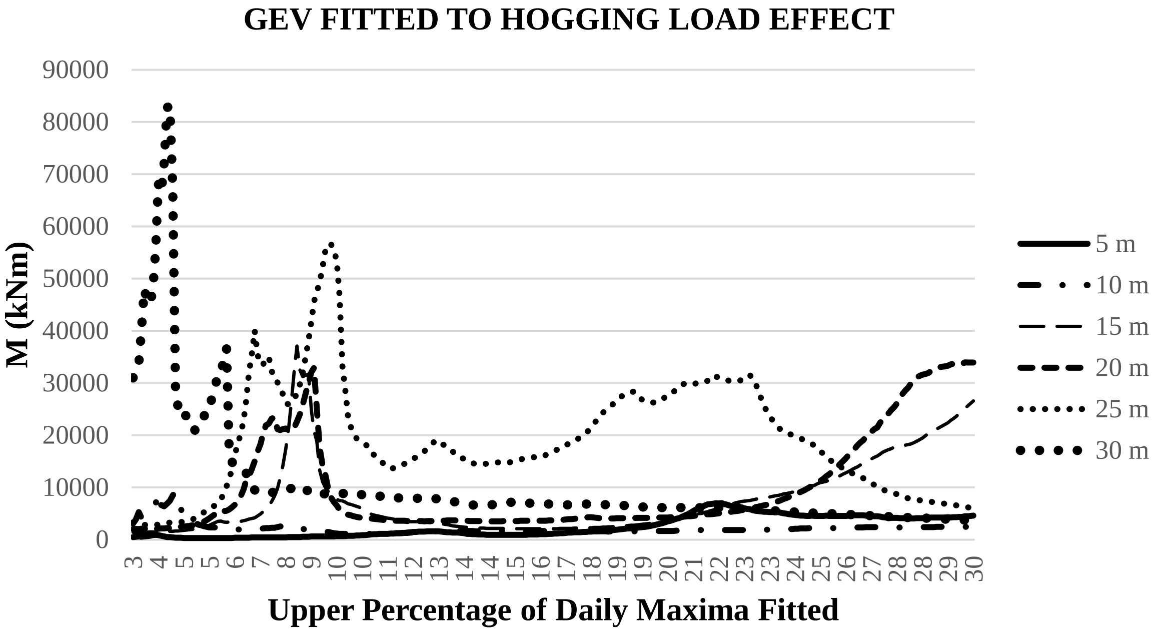

Figure 1: Hogging Load Effects Extrapolation

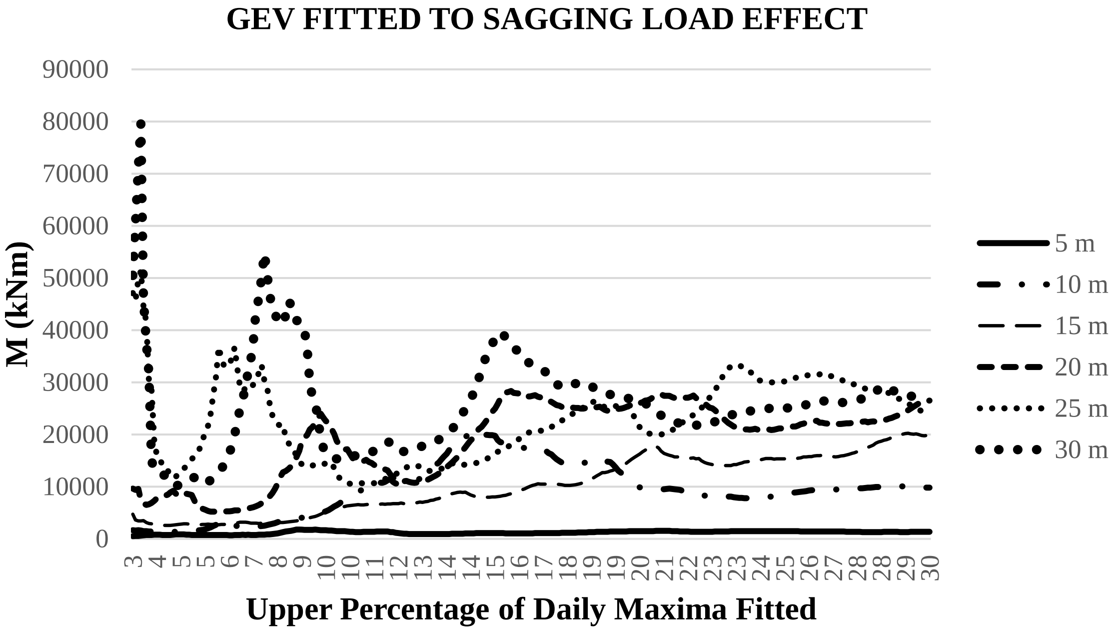

Figure 2: Sagging Load Effects Extrapolation

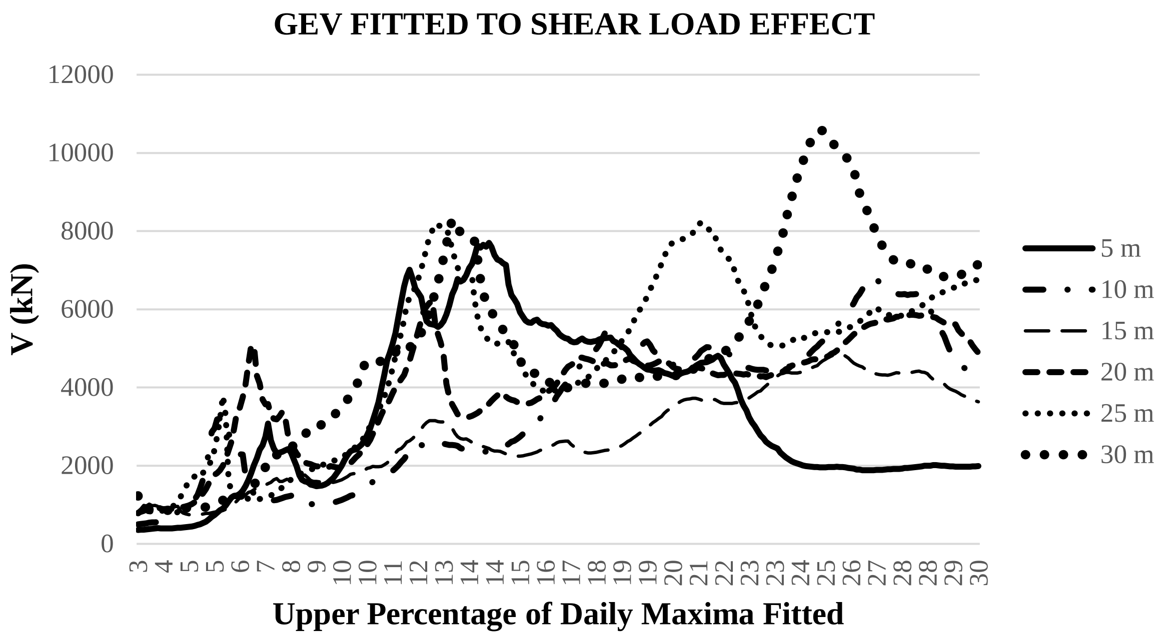

Figure 3: Shear Load Effects Extrapolation

6. CONCLUSIONS

Three years of WIM data was used in this study and extrapolated for different tail lengths. This study shows that it is not reasonable to assume some generic tail length for all cases, but rather that each case should be treated individually. A possible solution to this subjectivity is to perform long run Monte Carlo simulations to increase the number of points in the tail or to simulate the entire reference period. Extrapolating from limited data to long return periods introduces statistical uncertainties which should be addressed in future research. These uncertainties could lead to conservative load models.

REFERENCES

[1] Bailey SF. Basic Principles and Load Models for the Structural Safety Evaluation of Existing Road Bridges. EPFL; 1996.

[2] Zhou XY. Statistical Analysis of Traffic Loads and Traffic Load Effects on Bridges. Universite Paris Est; 2013.

[3] Zhou XY, Schmidt F, Jacob B. Extrapolation of Traffic Data for Development of Traffic Load Models: Assessment of Methods Used During Background Works of the Eurocode. In: Bridge Maintenance, Safety, Management, Resilience and Sustainability - Proceedings of the Sixth International Conference on Bridge Maintenance, Safety and Management. 2012. p. 1503–9.

[4] Castillo E. Extreme value theory in engineering. First edit. Academic Press Inc; 1988.

[5] Crespo-Minguillón C, Casas JR. A Comprehensive Traffic Load Model for Bridge Safety Checking. Struct Saf. 1997;19(4):339–59.

[6] Enright B, OBrien EJ. Monte Carlo Simulation of Extreme Traffic Loading on Short and Medium Span Bridges. Struct Infrastruct Eng. 2012;9(Online):1267–82.

[7] OBrien EJ, Schmidt F, Hajializadeh D, Zhou XY, Enright B, Caprani CC, et al. A review of probabilistic methods of assessment of load effects in bridges. Struct Saf. 2015;53:44–56.

[8] Heitner B, OBrien EJ, Schoefs F, Yalamas T, Décatoire R, Leahy C. Evaluation of bridge safety based on Weigh-in-Motion data. Civ Eng Res Irel 2016. 2016;

[9] Van der Spuy PF, Lenner R. Developing a new bridge live load model for South Africa. In: Powers, Frangopol, Al-Mahaidi, Caprani, editors. Proceedings of the ninth international conference on bridge maintenance, safety and management (IABMAS). Melbourne: Taylor & Francis; 2018. p. 1405–10.

[10] Lenner R, de Wet DPG, Viljoen C. Bridge Loading and Traffic Characteristics in South Africa. J South African Inst Civ Eng. 2017;59(4):34–46.

[11] de Wet DPG. Post-Calibration and Quality Management of Weigh-in-Motion Traffic Data. Stellenbosch University; 2010.

[12] Enright B. Simulation of Traffic Loading on Highway Bridges. University College Dublin; 2010.

[13] de Wet DPG. WIM Calibration and Data Quality Management. J South African Inst Civ Eng. 2010;52(2):70–6.

[14] Lenner R. Safety Concept and Partial Factors for Military Assessment of Existing Concrete Bridges. Universitat der Bundeswehr Munchen; 2014.

[15] Lenner R, Keuser M, Sykora M. Safety Concept and Partial Factors for Bridge Assessment under Military Loading. Adv Mil Technol. 2014;9(2).

[16] Caprani CC. Probabilistic Analysis of Highway Bridge Traffic Loading. University College Dublin; 2005.

[17] Coles SG. An introduction to Statistical Modeling of Extreme Values. Springer Series in Statistics. 2001.

[18] Caprani CC, Belay A, O'Connor AJ. Site-specific Probabilistic Load Modelling for Bridge Reliability. In: Proceedings of the 3rd International Conference on Current and Future Trends in Bridge Design. 2003. p. 341 to 348.

[19] OBrien EJ, O'Connor AJ, Arrigan JE. Procedures for Calibrating Eurocode Traffic Load Model 1 for National Conditions. In: Bridge Maintenance, Safety, Management, Resilience and Sustainability - Proceedings of the Sixth International Conference on Bridge Maintenance, Safety and Management. Lake Maggiore; 2012. p. 2597–603.

[20] O'Connor AJ, OBrien EJ. An Assessment of the Influence of Dynamic Interaction Modelling on Predicted Characteristic Load Effects in Bridges. In: 3rd International Conference on Current and Future Trends in Bridge Design. Shanghai: Thomas Telford; 2003.

[21] Sivakumar B, Moses F, Ghosn M. Protocols for Collecting and Using Traffic Data in Bridge Design Prepared for NCHRP. Paramus; 2008.

[22] Fu G, You J. Truck Loads and Bridge Capacity Evaluation in China. J Bridg Eng. 2009;14(5):327–35.

[23] OBrien EJ, Enright B, Getachew A. Importance of the Tail in Truck Weight Modeling for Bridge Assessment. J Bridg Eng. 2010;15(2):210–3.

[24] Hellebrandt L, Blom CBM, Steenbergen RDJM. Probabilistic Traffic Load Model for Short-span City Bridges. Heron. 2014;59(2/3):147–68.

[25] Holicky. Reliability analysis for structural design. First. Stellenbosch: SUN meDIA; 2009. 1-199 p.

[26] CEN. EN1991-2: Traffic loads on bridges. Brussels; 2003.
[27] SABS. Basis of structural design and actions for buildings and industrial structures Part 1. 1.1. Pretoria: SABS; 2011. 1-82 p.

CONSECUTIVE MULTI-LEVEL BRIDGE ASSESSMENT

Ana Mandić Ivanković, Dominik Skokandić and Mladen Srbić

Faculty of Civil Engineering, University of Zagreb, Croatia

Abstract

When assessing an existing bridge, the application of conservative design load and resistance models can cause unnecessarily high maintenance costs. On the other hand, sophisticated methods based on probabilistic approach require greater effort and are also demanding for practical application. Consequently, multi-level assessment procedures are considered appropriate, whereby complexity and accuracy increase consecutively through the levels. Namely, if the bridge meets the requirements at the first assessment level - on the safe side, no further complicated steps are needed. Otherwise, a more complex assessment step should be carried out in which we are closer to the real values of the structure's performance and resistance.

In this paper, (i) the multi-level assessment of road bridges for traffic load and (ii) the multi-level seismic assessment of arch bridges, will be overviewed.

In addition, recommendations for further development of assessment procedures will be provided, based on undergoing research. The first research branch explores the value of implementing the Bridge-Weigh-in-Motion measurements together with the probabilistic approach in assessment of existing road bridges. The second research branch aims to reveal seismic resistance of bridge elements with nonstandard sections and smooth reinforcement designed without contemporary rules for ductile behaviour.

Keywords: bridges, arch bridges, multi-level assessment, traffic load, seismic assessment

1. INTRODUCTION

Deterioration of bridge structures occurs due to weathering (eg. corrosion, fatigue) or due to structural defects caused by accidental actions (eg. truck collision on substructure elements). Combination of aggressive exposure conditions, inadequate detailing, neglecting durability issues, construction errors and underestimating the importance of maintenance, may result in serious damages. Furthermore, loads change during lifetime of the bridge (eg. traffic load) or extension of the design life is imposed [1]. In addition, requirements on structures change in terms of development and updating of regulations and normative standards in line with contemporary approaches to safety and serviceability of structures and novel scientific contributions. Therefore, existing structures, often do not satisfy current needs, respectively do not poses adequate safety levels, particularly in relation to seismic performance.

For the successful evaluation of bridge performance in remaining service life, in order to determine whether it requires repair or retrofitting, it is extremely important to properly assess it. Current codes for the design of new bridges do not offer optimum approach for assessment of existing bridges, as they are based on conservative assumptions regarding loads and resistance and could result in extremely large costs for bridge maintenance [2]. On the other hand, sophisticated methods, based on probabilistic approach require additional knowledge and assets, and they are more complicated for practical application.

Therefore, multi-level assessment methods, where accuracy, along with complexity increases on subsequent levels, are considered to be more appropriate for assessment of existing bridges. If the bridge passes the initial level of assessment, no further actions are required. Otherwise, the bridge is revaluated with advanced methods on subsequent levels, in order to determine realistic values of load effects and bridge load carrying capacity.

2. MULTI-LEVEL ASSESSMENT OF ROAD BRIDGES FOR TRAFFIC LOAD

Most often, bridges are assessed in terms of traffic load effect. Traffic load is the basic bridge load, of highly variable characterisation, both in space and in time, so its modelling for the design of new bridges is very conservative. In most of the European countries that have adopted national standards for assessment of existing structures (Switzerland, Austria, Germany), adjusted partial factors method is used with the same reliability levels requirements as for new structures. The exception is the Netherlands, where reduced reliability levels are suggested for existing structures [3].

A large number of road bridges and overpasses of small and medium spans in Croatia, built during seventies and eighties, are designed according to outdated regulations. In order to evaluate their reliability for traffic loading, multi-level method (Figure 1) is developed [4]. If condition assessment based on visual inspection and documentation overview, points to deficiencies which might endanger the safety of the bridge and its users, three-level assessment procedure should start. At each level, adequate checks, based on limit state equation are to be evaluated, thus proving whether the bridge is enough safe/ reliable for continued use [4].

At the initial level, assessment is performed using conservative methods similar to those used when designing new bridge, employing codified partial safety factors for material and load. If the bridge passes the initial level, no further actions are performed.

Otherwise, the bridge should be re-evaluated using advanced non-linear analysis methods at the second assessment level in order to reveal global safety factor γ as shown in Figure 1. Applying non-linear behavior of bridge materials may result in higher levels of bridge resistance compared to those obtained from the first assessment level [3].

Third level of proposed assessment method is based on probabilistic approach, which makes it more demanding for practical use. All variables in limit state equation are modelled as stochastic variables, described with its statistical parameters (mean value μ and standard deviation σ). Probability index β is calculated and compared to target reliability for existing bridges. To carry out this assessment level, data on materials based on in-site and laboratory testing are to be collected to calculate the relevant statistical parameters. Uncertainties in resistance and load effects will not be covered with partial factors as in previous two levels;

namely adequate uncertainty will be joined to each separate variable depending on its type and amount of data. Valuing of uncertainties will highly impact the final assessment result [4].

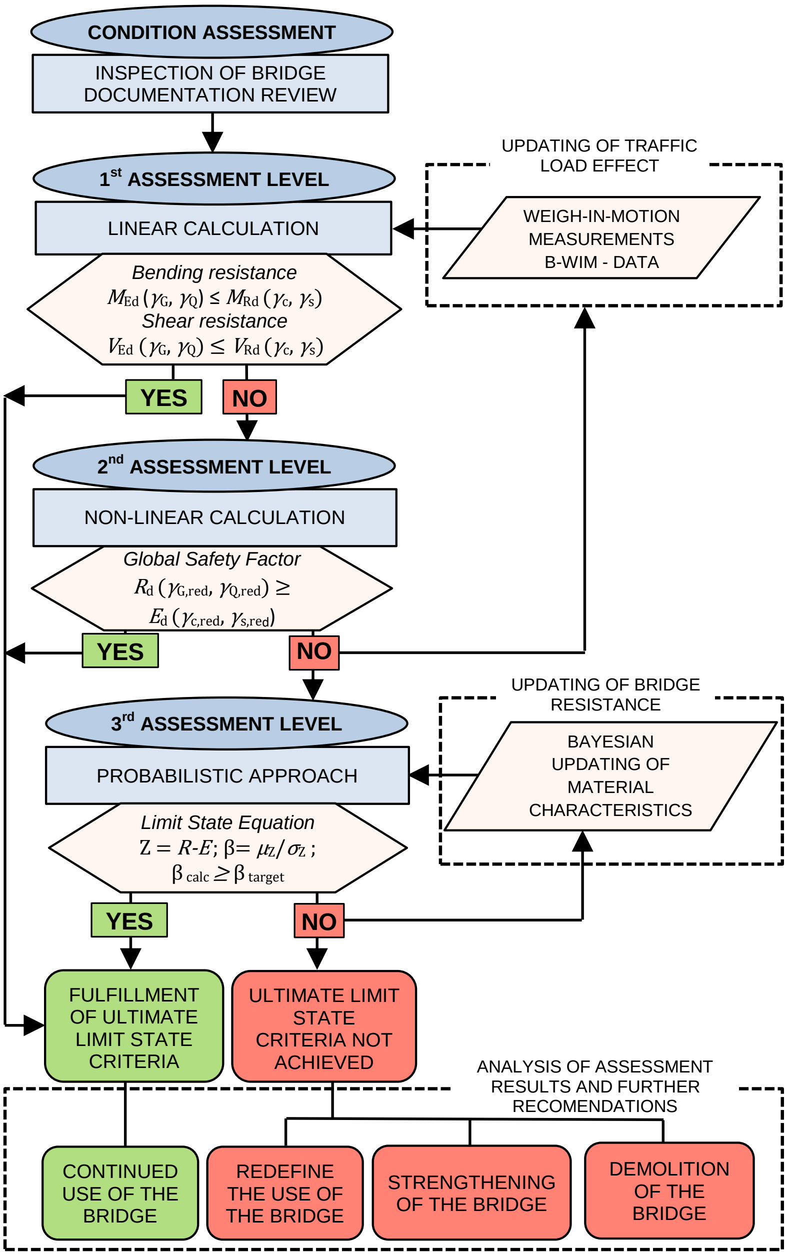

Figure 1: Flow chart diagram of multi-level assessment of road bridges for traffic load

Above mentioned bridge evaluation procedure may be improved by additional methods for determining localised load effects and realistic material/structural resistance indicators. This requires additional research and gathering more data.

Based on measurements of in-service traffic load using Bridge Weight in Motion System, it is possible to reveal exact traffic effect for a certain bridge including changes in bridge boundary condition, hidden degradation and also the values of dynamic amplification factor which may have significant influence in assessment of small and medium span bridges [5, 6].

In probabilistic based approach at the third level of assessment method, material resistance indicators are to be presented as random variables with adequate statistical parameters. Valuing of this indicators is based on inspections and tests which extent greatly depend on the available costs provided by the investor so very often the engineer will need to assess the bridge based on a limited data collection. In these cases, the use of Bayesian method [7] of probability estimation proved to be very effective. It provides reliable values of material characteristics, combining prior information, obtained from literature or past experiments, with test results in order to reduce uncertainties in probabilistic based assessment approach.

Based on the assessment procedure results, we come to the conclusions for further bridge performance. In case the assessed bridge does not meet the ultimate and serviceability limit state criteria, it is necessary to decide whether the traffic should be restricted, bridge strengthened or completely closed or/and removed.

3. MULTI-LEVEL SEISMIC ASSESSMENT OF ARCH BRIDGES

Considering that the whole of Croatian territory is seismically active, earthquake loading is often governing for element design (especially columns), material consumption, detailing, and overall mechanical resistance and stability of bridges.

The current European seismic code does not offer a procedure for seismic assessment of bridges, arch bridges in particular [8]. Non-linear static pushover methods have been the focus of extensive research in the recent years [9], particularly in the direction of extending them to structures with significant higher mode effects as are many bridge types.

Reinforced concrete arch bridges are particular structures owing to their robustness and not much may be found in existing literature about seismic assessment of this type of bridges. The tradition in construction of such structures in Croatia and gathering knowledge on them through their use and maintenance, enabled us to further develop and improve certain aspects of available seismic performance methods and to properly incorporate them in a new procedure dedicated to seismic assessment of reinforced concrete arch bridges, presented at the figure 2. The procedure, running through levels of assessment, is applicable for the whole arch bridge structure and it indicates the most critical bridge details and elements in seismic response [8, 10].

First of all, it is necessary to collect bridge data. To define a correct structural model of the existing structure and to perform adequate structural analysis it is necessary to identify existing and desired knowledge level of the existing structure based on the bridge importance. These knowledge levels may be obtained with adequate data collection on geometrical properties of both structural and non-structural elements which may affect structural response, structural details including amount and detailing of reinforcement, concrete cover, connection between members and the mechanical properties of the constituent materials in conjunction with the appropriate confidence factors [8,10].

The procedure is consisted of two levels and several evaluation checks at each assessment level (table 1). Each evaluation check gives an answer if appointed demand is fulfilled or not. With these answers quite precise guideline for seismic retrofit of assessed arch bridge may be brought, which than can be presented to the bridge owner who will bring the final decision to retrofit the bridge or not.

First level of assessment results with more conservative estimate of the bridge state considering seismic response than the second level. Therefore for bridges that do not fulfill all checks of the first level it is necessary to go through the second level of assessment. As reinforced concrete arch bridges are particular structures owing to their robustness, it is found out that performance of arches under seismic design situation may be proved already at the first level using linear multimodal analysis. For spandrel columns (particularly short ones near the arch crown) it will be necessary to go through the second level of assessment based on non-linear pushover analysis [8,10].

Second level requires more numerical and computational effort but it results with less conservative estimate of bridge state than the first one and thus with economically favourable retrofitting measures. If retrofitting measures will be taken, it is important to apply this same procedure again on the model of retrofitted bridge and evaluate the results following the same steps [8,10].

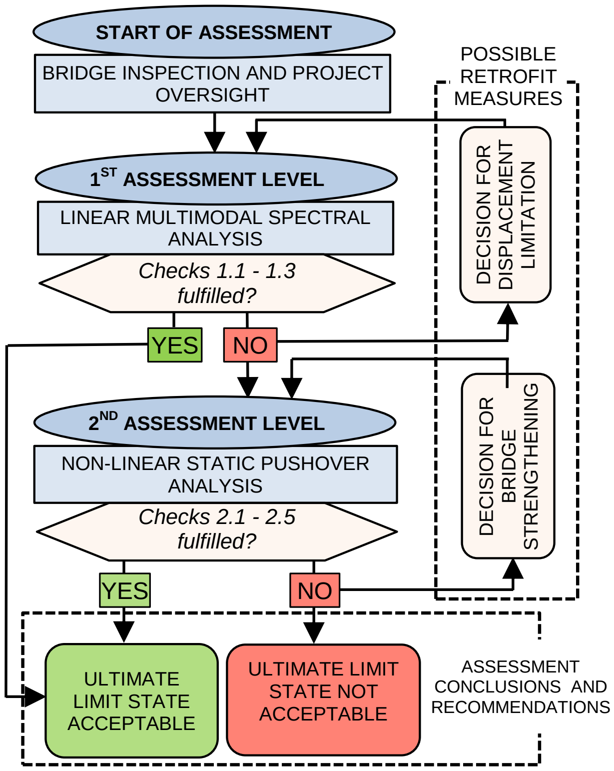

Figure 2: Seismic assessment procedure flowchart

Dynamic specificity of arch bridges is the flexibility of an arch as support for spandrel columns and great amount of the bridge mass located generally in the middle of the bridge, what comes from the position and the mass of arch.

During inelastic response of arch bridge due to the initial seismic stroke, the greatest deformation demands are posed on the shortest columns which results in their excessive cracking and finally after damage causing earthquake the need for their repair or retrofit. Upon the cracking of shortest columns and appurtenant stiffness reduction, deformation requirements are moved following from the crown to the coastal columns which results with their degradation as well. That excessive cracking should be taken into the account appropriately with effective stiffness of column cross sections [8].

Table 1: Assessment checks through consecutive levels

Assessment checks related to linear multimodal spectral analysis	
1.1 Displacements compared to allowable ones at the abutment	$d_{allow} \geq d_e$
1.2 Design resistances for the interaction of axial force and bending moment	$f(N_{Rd}, M_{Rd}) \geq f(N_E, M_E)$; $f_{i,m}$ za $f(N_{Rd}, M_{Rd})$ i $f(N_E, M_E)$
1.3 Seismic shear force demand	$V_{Bd,1}=V_{Rd}/\gamma_{Bd,1} \geq V_E$; $CF \times f_{i,m}$ za V_E; $f_{i,m}/CF \times \gamma$ *za* V_{Rd}
Assessment checks related to non-linear static pushover assessment	
2.1 Rotation capability at locations of potential plastic hinges	$\theta_{ls} \geq \theta_{p,E}$
2.2 a) Stresses of unconfined i b) and confined concrete	$f_{cm}/(CF \times \gamma_{c,acc}) \geq \sigma_{c,E}$ (in elastic regions) $f_{cm,c}/(CF \times \gamma_{c,acc}) \geq \sigma_{c,E}$ (in plastic regions)
2.3 Stresses in reinforcing steel	$f_{ym}/(CF \times \gamma_{s,acc}) \geq \sigma_{y,E}$
2.4 Verification against non-ductile failure through shear	$V_{Bd,1}=V_{Rd}/\gamma_{Bd,1} \geq V_E$; $CF \times f_{i,m}$ za V_E; $f_{i,m}/CF \times \gamma$ *za* V_{Rd}
2.5 Outward buckling of longitudinal compression reinforcement between transverse ties	$A_{t,built}/s_{T,built} \geq \min(A_t/s_T)$

The topic that requires additional research is the rotational capability of elements with unusual section (such is the extended hexagon shown at the figure 3 right), which so far are to be conservatively approximated with rectangular sections.

Accurate evaluation of the ultimate rotational capacity of reinforced concrete members may only be based on experimental data [11] due to numerous geometrical and mechanical parameters and uncertainties involved (loading type: cyclic or monotonic, seismic detailing, concrete confinement, spalling of concrete cover, ribbed or smooth bars, overlapping length, plastic hinge length, bending contribution, height of the section, etc.).

4. UNDERGOING RESEARCH

Further development of assessment procedures will be based on two undergoing research branches.

The first research branch explores the value of implementing the Bridge-Weigh-in-Motion measurements together with the probabilistic approach in assessment of existing road bridges. This is related to the 3rd assessment level after the updating of traffic load effect as presented in the figure 1.

So far, this approach is applied at the case study simply supported highway bridge with a single span of 24,8 meters, and superstructure composed of five prefabricated I-type prestressed concrete girders connected with monolithic deck. B-WIM monitoring strategies include (i) short term monitoring, which provides realistic influence lines and girder distribution factors and (ii) long term monitoring, which provides dynamic amplification factors and site-specific load models, along with the data obtained also in short term monitoring.

Results showed that this improvement may reveal hidden bridge reserves and predict bridge reliability development over a specified lifetime. Consequently, such measurements can permit unrestricted use of a bridge over a much longer remaining service life [6].

Undergoing research involves Value of Information analysis, and associated decision trees as convenient tools that can be used to justify initial investments in SHM to bridge owners. Currently modelling of all the associated probabilities, costs and benefits required for the decision tree, along with classification of bridge based on his importance in the infrastructure networks is under progress (Figure 3 left) [12].

The second research branch aims to reveal seismic resistance of bridge elements with nonstandard sections and smooth reinforcement designed without contemporary rules for ductile behaviour [13].

Namely, the question of ductility of such columns, as well as plastic hinge development, and overall nonlinear behaviour, is largely unanswered. Therefore, research into the behaviour of such sections could reveal their ductility levels and show much better performance in seismically active areas. Seismic performance indicators of bridge columns to be revealed are: (i) M/φ diagrams - bending moment and section curvature relationship curves which best show the rotational capability of plastic hinges, (ii) chord rotation capacity as rotational capability of sections and elements in the hinges and (iii) real effective stiffness after cracking near the hinge.

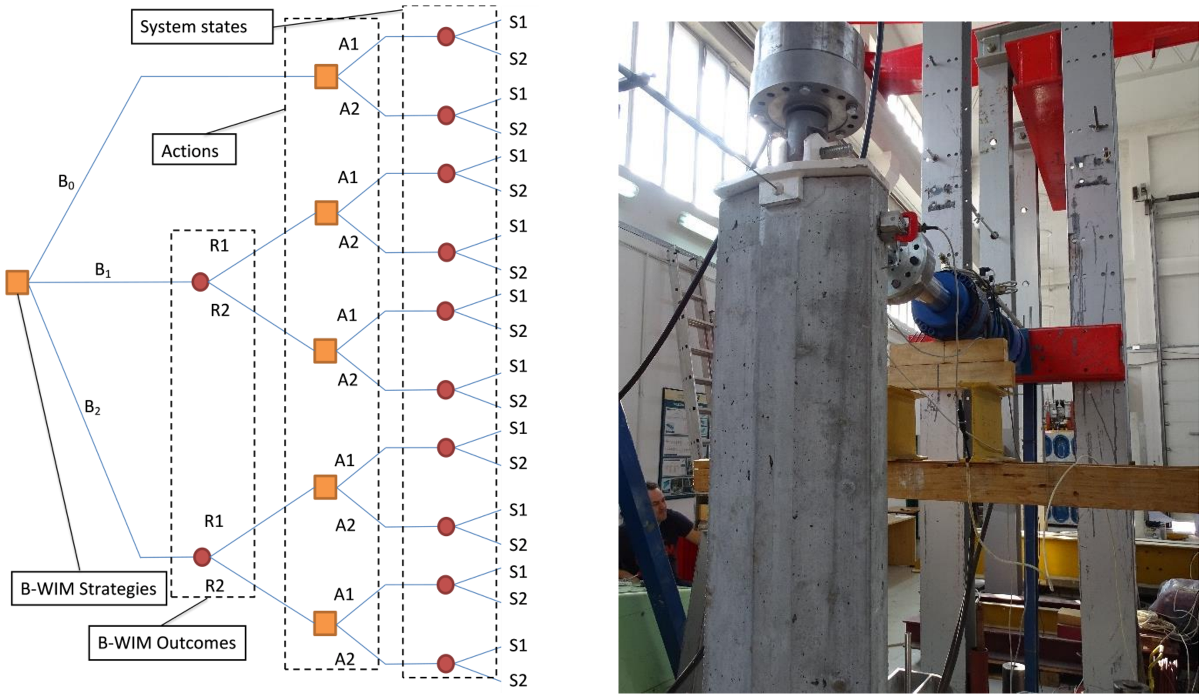

Figure 3: Undergoing research for further development of assessment procedures – Left: implementation of VoI for quantifying the value of B-WIM; Right: testing of piers with nonstandard cross sections and smooth reinforcement for revealing ductility levels

The experiment planned to reveal this indicators for bridge columns of nonstandard sections with smooth reinforcement, designed without contemporary detailing for ductile behaviour, is under progress (Figure 3 right). Experiment will serve to update analytical models and investigate the applicability of existing building code formulas for assessment of seismic resistance of existing bridges with atypical cross sections.

5. CONCLUSIONS

Assessment of existing bridges should be based on consecutive levels becoming more demanding but also more accurate, which are gradually approaching the realistic load effects and structural resistance. Only this way, the application of scientific achievements in practice, resulting in optimal and efficient maintenance of the bridges, will be possible. Two undergoing researches will hopefully (i) prove the value of implementing the Bridge-Weigh-in-Motion measurements together with the probabilistic approach in assessment of existing road bridges and (ii) reveal ductility levels of nonstandard bridge column sections with smooth reinforcement in seismically active areas.

REFERENCES

[1] Radić, J., Mandić, A., Augustinović, I.: Ocjenjivanje postojećih konstrukcija, Građevinar 61 (2009) 9, 901 – 912

[2] Mandić, A., Radić, J., Šavor, Z.: Ocjenjivanje graničnih stanja postojećih mostova, Građevinar 61 (2009) 6, 533 – 545

[3] Skokandić, D., Mandić Ivanković, A.: Ocjena pouzdanosti postojećih cestovnih mostova, Simpozij doktorskog studija građevinarstva, Zagreb, 2015.

[4] Skokandić, D., Mandić - Ivanković, A., & Džeba, I. (2016). Multi - level road bridge assessment. In Proceedings of 19th IABSE Congress Stockholm (pp. 21–23+CD)

[5] Žnidarič, A., Lavrič, I., Kalin, J.: The next generation of bridge weigh-in-motion systems, International Conference on Weigh-in-Motion, Orlando, 2002.

[6] Mandić Ivanković A, Skokandić D, Žnidarič A, Kreslin M.: Bridge performance indicators based on traffic load monitoring. Struct Infrastruct Eng. 2017;2479 (December):1–13.

[7] Holicky, M.: Introduction to probability and statistics for engineers, Elsevier Science Publishers ltd., London, 2013.

[8] Franetović M., Mandić Ivanković A., Radić J. Seismic assessment of existing reinforced-concrete arch bridges, Journal of Croatian Association of Civil Engineers 66 (2014) 8, 691 – 703

[9] Kappos A. J., Saiidi, M. S., Aydinoğlu, M. N. & Isaković, T. (eds.): Seismic design and assessment of bridges – Inelastic methods of analysis and case studies. Geotechnical, Geological and Earthquake Engineering, Volume 21, Springer, 2012.

[10] Mandić Ivanković, A., Srbić, M., Radić, J.: Seismic performance of concrete arch bridges, fib Symposium 2016: Performance – Based Approaches for Concrete Structures / Beushausen, Hans (ur.), Cape Town, South Africa, pg 237-238 + cd

[11] Verderame G.M., Ricci, P., Manfredi, G. & Cosenza, E.: Ultimate chord rotation of RC columns with smooth bars: some considerations about EC8 prescriptions Bull Earthquake Eng 8 (2010), pp.1351–1373.

[12] Skokandić D., Mandić Ivanković A., Žnidarić A.: Structural Health Monitoring of existing bridges using Bridge Weigh-in-Motion measurements – Value of Information analysis, paper submitted for the 40th IABSE Symposium to be held in September 2018, Nantes France

[13] Srbić M.: Seismic resistance indicators of bridge piers designed without contemporary detailing for ductile, (2017), approved topic of the PhD dissertation

International Conference on Sustainable Materials, Systems and Structures (SMSS 2019)
Challenges in Design and Management of Structures
20-22 March 2019 – Rovinj, Croatia

LIFE CYCLE ASSESSMENT OF RETROFIT STRATEGIES APPLIED TO CONCRETE INFRASTRUCTURE AT RAILWAY STATIONS EXPOSED TO FUTURE EXTREME EVENTS

Kundai L Sibanda (1) and Sakdirat Kaewunruen (2)

(1) Arup, Solihul, Birmingham, UK

(2) The University of Birmingham, Birmingham, UK

Abstract

Critical infrastructures such as railway stations are important assets to society which over time have been shown to be susceptible to multiple hazards that could hinder their ability to function as intended. This study focuses on two unique extreme events, flooding and terror attacks, and the sustainability of the retrofits that are typically prescribed to these facilities to enhance their resilience to these hazards under the influence of uncertainty. A framework that incorporates life cycle assessment was applied during the selection process of the retrofits which allowed each of the solutions to be categorised as either being a "No regret", "Reversible" or "High Safety Margin" option. The sustainability of each retrofit was determined by computing the whole-life costs over a 20-year service life and the net present value as well as by measuring net carbon footprint associated with different processes during this service life.

Keywords: life cycle, assessment, retrofit, railway infrastructure, extreme events

1. INTRODUCTION

Buildings designed to accommodate critical infrastructures should possess a high level of resilience to any events or actions that may threaten its ability to function as intended, and should also remain environmentally sustainable. For the purpose of this study, the resilience of a critical infrastructure has been defined as the ability to prepare for and adapt to changing conditions and withstand and recover rapidly from deliberate attacks, accidents or naturally occurring threats or incidents" [1, 2]. Over time, the resilience and overall performance of a structure will reduce and without adequate maintenance, this will increase its vulnerability to extreme events. Critical infrastructures such as transport systems, which decisively affect a bevy of societal and economic functions, cannot afford to be vulnerable to extreme events because of the adverse impacts that could arise. For instance, the vulnerability of a railway station to extreme events such as flooding and terrorism presents primary impacts which could create a succession of secondary damages and inconveniences that could render it incapable of providing normal levels of service to customers as outlined in Table 1. While railway stations are subject to other hazards, two particular extreme events have been selected for evaluation due to the inherent differences in the ways in which they occur, the time-scales within which they occur and the impacts they present to the building when they do occur.

Table 1: Primary and Secondary impacts of flooding and terror attacks on a railway station

Extreme event	**Causes**	**Likelihood /Timescale**	**Primary impact**	**Secondary impact**
Flood	Storm surges, heavy rainfall	Variable likelihood however, the risk is reoccurring due to natural processes	Water inundation; soil/slope erosion, debris impact, sudden surges of large volumes of water, flood risks to HVAC components, encroachment onto railway track	Site pollution, erosion to landscape such as cuttings which may be susceptible to landslides; disruption to services
Terrorist attack	Political, religious and/or socioeconomic motivations	Occur in short and sudden sequences. Infrequent at the same location	Structural damage, debris impact, death, fatal and non-fatal injuries	Progressive collapse of building, fire, traumatising of people ; disruption to services

Since 2016 there has been a 68% surge of terrorism-linked offences in the UK with most notable terror attacks on railway infrastructure leading to the loss of life and injuries, disruptions to the services and significant damage to the buildings themselves [3, 4]. This is particularly true for the bombings that took place in the Brussels airport and metro station in March of 2016 as well as those in May 2017 in the Manchester Victoria station where 32 and 22 deaths occurred respectively as a direct impact of the explosions and millions worth of pounds of cosmetic and structural damages were incurred according to BBC News [5] and Bardsley [6].

While disparities do exist between both extreme events, when attempting to retrofit an existing critical infrastructure that is susceptible to both hazards, similarities in the constraints can be drawn between them as they both introduce elements of uncertainty into the planning process. There is a great deal of difficulty associated with attempting to predict both the environmental and political/socioeconomic climates of the future; therefore a great deal difficulty associated with prescribing the most appropriate retrofit solution that is not over-engineered yet operates with adequate resilience to prevent future risks. Menassa, et al. [7] argued that in some cases this lack of information & adequate benchmarks associated with the uncertainty can drive reluctant stakeholders and decision-makers to either choose or avoid solutions primarily based on the initial capital investment required. In normal circumstances where there is not a high degree of uncertainty, designers typically prioritise a few parameters such as structural performance, costs, speed of installation and suspension time while sustainability is often considered as an afterthought [8, 9, 10]. However, in this context, the consideration of the environmental impacts of the retrofit to be applied to the critical infrastructure should be regarded as critical component of the decision-making process in order to achieve a sustainable design. Furthermore, a truly sustainable design is only achievable if these impacts of the retrofits are holistically assessed over the entirety of the retrofit's service life; a task which is usually undertaken by using a using decision-support tool by many authors using a life cycle assessment (LCA) [11, 12]. Therefore, this study aims to conduct a life cycle assessment of the retrofit strategies that are introduced to railway stations to enhance resilience against extreme events such as terrorisms under the influence of uncertainty.

2. RETROFIT SOLUTIONS

The approach used in this study evaluated the sustainability of different retrofit solutions that can be introduced to enhance the resilience of a train station that is vulnerable to multiple hazards such as flooding and terror attacks by measuring their economic and environmental impacts over a period of time. Using the framework that was set out by Hallegatte [13], 3 approaches that could be specified to address each extreme event without exact knowledge of the time it will occur or severity of the consequences they could present beforehand were identified in Table 2 on the basis that they could be categorised either as a 'No regret', 'Reversible' or a 'High Safety Margin' option. While the most suitable category has been selected for each solution, it should be noted that some solutions, such as vegetated swales, could be placed in multiple categories (i.e. No regrets).

Table 2: Categorised retrofit solutions to enhance resilience against each extreme event

Solution	**Description**	**Method**
1.No Regrets Option	Solutions that can yield secondary benefits even in the absence of the hazard for which they were primarily designed for	**Carbon Fibre Reinforced Polymer (CFRP)** – lightweight material that can be applied to columns to improve resilience against blast loads, as well as deterioration caused by chemical processes propagated by moisture in the air [14].
2.Reversible Option	Solutions which can be easily reversed/removed should the hazard they were designed for not occur or be deemed unlikely to.	**Modified Steel Jacketing (MSJ)** – removable protective coating that can be applied to concrete columns using bolts to improve resilience against blast loads [15].
3.High Safety Margin Option	Solutions for which additional safety measures are provided to significantly reduce the impact	**Ductile CONcrete (DUCON)–** marketed based on basis of the security applications of its ductility, DUCON is a high performance concrete characterised by its high blast and ballistic resistance that allows it to retain 50-100% loading capacity following a contact detonation in comparison to reinforced concrete which could only achieve 4-15% under the same conditions [16].

3. CASE STUDY: BIRMINGHAM INTERNATIONAL RAILWAY STATION

For the purposes of this study, it has been assumed that Birmingham International Railway Station can be categorised amongst the select few railway stations in the United Kingdom that are at a higher risk of suffering from both flooding and terrorism risks. This assumption has been based on the fact the station serves the NEC Genting Arena and Resorts World which generate high volumes of pedestrian traffic each year for concerts, conferences and other large events and the fact that it supports another critical infrastructure; Birmingham International airport, the 3rd largest airport outside of London that saw a record breaking 11.6 million passengers in 2016 [17].

The site to which the retrofit solutions discussed in the previous section have been applied has been illustrated in Figure 1 which depict the plan layout of the entirety of the site that is being considered, the front elevation of the building and a plan view of the ground floor respectively. For the purposes of this study, the corresponding dimensions of the short stay parking lot, taxi ranks and staff parking pavements and the dimensions of the vegetated belts of land which characterise the site boundaries outside the building have been measured using Google Maps to be approximately 1600m^2 and 6710m^2.

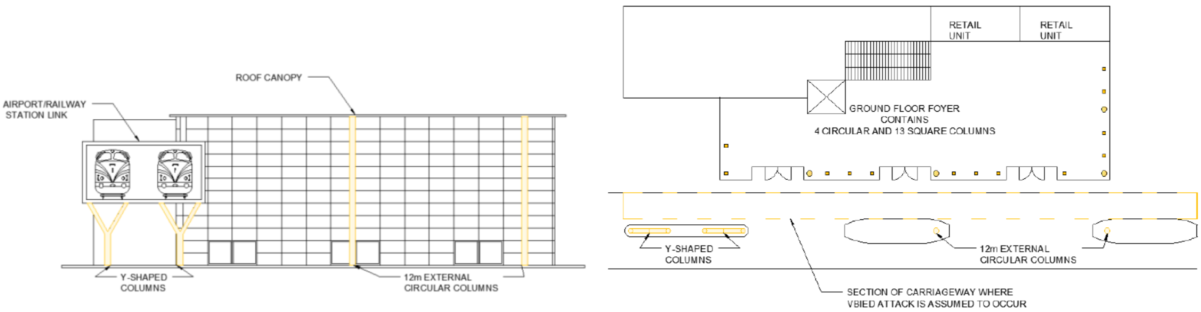

Figure 1: Train station views

4. LIFE CYCLE ANALYSIS

Unlike typical residential and commercial properties, there is an implicit difficulty that can be awarded to the process of assigning a monetary value to a critical infrastructure such as Birmingham International Railway Station and estimating the true costs that would be incurred by either extreme event due to the number of stakeholders (e.g. station managers, rail operators, passengers, staff). The cost of the structural damage experienced will depend on the level of resilience offered by the existing infrastructure and proposed retrofits as well as the magnitude of the event. However, in addition to the structural damage, one must also consider the losses suffered due to a reduced service in the station and the loss of passengers. While it is known that the amount of passengers that exit and enter Birmingham International Railway station annually will be directly affected, currently estimated to be 6.5 million, the ways in which this figure will be affected as a result of either events is beyond the scope of this study. Details of the structural columns within the interior and the exterior of the building have been outlined in Table 3 and have been illustrated in Figure 1.

Although various experiments have been conducted on the materials outlined in this study to observe and determine their blast resilience, there exists limited literature that focuses on their application to columns. Therefore, the thicknesses that have been specified in Table 4 have been adopted from relevant studies and literature where structural columns were retrofitted with CFRP, MSJ and DUCON and they displayed greater residual load capacities following the detonation of an explosive device.

Table 3: Geometrical details of structural columns distributed on ground floor

	Diameter/Width (m)	**Height (m)**	**Area (m^2)**	**Quantity**
Internal square steel columns	0.3	12	0.09	13
Internal circular concrete columns	0.5	12	0.20	4
External circular concrete columns	0.5 0.5	12 (straight columns) 6 (Y-shaped columns)	0.20 0.20	2 2

Table 4: Initial costs and production/extraction carbon emissions of column retrofits solutions

Method	**Thickness (mm)**		**Cost (£/kg)**		**Constituent Materials**	**eCO2 kg/kg**	
		Source		Source			Source
CFRP	2	(Elsanadedy, et al., 2011)	9.66	(Shama Rao, et al., 2017)	Epoxy Resin	2.3300	(Ye & Yue, 2010)
					Polyacrylonitrile (PAN)	31.000	(Das, 2011)
MSJ	8	(Fouche, et al., 2016)	0.59	(S&P Global Platts, 2018)	Iron ore	0.3570	(NSC, 2010)
DUCON	60	(DUCON® Security, 2017)	0.13	(BUILT, 2018)	Quartz sand	0.0026	(Kim, et al., 2015)
					Portland Cement	0.9590	(Norchem, 2011)
					Silica fume	0.0140	(Norchem, 2011)
					Water	0.0002	(Kim, et al., 2015)
					Superplasticiser	1.0643	(Ma, et al., 2016)
			2.65	(UltimateOne, 2018)	Mat Reinforcement (10% of the volume)	2.5000	(Geyer, n.d.)

The capital investment initially required for each material for retrofitting has been computed using the values in Table 4. The equivalent mass of carbon dioxide emissions per kilogram of each constituent material within the retrofit solutions has been specified in order to compute the contribution made to global warming from their individual extraction and production processes. The values associated with each of the retrofit solutions provided in Table 4 have been applied to the appropriate columns within the site and used to determine the financial costs and global warming potential of their application which would aid the determination of their sustainability and feasibility for their purpose. Given the complexity and the number of variables associated with planning for terror attacks, it is often difficult for decision-makers to determine the return on investment that is associated with each retrofit. Several assumptions must be made given that the value of the assets, the number of people in the vicinity of the attack, the true value of the assets to all stakeholders, the magnitude and the extent of the possible damage are all unknown when conducting the calculation of the net present value (NPV) of each solution before the extreme event. The value of the NPV is given by $NPV = \sum[(B_t - C_t)/(1+i)^t]$. where t represents the design life, B_t represents the total monetary benefits in each year between zero and the end of life t, C_t represents the total monetary costs in each year between zero and the end of life *t* and *i* represents discount rate applied for the year under consideration.

Given a scenario where a VBIED attack similar to that of the 1995 Murrah Federal Building bombing occurred in this station with a magnitude sufficient enough to cause the failure of unprotected columns in the absence of protective coatings, but insufficient magnitude to cause the progressive collapse of the building if any of the retrofit solutions that had been applied to the columns, it could be possible to deduce a return on the investment made in a given year. By avoiding the loss of life/fatal injuries to staff and passengers, the value of Bt could be derived by considering it to be a fraction of the monetary value attributed to the life of a single human being. While in most cases this is considered to be an intangible cost, the value can be assumed to be equivalent to 'the cost to society per case of fatal injuries to a single person is equivalent to £1,597,000 [18]. The decision-maker then has the responsibility of crediting a percentage of the benefits to the retrofit initiative based on its15contribution to the prevention of the failure of the structure but must take care to avoid over-valuing the benefits [19]. It has also been assumed that following the explosion; none of the retrofits will remain fit for their intended purpose as a result of the incurred damage and must be replaced and recycled for future use. While it has been assumed for there to be no monetary gain from recycling the remnants of the CFRP and DUCON, any valuable MSJ and mat reinforcement within the DUCON (10% of volume) can be sold for £0.05-0.14 per kg following the VBIED attack [20]. The return of this benefit in each year has been discounted at 3.5% [21].

5. RESULTS AND DISCUSSION

The initial costs of retrofitting the columns within the ground floor of the train station entrance using MSJ, DUCON and CFRP wraps based on the geometric parameters outlined in Table 6 have been calculated and displayed in Figure 2. When considering the option of protecting all of the columns to a height of 6m, MSJs incur the lowest initial capital costs of £14,295; immediately followed by CFRP wraps at an initial cost of £16,896; and lastly DUCON coating costing £30,405. This trend is shown to be consistent between all of the different retrofit combinations that could be made whether only the internal circular columns, only the external columns or whether only the internal square columns are protected. It has been assumed that no steel jacketing would be provided for the internal square steel columns.

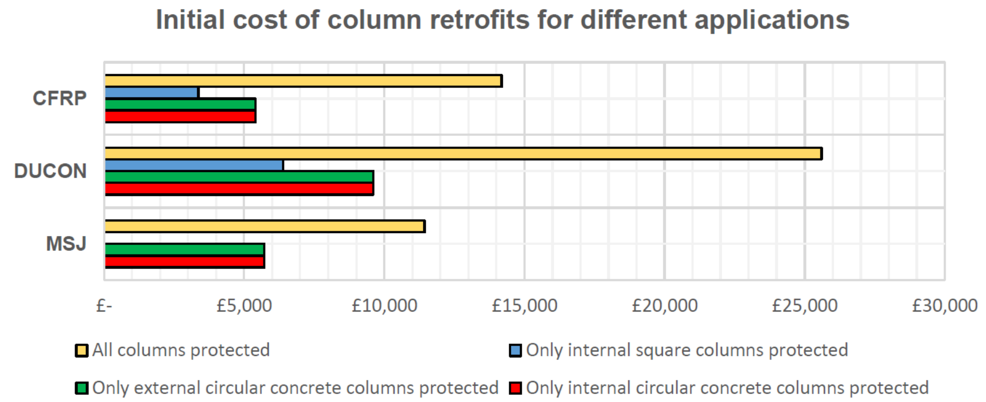

Figure 2: Initial cost of column retrofits for different applications

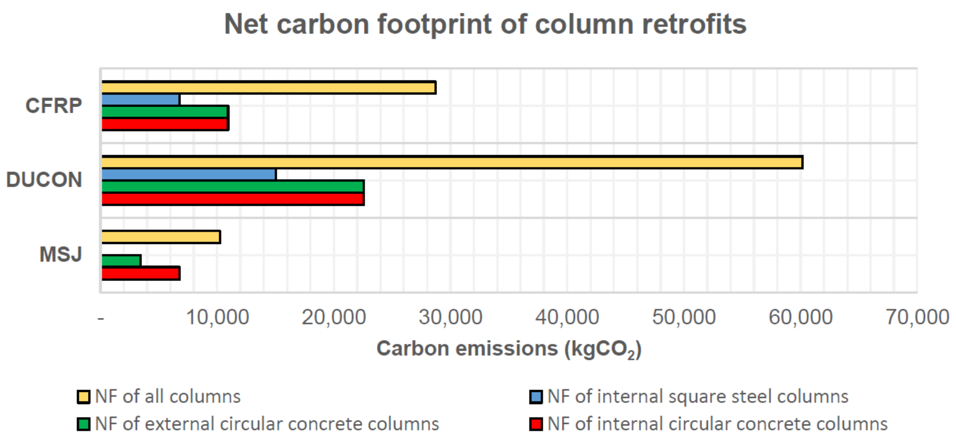

Figure 3: Net carbon footprint of column retrofits

As highlighted in Figures 2 and 3, while the use of DUCON (i.e.“High Safety Margin” option) will significantly enhance the robustness and resilience of the columns, it does so at a higher cost to the decision-maker and the environment than the other protective retrofits do. Unlike the porous pavements in Section 4.1, the DUCON retrofits are not multifunctional applications and do not yield additional benefits which would otherwise be used to justify the fact that the net carbon footprint of 6 circular columns is shown to emit 33,862 kgCO2 during production/extraction; nearly 4 times as much 23 MSJs that produce 8,840kgCO2; roughly similar to the emissions from all 23 CFRP wraps of 34,162 kgCO2. In a similar fashion to Philips, et al. [22]’s results which showed that 20% of the resilience frameworks they examined harboured a negative relationship with sustainability, the results of this study with regards to DUCON coating seek to reinforce the notion that the most resilient solutions tend to be the least sustainable.

6. CONCLUSION

This study reviewed various resilience and sustainability frameworks from previous studies relevant to this topic and in doing so highlighted the difficulties and impacts associated with retrofitting for future hazards when there are several unknowns and uncertainties that must be considered. It has shown how LCA’s can be practical decision-support tools that could be utilised by decision-makers when planning for future extreme events. By assessing the environmental and economic impacts of different retrofit options that enhance the resilience of a critical infrastructure when faced with uncertainty, this study is able to determine the sustainability of each option. The modified steel jacketing (MSJ) is found to be the most suitable method in terms of both economical and environmental sustainability.

ACKNOWLEDGEMENTS

The authors are sincerely grateful to European Commission for the financial sponsorship of the H2020-MSCA-RISE Project No. 691135 “RISEN: Rail Infrastructure Systems Engineering Network,” which enables a global research network that tackles the grand challenge of railway infrastructure resilience and advanced sensing in extreme environments (www.risen2rail.eu).

REFERENCES

[1] Kaewunruen S, Sussman JM, Matsumoto A. Grand challenges in transportation and transit systems. *Front Built Environ* 2016; 2(4).

[2] Homeland Security, *Critical Infrastructure Security and Resilience*. s.l., International Committee on Global Navigation Satellite Systems, 2014.

[3] Travis, A., UK terror arrests rise 68% to record level during year of attacks, 2017. [Online] Available at: https://www.theguardian.com/uk-news/2017/sep/14/uk-terror-arrests-rise-68-record-level-during-year-attacks .

[4] Rennie J, Kaewunruen S, Baniotopoulos C. Blast effects on spatial glass shells for a long-span roof structure, *IASS Symposium 2018*, Massachusetts Institute of Technology (MIT), IASS 2018, Cambridge, United States.

[5] BBC News, Brussels explosions: What we know about airport and metro attacks, 2016. [Online] Available at: http://www.bbc.co.uk/news/world-europe-35869985

[6] Bradsley, S., Cost to line a stripe a parking lot, 2015. [Online] Available at: http://www.fixasphalt.com/blog/cost-to-line-stripe-a-parking-lot

[7] Menassa, C. C., Evaluating sustainable retrofits in existing buildings under uncertainty. *Energy and Buildings*, 43(12), pp. 3576 - 3583. (2011).

[8] Setsobhonkul S, Kaewunruen S and Sussman JM., Lifecycle Assessments of Railway Bridge Transitions Exposed to Extreme Climate Events. *Front. Built Environ*. 3:35. (2017) doi: 10.3389/fbuil.2017.00035

[9] Vitiello, U. et al., Life-cycle assessment of seismic retrofit strategies applied to existing building structures. *Sustainability*, 8(12), 1275. (2016).

[10] Kaewunruen, S., Sussman, J. M., and Einstein, H. H. Strategic framework to achieve carbon-efficient construction and maintenance of railway infrastructure systems. *Front. Environ. Sci.* 3:6. (2015). doi:10.3389/fenvs.2015.00006

[11] Tuler, M.V. and Kaewunruen, S. Life cycle analysis of mitigation methodologies for railway rolling noise and groundbourne vibration. *J. Environ. Manag.* (2017), *191*, 75–82.

[12] Tavares de Freitas, R. and Kaewunruen, S. Life Cycle Cost Evaluation of Noise and Vibration Control Methods at Urban Railway Turnouts. *Environments* (2016), 3, 34.

[13] Hallegatte, S., Strategies to adapt to an uncertain climate change. *Global Environmental Change*, 19(2), pp. 240 -247, (2009).

[14] Burgoyne, C. and Balafas, I., *Why is FRP not a financial success?*. Patras, Greece: s.n. (2007).

[15] Fouche, P., Bruneau, M. and Chiarito, V. P., Modified Steel-Jacketed Columns for Combined Blast and Seismic Retrofit of Exisiting Bridge Columns. *Journal of Bridge Engineering*, 21(7). (2016).

[16] DUCON® Security, *Structural Flexibility and Resilience*, Darmstadt: s.n. (2017).

[17] Birmingham Updates, Birmingham Airport celebrates a record breaking year – 11.6 million passengers in 2016. (2017). [Online] Available at: http://www.birminghamupdates.com/birmingham-airport-celebrates-a-record-breaking-year-11-6-million-passengers-in-2016

[18] Health and Safety Executive, Appraisal values or 'unit costs'. (2015). [Online] Available at: http://www.hse.gov.uk/economics/eauappraisal.htm

[19] Office of Rail and Road, *Estimates of station usage*. London, UK. (2017).

[20] Kaewunruen, S., Wu, L., Goto, K., Najih, Y.M. Vulnerability of Structural Concrete to Extreme Climate Variances. *Climate* 2018, 6, 40 (2018).

[21] HM Treasury, *Green Book*, s.l.: s.n. (2013).

[22] Philips, R., Troup, L., Fannon, D. & Eckelman, M. J., 2017. Do resilient and sustainable design strategies conflict in commercial buildings? A critical analysis of existing resilient building frameworks and their sustainability implications. *Energy and Buildings*, 146, pp. 295-311.

DURABILITY DESIGN FOR CONCRETE BRIDGE STRUCTURES IN THE GERMAN FEDERAL HIGHWAY NETWORK: STATUS QUO

Maria Teresa Alonso Junghanns and Peter Haardt

Federal Highway Research Institute (BASt)/ Concrete Structures, Germany

Abstract

According to valid standards and guidelines, concrete bridge structures should ensure their structural safety, serviceability and durability during their service life. Durability design of new infrastructure is usually carried out based on a descriptive approach appropriate to exposure-dependent information. By regular inspection, structural changes and damages are evaluated. It is not possible to estimate the reliability with regard to the durability. This design format does not allow any prediction of the service life and stands in contrast to the structural design for static and dynamic loads. However, other approaches are already included in the regulations.

For durability designs referring to carbonation- and chloride-induced reinforcement corrosion probabilistic prediction models are available. They define the limit state as the condition state when a critical chloride content reaches the reinforcing steel surface or the carbonation front penetrates to the first reinforcement layer.

A calculated durability design requires laboratory tests for calibration and results of in-situ tests for validation. In principle it must be answered whether and, if so, how an operational assessment of durability should be applied. This paper presents an overview of the status of the current application of this design approach for concrete bridge structures in the federal german highway network.

Keywords: durability, design, concrete, bridges, Germany

1. INTRODUCTION

According to DIN EN 1992-2 [1], the requirements on an adequately durable concrete structure are met, if it fulfills its function during the design working life. Durability is therefore an inherent aspect in the design of engineering structures.

RI-ERH-ING [2] defines durability in the german federal highway network as the resistance of the structure or individual elements of the structure to actions in order to achieve a service life as long as possible, while maintaining structural stability and traffic safety under scheduled use and maintenance as planned. Thus the guarantee of durability means that even the physical and chemical actions caused by environmental conditions should not have any detriment on the concrete properties. Durability is considered exclusively under consideration of environmental and storage-related influences.

Physical and chemical action on concrete can change the concrete properties. These changes are referred to as damage. After initation the damage can progress to failure during the propagation period. In reinforced concrete bridges, for example, the initiation period ends with the depassivation of the reinforcement surface due to carbonation or chloride penetration. The subsequent damage period presupposes boundary conditions for example resulting from the moisture balance and oxygen supply.

The durability design in the german federal highway network currently follows a deemed to satisfy approach based on descriptive rules. However, the safety of a descriptive design remains unknown and the remaining service life cannot be determined. Probablisitic design approaches could provide a mathematical proof of the service life. According to the valid standards and guidelines, a probablisitic approach is also possible in addition to a descriptive design approach according to EN 206.

A calculated durability design requires models which represent a quantification of the action and resistance of the bridge element. These models consider the physical, chemical, storage related, geometric data and concrete technological influences up to the end of the initiation period. It is assumed that damage will reach a certain limit value with a certain probability. These limit states are currently already recorded and evaluated today by regular inspections.

Typical damage in concrete bridges with regards to durability are carbonation-induced corrosion, chloride-induced corrosion and freeze-thaw attack with/ and without de-icing agents. At current time, a mathematical damage modelling of frost with de-icing salt, necessary for the durability design calculation, is not possible due to the complexity of the underlying mechanisms. In this paper only the carbonation-induced and chloride-induced reinforcement corrosion is considered.

2. CURRENT DURABILITY DESIGN FOR CONCRETE BRIDGE

2.1 Current planning and detailing of new concrete bridge structures

The durability design of new concrete bridges is currently carried out on the basis of exposure-dependent data on concrete composition, geometry data and execution rules [1, 3, 4]. Descriptive values are based on laboratory test and inspection tests, empirical correlations and experience.

Regulations define exposure classes related to the environmental and storage conditions. Specific exposure conditions for bridges are specified in ZTV-ING [4]. In addition to the microclimatic conditions, the specific properties of the bridge elements are also taken into account. For example, surfaces in the spray area (e.g. piers under a high viaduct) are exclusively assigned to exposure class XC4 and XD3 and not predominantly horizontal surfaces in the splash water area, e.g. abutments, to exposure class XC4 and XD2.

Depending on the exposure classes, minimum requirements are set for the concrete composition and for the concrete cover. These minimum requirements are intended to ensure a planned service life of the concrete of at least 50 years under normal maintenance conditions. Verifications of the concrete properties of the concrete with regard to durability are not carried out. Only for approvals in individual cases proof is required within the scope of unregulated concretes.

2.2 Current assessment of existing concrete bridge structures

The condition of bridge structures is determined according to RI-EBW-PRÜ [5] by scheduled inspections according to DIN 1076 [6]. Each individual damage noticed during the inspection is assessed separately according to the criteria stability (S), traffic safety (V) and durability (D) and the grade of element groups is taken into account. The element group grades allow the determination of the condition grade of the overall structure using algorithms [7].

The damage assessment is carried out for the individual criteria with grades from 0 to 4. With a grade of 0, the damage has no influence on the respective criterion. In the case of grade 4, immediate actions are required, restrictions on use may be imposed and repair or renewal may be initiated. The results of the bridge inspection are documented in the data base SIB-Bauwerke (Road Information Database-Structures), wich contains also technical data concerning construction type and characteristics according to the guideline ASB-ING [8] in order to enable systematic bridge maintenance.

According to RI-EBW-PRÜF [5], a certain damage level is reached as soon as the carbonation or chloride front has penetrated the concrete. If they reach 1/3 of the depth of the concrete cover, the grade is D=1, between 1/3 and 2/3 D=2 and up to the concrete cover D=3. Limit values for the chloride front in reinforced concrete or prestressed concrete are specified for a concentration of 0.4 wt.%z or 0.02 wt.%z respectively.

Furthermore, in RI-EBW-PRÜF [5] crack width and exposure are evaluated with regard to chloride-induced corrosion. For example, cracks under chloride exposure in the spray water area with crack widths between 0.1 and 0.2 mm are given the durability grade D=2. For crack widths between 0.2 and 0.4, the state grade D=3 is given.

A handbook of damage potentials for defined groups of structures in steel and prestressed concrete bridges is presented in [9]. For this purpose, bridges of the construction years 1935 to 2010 were analysed on the basis of the relevant current damage. It was found that only 14.5% of all damage had no effect on durability, whereas 81% and 94% respectively had no effect on road safety or stability. It should be noted that damage to stability and traffic safety always has an impact on durability in the assessments [7].

If bridges constructed after 2003 are explicitly analysed, a shift in the damage towards a more favourable assessment number for each element group can be seen in comparison with bridges built between 1935 and 2003. For example, damage with a grade D=2 is reduced to about 50% for all elements and, for example, damage of the superstructure drops from approx. 46% to approx. 22% and damage of the substructure from approx. 37% to approx. 15%. This improvement is attributed to the tightening of standards. A dependence on traffic intensity with regard to damage with regard on durability is not discernible from the results [9,10].

The assessment according to RI-EBW-PRÜF [5] usually takes place visually after the damage has occurred. This corresponds to a stage in which the initiation period has ended. Therefore, these results do not allow an evaluation of the initiation period and reliability considerations of the service life are not possible.

3. CALCULATED DURABILITY DESIGN FOR CONCRETE BRIDGES

3.1 Semi-Empirical methods for durability calculations

Damage models for the depassivation of reinforcement are often represented by a simple $\sqrt{t}$ function. Carbonation factors and chloride diffusion parameters are determined by regression calculations based on results from laboratory or inspection testing.

Empirical factors based on measurements from 156 German bridges built between 1905 and 1994 and tested between the ages of 7 and 90 years are included in [11]. The results were classified according to the bridge elements. The evaluation shows reasonable engineering results regarding transport phenomena, e.g. that damage due to carbonation is not relevant for the edge beams and that higher carbonation is generally to be expected in abutments. The results also show that an increase in chloride penetration velocity due to surface damage is to be expected and that the highest values of chloride concentration can be expected in edge beams. However, the dispersion is very large. The compiled data have a very heterogeneous structure, which can be traced back, among other things, to the non-uniform collection of data. The data were obtained from several reports, which do not always contain all geometric and/or concrete technological properties as well as enviroment dependent data.

These semi-empirical methos allow a simple estimation of the factors after assesments or using Lab-Results but they do not allow a prediction of damage a "priori".

3.2 Probabilistic calculation of durability

Neither the actions nor the behaviour of bridge elements are known exactly in the structure. Stochastically distributed input parameters are applied by means of laboratory or field measurements with scatters and distributions in order to determine the stochastically distributed time dependent damage.

A full-probabilistic prediction for concrete bridges with regard to carbonation-induced and chloride-induced corrosion was investigated in a research project [12] commissioned by BASt using the descriptive rules for concrete bridge structures according to ZTV-ING [4]. Various design situations were selected: High actions and low material resistances as well as high material resistances and low actions were compared. The climatic conditions were taken into account on the basis of real climate data from various locations in Germany.

For bridges it can be assumed that if an XC exposure is given, the element is also exposed to both XD and XF exposures. XD or XF exposure require the higher material resistances. For concrete bridges, a water-cement ratio of 0.50 and a minimum cement content of 320 kg/mm² are uniformly specified in ZTV-ING [4]. For the nominal value of the concrete cover, 40 mm are assumed for exposed surfaces of the structural concrete with an allowance in design for deviation of the cover of 5 mm. For the parameter study in [12] also an allowance for deviation of 15 mm was included.

The reliability spectra for these design situations were determined in [12] using pre-normative work [13, 14, 15]. Model input parameters were selected for the prediction "a priori" from the literature [12]. The dependence of the computed results on the input variables was investigated with probabilistic sensitivity and dominance analyses, see Figure 1:

- for XC-exposed elements the concrete cover is the most sensitive parameter in most of the design situations and especially in exposure class XC2. For XC3, both the carbonation resistance and the test parameter k_t to take into account the test method for determining carbonatation resistance (R_{NAC} or R_{ACC}) show a high sensitivity. The regression exponent has a particularly sensitive effect in exposure class XC4.

- for XD-exposed elements, a precise information on the ageing exponent α, on the chloride diffusion coefficient D_{app}, on the chloride content at the surface, and on the temperature reduce model uncertainty

In the frame of the current investigation, whether the results of the "a priori" prediction correspond to realistic values in bridge structures could only be checked on the basis of a few structures assigned to exposure classes XD1 and XC3. For the critical chloride content, 0.6 wt.% was used for the calculation according to [15,16]. In [5] the limit value is defined as the maximum initial chloride content of concrete of reinforced concrete structures according to EN 206-1.

Carbonation depth $x_c(t)$ at a time t.

$$x_c(t) = \sqrt{2 \cdot R_{NAC,0}^{-1} \cdot C_S \cdot k_e \cdot k_c} \cdot \sqrt{t} \cdot W(t)$$

Cs:	CO_2-Concentration
ke:	enviromental funktion
k_c:	execution transfer parameter
W(t):	weather funktion
R_{NAC}: and R_{ACC}:	effective carbonation resistance of concrete under natural conditions (ACC) and in accelerated test (NAC)
k_t:	Test method factor
c:	concrete cover
RH	relative humidity

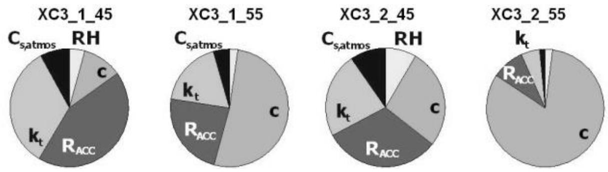

Chlorid content C (x,t) at a depth x at atime t t

$$C(x,t) = C_0 + (C_{S,\Delta x} - C_0) \cdot \left[1 - erf \frac{x - \Delta x}{2 \cdot \sqrt{D_{app}(t) \cdot t}}\right]$$

C_0:	initial chloride content
$C_{S,\Delta x}$:	chloride content at a the depth of the convection zone Δx
D_{app} :	apparent chloride diffusion coefficient
α	age exponent
be	regression variable
c:	concrete cover
C_{crit}:	critical chlorid content

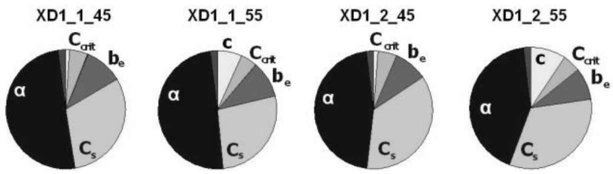

1: >S, <R; 2: <S, >R; c: 45 mm und 55 mm;
S: exposure condition; R :material and geometry conditions
c=320 kg/m³; w/c=0.50

Figure 1: Example for the sensitivity analyse for the exposure classes XC3 und XD: mathematical Model, influence of the parameters on the results according the design situations [12]

Values for the required reliability index for the limit state depassivation are contained in [16]. For example for XD1 or XC3 should be ß ≥ 1.5 or ß ≥ 0.5. In the investigated cases [12] the reliability of the actual condition was above the target condition, and after 100 years service life the determined actual reliability is greater than the target reliability.

Figure 2 shows results on the development of the calculated reliabilty spectra as well as the target and actual condition for a real bridge from 1965 in the exposure XD1. Figure 2 shows that the target reliability of $\beta = 1.5$ for the spectrum case of high exposure effects (actions) and low material resistance is not mathematically met over 100 years. If, however, there are high material resistances with low actions, the calculated reliability, even after 100 years, does not fall below 3.8 and is therefore on the safe side.

The reliability development in the target state according to fig. 2 is located in the reliability spectrum for the general design situation correspondig to XD1 and for this bridge as used in the research [12]. The reliability indices in the actual state are again higher than those in the target state, although the real concrete cover of 33 mm is low compared to the assumed value of 45 mm. However, the real surface chloride content is also considerably smaller than the initially assumed. Also after 100 years a calculated reliability is higher than the required target reliability index.

Figure 2 contains a few of the model input parameters. For the target state, parameters depending on the actual concrete composition were selected from the literature; for the actual state, data from an inspection of undamaged areas were used [12]. The chloride diffusion coefficient was determined as the mean value of six chloride profiles in three depths each and the surface chloride concentration was summarized as the mean value of the measuring points.

Input-Parameters (μ: mean; σ: deviation)

	D_{RCM} (t_0) [10^{-12}m²/s]	$C_{S,\Delta x}$ [M %/b]	C [mm]
Spectrum: XD1_1_45; XD1_2_45 z=320kg/m³; w/z=0,50			
μ	15.8; 2.8	1.5; 0.5	45
σ	3.16; 0.56	1.1; 0.4	3
Construction 1965; Inspection 1999 CEM I; z=350 kg/mm³, w/z= 0.38			
Target; Actual			
μ	8.9; 0.3	1.0; 0.35	45; 33
σ	1.78; 0.3	0.75; 0.2	5.0; 5.5

Reliability: Spectrum; Target and Actual State

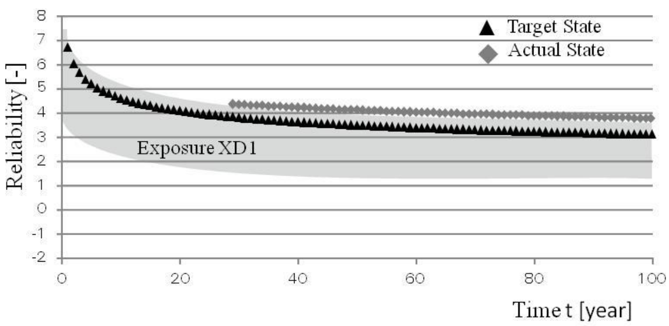

α=0.65±0.12; b_e=4800±700 K; Δx=0 mm;
C_0=0 M.-%/b; C_{crit} = 0.6±0.15 M.-%/b
(Model after Figure 1)

Figure 2: Examples of the evolution of the calculated reliability for the exposure XD1 [12]

The results in [12] cannot be applied directly in practice, since for a safe application significantly more engineering structures from all exposure classes with a broader selection of locations/exposures and concrete compositions are necessary to verify the model analysis. The large data sets according to 3.1 could not be evaluated for the validation because only a few profiles fulfill the requirements for the calculations. A meaningful application of fully probabilistic models places high demands on the quantity and quality of the inspection results. For example, the measurement of the real concrete cover during inspection is recommended if it was not determined during production. In addition, in the case of chloride exposure, for example, taking samples in at least four, preferably five depths is recommended. For a regression analysis, at least three depths are required and for XD3 components, the results from the convection zone are not to be included in the regression analysis. The concrete composition should be known and measured data on concrete coverage should be available

[12]. The samples in the structure are to be taken from undamaged concrete surfaces to ensure that the results correspond to the initation period. According to [13], cracks up to 0.2 mm are not considered for durability and the depassivation progress of concrete with cracks up to 0.2 mm is assumed analogous to non-cracked concrete.

3.3 Consideration for design with partial safety factors

Analogous to the structural design, sufficient safety is achieved with partial safety factors if the design values for the actions are smaller than the design values for the resistances. The characteristic values and the partial safety factor are considered as design values. Partial safety factors for carbonation and chloride-induced corrosion are derived in [15] e.g. from probabilistic considerations. Partial safety factors for bridges in the german federal highway network are unknown at this time; verification is required.

The described calculation design methods are based on damage models at the individual damage level. A transfer to the entire structure should consider combinations of different damage mechanisms and the spatial distribution of "singular damages". However, this is still associated with a high need for research. For example, the necessary tests for the entire structure must be determined and the effects of interactions should be proven experimentally.

5. CONCLUSIONS

- The durability design in the german federal highway network currently takes place descriptively for new and existing concrete bridges.
- The application of probabilistic methods for durability design could also be possible for bridges. However, the methods require a large amount of results from laboratory and field testing in order to determine reliably age-dependent input parameters in the models. The properties should be determined before visual macro damage occurs and the extent of testing should be determined taking into account the data required for the models.
- Simplifications of computational methods, selection of input parameters in the model and representation of its effect on the results could facilitate the estimation of the accuracy of the calculation.
- It is imaginable that the calculation methods could provide a basis for predicting the service life in concrete bridge structures in the german federal highway network and that these methods could enable a transition from the current assessment procedures to a reliability-based procedure. Currently only imprecise statements on the actual service life of a concrete bridge with regard to durability are possible.

REFERENCES

[1] DIN EN 1992-2: Eurocode 2: Bemessung und Konstruktion von Stahlbeton- und Spannbetontragwerken - Teil 2: Betonbrücken - Bemessungs- und Konstruktionsregeln; Nationaler Anhang - National festgelegte Parameter.
[2] RI-ERH-ING: Richtlinien für die Erhaltung von Ingenieurbauten. Leitfaden Objektbezogene Schadensanalyse OSA. Ausgabe 2007
[3] DIN 1045-2:2008; DIN 1045-3:2012-3 Tragwerke aus Beton, Stahlbeton und Spannbeton – Teil 2: Beton –Festlegung, Eigenschaften, Herstellung und Konformität – Anwendungsregeln zu DIN EN 206-1. Teil 3: Bauausführung - Anwendungsregeln zu DIN EN 13670

[4] ZTV-ING: Zusätzliche Technische Vertragsbedingungen und Richtlinien für Ingenieurbauten, Teil 3 Massivbau, Bundesanstalt für Straßenwesen, 2018
[5] RI-EBW-PRÜF: Richtlinie zur einheitlichen Erfassung, Bewertung, Aufzeichnung und Auswertung von Ergebnissen der Bauwerksprüfungen nach DIN 1076. Ausgabe 2013
[6] DIN 1076: 1999-11: Ingenieurbauwerke im Zuge von Straßen und Wegen - Überwachung und Prüfung
[7] Haardt, P.: Algorithmen zur Zustandsbewertung von Ingenieurbauwerken. Reports of the Federal Highway Research Institute (Bundesanstalt für Straßenwesen). Number B22. Bergisch Gladbach, 1999
[8] ASB-ING: Bundesministerium für Verkehr, Bau- und Stadtentwicklung. Abteilung Straßenbau. Anweisung Straßeninformationsbank. Segment Bauwerksdaten. Erhaltung. Sammlung Brücken- und Ingenieurbau., 2013
[9] Schnellenbach-Held, M.; Peters, M.; Miedzinski, G.: Intelligente Bauwerke. Schädigungsrelevante Einwirkungen und Schädigungspotenziale von Brückenbauwerken aus Beton. Reports of the Federal Highway Research Institute (Bundesanstalt für Straßenwesen). Number 110, Bergisch Gladbach 2015
[10] Schnellenbach-Held, M.; Karczewski, B.; Kühn, O.: Intelligente Brücke. Machbarkeitsstudie für ein System zur Informationsbereitstellung und ganzheitlichen Bewertung in Echtzeit für Brückenbauwerke. Reports of the Federal Highway Research Institute (Bundesanstalt für Straßenwesen). Number 105, Bergisch Gladbach, 2014.
[11] Novák, B.; Brosge, S.; Ananiev, S.; Meiss, K.; Wagner, R., Weißbach, M.: Weiterentwicklung des Modelansatzes der Schadensprognose und Wirkung von Erhaltungsmaßnahmen im BMS. Final report on the research project FE 15.383/2003/HRB, commissioned by the Federal Highway Research Institute (Bundesanstalt für Straßenwesen), Bergisch Gladbach, 2003
[12] Keßler, S.; Gehlen, C.: Untersuchungen zum Einfluss von Modellparametern auf die Lebensdauerprognose für Brückenbauwerke. Final report on the research project FE 15.0481/2009/DRB, commissioned by the Federal Highway Research Institute (Bundesanstalt für Straßenwesen), Bergisch Gladbach, 2018
[13] Fib Model Code for Concrete Structures 2010. Ernst&Sohn , Berlin 2013
[14] Fib Bulletin 34: Model Code for Service Life Design. International Federation for Structural Concrete, Lausanne, February 2006
[15] Fib Bulletin 76: Benchmarking of Deemed-To-Satisfy Provisions in Standards. . International Federation for Structural Concrete, Lausanne, May 2015
[16] Deutscher Ausschuss für Stahlbeton: Positionspapier des DAfStb zur Umsetzung des Konzepts von leistungsbezogenen Entwurfsverfahren unter Berücksichtigung von DIN EN 206-1, Anhang J. Beton- und Stahlbetonbau 103 (2008), Heft 12, 837-839.

RISK BASED INSPECTION PLANNING METHODOLOGY FOR CONCRETE BRIDGES

S.M. Samindi, M.K. Samarakoon and R.M. Chandima Ratnayake

Department of Mechanical and Structural Engineering and Materials Science, University of Stavanger, Norway

Abstract
The inspection of reinforced concrete bridges is vital to assure load-bearing capacity, traffic safety (health and societal safety) and aesthetics and the ability to cope with environmental challenges and, as well as to minimize maintenance costs. Bridge inspection accrues significant costs due to lack of cross fertilization with the standard approaches that have been developed in other inspection disciplines. This study focuses on developing a risk-based inspection (RBI) planning procedure for concrete bridges, using the salient features of RBI planning in other disciplines. To develop the RBI planning procedure, a comprehensive study is carried out, using the inspection data available in the Norwegian Public Roads Administration (NPRA) database. The existing inspection recommendation approach in NPRA is studied to understand the deficiencies. A risk matrix is developed to assist RBI planning-associated prioritizations, focusing on concrete crack size and potential maintenance and repair cost. Then, to overcome the variability of recommending future inspection measures, a fuzzy set theory-based approach is used. A set of rules is derived, using the table look-up method. The overall methodology to incorporate the RBI planning is illustrated.

Keywords: Risk-based inspection, concrete bridges, cracks, Fuzzy set theory, maintenance

1. INTRODUCTION

The inspection of reinforced concrete bridges helps to discover harmful deterioration and other types of deficiencies in structural members [1]. In general, periodic bridge inspection programs are carried out to reduce the health, safety and environmental (HSE) challenges, as well as the maintenance and repair costs [2]. Moreover, every country applies bridge inspection programs based on its national regulations by satisfying the owners' requirements. However, it is still a challenge to select an efficient inspection method, the optimal inspection interval, and the extent of inspection. To overcome deficiencies in the present inspection methods, it is vital to implement risk-based inspection (RBI) analyses, assessments and planning [3]. The RBI approach improves safety, whilst allowing inspection resources to be allocated more efficiently and effectively [4]. Hence, the integration of risk-based assessment and control approaches into inspection programs enables the quantification of the current condition of the existing structure and the consequences due to that condition with optimal resource allocations.

RBI is widely utilized for the mechanical equipment and steel structures in offshore oil and gas production facilities [5] and highway structures [6]. However, after the implementation of RBI, in practice, there can be considerable variability among the recommendations for future inspections. Therefore, it is vital to improve the existing RBI method, to reduce the variability of inspection recommendations. This paper discusses the existing inspection program in NPRA as a case study. It proposes modifications to improve the efficiency of the existing program, by reducing the variability of decision makers via a fuzzy set theory based approach.

2. OVERVIEW OF THE EXISTING INSPECTION PROGRAM IN NPRA

Figure 1 shows an overview of the inspection program in NPRA after significant modification in 2018 [7]. According to Figure 1, once a bridge needs to be inspected, visual inspection, combined with non-destructive/destructive testing, is performed to assess the condition and safety of the bridge. Then, any damage or deficiencies in structural members (i.e. location) in the bridge should be recorded in a database. The list of possible damage/deficiencies (i.e. corrosion, cracks, spalling, discoloring, etc.) in bridges is given in the NPRA handbook [7] with a corresponding number. Moreover, NPRA has established a bridge management system called 'Brutus' for the input of all the information about all bridges in Norway. Therefore, 'Brutus' (i.e. the bridge inspection database – BIDB) consists of the historical inspection data of the bridges. Then, after an inspection, it is vital to analyze the data to recommend the next inspection interval. When assessing damage, it is crucial to classify the type, level (use Table 1), cause and consequences of the damage to the entire bridge and/or the environment (use Table 2 and Table 3). Then, to recommend the level of action required, a priority number is calculated, using equation 1. Furthermore, the higher the priority number, the greater the indication that immediate action/measure is required.

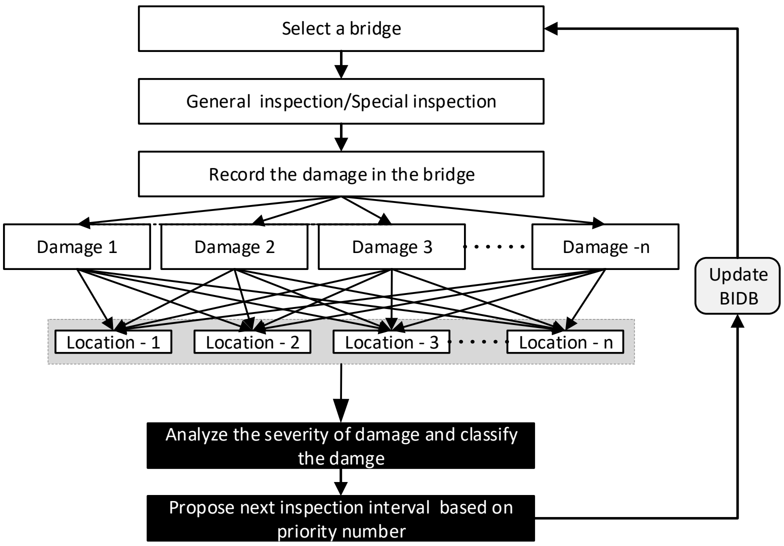

Figure 1: Existing inspection program at NPRA

Table 1: Damage/defect level and rank [7]

Rank	Damage/deficiency level	
1	Low (L)	
2	Medium (M)	
3	High (H)	
4	Very high (VH)	

Table 2: Consequence type and level [7]

Consequence type	*Abb.
Damage/defect(s) threatening bearing capacity	B
Damage/defect(s) threatening road safety	RS
Damage/defect(s) that may increase maintenance costs	M/R
Damage/defect(s) that may affect the environment/aesthetics	E/A

Consequence level	Measures to be taken	Rank
L	No action required	1
M	Register the recommended measures in BIDB	2
H	• Register the recommended measures in BIDB, and • Inspection interval shall be recommended	3
VH	Immediate action is required	4

**Abbreviation - B: Bearing capacity; RS: Road safety; M/R: Maintenance/Repair; E/A: Environment and aesthetic appearance*

Table 3: Damage level and rank in relation to the damage type – crack width (CW) [7]

Damage level	Rank	CW in mm
Low (L)	1	CW < 0.3
Medium (M)	2	0.3 < CW < 1.0
High (H)	3	1.0 < CW <2.0
Very high (VH)	4	CW > 2.0

$$\textbf{\textit{Priority (P) = Damage level}} \times \textbf{\textit{Consequence of damage}} \times \textbf{\textit{Consequence type}} \quad (1)$$

When
$P \leq 6$: Recommended measures are normally not assessed before the next inspection
$8 \leq P \leq 12$: Recommended measures are assessed with the proposed time of execution
$P = 16$: Measures taken immediately

Initially, a fixed time interval based inspection program was used in NPRA, but this was revealed to be relatively inefficient (i.e. compared to the current consequence classification-based inspection prioritization). Before 2018, the inspection recommendations were carried out without a consequence classification based priority number (i.e. the current approach recommends measures to prevent the risk of potential failures, based on the consequence classification). The revised approach enables a significant reduction in unnecessary inspection cost and the risk of potential failures (i.e. decreasing health and safety challenges). Table 4 gives an example of the application of the revised method. However, the revised inspection plan does not take into account the variability of future recommendations.

Table 4: Example to demonstrate the current use of the inspection procedure [7]

Crack illustration	Description
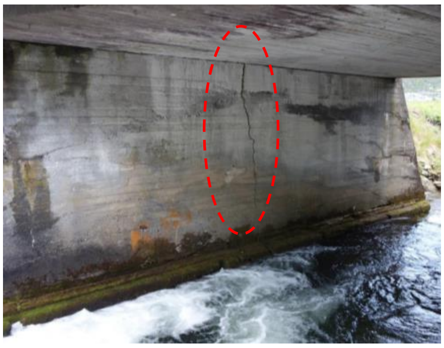	**Comment:** • Coarse vertical crack on reinforced concrete abutment. • No evidence of sequential loss or lack of support to the slab. • The crack may have developed due to the movement/rotation in abutment due to soil erosion. **Damage type**: Crack **Damage level**: 4 (crack width is greater than 2mm) **Consequence category**: 2M (Consequence level and type) **Priority**: 8M **Cause**: Erosion under the abutment **Measures to be taken**: • Repair the abutment. • Any development of crack or lack of support for the plate must be followed by periodic inspection.

3. FRAMEWORK FOR RBI ASSESSMENT AND CONTROL

Figure 2 illustrates the framework that has been developed to carry out RBI assessments and evaluation on concrete bridge structures. The suggested approach involves a risk matrix, which has been developed to assess the risk of a potential failure by careful consideration of the probability of a potential failure (PoF) and the consequence of such a potential failure (CoF).

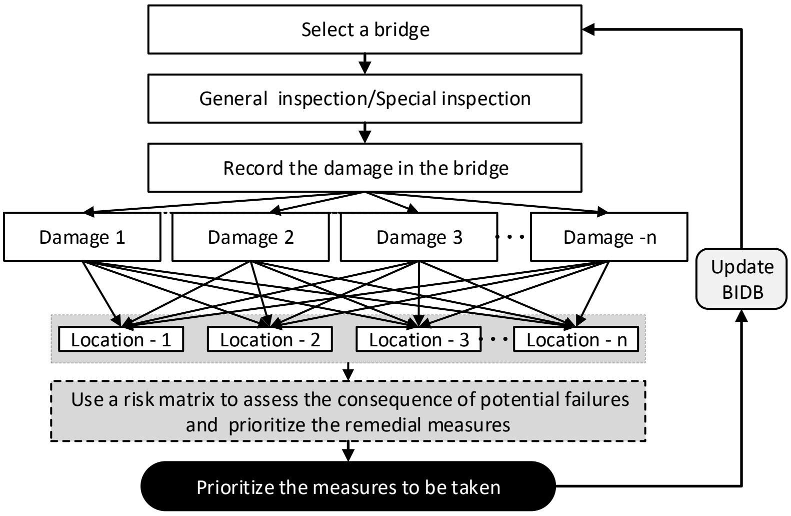

Figure 2: Suggested approach to RBI assessment and control at NPRA

Figure 3 illustrates the factors (i.e. time-dependent and -independent) that need to be taken when assessing the risk of potential failure on bridges. The PoF is assessed in relation to the bridge category, damage/defect/deterioration level, environment where it is located, and degree of inspectability.

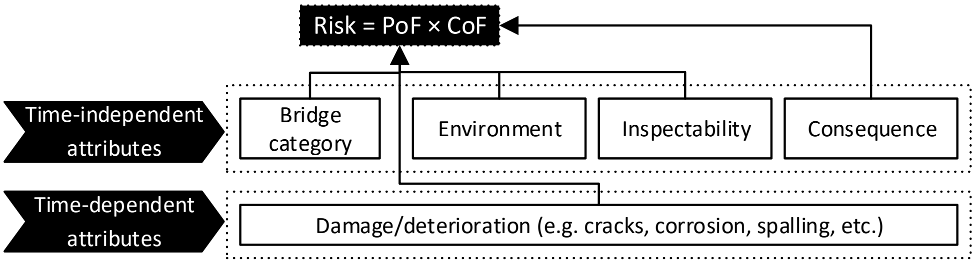

Figure 3: Assessment of the risk of potential failures on concrete bridges

The CoF is assessed in relation to: the potential loss of bearing capacity (B), due to damage/defect/deterioration level; the potential danger to road safety (RS); the potential increase in maintenance/repair (M/R) cost; and the nature of the environment and the aesthetic appearance (E/A) [e.g. the level of graffiti on the bridge structure, whether the bridge is located at the coast or inland, etc.].

4. ILLUSTRATIVE EXAMPLE

4.1 Risk matrix development

Table 5 illustrates the risk matrix (i.e. to evaluate the risk of potential failure due to cracks. It is worth noting that a similar risk matrix shall be developed for each of the other key damage mechanisms) that has been developed to evaluate the risk of potential failure due to cracks on concrete bridges. It has been developed as an extension to the currently used method. In order to illustrate the evaluation approach, the 'crack width' (CW) [i.e. chosen as a measure of PoF] and maintenance/repair (M/R) cost (C) has been chosen as the CoF. In this context, cost ranges have been used to designate the CoF levels. It is also possible to choose bearing capacity (B); road safety (RS); maintenance/repair (M/R); and/or environment and aesthetic appearance (E/A) as the CoF, depending on the case and circumstances.

Table 5: Risk matrix for crack consequence classification

		Consequence type	***CoF levels***			
Crack width		B	L	M	H	VH
		RS	L	M	H	VH
		M/R (Euro)	L (*C < 5K)	M (5K< C < 10K)	H (10K< C < 50K)	VH (C > 50K)
		E/A	L	M	H	VH
PoF levels	**CW in mm**	***Rank***	***1***	***2***	***3***	***4***
	CW < 0.3	***1***	L	L	M	H
	0.3 < CW < 1.0	***2***	L	M	M	H
	1.0 < CW <2.0	***3***	L	M	H	VH
	CW > 2.0	***4***	M	H	VH	VH

*C = Cost of M/R

Table 6 illustrates the risk level vs. the measures to be taken. The recommendations for the measures (i.e. to be taken) have been assigned at different risk levels, based on the NPRA guidelines [3].

Table 6: Risk vs. measures to be taken

Risk level	Recommendations	Rank
L	No action required	1
M	Register the recommended measures in BIDB	2
H	Register the measures in BIDB and inspection interval shall be recommended	3
VH	Immediate action is required	4

It is important to minimize the variability that may be caused during the RBI evaluations due to lack of overall knowledge, experience, etc. The variability especially occurs when the PoF and/or CoF value for a certain situation gets closer to the boundary of the corresponding ranges. In order to avoid such variability and to enable the recycling of the experts' knowledge, a Mamdani-type fuzzy inference system (FIS) has been used [8]. The FIS's parameters were selected as follows: 'and' method with 'minimum', 'or' method with 'maximum', 'implication' with 'minimum', 'aggregation' with 'maximum' and 'defuzzification' with 'centroid' algorithm. Fuzzy rules were developed by the table-look-up (refer Table 6) approach [8]. The toolbox simulator of the MATLAB (R2016a) toolbox was utilized to develop and execute the FIS [9].

4.2 Fuzzy set theory based RBI assessments

Triangular and trapezoidal fuzzy membership functions (MFs) have been selected in order to model the potential PoF and CoF ranges. Figure 4 provides an overview of the suggested FIS. Figures 5, 6 and 7 illustrate the MFs of PoF, CoF and risk, respectively.

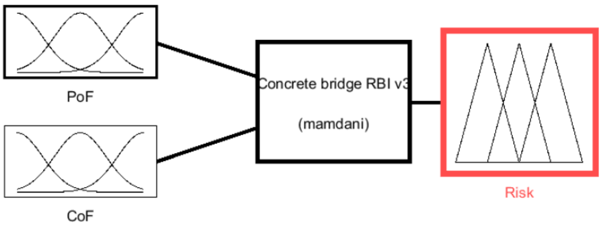

Figure 4: Overview of FIS

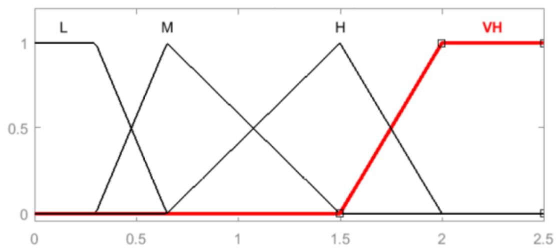

Figure 5: PoF MFs

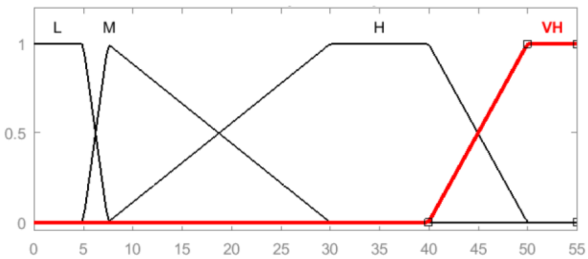

Figure 6: CoF MFs

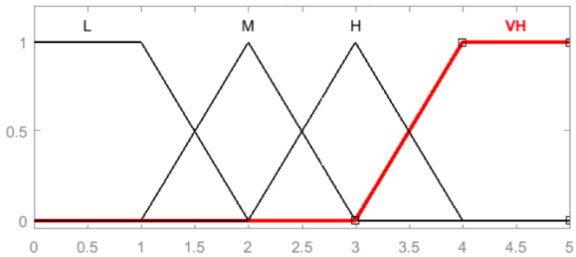

Figure 7: Risk MFs

Table 7 illustrates the rules that have been derived from the table-look-up method to evaluate the risk of potential failure.

Table 7: Rules for evaluating risk of potential failure

Rule no.	Description
1	If (PoF is L) and (CoF is L) then (Risk is L)
2	If (PoF is L) and (CoF is M) then (Risk is L)
3	If (PoF is L) and (CoF is H) then (Risk is M)
4	If (PoF is L) and (CoF is VH) then (Risk is H)
5	If (PoF is M) and (CoF is L) then (Risk is L)
6	If (PoF is M) and (CoF is M) then (Risk is M)
7	If (PoF is M) and (CoF is H) then (Risk is M)
8	If (PoF is M) and (CoF is VH) then (Risk is H)
9	If (PoF is H) and (CoF is L) then (Risk is L)
10	If (PoF is H) and (CoF is M) then (Risk is M)
11	If (PoF is H) and (CoF is H) then (Risk is H)
12	If (PoF is H) and (CoF is VH) then (Risk is VH)
13	If (PoF is VH) and (CoF is L) then (Risk is M)
14	If (PoF is VH) and (CoF is M) then (Risk is H)
15	If (PoF is VH) and (CoF is H) then (Risk is VH)
16	If (PoF is VH) and (CoF is VH) then (Risk is VH)

4.3 Analysis and results

Figure 8 illustrates the risk surface that is used in the developed FIS. Figure 9 demonstrates an FIS-based risk rank calculation (i.e. If CW = 1.9 mm and cost M/R = 40K Euro then risk rank = 3.98).

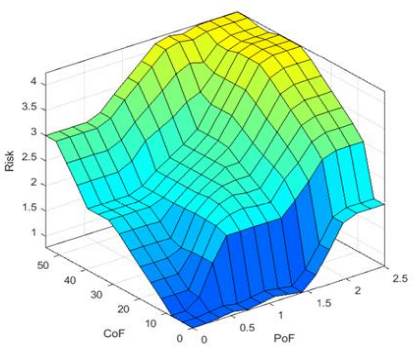

Figure 8: Risk surface

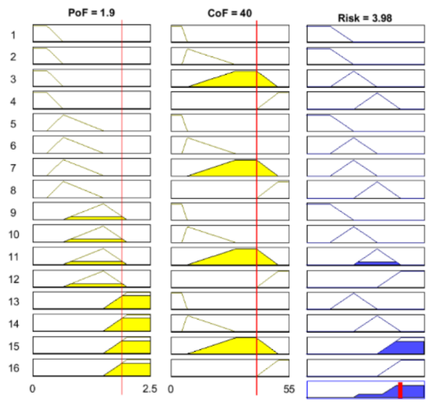

Figure 9: FIS-based risk rank calculation

Table 8 illustrates the results of the FIS-based risk level (refer Figure 5) investigation and the recommended measures to be taken by the NPRA technical authorities.

Table 8: FIS based risk level investigation and recommendations

Crack size/ (mm)	Estimated cost of M/R (Euro)	FIS calculated risk rank	Risk level (refer Figure 7)	Recommendations
0.4	6K	1.17	L	No action required
1.5	12K	2.24	M	Register in BIDB for future inspection planning
1.9	40K	3.98	VH	Immediate action is required

5. DISCUSSION AND CONCLUSIONS

This manuscript demonstrated the development of an RBI risk matrix and an approach for performing RBI assessments and recommendations for concrete bridges. The development has been aligned with NPRA requirements. An FIS has been developed to minimize the variability that can be caused during the RBI assessments and recommendations. The suggested approach also provides the possibility for the recycling of expert knowledge via developing MFs with the support of a group of technical experts on bridge inspection. Also, the FIS enables the ambiguity that can be caused when the values of PoF and CoF are closer to the lower or upper values of the respective ranges to be minimized. The suggested approach enables the bridge inspection process to be made lean, whilst increasing inspection performance. Future research shall be carried out to investigate the ranges of different damage mechanisms and the corresponding consequences.

ACKNOWLEDGEMENTS

This study has been carried out as part of the ILA-Lean project: Innovative Learning Approaches for Implementation of Lean Thinking to Enhance Office and Knowledge Work Productivity, project number 2016-1-PL01-KA203-026293. The project has been co-funded with support from the European Commission.

REFERENCES

[1] Samarakoon, S.M.S.M.K and Ratnayake, R.M.C., ‘In-service inspection of offshore concrete structures: Application of an expert system’, IEEE International Conference on Industrial, Engineering and Engineering Management, Bangkok, Thailand, 10-13 December 2013.

[2] Ratnayake, R.M.C. and Markeset, T., ‘Technical integrity management: measuring HSE awareness using AHP in selecting a maintenance strategy’, *JQME* **16** (1) (2010) 44-63.

[3] Ratnayake, R.M.C., ‘A decision model for executing plant strategy: Maintaining the technical integrity of petroleum flowlines’, *IDJRSM* **4** (1/2) (2012) 1-24.

[4] Ratnayake, R.M.C., ‘KBE development for criticality classification of mechanical equipment: A fuzzy expert system’, *Int. J. Disast. Risk Re.* **9** (2014) 84-98.

[5] Samarakoon, S.M.S.M.K and Ratnayake, R.M.C., ‘Risk-based in-service inspection framework for offshore concrete wind turbine structures and application of Fuzzy Inference System’, Proceedings of the ASME 2018 37th International Conference on Ocean, Offshore and Arctic Engineering (OMAE2018), June 17-22, 2018, Madrid, Spain.

[6] Atkins, ‘Risk Based Inspection for Highway Structures’ (Transport for London, 2011).

[7] Staten Vegvesen, ‘Håndbok V441 Inspeksjonshåndbok for bruer’ (Norway, 2014). https://www.vegvesen.no/fag/publikasjoner/handboker.

[8] Ratnayake, R.M.C., ‘Integrity assessment and control of offshore topside piping: An expert system based approach’, Proceedings of the ASME 2018 37th International Conference on Ocean, Offshore and Arctic Engineering (OMAE2018), June 17-22, 2018, Madrid, Spain. doi:10.1115/OMAE2018-78267.

[9] MATLAB. ‘R2016a: Fuzzy Logic Toolbox’ (The MathWorks, Inc., 2016).

SUSTIMS – SUSTAINABLE INFRASTRUCTURE MANAGEMENT SYSTEM

Álvaro A. Soares

Ascendi Inovação e Gestão de Infraestruturas, S.A., Information Systems Department, Antero de Quental Street, 381 - 3º floor - Building Ariane, 4455-586 Perafita, Matosinhos, Portugal

Abstract

In the present context of digital transformation there's a higher need for the adoption of new technologies that support the processes of an intelligent and sustained asset. The quantity and complexity of information that needs to be collected and treated requires the use of appropriate systems and tools that support operatives, supervisors and decision-makers activities. There's also the need to create a shared information and knowledge base, compatible with other internal and external systems, which could be used as a powerful tool. This knowledge base becomes a tool of great value and importance for an efficient and sustained asset management.

Keywords: SustIMS; Asset Management; Digital Transformation; Sustainability; System

1. INTRODUCTION

SustIMS, abbreviation for Sustainable Infrastructure Management System, is the result of a partnership project between Ascendi, Universidade do Minho and Universidade Nova of Lisboa, co-funded by QREN and developed between 2012 and 2015. The project's main goal was to develop an integrated system that enabled its users to effectively and sustainably manage road infrastructures.

Ascendi´s needs as a road asset concessionaire and manager were shared by many of its counterparts, as there was a lack in the market capable of providing tools that support the management of the main types of road infrastructures. This was the motivation factor for Ascendi and its project partners to start the SustIMS project: develop a platform that could become a reference solution for not only Ascendi but also other potentially interested infrastructure managers.

In mid-November 2015, the project was completed and approved by the Agency for Development and Innovation, thus beginning the implementation stage of the solution, comprising the essential components: inventory installation, configuration, and loading. In

November 2018, this stage was successfully completed and the system went into production, providing an integrated management of the following types of road infrastructures: Bridges, Pavements, Walls, Slopes and ITS Equipment.

The life cycle between project and finished product was filled with several challenges which questioned the skills of all the involved entities, compelling them to evolve and expand their own limits as implementers and asset managers. Despite all the breakthroughs, the challenges remain and the emergence of new technologies capable of enhancing the various types of operational processes, give rise to new evolving needs.

This long journey was also marked by the tool's worldwide recognition by the IRF - International Road Federation, in 2017, awarding it with the Global Road Achievement Awards (GRAA) in the Asset Preservation & Maintenance Management category, a 1st time distinction for a Portuguese project in this category.

2. THE SUSTIMS SOLUTION

SustIMS is an integrated system for the management of the main types of road infrastructures – Bridges, Pavements, Walls, Slopes and ITS Equipment, comprising a Management Platform, a Mobile Platform and Monitoring Systems.

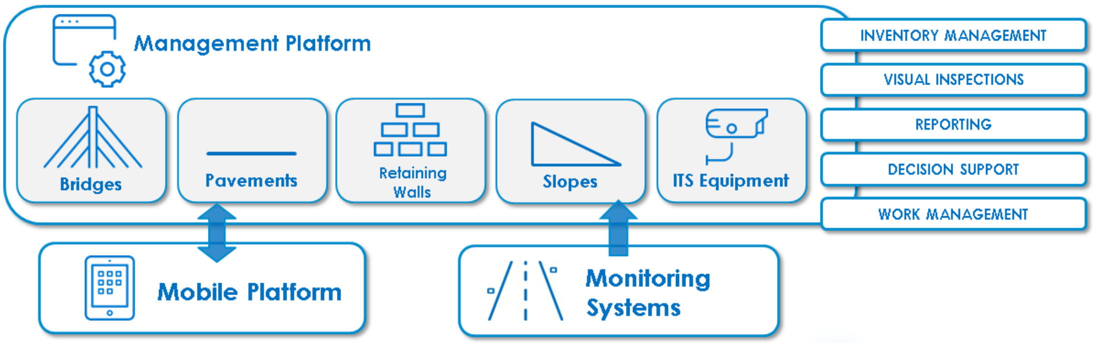

Figure1: System´s Functional Design

The system allows its users to carry out an efficient, modular and integrated management of their road assets through a wide set of tools and processes aimed at managing different types of infrastructures.

Despite sharing a common core, SustIMS allows different management methodologies, according to each module's technical and procedural characteristics, making SustIMS a customizable solution, allowing its users to adapt the most relevant aspects of their management through the configuration and adaptation of the system, to their more specific needs.

2.1. Platforms and main features

2.1.1. Management Platform

The management platform is the heart of the system, centralizing all logic and core business operations through a wide range of asset management processes in a simple and standardized way.

The system offers the same basic functionalities for all types of infrastructures: "Inventory Management", "Visual Inspection Management", "Reports", "Decision Support" and "Works Management". The SustIMS information structure has been implemented on a layer logic where filling the data of each layer is critical to advance to the next.

In a systematic and functional way, the asset information is being processed from the initial registration stage, through the assessment of its condition and finally proceeding to a predictive evaluation in order to find the best preventive and/or corrective solutions on each asset.

The management platform also ensures integration with other systems such as the mobile platform, auscultations, data instrumentation and alerts provided by the monitoring systems.

2.1.2. Mobile Platform

The mobile platform supports all field data collection processes such as visual inspections. It provides a set of functionalities that enable the management and execution of visual inspections assigned to each inspector. The mobile platform allows the following operations:

- Download/Upload of visual inspections;
- Infrastructures selection according to their location;
- Pathology or Check-list registration;
- Collection of evidence through different multimedia elements (photo, video or audio);
- Representative schematics of each infrastructure;
- Availability to access to reports of previous inspections;
- Geo-referenced information.

2.1.3. Monitoring Systems

Monitoring systems are based on sensors managed by a central platform and spread throughout the network for the control of critical points of the infrastructure in real time. Two sensor prototypes were developed to monitor two types of incident alert: collisions with safety rails and movement on slopes. With the placement of these sensors, it´s possible to receive real-time alerts ensuring greater agility in incident response and better consequence control/mitigation.

2.1.4. Reports

SustIMS offers its users a reporting platform to access custom reports. The platform provides access to all kinds of reports, from the inspection reports automatically available when its information is integrated, to reports designed to support the decision process such as "Risk Assessment Maps".

This Platform also enables users mass report creation and the possibility to export results in several formats, allowing an additional degree of data processing and customization.

						Evolução Estados Conservação																									
infraestrutura	Tipo	Última Inspeção (i)		Data Modelo (m)	Ano Risco	i	m+ 0	m+ 1	m+ 2	m+ 3	m+ 4	m+ 5	m+ 6	m+ 7	m+ 8	m+ 9	m+ 10	m+ 11	m+ 12	m+ 13	m+ 14	m+ 15	m+ 16	m+ 17	m+ 18	m+ 19	m+ 20	m+ 21	m+ 22	m+ 23	m+ 24
AGL.LSB-A16.000+000.PI.1.-1#-1.0	Passagem Superior	2018	Muito Bom	2019	2044	1	1	1	1	1	1	1	2	2	2	2	2	2	2	2	2	2	2	2	2	2	2	2	2	2	2
AGL.LSB-A16.000+000.PI.1.-1#1.0	Passagem Superior	2018	Muito Bom	2019	2041	1	1	1	1	1	1	1	2	2	2	2	2	2	2	2	2	2	2	2	2	2	2	2	3	3	3
AGL.LSB-A16.000+000.PI.1.0#0.0	Passagem Superior	2018	Muito Bom	2019	2041	1	1	1	1	1	1	2	2	2	2	2	2	2	2	2	2	2	2	2	2	2	2	2	3	3	3
AGL.LSB-A16.000+000.PP.1.1#1.-1	Passagem Peões	2018	Muito Bom	2019	2042	1	1	1	1	1	1	1	2	2	2	2	2	2	2	2	2	2	2	2	2	2	2	2	2	3	3
AGL.LSB-A16.000+000.PP.1.1#1.0	Passagem Peões	2018	Muito Bom	2019	2041	1	1	1	1	1	1	1	1	2	2	2	2	2	2	2	2	2	2	2	2	2	2	2	3	3	3
AGL.LSB-A16.000+291.PS.2.0#0.0	Passagem Superior	2018	Muito Bom	2019	2038	1	1	1	1	1	1	1	2	2	2	2	2	2	2	2	2	2	2	2	2	3	3	3	3	3	3
AGL.LSB-A16.000+800.PI.3.0#0.0	Passagem Inferior	2018	Muito Bom	2019	2042	1	1	1	1	1	1	1	2	2	2	2	2	2	2	2	2	2	2	2	2	2	2	2	2	3	3
AGL.LSB-A16.001+090.PI.4.0#0.0	Passagem Inferior	2018	Muito Bom	2019	2048	1	1	1	1	1	1	2	2	2	2	2	2	2	2	2	2	2	2	2	2	2	2	2	2	2	2
AGL.LSB-A16.001+662.PI.5.0#0.0	Passagem Inferior	2018	Muito Bom	2019	2047	1	1	1	1	1	1	2	2	2	2	2	2	2	2	2	2	2	2	2	2	2	2	2	2	2	2

infraestrutura	m+ 25	m+ 26	m+ 27	m+ 28	m+ 29	m+ 30	m+ 31	m+ 32	m+ 33	m+ 34	m+ 35	m+ 36	m+ 37	m+ 38	m+ 39	m+ 40	m+ 41	m+ 42	m+ 43	m+ 44	m+ 45	m+ 46	m+ 47	m+ 48	m+ 49
AGL.LSB-A16.000+000.PI.1.-1#-1.0	3	3	3	3	3	3	3	3	3	3	3	3	3	3	3	3	3	3	3	3	3	4	4	4	4
AGL.LSB-A16.000+000.PI.1.-1#1.0	3	3	3	3	3	3	3	3	3	3	3	3	3	3	3	3	3	3	3	3	3	4	4	4	4
AGL.LSB-A16.000+000.PI.1.0#0.0	3	3	3	3	3	3	3	3	3	3	3	3	3	3	3	3	3	3	3	3	3	3	3	4	4
AGL.LSB-A16.000+000.PP.1.1#1.-1	3	3	3	3	3	3	3	3	3	3	3	3	3	3	3	3	3	3	3	3	3	3	3	3	3
AGL.LSB-A16.000+000.PP.1.1#1.0	3	3	3	3	3	3	3	3	3	3	3	3	3	3	3	3	3	3	3	3	4	4	4	4	4
AGL.LSB-A16.000+291.PS.2.0#0.0	3	3	3	3	3	3	3	3	3	3	3	3	3	3	4	4	4	4	4	4	4	4	4	4	4
AGL.LSB-A16.000+800.PI.3.0#0.0	3	3	3	3	3	3	3	3	3	3	3	3	3	3	3	3	3	3	3	3	3	3	4	4	4
AGL.LSB-A16.001+090.PI.4.0#0.0	2	2	2	2	3	3	3	3	3	3	3	3	3	3	3	3	3	3	3	3	3	3	3	3	3
AGL.LSB-A16.001+662.PI.5.0#0.0	2	2	3	3	3	3	3	3	3	3	3	3	3	3	3	3	3	3	3	3	3	3	3	3	3

Figure 3: Risk Assessment Map Example

2.2. Management and Decision-Making Processes

2.2.1. Inventory Management

Inventory management is fundamental for the correct functioning of the entire system. The information of the road network and the inventory data of each infrastructure are vital to the execution of any process. The complexity of this process is directly related to the granularity and desired detail level. Although the system requires a basic structure for the execution of its processes, its level of detail may differ and can be the deciding factor for the complexity of the inventory management process. It is up to the manager of each module to define its basic structure according to its needs and objectives.

2.2.2. Quality Indicators

The assessment processes of each infrastructure's condition represent the beginning of its life cycle regarding maintenance and conservation. SustIMS provides several ways of assessing these conditions, the most common being the visual inspection process using the mobile platform, but there are still other ways of assessment, namely through the auscultation process applied in pavements and also data from the monitoring equipment of walls and slopes.

All of these processes are based on data collection in order to obtain the conservation and/or maintenance state. As soon as the data enters the system it starts an automatic calculation process based on two distinct types of data: the visual inspection data indicating the gross results collected on the field and the business rules (parameters) to be applied to each calculation. The following example demonstrates a standard infrastructure calculation:

Infrastructure

- Component type
  - Subcomponent
    - Pathologies or Verification (checklist)

These calculations are applied to the whole structure in a drill-up perspective based on predefined formulas (Maximum, Minimum, Average or Weighted Average) where each level has a condition of its own. By default, the upper levels results from the calculation of the previous and lower levels. It is also possible to apply custom formulas and logics.

Through this method the user obtains total control over the processes and calculation formulas, ensuring not only a better fit of the tool but also its transparency and uniformity in the entire calculation process. Another important factor is a total reduction of subjectivity in the inspection process since the technicians at no time define state values. Instead they fill the forms with the data collected and afterwards, the system integration will recursively calculate the state of the entire infrastructure. This methodology applies mainly to the calculation of the conservation and/or maintenance of infrastructures organized by levels of components such as Bridges, Walls, Slopes and ITS Equipment's, implementing the good practices respecting our Quality Control Plan.

Table 2. Conservation/Maintenance States

Conservation States	Maintenance States
1 – Very Good 2 – Good 3 – Medium 4 – Bad 5 – Very Bad	1 – Very Good 2 – Good 3 – Medium

SustIMS also provides a pavement condition assessment based on "Performance Indicators", according to the methodology COST 354 (2008). These indicators are calculated from the data gathered in visual inspections and auscultations. SustIMS presents a fully custom platform for the creation and calculation of indicators based on multiple types of data collected on the field. The system includes the following indicators:

Table 3. Pavement Condition Status Indicators

Indicator	**Origin**	**Detail**	**GPI**
PI_E - Longitudinal Evenness	Auscultations	IRI	X
PI_R – Rutting	Auscultations	RD	X
PI_CR - Cracking	Visual Inspections	Cracking Pathologies	X
PI_F – Friction	Auscultations	LFC	X
PI_B - Bearing Capacity	Auscultations	FDW	X
PI_SD - Surface Defects	Visual Inspections	Surface Defects Pathologies	
PI_T - Macro-Texture	Auscultations	MPD	

In addition, the system provides the overall Pavement calculation (GPI – Global Performance Indicator) by combining the indicators referenced in Table 3.

2.2.3. Decision Support Module

SustIMS decision support system features the predictive ability, achieved through the application of degradation and optimization models, based on Markov Chains featured by the calculation of the probability of a certain component reaching a certain quality index at a future point, through the use of a transition matrix applied on an initial quality index. These curves represent the natural degradation of the infrastructures and their components, when they aren't subject to any maintenance/conservation actions. The transition matrixes were developed through the progressive method, based on the historical conservation/maintenance data, therefore it was imperative to have at least two consecutive observations of the same object at different times.

Through the application of these predictive models, SustIMS delivers a long-term view of the state of the infrastructures having as sole requirement the information of the current state of the infrastructure(s).

An additional level of decision support offered by SustIMS is the automatic suggestion of maintenance/conservation strategies that guarantee pre-defined levels of quality indexes. Based on the application of the degradation models, which are responsible for predicting the degradation of the infrastructures, the system can signal when a determined level of restriction is going to be reached. When this occurs, the system points the need for an action that can improve the quality index so that it continues to respect the initially defined restriction. It is a multi-objective recursive process where all the variants between performance and cost are tested, so that at the end, a set of intervention scenarios is suggested according to the imposed constraints.

Data quality is decisive in the application of these models, and the data that most affect these calculations is the actions/works data, more specifically their effects and associated costs. For an action/work to be valid, it must quantify an improvement after its application as well as a cost that can be fixed or variable, depending on the technical characteristics of the component to which it applies namely: extension, area, quantity or other reference dimension.

All of these parameters are available for customization, but the challenge lies on their calibration. A complex and sensible trial-error process takes place with the constant cross analyses between the suggested data and the real data obtained by the operation.

3. FROM VISION TO DEPLOYMENT

In the last two years (2017 and 2018) SustIMS has been Ascendi´s elected platform used for the management of its road assets in detriment of other old systems. The introduction of a system of this nature that is totally dependent on the quality of its information, it becomes fundamental to raise user's awareness to the importance of managing a new kind of asset as important as the assets managed by the system (infrastructures) which is the "Information Asset". In this sense, new challenges arise to ensure consistency and accuracy of data. Alarm-based processes and online recording have been implemented in order to help users resolve inconsistencies and filling in missing data. The online inventory functionality is critical to address data gaps, nobody better than the person on the field to detect potential deviations in the information, reacting immediately towards its correction.

Table 4. Indicators

Indicator	**Value**
Concessions under operation	5 concessions + 2 sub concessions
Infrastructures	> **15.000** registered
Visual Inspections	> **3.200** inspections carried out
Multimedia Records	> **48.000** evidence gathered
Training	> **50** trained users
Equipment	> **20** mobile platforms
Service Providers	> **10** different entities

Two years of massive use of the system, reveal some indicators of the quantity and potential growth of the information.

A system's success is far beyond its figures, a fundamental aspect is the acceptance by its users and the real benefits recognized from its use. The feedback from users has been widely positive, but when it is not, this information usually arrives in the form of improvement suggestion, largely coming from service providers, since these users are the ones that deal with the most operational aspects of the system. In its conception the system meant to achieve a set of operational and corporate advantages, some of them obvious but still, necessary to materialize and prove. The following benefits were identified from our experience and user´s feedback.

Table 5. Benefits

Benefit	Arguments
Administrative Overhead Reduction	Probably the greatest and most perceptible benefit of all. The introduction of digital platforms to support operational processes facilitates data acquisition and reduces manual registration which normally implies a greater error probability.
Quality of Information	The introduction of automated and systematized processes supported in technology minimizes the subjectivity of the visual inspection.
Reduced subjectivity in data collection	
Decrease of Paper Consumption	The use of the mobile platform promotes in a direct way, the suppression of the need for the use paper.
Maximize Planning & Execution	These less tangible benefits are the ones that add real value to the solution. The use of an integrated platform with a whole set of optimized tools and processes, grants above all, global and integrated evidence-based management.
Minimize Risk	
Support the Decision Making Process	

4. FUTURE

With the solution fully operational it is fundamental that it continues to meet the needs of its users and at the same time follow the trends and new immersive technologies. Ascendi as the implementing entity is committed to ensure these two realities, therefore two strategic lines of evolution for the system were defined, one dedicated to the functional evolution, focused on increasing its scope through the development of new modules and another, oriented for innovation, through the introduction of innovative technologies.

4.1. New Modules

The functional scope of SustIMS will be widened in the short term from five to eight functional modules, with the development of the Vertical Signs, Culverts and Road Markings modules respectively in this order. The introduction of these new modules will allow Ascendi to expand its current range of infrastructures managed by SustIMS, and to progressively make way towards a fully integrated management on a single platform.

4.2 New Technologies

Ascendi started a new project which aims to redesign and improve the pavements visual inspection process, introducing video-verification and Artificial Intelligence (AI) in the collection and data processing. This project intends to develop a technological architecture capable of collecting videos/frames of the pavement through equipment's coupled to the vehicles to be treated by algorithms of AI in an attempt to automatically register pathologies. It is an interactive process where human supervision will always be necessary to continuously "teach" the system namely confirming automatically detected pathologies, registering undetected pathologies and identifying false positives.

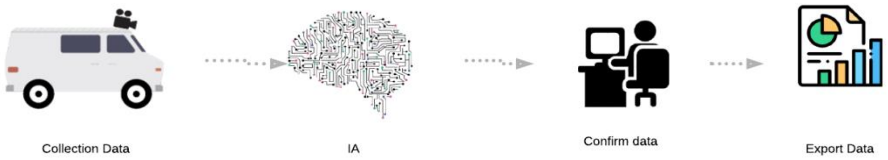

Figure 5: Continuous Learning Process

We aim for 3 levels of improvement: Safety, Quality of Information and Performance:

Viewpoint	Advantages
Safety	Pathology monitoring is currently performed from the interior of the vehicle, traveling at the outer edge at idle. Pathology monitoring would be done by the vehicle passing through the main lanes (Right, Left and Centre lanes) at normal speed.
Quality of Information	The current process of collecting evidences doesn't facilitate the recognition of less evident pathologies. The photographic records would be obtained in 90 degrees rather than in perspective at distances from 3 to 7m.
Performance	The process would be simpler, faster and can even be carried out by patrols, thus freeing inspection technicians for other activities The introduction of artificial intelligence can bring significant gains in the automatic detection of pathologies.

5. CONCLUSION

Asset management is founded on the organization of a series of processes, procedures and operations that involve the conservation and maintenance, focusing on the achievement of a set of pre-established results and objectives.

Managing road infrastructures is a complex process and the complexity increases in proportion to assets characteristics and quantity, thus making it fundamental to adopt facilitating systems that can provide an integrated and sustainable management.

SustIMS arises and grows as a solution capable of responding to the more general management needs, applicable to different types of road infrastructures, being also prepared to adapt to more specific needs of any company and always in line with new trends and immersive technologies.

APPLICATION OF NON-DESTRUCTIVE TESTING IN ASSESSMENT AND SERVICE LIFE PREDICTION OF CONCRETE BRIDGES

Marija Kušter Marić, Ana Mandić Ivanković, Anđelko Vlašić, Jelena Bleiziffer, Mladen Srbić and Dominik Skokandić

Faculty of Civil Engineering, University of Zagreb, Croatia

Abstract

Existing bridge maintenance policy, where bridge assessment is based on results of visual inspection is not sufficient since reinforcement corrosion, as the main degradation process of concrete bridges, cannot be timely detected. Hence, new approach, where visual inspection is combined with simple, rapid and cost-effective non-destructive testing (NDT) is presented and demonstrated on the case study: Adriatic Bridge across Sava River in Zagreb.

NDT on the bridges includes crack detection, determination of geometry and crack cause identification, estimation of strength and dynamic elastic modulus of concrete, rebar detection, measurements of rebar diameter, concrete cover, electrical resistivity of concrete and half-cell potential.

Application of NDT increases the objectivity of the visual inspection results and allows detection of invisible defects, what was confirmed by additional destructive testing on the case study. Utilization of results obtained by visual inspection and NDTs in numerical models for service life prediction of structure is discussed, highlighting the importance of inclusion of performance indicators variation due to non-uniformity of concrete quality (local cracks, damage).

Keywords: bridge, corrosion, crack, non-destructive testing

1. INTRODUCTION

Most road bridges are made of concrete. Although they are designed for 100 years of service, most of them show significant damages already after 20-30 years. The major cause of deterioration and service life reduction of reinforced concrete bridges is chloride-induced corrosion of steel reinforcement in concrete due to exposure to sea and/or de-icing salts.

Visual inspection is the most commonly used method to assess bridges and to make decision on non-regular maintenance such as repair, strengthening and reconstruction. Investigation works including destructive and non-destructive testing used to be conducted once the decision on bridge intervention is made based on the results of visual inspection, in order to define required scope of the repair design project. Accuracy of visual inspection depends a lot on the skills of the individual inspector and spent time [1,2]. Time intervals between main inspections used to be longer than prescribed 6 years and carried out on an “as-needed” basis [3]. Many road authorities do not have uniform and standardized inspection protocol in order to assure objectivity of condition assessment. Furthermore, deficient comparison of condition assessment between current and previous results disables reliable estimation of current and future degradation rate of structure or its element, crucial for cost-effective management.

On the other side, reinforcement corrosion in concrete, as the main cause of concrete bridge deterioration, cannot be timely detected by visual inspection. During the initiation phase of reinforcement corrosion, there are no visible damages on concrete surface, while at the beginning of the propagation phase damage are hardly detected. Only damages in advanced stage of reinforcement corrosion, manifested in the form of cracking and spalling of concrete cover, can be detected during visual inspection. Hence, new approach of pro-active maintenance of concrete bridges is proposed including visual inspection complemented with the non-destructive testing (NDT) and application of numerical model for service life prediction [4–6] and demonstrate on a case study.

2. CASE STUDY: ADRIATIC BRIDGE ACROSS SAVA RIVER IN ZAGREB

Adriatic bridge across Sava River in Zagreb was built in 1981 and was the first contemporary prestressed concrete bridge in the Croatian capital. It comprises: main bridge (central dilatation) with seven spans and north and south approach viaducts with one and four spans, respectively. Most of the superstructure comprises 39 m long prefabricated girders, a concrete deck and cross girders. The largest span above the river was achieved by utilizing 12 m pier cantilevers comprising box cross sections. Together with the aforementioned prestressed girders placed in between these cantilevers, a 63 m span was erected [7]. During the last visual inspection in 2017, investigative works were done to determine carbonatization depth according to the code HRN EN 1542, chloride content in concrete using rapid chloride penetration test, tensile and compressive strength according to the HRN EN 1542 and HRN EN 12504-1, respectively [8]. Inspection determined that the damage to structural parts of the bridge are of such a scope that the bearing capacity of the bridge is reduced. The damage is as follows: sidewalks cantilevers are supposed to concrete delamination due to reinforcement corrosion, asphalt cracking, curb damage, railing corrosion, cornice delamination and cracking, expansion joints blockage, main girders severe reinforcement corrosion and concrete cracking, drainage clogging, columns and

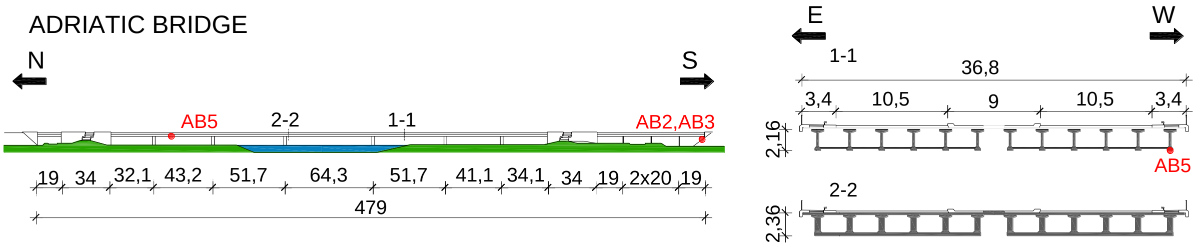

Figure 1: Adriatic Bridge layout with specified measuring locations

abutments with advanced reinforcement corrosion, bearings corrosion and misalignment, cracking of concrete bearing pedestals. Box girders of the main central part of the bridge over Sava River are heavily damaged due to reinforcement corrosion, with large parts of the concrete protective layer missing and reinforcement area significantly reduced. Drainage leakage inside box girders is recorded with fills of mud and water. South abutment is severally damaged from water leakage and reinforcement corrosion, with bearings damage. Extensive rehabilitation is in plan in near future.

3. NON-DESTRUCTIVE TESTING (NDT)

3.1 Chosen NDT methods

The non-destructive testing methods, used to evaluate bridge performance indicators (PIs) associated with structure load-bearing capacity and reinforcement corrosion, are selected based on the following favourable characteristics (Table 3):

- Simple for use, fast to perform and cost-effective testing;
- Complemented by visual inspection to assure more reliable bridge assessment
- NDT device availability among inspectors
- Measured PIs are included in the 3D CHTM model for service life prediction.

Preparation for bridge testing starts by obtaining and reviewing the documentation on design and maintenance available for the Adriatic bridge. During preliminary visual inspection locations for testing are defined (Figure 1). Measuring locations are distributed among the bridge portions that can be accessed without special platforms, but in such a manner to include different structural members i.e. abutments and girders.

Table 1: Applied NDT methods and measured performance indicators (PIs)

NDT methods and techniques	PI	Impact on structure load – bearing capacity	Impact on reinforcement corrosion
Schmidt hammer	Compressive strength	●	
Ultrasonic pulse velocity (UPV)	Modulus of elasticity	●	
	Crack depth	●	●
Optical microscope	Crack width	●	●
Cover meter	Position and alignment of reinforcement	●	●
	Rebar diameter	●	●
	Concrete cover thickness	●	●
Wenner probe	Electrical resistivity of concrete		●
Voltmeter	Half-cell potential		●

NDT starts with cleaning of concrete surface and identification of position and alignment of reinforcement, then concrete cover and rebar diameter are measured. Crack width is measured by ruler (crack width rod) and optical microscope, while crack depth and dynamic elastic modulus is estimated by ultrasonic pulse velocity device. Crack pattern and concrete cover delamination for the location with significantly damaged concrete due to reinforcement corrosion is recorded based on visual inspection and by sounding it (tapping it) with a hammer. Schmidt hammer is used to assess the uniformity of concrete strength, discover potential location of lower quality and determine concrete compressive strength. At the end of testing, half-cell potential and concrete resistivity are measured after wetting of the concrete surface.

3.2 Results and discussion

Summarized results of provided testing on the Adriatic Bridge are presented in Table 2. Surface plots of measured half-cell potential and electrical resistivity on the south U4 abutment wall (AB2) are shown in Figure 2. Correlation between half-cell potential and electrical resistivity is shown for all provided measurements in Figure 3. Each measuring location includes at least one crack, mainly or partially caused or progressed by reinforcement corrosion.

Table 2: Summarized results of provided NDT measurements on Adriatic Bridge

Measuring location		AB2				AB3				AB5			
Structural element		Abutment U4 - wall				Abutment U4 - wing				Girder N6-bottom			
Values		min	max	mean	St. dev	min	max	mean	St. dev	min	max	mean	St. dev
Transverse/ vertical reinforcement	Concrete cover [mm]	34	56	43.21	6.12	32	47	40.75	6.34	0-5 (absence or delamination of concrete cover)			
	Diameter [mm]	18	27	23.75		11	17	13.5		12			
Longitudinal/ horizontal reinforcement	Concrete cover [mm]	52	52	52		Location only				33	40	36.4	2.7
	Diameter [mm]	28	28	28		Location only				18	23	21	
Half-cell potential	[mV]	-434	-126	-291.51	71.9	-390	-73	-250.17	87	-215	-50	-85.64	30.88
El. resitivity	[kΩcm]	6.3	39.1	16.54	6.33	20.3	44.4	30.91	6.58	16.1	388	132.3	117.36
Compressive strength [MPa]	Schmidt hammer test	Q	Q st. dev.	fck (Schmidt Hammer)		Q	Q st. dev.	fck (Schmidt Hammer)		Q	Q st. dev.	fck (Schmidt Hammer)	
		39.2-65.1	3-9.7	18-63		57-58.5	4.3-5.4	44-46		70.7	1.6	82.5	
Crack	Width [mm]	1.2				0.5 - 1.05				0.078			
	Depth [mm]	52 (cc)				30 ; 118				131			
	Length [mm]	1000				750				300 (flange width)			

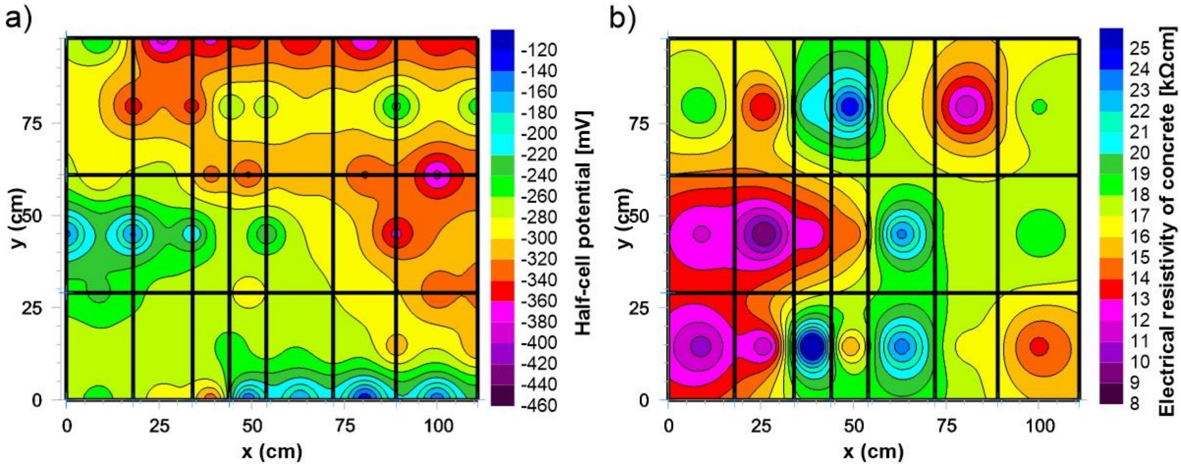

Figure 2: Surface plot of measured a) half-cell potential and b) electrical resistivity for U4 abutment wall of the Adriatic Bridge (AB2)

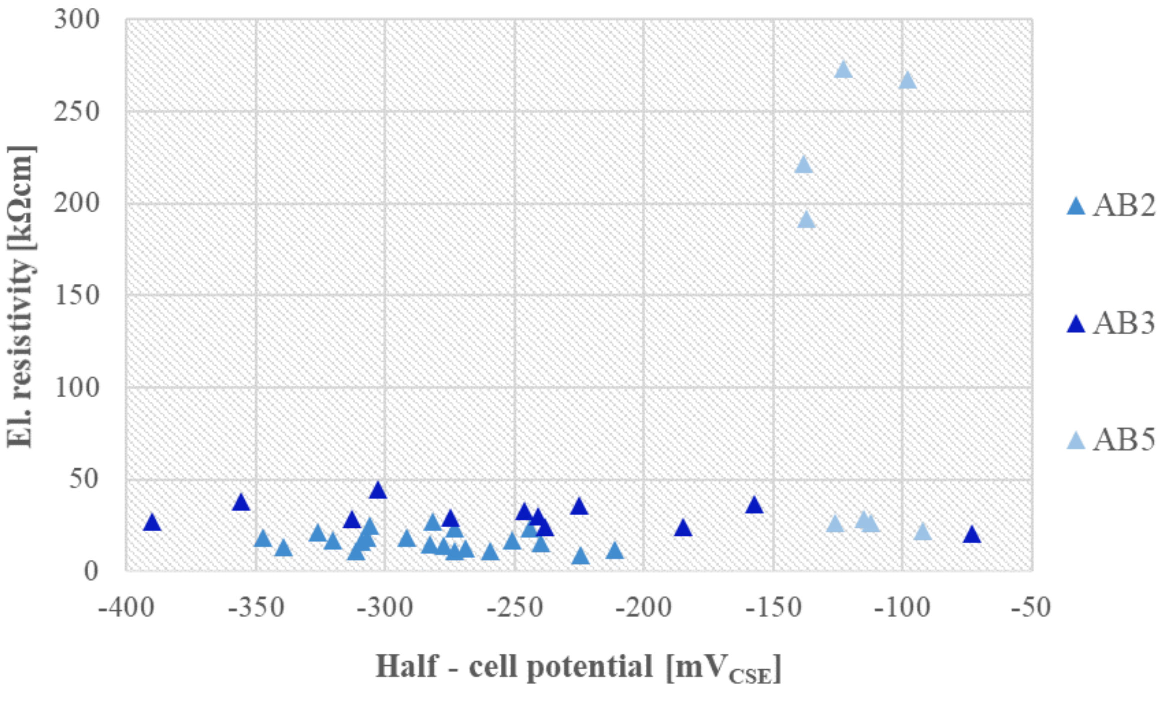

Figure 3: Correlation between measured half-cell potential and electrical resistivity for all measuring location

The measured values of electrical resistivity and half-cell potential show moderate risk of corrosion on all three location among which the south abutment wall (AB2) is most vulnerable, with the lowest electrical resistivity and half-cell potential and the highest half-cell potential gradients. On this location determined chloride content in concrete at the reinforcement level (depth of 4 mm) is above threshold value of 0.05% of concrete mass [8]. Moreover, concrete has non-uniform quality containing wide and deep cracks. The lowest measured tensile strength is 1.6 MPa. The cause of the abutment wall decay is with de-icing salts contaminated water leakage through the deteriorated expansion joints.

The wing of the south abutment (AB3) is less exposed to de-icing salts but executed concrete cover does not exist or it is very thin and delaminated (0-5 mm) enabling faster penetration of aggressive substances and depassivation of reinforcement corrosion.

Typical pitting corrosion is detected on the bottom of the girder (AB5), where the measured electrical resistivity is very low in cracked region with reinforcement corrosion, while the resistivity of sound (un-cracked) concrete 80 cm away is more than 20 times higher.

4. APPLICATION OF NDT RESULTS IN STRUCTURE SERVICE LIFE PREDICTION

Visual inspection combined by non-destructive testing provides current bridge condition assessment. However, to achieve sustainable bridge management system with effective and efficient bridge maintenance, it is necessary to predict future degradation processes on the structure. For this purpose, numerical models have been developed and subsequently improved in last three decades.

Recently developed 3D chemo-hygro-thermo mechanical (CHTM) model is one of the most comprehensive models for realistic simulation of transport and corrosion processes before and after depassivation of reinforcement bar in concrete considering damage and cracks in concrete caused by mechanical loads and reinforcement corrosion [9–14]. The 3D CHTM model has proved its ability for realistic simulation of mechanical and corrosion processes on several case studies [15]. However, quantifying the material, mechanical and corrosion related parameters and their interactions are still challenging tasks and main objective of the current research project.

To assure more realistic simulation of degradation processes in future, more comprehensive and accurate input data for a numerical model is required, which can be obtained by visual inspection and NDT, e.g. concrete cover thickness, rebar alignment, crack position and geometry, electrical resistivity[16].

One of the most important PI related to reinforcement corrosion is concrete cover with sufficient quality and thickness. Executed concrete cover used to be lower than designed value.

Damage and cracks in concrete caused during construction and/or service life significantly accelerate reinforcement corrosion. Namely, crack with width from 0.2 to 0.4 mm can increase chloride diffusivity from 10 to 10^3 times comparing to un-cracked concrete of the same quality.

Another time-varying PI important for durability is electrical resistivity of concrete, inversely proportional to corrosion rate - current density. Electrical resistivity depends on many parameters, e.g. porosity, water to cement ratio, aggregate, concrete curing, water and ions content in concrete, etc [17,18]. Although several researches have been focused on determining influence of various parameters on electrical resistivity, development of numerical models of resistivity as a function of the most influencing parameters is still challenging tasks. On the other side, electrical resistivity measurement technique is becoming popular non-destructive method in last two decades, due to its simplicity, rapidness, and cost during test conduction. Hence, measured electrical resistivity presents an important input parameter for service life prediction of concrete structure.

Although measured half-cell potential cannot be directly compared with calculated values of electric potential in numerical model, great gradients and very negative potential values measured on real structures, provide useful information for anode and cathode configuration in model, whose surface and position should be assumed in advance due to computation issue.

5. CONCLUSION

Existing bridge maintenance policy, where bridge assessment is based on results of visual inspection is not sufficient since reinforcement corrosion, as the main degradation process of concrete bridges, cannot be timely detected. On the other site, comprehensive and continuous structural health monitoring including installation of large number of different type of sensors, due high cost, is feasible only for megastructures and the most important structures. Hence, new approach, where visual inspection is combined with simple, rapid and cost-effective non-destructive technique (NDT) is presented and demonstrated on the case study: Adriatic Bridge across Sava River in Zagreb.

Although, each NDT has limitations in terms of measurement accuracy, use of NDT increases the objectivity of visual inspection results and allows detection of invisible defects, what was confirmed by additional destructive testing on the case study.

Moreover, the speed of structure degradation can be determined by comparing the periodic results. Results obtained by visual inspection and NDTs presents valuable input data for numerical model for service life prediction of structure, especially to include performance indicators variation due to non-uniformity of concrete quality (local cracks, damage), as it was shown for variation example of electrical resistivity which is more than 20 times lower in cracked concrete compared to the uncracked concrete of the same quality.

ACKNOWLEDGEMENTS

This research was carried out in the framework of the UKF project 04/17 "Influence of concrete damage on reinforcement corrosion - computer simulation and in-service performance of bridges (CODEbridges)" [19] supported by Unity through Knowledge Fund.

REFERENCES

[1] Graybeal, B. A., Phares, B. M., Rolander, D. D., Moore, M. Washer, G. Visual Inspection of Highway Bridges. J Nondestruct Eval. (2002) 67–83.

[2] Tenžera, D., Puž, G., Radić, J. Visual Inspection in Evaluation of Bridge Condition. Gradevinar. (2012) 717–26.

[3] Klanker, G., Stipanović Oslaković, I., Škarić Palić, S. The Impact of Different Maintenance Policies on Ownerscosts: Case Studies from Croatia and the Netherlands. In: Mandić Ivanković, A., Matos, J., Thöns, S., Høj ,N.P., editor. Proceedings of Joint COST TU1402 – COST TU1406 – IABSE WC1 Workshop: The value of SHM for the reliable Bridge Management (2017)

[4] Kušter Marić, M., Ožbolt, J., Mandić Ivanković, A., Bleiziffer, J., Srbić, M., Skokandić, D., et al. Quality specification for concrete bridges vulnerable to reinforcement corrosion. In: Matos, Jose ; Casas, Joan ; Bien, Jan ; Kaminski ,T., editor. eBook of the 3rd Workshop Meeting Cost Action TU1406. Wroclaw (2018) 1–8.

[5] Kušter Marić, M., Bleiziffer, J., Vlašić, A., Ožbolt, J., Mandić Ivanković, A., Srbić, M., et al. In-service performance of road concrete bridges – set up of case studies for novel pro-active maintenance methodology. In: Lakušić, S., editor. Proceedings of the 5th International Conference on Road and Rail Infrastructures - CETRA 2018. Zagreb: Department of

Transportation Faculty of Civil Engineering; (2018) 139–45.

[6] Kušter Marić, M., Bleiziffer, J., Vlašić, A., Ožbolt, J., Mandić Ivanković, A., Srbić, M., Skokandić, D. Assessment of reinforcement corrosion and concrete damages using non-destructive testing on bridges, J Croat Assoc Civ Eng., submitted to peer-review.

[7] Radić, J., Vlašić, A., Puž, G., Kolić, D. Zagreb Bridges. In: Radić, J., editor. Proceedings of Gold Parliament of CSSE. 2003. p. 117–35.

[8] Main six-year inspection report of Adriatic Bridge, Geoexpert-I.G.M. d.o.o., Zagreb (2017) (in Croatian)

[9] Ožbolt, J., Balabanić, G., Periškić, G., Kušter, M. Modelling the Effect of Damage on Transport Processes in Concrete. Constr Build Mater. 2010;1638–48.

[10] Ožbolt, J., Balabanić, G., Kušter, M. 3D Numerical Modelling of Steel Corrosion in Concrete Structures. Corros Sci. 2011;4166–77.

[11] Ožbolt, J., Oršanić, F., Balabanić, G., Kušter, M. Modeling Damage in Concrete Caused by Corrosion of Reinforcement: Coupled 3D FE Model. Int J Fract. 2012;233–44.

[12] Ožbolt, J., Oršanić, F., Balabanić, G. Modeling Influence of Hysteretic Moisture Behavior on Distribution of Chlorides in Concrete. Cem Concr Compos. 2016;73–84.

[13] Ožbolt, J., Oršanic, F., Balabanic, G. Modeling Corrosion-Induced Damage of Reinforced Concrete Elements with Multiple-Arranged Reinforcement Bars. Mater Corros. 2016;542–52.

[14] Ožbolt, J., Balabanić, G., Sola, E. Determination of Critical Anodic and Cathodic Areas in Corrosion Processes of Steel Reinforcement in Concrete. Mater Corros. 2017;622–31.

[15] Kušter Marić, M., Ožbolt, J., Balabanić, G., Mandić Ivanković, A. & Zarić, D. Service life prediction of concrete structures in maritime environment – case study: Maslenica Motorway Bridge. In I. Banjad Pečur, A. Baričević, N. Štirmer & D. Bjegović (eds) Proceedings of the 1st International Conference on Construction Materials for Sustainable Future (CoMS_2017), (2017) 629-636. Zagreb: Faculty of Civil Engineering, University of Zagreb.

[16] Wang, H.L., Dai, J.G., Sun, X.Y., Zhang, X.L. Characteristics of Concrete Cracks and Their Influence on Chloride Penetration. Vol. 107, Construction and Building Materials (2016) (107) 216–225

[17] Sanchez, J., Andrade, C., Torres, J., Rebolledo, N., Fullea, J. Determination of Reinforced Concrete Durability with On-Site Resistivity Measurements. Mater Struct Constr. (2017) 1–9.

[18] Azarsa, P., Gupta, R. Electrical Resistivity of Concrete for Durability Evaluation: A Review. Adv Mater Sci Eng. (2017)

[19] Influence of concrete damage on reinforcement corrosion - computer simulation and in service performance of bridges (CODEbridges), www.grad.unizg.hr/codebridges , 01.10.2018

International Conference on Sustainable Materials, Systems and Structures (SMSS 2019)
Challenges in Design and Management of Structures
20-22 March 2019 – Rovinj, Croatia

MAPPING OF RUNWAY PAVEMENT LAYERS THICKNESS BY GPR

Josipa Domitrović, Tatjana Rukavina, Šime Bezina and Ivica Stančerić

Faculty of Civil Engineering, University of Zagreb, Croatia

Abstract

In the era of rehabilitation projects non-destructive test methods are becoming irreplaceable tool for pavement condition assessment and selection of reconstruction strategies. This is especially important for airports where there is no room for ″surprises″ and every step of the reconstruction project has to be carefully planned in respect to time and technology. Since, layers thickness of existing pavement is an important factor in choosing rehabilitation technique all variations in layers thickness need to be located. The only tool one can use to gain insight into thickness variations, without disturbing pavement integrity, is Ground Penetrating Radar (GPR).

The paper presents experiences in determination of runway pavement layers thickness by GPR at Split Airport. Measurements were carried out on 15 m wide and 750 m long runway section. The results of measurement and conducted analyses were used in mapping pavement layers thicknesses. Obtained maps together with pavement material properties represented the baseline for the design of rehabilitation project. From the presented it can be concluded that employing GPR at project level as complement to traditional investigation methods is technically and economically sound program.

Keywords: pavement rehabilitation; non-destructive method; layer thickness; Ground Penetrating Radar

1. INTRODUCTION

Prior to any pavement rehabilitation work, it is recommendable to perform a structural evaluation in order to select the type of rehabilitation (structural rehabilitation, inlay or overlay) [1]. One of the key parameters in pavement structural evaluation is information on pavement layers thickness. Pavement layers thickness can be obtained from historical data, coring, trial pits or Ground Penetrating Radar (GPR), and each of these methods has its own advantages and disadvantages [2]. The problem with historical data is that is not always available or accurate especially in the case of old pavements. Coring and trial pits give accurate data on layers thickness but are destructive and affect the strength and durability properties of pavement. Furthermore, a core only brings local information about the layers thickness, so the variations between the cores locations can go unnoticed [1, 3]. Since layer thickness may be quite variable along a pavement structure continuous information on thickness is desirable. A continuous measurement of the layer thicknesses can be obtained non-destructively with application of GPR.

The use of GPR for pavement thickness evaluation is based on the measurement of the travel time and reflection amplitude of an electromagnetic pulse transmitted through a pavement and then partly reflected from electrical interfaces within the structure [4]. GPR is excellent tool in locating changes in pavement structure and hence defining homogenous pavement sections and can serve as a basis for planning structural tests.

The paper presents case study on mapping the runway pavement layers thickness (depth) on Split Airport by GPR. GPR data interpretation was done only on the bases of surface reflection method. Verification of method accuracy was done by comparing GPR results with thickness measured on cores.

2. GPR METHOD

High-frequency air-coupled antennas are typically used for concrete and flexible pavement inspection, e.g. determination of layers thickness and locating embedded reinforcement [5]. In this section short overview of air-coupled antennas basic operational principles, equipment used in presented study as well as data processing and interpretation are described.

2.1 GPR basics

Air-coupled antenna systems are pulse radar systems with frequency range from 500 MHz to 2.5 GHz and typical penetration depth between 0.5 and 0.9 m [6]. GPR antennas are bistatic with transmitter and receiver electronics installed in the same box. Transmitter emits pulses of electromagnetic waves into pavement. When GPR signal encounters the boundary between two materials part of the energy reflects to receiver and rest of the energy is transmitted across the boundary (Figure 1). Reflected signal is registered as amplitude and polarity versus two-way travel time.

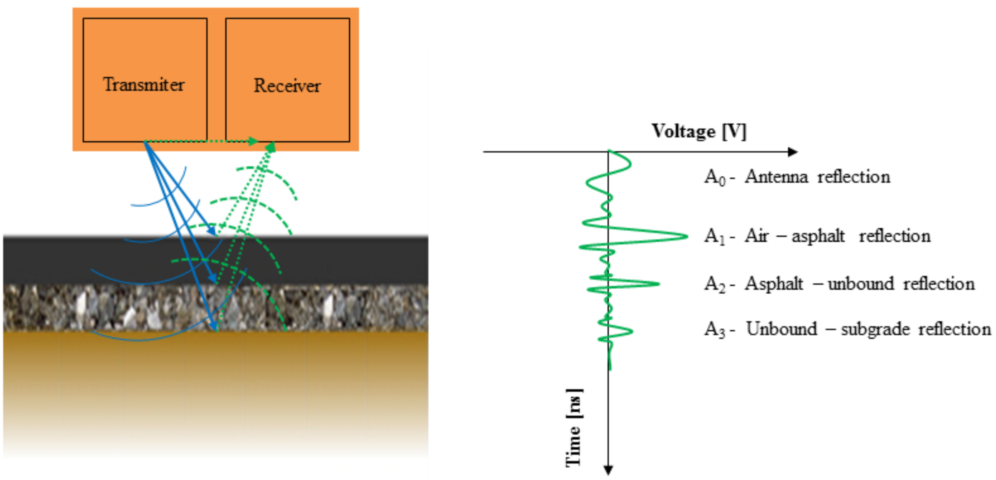

Figure 1: Electromagnetic wave transmitted to the pavement structure

The speed of EM wave propagation through subsurface is influenced by relative dielectric constant of the materials. To determine the thickness of layer the equation (1) is used:

$$h_i = \frac{c\Delta t_i}{\sqrt{\varepsilon_r}} \tag{1}$$

where c – the speed of the EM wave through the vacuum (3×10^8 m/s); Δt_i – the time between the amplitudes A_i and A_{i+1}; ε_r – the relative dielectric constant of the medium [2].

Relative dielectric constant of pavement materials can be either determinate in the laboratory or calculated on the basis of surface reflection method or by performing back calculation from ground truth data [7]. In this study surface reflection method was used and detailed explanation of the calculation process can be found in Ožbolt et al [8].

2.2 GPR equipment

The equipment used in the case study was GSSI impulse radar model SIR-20, with two air-coupled antennas with central frequency of 1.0 and 2.0 GHz. GPR system was complemented by a high definition digital camera (Figure 2).

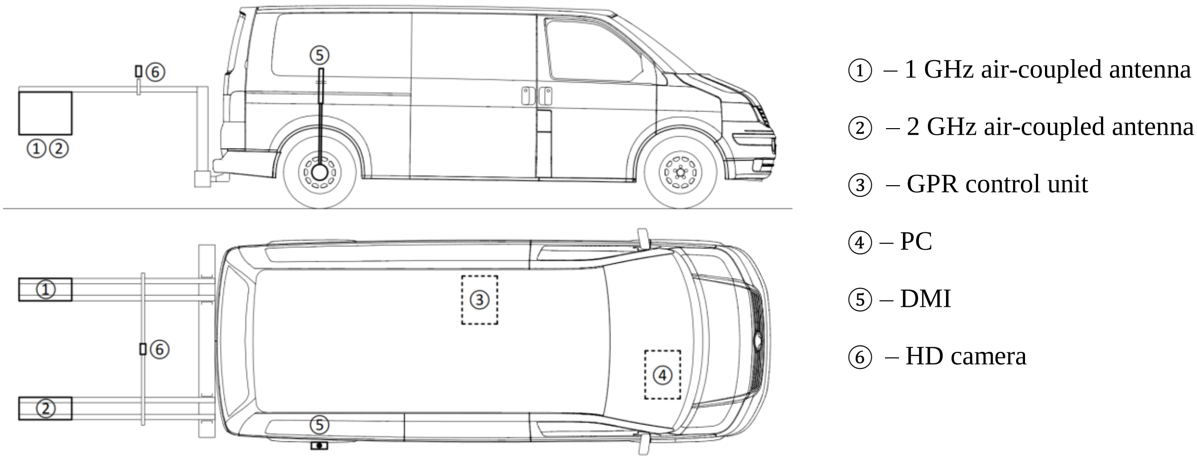

Figure 2: Schematic display of measuring equipment

The GPR profiles were recorded by distance measuring instrument (DMI) and scans were collected every 0.1 m (10 scans/m) with 512 samples per scan. Positioning of GPR data was done by placing the metal plate at the beginning and end of every profile. The processing and interpretation of collected GPR data was done in RADAN 6.6 software.

2.3 GPR data processing and interpretation

In processing phase raw GPR data (Figure 3, left) is combined with calibration data (Figure 3, middle) collected over a metal plate, to gain processed data (Figure 3, right). This step is required to compensate for the bouncing of the antennas during data collection, to set time-zero correction and to calculate velocity of GPR signal.

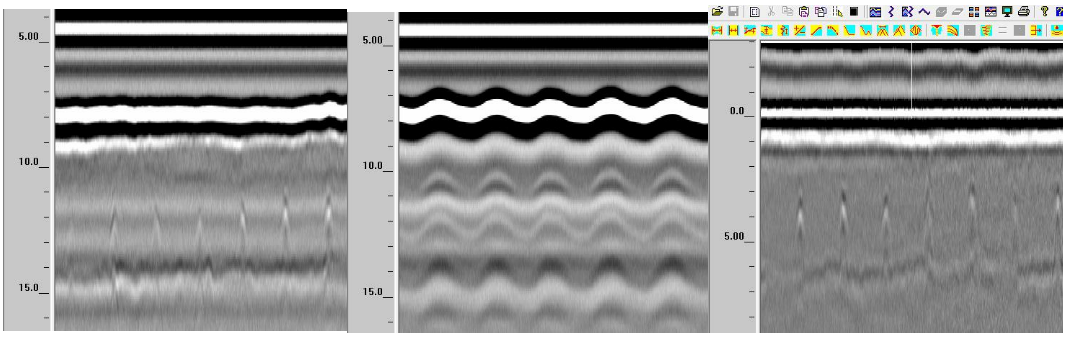

Figure 3: Radargram of raw (left), calibration (middle) and processed data (right)

The reflections of EM wave from the various layer interfaces within the pavement were visually identified on radargram (Figure 4). Positive reflections (white) are register when lower layer has higher dielectric value, and negative (black) reflections appear when the lower layer has lower dielectric value than the upper layer [6].

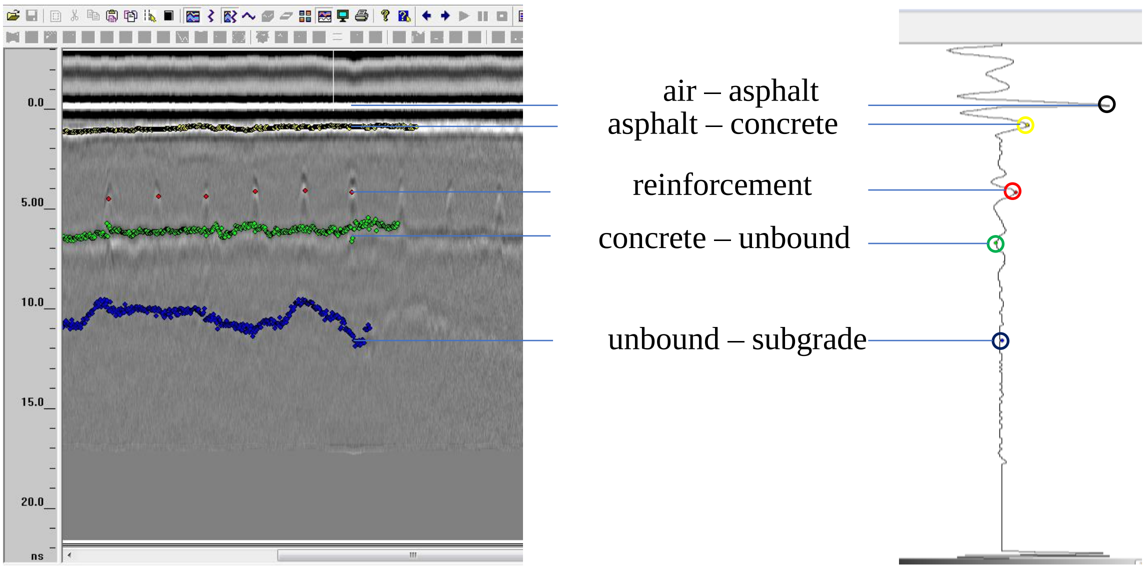

Figure 4: Interpretation of GPR data on radargram (left) and single scan (right)

As it can be seen on figure 4 continuous strong positive reflection defines obvious interface between air and asphalt layer and asphalt layer and concrete slab. Distinguishable interface between concreate slab and unbound base is seen as negative reflection. Interface between unbound base and subgrade is seen as positive mild reflection and it can be classified only as possible interface. Reinforcement, such as dowel, rebar etc., are seen on radargram as hyperbolic pattern.

3. SITE DESCRIPTION

According to project documentation runway was built in 1966 as concrete pavement with 22 cm thick concrete slabs on 28 cm thick unbound base. Due to increase in number of aircraft operations and loading in 1985 concrete pavement was overlaid with 8 cm of asphalt. Since than till today, beside routine maintenance, filling the cracks and patching as needed, there was no mayor rehabilitation. Upon visual inspection in 2014 it was concluded that the surface is in poor condition, especially the section stretching 7.5 m left and 7.5 m right from the axis in total length of 750 m from chainage 0-750.00 to 0+000.00. On this section six cores were drilled to determine pavement composition, layers thickness and materials condition.

Thicknesses measured on cores varied from 21 to 30 cm for unbound base layer, from 22 and 25 cm for concrete slab and between 5 and 9 cm for asphalt overlay. Due to large variation in layers thicknesses, it was decided to carry out GPR measurements, in order to obtain a continuous overview of layers thickness. Measurements were conducted in 16 measurement lines, with approximately one meter distance between the lines.

4. RESULTS

For all measurement lines thickness of asphalt overlay was determinate on every 10 cm, and thickness of concrete slab and unbound granular material on every meter. Layer depth was determinate by manually controlled semiautomatic interpretation which is based on finding nearest positive or negative peak. The results are shown by the depth versus distance diagrams for every measurement line (Figure 5) and depth maps in which the points of the same depth are connected with contours of the same colour (Figure 6). Maps were created by triangulating points obtained from GPR measurements in OpenRoads Designer Softwer.

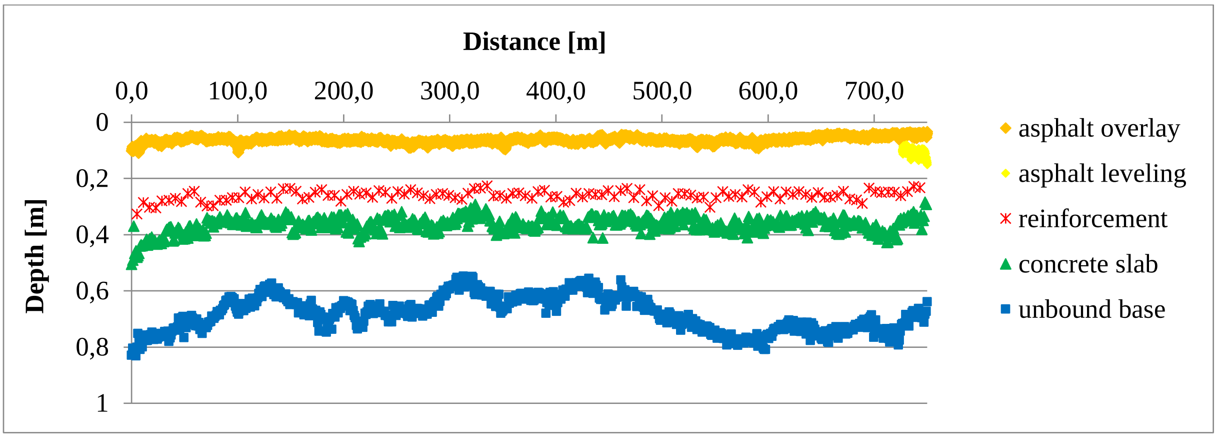

Figure 5: Depth vs distance diagram for measurement line 14

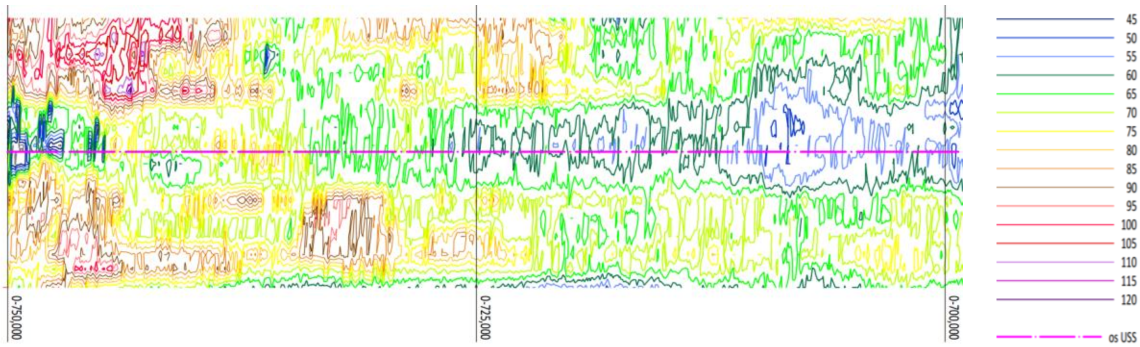

Figure 6: Map of asphalt layer depth from chainage 0-750.00 to 0-700.00

Created maps were used to identify changes in pavement structure and determination of homogeneous pavement sections. Defined homogeneous section together with pavement material properties served as a basis for pavement rehabilitation design and selection of optimal construction technology.

For every layer average thickness and interval in which 90% of the values appear are determinate. To verify results obtained by GPR, determinate thicknesses were compared to those measured on cores.

4.1 Asphalt overlay

Thickness of asphalt overlay varies from 2 cm to 12.3 cm, with average value of 5.9 cm and 95% of the results between 4.5 and 8.0 cm. In table 1 thicknesses of asphalt overlay measured on cores and by GPR are compared. Due to the fact that cores were drilled before GPR measurements, it was not possible to obtain GPR data on exact core location. That is why GPR thicknesses were determinate in the same chainage but with offset of 10 to 30 cm left or right from core location.

Table 1: Comparison of asphalt overlay thicknesses

Core number	**B-1**	**B-2**	**B-3**	**B-4**	**B-5**	**B-6**
Chainage	0-710.00	0-600.00	0-550.00	0-451.00	0-248.00	0-050.00
Core (cm)	7.8	8.7	5.5	7.3	5.8	4.9
GPR (cm)	7.0	8.9	5.4	7.0	5.9	4.4
Difference (%)	-10.3	2.3	-1.8	-4.1	1.7	-10.2

Difference between GPR and core varied from 1.7% to 10.3%. Obtained errors are rather low and consistent with previous studies [9]. This accuracy is considered acceptable for overlay design or reconstruction, especially taking into account age of the pavement and different measurement locations [8].

Between asphalt overlay and concreate slab from chainage 0+025.00 to 0+000.00 there was one more asphalt layer with average thickness of 5.9 cm. Therefore the total thickness of asphalt layers on this section was between 5.2 and 16.1 cm. This layer was not detected during coring and there was no information about its existence in project documentation. Situations like this emphasize the importance of implementing GPR measurements prior to coring or excavation in order to determine the homogeneous zone and properly locate investigation works.

4.2 Reinforcement

Reinforcement is located in middle of concrete slab, 20 to 30 cm from runway surface, positioned in longitudinal direction on every six meters. This distance corresponds to length of concrete slabs, i.e. position of transversal joint, indicating position of dowel basket. Since there was no information on the position of dowels, from project documentation or investigation work, it was not possible to estimate the accuracy of the measurement.

4.3 Concrete slab

Thickness of concrete slab varies between 16 and 43 cm with average thickness of 31 cm, and 90% of the data between 25 and 40 cm. Compared with the data obtained from cores

(Table 2) it is evident that on some locations there is a great difference between obtained results that could not be explained only by difference in position of the measurements.

Table 2: Comparison of concrete slab thicknesses

Core number	**B-1**	**B-2**	**B-3**	**B-4**	**B-5**	**B-6**
Chainage	0-710.00	0-600.00	0-550.00	0-451.00	0-248.00	0-050.00
Core (cm)	25	24	23	22	23	22
GPR (cm)	26	25	30	28	31	30
Difference (%)	4.0	4.2	30.4	27.3	34.8	36.4

According to project documentation thickness of concrete slab should be between 18 and 25 cm. In years 1983 and 1984 analysed section was repaired by injecting a mixture of cement and water at a ratio of 1:2. This mixture penetrated approximately 5 cm into unbound base layer making it hard to locate exact interface of concrete slab and unbound base on radargram due to similarity of dielectric values of the materials. Furthermore, since layer thickness was calculated only on the bases of surface reflection method by RADAN software the error cumulatively increased with the depth [8]. So, it can be concluded that calculation of layer depth only on the basis of refection method results in overestimation of thickness. To gain more accurate thickness GPR data should be calibrated with core data.

4.4 Unbound base

Thickness of unbound base varies between 15 and 54 cm with average thickness of 32 cm, and 90% of the data between 20 and 40 cm. Thicknesses obtained from GPR data were larger than those obtained from cores (Table 3).

Table 3. Comparison of unbound base thicknesses

Core number	**B-1**	**B-2**	**B-3**	**B-4**	**B-5**	**B-6**
Chainage	0-710.00	0-600.00	0-550.00	0-451.00	0-248.00	0-050.00
Core (cm)	27	28	27	21	21	30
GPR (cm)	34	34	30	24	24	37
Difference (%)	25.9	21.4	11.1	14.3	14.3	23.3

There are several possible reasons for thickness overestimation. First, the average depth of unbound base and subgrade interface was around 0.7 m which is on the border of penetration depth for 1 GHz air-coupled antenna [10]. Second, on some locations subgrade consisted of crushed limestone with similar dielectric properties as unbound base material making it hard to differentiate between the two layers. And third, accumulation of error with increased depth when reflection method is used. For higher accuracy GPR data interpretation should be conducted on the basis of core data.

5. CONCLUSIONS

In presented study GPR system was used to create map of runway pavement layers thickness. Measurements were conducted with two air-coupled antennas with central frequency of 1 and 2 GHz on 15 m wide and 750 m long section of the runway. The thickness of asphalt overlay, concrete slab and unbound base was determinate by employing surface reflection method. Thicknesses determinate from GPR data were compared with thicknesses measured on cores to estimate the accuracy of the results.

From the conducted analysis following conclusions have been drawn:

1. Graphic representation of layer thickness (depth) can be used for determination of homogenous pavement sections which facilitates selection of optimal construction technology;
2. Thickness of asphalt layers determinate by surface reflection method results in accuracy that is acceptable for rehabilitation projects and overlay design;
3. Calculation of concreate slab and unbound base thickness on the basis of surface refection method results in overestimation of thickness, for higher accuracy it is desirable to calibrate GPR data with thickness information from cores.

Creating layer thickness maps and determining homogeneous pavement sections is especially important for projects where rehabilitation activities are scheduled per hour with minimum traffic disturbance.

REFERENCES

[1] Van der Wiele, A., 'Thickness estimation of road pavement layers using Ground Penetrating Radar', retrieved from European Research Association for Sustainable and Multimodal Mobility website:
http://www.ectri.org/YRS15/Documents/Papers&presentations/Session%202B%20Transport%20Civil%20&%20Road%20Engineering.%20Tutor%20Laszlo%20GASPAR/Papers/Road_thickness_estimation_using_Ground_Penetrating_Radar_VAN%20DER%20WIELEN.pdf

[2] Fontul, S., 'Structural Evaluation of Flexible Pavements Using Non-Destructive Tests', Ph.D. Thesis, Departamento de Engenharia Civil, Universidade de Coimbra, Coimbra, Portugal, 2004.

[3] Maser, K.R., 'Condition Assessment of Transportation Infrastructure Using Ground-Penetrating Radar, Journal of Infrastructure Systems 2 (2) (1996) 94-101.

[4] Stryk, J., Matula, R. and Pospisil, K., 'Possibilities of ground penetrating radar usage within acceptance tests of rigid pavements', Journal of Applied Geophysics 97 (2013) 11–26.

[5] Khamzin, A.K., Varnavina, A.V., Torgashov, E.V., Anderson, N.L.and Sneed, L.H., 'Utilization of air-launched ground penetrating radar (GPR) for pavement condition assessment', Construction and Building Materials 141 (2017) 130–139.

[6] Saarenketo, T., 'Electrical properties of road materials and subgrade soils and the use of Ground Penetrating Radar in traffic infrastructure surveys', Ph.D. Thesis, Faculty of Science, Department of Geosciences, University of Oulu, Finland, 2006.

[7] Marecos, V., Fontul, S., Antunes, M.L. and Solla, M., 'Assessment of a concrete pre-stressed runway pavement with Ground Penetrating Radar', 8th International Workshop on Advanced Ground Penetrating Radar (IWAGPR), 2015.

[8] Ožbolt, M., Rukavina, T. and Domitrović, J., 'Comparison of the Pavement Layers Thickness Measured by Georadar and Conventional Methods – Examples from Croatia', Baltic Journal of Road and Bridge Engineering 7 (1) (2012) 30-35.

[9] Loizos, A. and Plati, C., 'Accuracy of Ground Penetrating Radar horn-antenna technique for sensing pavement subsurface', IEEE Sensors Journal 7 (5) (2007) 842-850.

[10] Grégoire, C., Van der Wielen, A., Van Geem, C. and Drevet, J.P., 'Methodologies for the Use of Ground-Penetrating Radar in Road Condition Surveys', Belgian Road Research Centre, Brussels, 2016.

METHODOLOGY AND CASE STUDIES FOR THE ASSESSMENT OF CONCERETE SUSTAINABILITY

Teplý Břetislav and Tomáš Vymazal

Brno University of Technology, Faculty of Civil Engineering, 602 00 Brno, Czech Republic

Abstract

One of the basic performance categories is sustainability. Since concrete is one of the most important and useful materials in the construction sector, which, unfortunately, has an adverse impact on the environment, it is evident that correct procedures for designing and/or assessing concrete structures need to be created. The present paper discusses a tool that enables the quantification and comparison of various cases. it introduces a simple equation for calculating the sustainability coefficient k_{SB}, taking into account lifespan, performance and eco-costs. Examples are shown for different definitions of service life, performance and impact on the environment.

Keywords: concrete, degradation, sustainability, lifetime, eco-costs, quantification

1. SUSTAINABILITY AND PERFORMANCE CATEGORIES

Civil engineers need an effective and simple way to quantify the advantages of a certain concrete type or a reinforced concrete structure with regards to its role as a sustainable material or a sustainable solution. It should be noted that the need to design structures following this approach is also expressed in the basic standard concerning the reliability of structures [1], specifically in article 4.2.1 (it emphasises service life as well). In addition, the international document fib Mode Code 2010 [2] focuses on a performance-based design of concrete structures, listing three basic performance categories: usability (i.e. also service life), safety and sustainability. Unfortunately, it does not draw any links between these categories. Moreover, civil engineers do not yet fully understand that all these design categories should also be considered in terms of the environmental design of concrete structures, as discussed in the ISO standard [3] (although not in full detail, unfortunately) – see later in this text. Performance-based thinking concerns life cycle analysis (LCA), sustainability and a relevant system boundary. The cradle-to-gate, or better, the modified cradle-to gate concept is advised for the purpose of evaluating concrete mix sustainability [15], as they comprise the environmental impact of the amount of concrete needed for the structure's maintenance.

It should be also noted - as discussed in *fib* currently - in 2020 a new, advanced *fib* Mode Code 2020 is awaited with the implementation of sustainability as a fundamental requirement.

The paper presents a methodology that enables the quantification and comparison of various cases, introducing a simple equation for calculating the sustainability coefficient k_{SB}, which takes into account lifespan, performance and eco-costs. The paper aims to show how this methodology can be applied using the example of several different types of concrete subjected to a chosen type of degradation. Such analyses can be optionally performed in a probabilistic manner. This methodology generally allows considering prior processes as well, such as raw material extraction, transport, manufacturing, maintenance and usage, through to processing as waste (recycling). In an ideal situation, economic, ecological and socio-cultural aspects can be included. However, for the sake of simplicity, these are not discussed in the presented methodology and examples.

2. SUSTAINABILITY COEFFICIENTS

Proper sustainability management requires effective tools that enable the quantification, measurement, optimization or comparison of material, technological and construction variants. In recent years, these tools have seen rapid development around the world. They include various indicators, indexes, certificates, comparison indicators, audits, evaluations and other systems, often using various databases. General principles concerning sustainability in building construction are discussed in ISO 15392 [4].

This paper concentrates on the assessment of concrete sustainability with focus on degradation resistance (due to mechanical and/or environmental load). Its aim is to present a suitable methodology which can broaden the decision-making perspective as to the design and choice of concrete mixtures, i.e. not considering only load-bearing capacity and serviceability, but also the quantification of sustainability measures. Generally, a sustainability potential can be understood, according to [5], as

$$\Omega = \frac{\text{service-life}\times\text{performance}}{\text{impact on the environment}} = \frac{L\cdot R}{E} \quad (1)$$

In this equation, *"performance" R* means, for instance, the load-bearing capacity, deformability, resistance to degradation or many other properties of the material or structure expressed in corresponding units.

Service life L is usually given in years. There are many definitions of service life, viewed e.g. in technical, operational, contractual or economic terms. However, when evaluating the sustainability of reinforced concrete structures, it is advisable to work with the definition stated in the 2010 document [6] in which the service life is described using relevant limit states, number of years and the corresponding level of reliability (i.e. the probability of achieving a limit state which must not be exceeded during this period).

The type of limit state and the limit probability value are critical figures. In order to determine them, it is often necessary to model the degradation of materials over time (e.g. using the tool described in [7]) or use estimations of the service life of a structure obtained using e.g. the Factor method ([8] - Part 8).

Quantity E (the "impact on the environment") is usually described as a string (sum) of data including such factors as bound emissions of various kinds, energy consumption, wear and tear, etc. All these are quantities that are often expressed in different units and thus need to be converted to common ones so as to combine all impacts into one value, *E*. This common unit is usually a monetary one, which is when *E* is called *eco-costs* and, according to e.g. [9], represents the total costs of measures taken to reduce the environmental impact down to a sustainable level. A useful choice is the global warming potential (GWP), as used e.g. in [25]. In order to correctly assess the potential environmental impacts of a concrete mix design, a review and explanation of several LCA approaches and models has been conducted; see, for instance, [24].

Quantity R can likewise be expressed in various units according to its type and thus the resultant unit for Ω will also differ from case to case. This is not practical and can complicate the decision process. Therefore, the authors suggest a simple normalisation of Eq. (1) using proper reference values [10, 11]. Sustainability can then be quantified using normalized sustainability coefficients k_{SB} according to Eq. (2), where quantities L, R and E are divided by reference values L_{ref}, R_{ref} and E_{ref}, meaning that k_{SB} is then a dimensionless quantity whose value usually approximates 1.0.

$$k_{SB} = \frac{\frac{L}{L_{ref}} \cdot \frac{R}{R_{ref}}}{\frac{E}{E_{ref}}} \tag{2}$$

This formula can be utilized for comparing the sustainability coefficient values between different groups of concrete and can be briefly described as follows: it must always be assumed that all concretes in a given group are at the same (or similar) location and suffering the same type of degradation and/or loading. When evaluating sustainability, a certain type of performance is considered and service life is determined with regard to that given type of degradation/loading. When applicable, concrete structures' ultimate and serviceability limit states have to be met (this also means that attention to the correct value of reliability index β has to be paid). In general, this analysis can be made in a probabilistic frame: input values are considered to be random quantities and a statistical, reliability or sensitivity analysis of equation (2) can be performed. Note: the authors will present examples of this approach in a separate paper later; the probability analysis is currently applied in the present text for service life L only using the software tool FReET [7].

A procedure for comparing sustainability coefficient values, k_{SB}, for groups of different concretes can be briefly described in this way: it is necessary to consider all concretes in a given group to be situated at the same location and to suffer the same type of degradation and/or loading. When evaluating sustainability, a certain type of performance is considered and service life is determined with regard to that given type of degradation. After the relevant eco-costs have been determined, equation (2) is used to arrive at the value of the sustainability coefficient; in this way concrete mix design can be optimized as well.

The paper presents a tool for sustainability management, which enables its quantification and the comparison of mixture variants for the production of concrete with certain properties, emphasising durability-related issues. The Eq. (2) in which service life, performance and eco-costs appear are used in a sustainability coefficients analysis, k_{SB}. The eco-costs make the task more complicated - its definition can have several forms and components, meaning that arriving at a single cost figure can be difficult for users if they are not able to draw on a suitable database or other resources. The approach to evaluating each different concrete mixture affects the final choice mixture or makes comparison possible.

The proposed methodology can serve as a policy-making tool for the cement industry with regard to, e.g. CO_2 emission issues. An advantage of this approach is also that it offers the possibility of using both test results or the results of mathematical models when searching for *L* or *R* values.

3. DEFINITION OF SERVICE LIFE, PERFORMANCE AND IMPACT ON THE ENVIRONMENT

Equations (1) and/or (2) seem to be quite simple, though they involve rather complex factors: service life *L*, performance *R* and impact on the environment *E* of a material or a structure. Depending on the definition of these quantities, there can be several variants of sustainability assessment:

3.1 A single degradation process

The simple case is where performance *R* is represented by a single degradation process, e.g. when concentrating on a single type of degradation resistance of the concrete structure: carbonation of concrete, chloride ingress, freezing-thawing, corrosion of reinforcement and others. A few such sustainability studies were presented in [10, 11], with *R* being represented by the strength of concrete, *L* by (i) the initiation period due to carbonation; i.e. the time until reinforcement begins to corrode; (ii) freeze-thaw cycles combined with concrete scaling [11]. These examples are not repeated in this paper. Note that the *service life* based on carbonation (and similarly on chloride ingress) is analysed by specifying the concrete cover value; it shows that such sustainability analyses are no longer based on pure *material level,* requiring some *structural parameters* as well. This may be one of the reasons why many authors often avoid the utilization of service life (e.g. [24]) and it should be stressed that the assessment of sustainability is then not complete, because sustainability is by default a function of time. Also, even the recent ISO 13315-4:2017 presents an example in Annex C in a similarly non-conformal way: a 30 % reduction of CO_2 is required in a concrete structure originally designed with a conventional concrete mix containing a portion of Portland cement. This reduction is achieved by including granulated blast furnace slag in the mix. No focus on durability and by extension also service life (SLS) is made. If, for example, focus of study is the influence of concrete carbonation and cover thickness a = 30 mm is chosen, the relevant service life of Portland-cement concrete is 97 years, whereas the concrete mix with slag (analysing the carbonation progress using a model [12]) has a service life of 34 years. This would influence the sustainability coefficient k_{SB} values considerably.

Note: The effectiveness of supplementary cementitious materials (SCM) in reducing CO_2 emissions is often subject to examination. The binder intensity *bi* index (measures the amount of binder necessary to deliver 1 MPa of concrete strength) and the CO_2 intensity index *ci* were recently introduced [14]. In [15], the binder intensity measure related to service life was expanded as follows: the total amount of binder per m^3 of concrete necessary to deliver 1 MPa of strength and 1 year of service life. This way, the unit of functional performance is given in two areas: strength and durability, which can also serve for concrete LCA. A similar approach was utilized in [16], where, based on data obtained by testing many laboratory and plant mixes, equations ware formulated for binder intensity and the CO_2 intensity index was introduced. Note such findings can be useful when analysing variables *L* and/or *R* and adopting Eq. (1) or (2). Also, other conditions can play a decisive role, e.g. different kinds of purpose for the structure, its location and others.

To show the effectiveness of Eq. (2) on sustainability assessment together with the ability to distinguish the influence of different degradation effects, four Portland-cement concrete mixtures (A to D, designed originally for concrete workability S3 according to EN 206-1) were tested. Data from [17] (Tab. 1) and Eq. (2) were utilized for the following cases: (i) frost; (ii) water penetration; (iii) concrete carbonation. Table 2 lists the values of sustainability coefficients: each line represents results for one degradation type and each column shows sustainability coefficients for each type of concrete tested for all three attacks. In normal practice it is not common to obtain results of such complexity, however, it is relevant for this paper since it sets out to thoroughly introduce the approach being discussed.

Note: the higher the value of the sustainability coefficient, the better the level of the associated sustainability. However, to the authors' best knowledge, no recommendation for a choice of the most suitable/relevant degradation effect is available. A crucial point can be assessed e.g. by the highest k_{SB} value, using an effect that occurs the most frequently, or the decision can be based on the exposure category used in the structure's design, or on the relevant resistance class [21]. Table 2 shows an example of how the value of sustainability coefficient can differ in real cases.

Table 1: Concrete mixture data and different degradation effects

Concrete	Unit	A	B	C	D*	Source
CEM I 42.5 R	kg/m^3	300	350	400	400	[17]
Aggregate 0 – 4 mm	kg/m^3	925	875	825	825	
Aggregate 4 – 8 mm	kg/m^3	185	185	185	185	
Aggregate 8 – 16 mm	kg/m^3	695	695	695	695	
Water	kg/m^3	204	179	174	164	
w/c	-	0.63	0.47	0.40	0.38	
28-day cube strength [MPa]	MPa	33.3	50.8	57.2	63.7	
Frost resistance [22]	-	61	49	44	98	
Water penetration [23]	mm	34	22	27	11	
Carbonation (considering cover 30 mm and reliability index β=1.3)	years	56	146	212	316	[12]
Carbon imprint	kg CO_2/m^3	240	279	321	318	
Eco-cost	€ /m^3	45.3	50.4	55.5	55.5	

* Air-entrained concrete

Table 2: Sustainability coefficients

Concrete	A	B	C	D
k_{SB} - frost resistance	1.00	0.70	0.54	1.22
k_{SB} – water penetration	1.00	0.72	1.06	0.43
k_{SB} - carbonation	1.00	2.24	2.83	4.26

3.2 A synergy of degradation processes

In reality, however, more than one degradation effects act simultaneously, which in turn has to be reflected in the analysis of sustainability coefficients, k_{SB}. It makes the problem rather complex since infrastructure performance - namely the durability of concrete structures and adequate reliability - can suffer from several forms of attack, namely chemical attack (e.g. concrete carbonation, chloride ingress, acid attack and others), electrochemical attack (corrosion of reinforcement), physical attack (e.g. freeze/thaw), and mechanical load (static or dynamic). In most cases the structural assessments for different forms of attack have, until recently, been treated separately. However, a general service life assessment or predictions which do not include the synergy of mechanical and environmental loads are neglecting a factor that can have a significant impact on structural safety and durability prognosis [18], [19]. In order to make service life design realistic it is necessary to take into consideration both mechanical and environmental loads acting simultaneously. The stress and/or deformation field may cause some significant changes in the pore structure and result in cracking. Moreover, damage due to reinforcement corrosion is recognized as one of the major causes of the deterioration of reinforced concrete structures and the presence of defects in the concrete may accelerate the corrosion rate.

All this can have a considerable impact also on sustainability measures of concrete structures. Generally, while accounting for synergy cases, the assessment of sustainability can be rather simple when using Eq. (1) or (2). However, this requires relevant experimental results or a numerical model. This is a major obstacle, because such results for the synergy of multiple and heterogeneous degradation effects are rarely available.

Evidently, mechanical load does affect the service life and the influence of its synergy with other types of degradation can be of interest. While assessing sustainability, some authors [19], [20] presented the example of an RC cooling tower, which was tested for carbonation depth. The tower, 206 m tall and 19.1 years old, was numerically analysed for the depth of carbonation as well as measured at 75 location on both the inner and outer surface. Thus, at $t \geq 19.1$ years the Bayes updating provides a corrected prognosis of the carbonation progress for future decades.

Concrete mix data [20]: CEM I 42.5 R 342 kg/m^3, fine aggregate 834 kg/m^3, coarse aggregate 987 kg/m^3, water 188 kg/m^3. The carbon imprint equals 273 kg CO_2/m^3, eco-costs = 21.3. More data are shown in Table 3 and were used for the sustainability coefficient analysis by Eq. (2), enabling the comparison of the effect of a single mechanical load and the synergy of a mechanical load with concrete carbonation. Resulting sustainability coefficients, k_{SB} are also shown in Tab. 3. Note both outer and inner surfaces of the cooling tower are distinguished as the relative humidity differs, leading to different carbonation rates and a slight difference in strength in both surfaces. The cover values of both surfaces differ as well.

Table 3: Concrete mixture data, structural data and resulting k_{SB}

	Unit	Outer surface	Inner surface	Source
Concrete strength in 19.1 year of age	MPa	33.6	34	
Cover	mm	28.4	23.6	[19] (mean values)
RH	%	70	97	
Depth of carbonation in 19.1 year of age	mm	14	8	
Service life relevant to reliability index β = 1.3 (carbonation)	years	37	86	
Service life relevant to reliability index β = 1.3 (carbonation + mechanical load)		19	66	
k_{SB} (carbonation)		1	2.3	
k_{SB} (carbonation + mechanical load)		0.51	1.8	

Note that this example analyses only one type of material and structure. A comparison of two models is presented (carbonation and carbonation + mechanical load effect), and the worst case is represented by the shortest service life.

Evidently (and not surprisingly), thanks to the faster carbonation rate, the outer surface value should be considered as the leading sustainability coefficient for the whole tower. Thus, the crucial case of the external surface results in a service life value of $k_{SB} = 0.51$, taking into account the synergy of surface carbonation and a mechanical load corresponding to a reliability index $\beta = 1.3$.

4. CONCLUSION

This paper presents a tool for the quantification and comparison of sustainability measures for various cases of concrete mixes or reinforced concrete structures. It introduces normalized equation for calculating the sustainability coefficient k_{SB}, taking into account service life, performance and eco-costs. A modified cradle-to gate concept is applied and two different examples are analysed and discussed.

The effect of more complex combinations of degradation types as well as a full probabilistic approach will be subject to future research.

ACKNOWLEDGEMENTS

This work has been supported by project No. 17-14302S "Experimental analysis of the early-age volume changes in cement-based composites", supported by the Czech Science Foundation and project No. No. LO1408 "AdMaS UP – Advanced Materials, Structures and Technologies", supported by Ministry of Education, Czech Republic.

REFERENCES

[1] ISO 2394:2015 - General principles on reliability for structures. International Organization for Standardization: Geneva, Switzerland.

[2] *fib* bulletin No. 65 and 66, *fib* Draft Model Code 2010 (2012). International Federation for Structural Concrete (*fib*), Lausanne, Switzerland.

[3] ISO 13315-4:2017 Environmental management for concrete structures – Part 4: Environmental design of concrete structures. International Organization for Standardization: Geneva, Switzerland.

[4] ISO 15392: 2008 Sustainability in building construction – General principles. International Organization for Standardization: Geneva, Switzerland.

[5] Müller, H.S. (2013). Sustainable structural concrete – from today´s approach to future challenge. *Structural Concrete*, 14 (4):299-300.

[6] *fib* bulletin No. 65 and 66, *fib* Draft Model Code 2010 (2012). International Federation for Structural Concrete (*fib*), Lausanne, Switzerland.

[7] Novák, D., Vořechovský, M. and Teplý, B. (2014). FReET – Software for the statistical and reliability analysis of engineering problems and FReET-D: Degradation Module.

[8] ISO 15686 Buildings and constructed assets -- Service life planning – Parts 1 to 8. International Organization for Standardization: Geneva, Switzerland.

[9] *fib* Bulletin No. 28 (2004). Environmental design. The International Federation for Structural Concrete, Lausanne, Switzerland

[10] TEPLÝ, B.; VYMAZAL, T.; ROVNANÍKOVÁ, P. Methodology for the quantification of concrete sustainability. MATEC Web of Conferences, 2018, vol. 174, no. 174, p. 1-7. ISSN: 2261-236X.

[11] Teplý, B., Rovnaníková, P., Vymazal., T. Sustainability quantification of concrete structures. In *Advanced Environmental in Research.* volume 63. New York, USA: Nova science publishers, 2018. p. 231-248. ISBN: 9781536139198.
[12] PAPADAKIS, V. G. - FARDIS, M. N. - VAYENAS, C. G.: Effect of Composition, Environmental Factors and Cement-lime Mortar Coating on Concrete Carbonation, Materials and Structures, 1992, Vol. 25, No. 149, 293-304.
[13] RCLifeTime – option of software tool [online]. BUT: ©2018 [cit. 26.7.2018]. Dostupné z: https://www.freet.cz/
[14] Daminely, BL, Kemeid, FM, Agular, PS and John, VM (2010) Measuring the eco-efficiency of cement use. Cement and Concrete Composites 2010 32(8):555-65
[15] P. Van den Heede, N. De Belie (2012) Environmental impact and life cycle assessment (LCA) of traditional and 'green' concretes: Literature review and theoretical calculations. Cement & Concrete Composites 34 (2012) 431–442
[16] Yang, K., Jung, Y., Cho, M. and Tae, S. (2015) Effect of supplementary cementitious materials on reduction of CO2 emissions from concrete. J. of Cleaner Production 103, 774-783.
[17] HALAMOVÁ, R.; KOCÁB, D.; VYMAZAL, T. The Influence of Concrete Composition on its Modulus of Elasticity: Comparison of Experiment and Values from Eurocode 2. In *Proceedings of The 12th International PhD Symposium in Civil Engineering.* Praha: Czech Technical University in Prague, 2018. p. 1103-1110. ISBN: 978-80-01-06401-6.
[18] Tang, S.W., Yao, Y., Andrade, C., li, Z.J. (2015) "Recent durability studies on concrete structures", *Cement and Concrete Research*, 78, 143-154.
[19] Dita Vořechovská, Martina Šomodíková, Jan Podroužek, David Lehký and Břetislav Teplý (2017) Concrete structures under combined mechanical and environmental actions: Modelling of durability and reliability. *Concrete and Computers*, TechnoPress, 20/1, 99-110
[20] Teplý, B., Chromá, M., Rovnaník, P. & Novák, D. 2013. The role of modeling in the probabilistic durability assessment of concrete structures. *Proc. Life-Cycle and Sustainability Infrastructure Systems (IALCCE 2012)* – Strauss, Frangopol & Bergmeister (Eds), Taylor & Francis Group, London: 876-882.
[21] Eckfeldt, L., Hintzen, W. and Breitschaftm G. (2016) Resistance classes for concrete – a discussion of a promising new approach. *fib Symposium Performance-based approaches for concrete structure*, Cape Town
[22] ČSN 73 1322, Determination of frost resistance of concrete, ČNI, 1969,
[23] EN 12390-8 Testing hardened concrete - Part 8: Depth of penetration of water under pressure, ČAS, 2009.
[24] M. W. Tait & W. M. Cheung (2016) A comparative cradle-to-gate life cycle assessment of three concrete mix designs. International Journal of Life Cycle Assessement (2016) 21:847–860 DOI 10.1007/s11367-016-1045-5
[25] Mueller, S. H.; Haist, M.; Moffatt, S. J; Vogel, M. Design, material properties and structural perfonmance of sustainable concrete. Proc. Eng. 2017, 171, 22 – 32, DOI 10.1016/j.proeng.2017.01.306

HYBRIDBEAM – COMPOSITION IN SLAB IS MORE THAN THE SUM OF STEEL AND CONCRETE

Matthias Kintscher (1), Jerzy Derysz (2) and C. Kryzstof Janczura (2)

(1) PFEIFER Seil- und Hebetechnik GmbH, Dr. –Karl-Lenz-Straße 66, G-87700 Memmingen

(2) PFEIFER Steel Production Poland Sp. z o.o., Wrocławska 68, PL-55330 Krępice

Abstract

Hybridbeam is a new concept of a 3 way composite steel-reinforced supporting beam for a slim floor concrete slab with newly designed interaction of rebars, precast concrete, steel beam and prefabricated hollow core slab.

It is a supporting member for a flush soffit of a slab system consisting predominantly from prestressed hollow core slab elements.

The nonlinear behavior of Hybridbeam is the result of a material minimizing composition of steel and concrete. The composite beam is acting as a steel concrete member in bond via horizontal studs to the steel beam as a sleeve. By the means of cross linking rebars through the Hybridbeam into the slab there is an interaction of slab and Hybridbeam activating an effective width of the composite slab which is more than the width of the Hybrid beam only. Combined with prefabricated camber in the Hybridbeam low bending deflections will be noted.

Advantages: Architectural it is a flush beam, not protruding from the slab underneath or at the top. Great spans without supporting column are realizable. The great stiffness makes mounting very easy without any supporting props. The resistance against torsion makes it independent of the sequence of loading. Fire resistance is given for R120.

The new interacting system between different materials activating more than only the sum of the effects, safes material, production energy, carbon dioxide emission and is therewith a contribution to sustainability.

Keywords: Flush Wide Span Steel Concrete Composite Beam, Hollow Core Slab, Fire Resistance, Sustainability, Material Minimization

1. INTRODUCTION

Architects and investors search for increased usable space per floor using a flush slab support within the floor thickness (Figure 1). This gives clean and flush soffit not wasting height floor and makes the technical installations at the ceiling easier. The Hybridbeam grants all, enabling for example, 11 instead of 10 storeys in administration or high rise buildings.

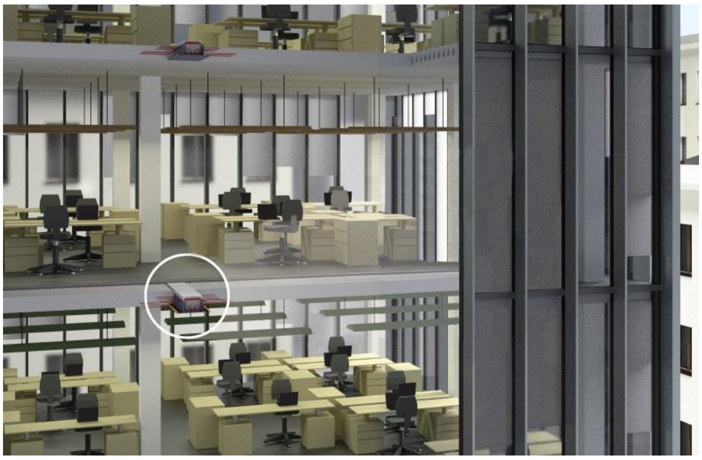

Figure 1: Administration building – section: slab with slim floor Hybridbeam support

Figure 2: Assembly of building structure with Hybridbeam

Economic benefits are clearly defined by a simple installation process by increased column spacing without any support projection through the floor (Figure 2). This and the reduced concrete work on site and a free not prescribed work sequence during installation of hollow core slab elements optimizes the assembly process and accelerates the construction decreasing the time wasting.

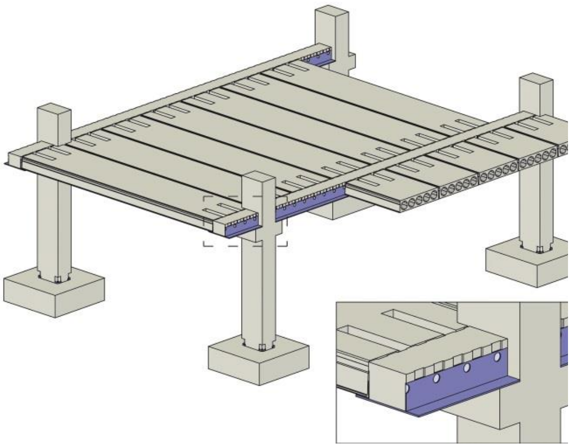

Figure 3: Hollow core slab supported by Hybridbeam

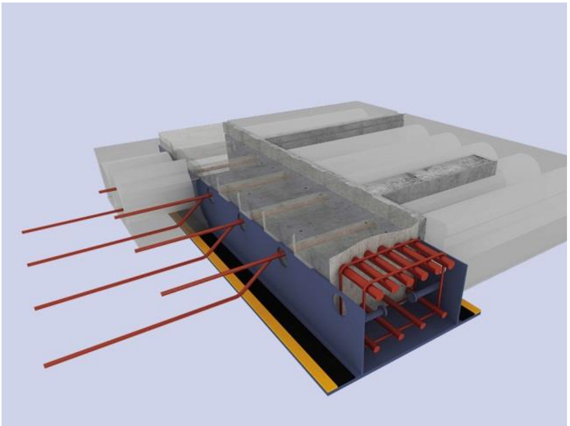

Figure 4: Hybridbeam with internal view and partially placed hollow core elements

The Hybridbeam (Figure 5) is a prefabricated load-bearing composite beam which is integrated flush with slabs to create so called slim floors – thin integrated structural slabs (Figure 3 and 4). The floor assembly is completed with single-spanned prestressed hollow core slabs. The Hybridbeams transfer the floor loads to columns or even walls. The beams allow precast floor slabs to be instantly supported. Installation is continued using continuity shear reinforcement and infill concrete is then used to bond the beam with the floor slabs.

The type BHM (Figure 5) is designed as an intermediate beam and uses two steel flanges to support the floor slabs meanwhile type BHR (Figure 12) is designed as an external beam and uses one single-sided bottom flange only to support the floor.

Figure 5: Hybridbeam – ready for installation composite element

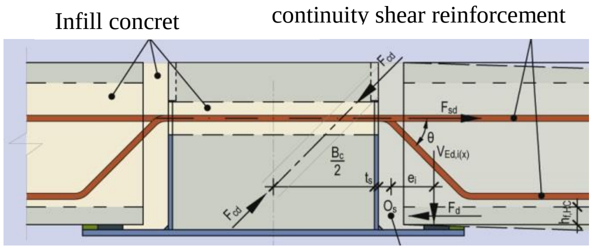

Figure 6: Supported slim floor slab cross section with shear reinforcement through cross holes

2. ACTIVATING THREE BOND INTERLOCKS CREATING STIFFNESS ON BASIS OF COMPOSITE EFFICIENCY

This steel concrete beam (Figure 4) itself is acting as a composite element by the ribs of the bars is stiff element itself. This is bond action one.

The steel components of the Hybridbeam (Figures 7 and 10) are composed of thin steel sheets as webs welded to a thicker steel bottom plate with left and right projecting bearing flanges. This steel structure forms an outer shell as u-shaped bar. It is filled with high-performance reinforced (Fig. 3 and 4) self-compacting concrete already in the production plant. Headed studs as shear bolts placed by contact welding with tip ignition inside the u-shaped welded steel beam at the webs are connecting the steel beam to the steel concrete beam (Figure 8). The steel around the concrete acts as additional reinforcement in the tension area of the beam lowering the centre of gravity and the neutral bending fibre and increases together the stiffness of the composite element. This is bond action two.

Cross holes through the beam built by thin walled corrugated metal tubes are intended to receive shear and continuity reinforcement used to join the beam with the floor slab elements after mounting in the building (Figures 9 and 10). Additional toothing of the concrete at the top of the Hybridbeam gives a mechanical shear interlock to the slab elements. When the voids – means all openings in the hollow cores, the gap between hollow cores and the beam and the cross holes in the beam - are later completely filled with infill concrete, areas of the whole slab and the beam structure of the floor are activated by bond to a wide efficient load bearing width. This increases the bending resistance again (Figure 10). This is the bond action three.

All three bond interactions are providing more efficiency than the pure sum of the parts would do (Figure 10).

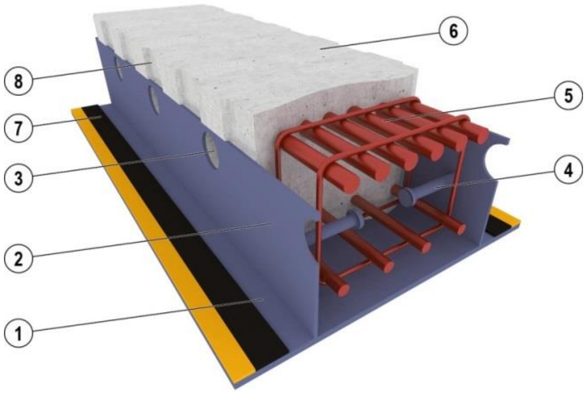

1. Bottom plate with flanges
2. Side wall as web
3. Cross hole
4. Headed stud as shear bolt
5. Longitudinal Reinforcement bars
6. Precast self-compacting high performance concrete
7. Load centring elastomer strip and stone wool fire protection
8. Lateral toothing of concrete as shear interlock

Figure 7: Components of Hybridbeam before installation on site – partially x-rayed for visualization

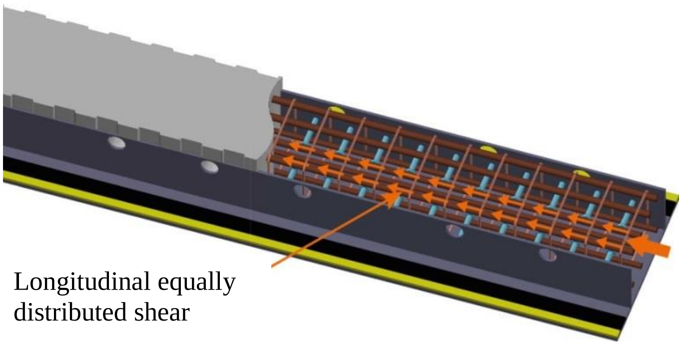

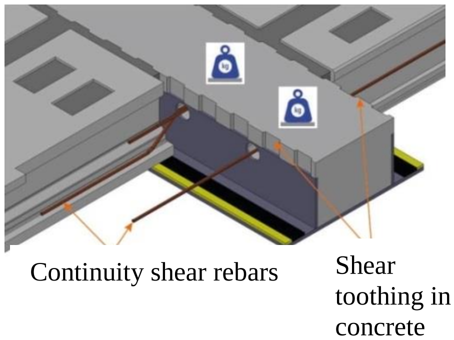

Figure 8: Shear bolts inside Hybridbeam connecting steel parts and concrete bar

Figure 9: Shear bars and concrete toothing for connection of Hybridbeam and slab as slim floor

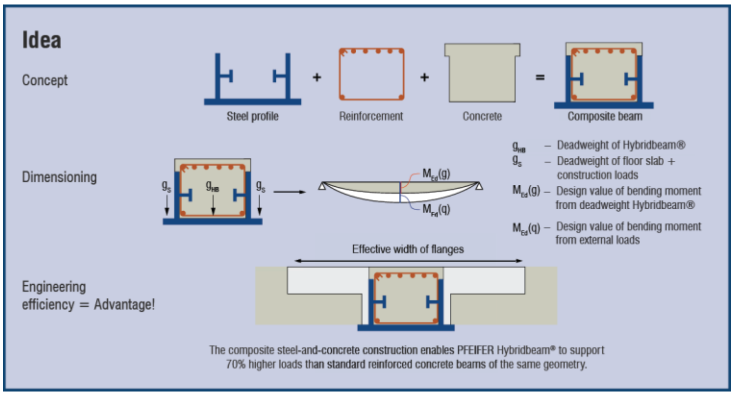

Figure 10: Idea of three actions of bond to create maximum stiffness activating an efficient contributing width of the slim floor slab

3. HYBRIDBEAM IN DESIGN AND USE

3.1 Shear resistance between slab and Hybridbeam

To achieve high load capacity, it is essential for the Hybridbeam to be completely connected by bond with the floor slabs. Therefore continuity reinforcement is passed through cross holes in both the beam into the channels of the hollow core slabs (Figure 6). Infill concrete of equivalent strength class is then cast into the voids and other gaps between the elements to bond the beam to the adjoining floor slabs (Figure 11). According to EN 1992-1-1:2010 the transmission of shear load at the reinforced joint between the beam and floor slab activates an extended section of the whole floor slab. The width of activated substitute area is determined from the equation of shearing force equilibrium in the joint and compressive forces in the substitute section and is dependent both on the surface (cross-section) of the joint reinforcement, and strength class of the infill concrete. As a result, additional load capacity with reduced deflection in the composite beam is achieved.

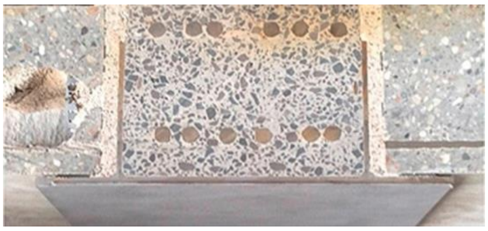

Figure 11: Cross section Hybridbeam and slab with infill concrete in voids

Figure 12: Hybridbeam BHR as one side supporting beam at the edge of the slab

During construction before the casting with infill concrete the load capacity of Hybridbeam is calculated assuming a weakened section due to the cross holes being unfilled with concrete.

After being fully installed, and because of the connection zone within the floor slabs, the limit load capacity of the Hybridbeam is calculated using a full combined section with plastic conditions according to EN 1994-1-1. For edge beams slabs or asymmetric load conditions torsion from the beam is transferred into the slabs via the continuity reinforcement once the voids and gaps are filled with infill concrete. The torsional rigidity of beam is determined according to EN 1992-1-1:2010 and EN 1993-1-1:2009

Hybridbeam are delivered to site as a complete steel-and-concrete composite element – acting with two of the three bond actions.

After laying the floor units, properly designed continuity reinforcement is positioned through holes in the beam and voids in the floor slabs. Infill concrete is cast into and voids, and after it is hardened, the full usable load capacity of the beam is attained – third bond action activated. Loads are transferred from the floor to the beam via the continuity reinforcement (Figure 6 and 9). The required cross-section of lateral reinforcement is calculated by excluding the bearing capacity of the composite beam's steel bearing flanges.

The Hybridbeam provides a high fire resistance rating in case of fire. A fire retardant coating on the bearing flanges of the beam enables a fire resistance rating of R60–R120. The thickness of the intumescent paint coating is provided by the manufacturer depending on U/A (perimeter/cross-section area) – the coefficient of the steel section's mass. Fire resistance can be determined according to EN 1994-1-2. Additional reinforcement is used in the tension zone of the composite beams to compensate for the loss of bearing capacity due the thermal effects of fire on the steel beam flanges according to EN 1991-1-7. A mineral wool strip positioned between the slab and the flange protects the slab's elastomeric bearing pad against high temperature. The fire resistance of the product is determined by a Polish National Technical Assessment issued by the Building Research Institute in Warsaw. Fire resistance is assessed in the range R60–R120.

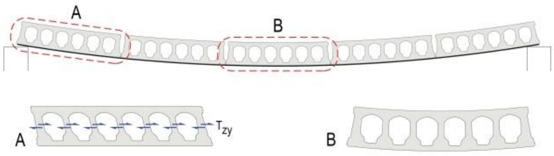

Figure 13: Typical displacements at hollow core on flexible supports with contact in pressure zone at the top and shear in the hollow core webs

Figure 14: Full scale testing of Hybridbeam in hollow core slab in Poland

It is well known that hollow core slabs have some problems in the case of support on flexible beams. In case of the Hybridbeam the expected deflection is compensated at production by a longitudinal camber. Every Hybridbeam is produced with camber that the dry installed hollow cores deflect the relative stiff Hybridbeam to the quasi final position from deadweight. The rest of loading from live loads then act on the slim flor with more little deflections.

All these effects have been studied in full scale tests in Poland where a slab supported on beams has been loaded by concrete blocks (deadweight of topping) and flexible water tanks (live loads) up to crash (Figure 13 and 14). Very positive results have been noticed therewith which are basis of the national polish assessment document.

3.2 Dimensioning of Hybridbeam

When selecting Hybridbeam, it is necessary to know technical data of the floor under design like beam span, a span of floor slabs, values of permanent loads (deadweight of the floor) and also the variables (live loads) (Fig. 15). The spans of effective floor elements are marked as lM (between middle beams) or as lR (at external beam), respectively. For preliminary dimensioning, it is necessary to determine the total floor load ($q_{E,d}$; $g_{E,d}$) excluding the deadweight of the beam. In Diagram Figure 16 it is a bundle of coloured lines shown to determine the loading on the beam dependant on span and load on the slab. With this loading on the beam as result of diagram 16 next diagram 17 can be entered. Each height of beam or slab has an individual diagram height are 20, 27, 32, up to 50 cm.

The designed slab height gives the indication where to look. In Figure 15 the Hybridbeam with 27 cm height is shown. The bundle of coloured lines shows for the 27 cm height a variety of widths of Hybridbeams. Dependent on span of the beam and the linear beam load from diagram 16 the right width can be selected. Both methods lead to an effective preselection of Hybridbeam.

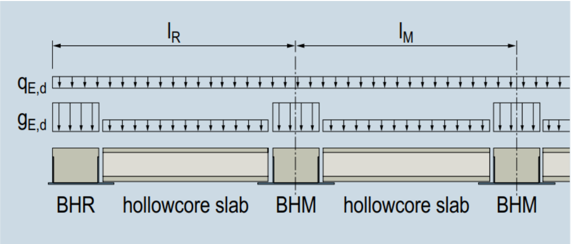

Figure 15: Loading scheme on slab and Hybridbeams

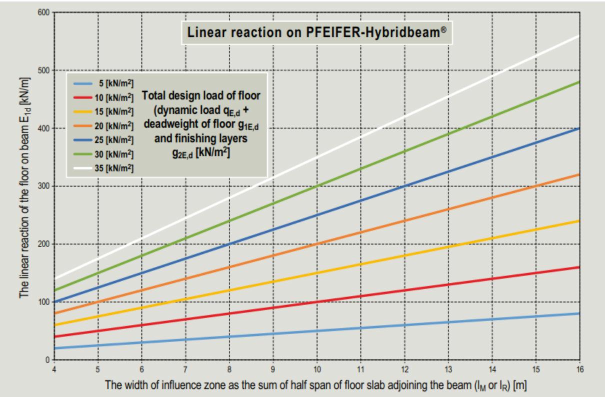

Figure 16 Loading selection of slab for predimensioning of supporting Hybridbeam

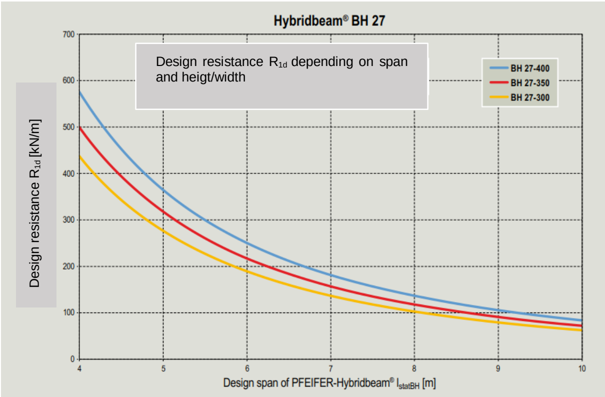

Figure 17 Example of Resistance Diagram of Hybridbeam with height of 27 cm

Specialized engineers of Advisory Centre at PSPP make the necessary calculations for each beam and provide design documentation.

3.3 Installation of Hybridbeams and floor slabs on construction site

Hybridbeams type BHM are usually installed as intermediate beams between two prestressed hollow core slabs of the same height (Fig. 15). In this application the top of the slab is opened at the core positions and after placing reinforcement these voids are filled with poured concrete along with the gaps between beam and slabs. It is also possible to use Hybridbeam type BHM with hollow core slabs to which a poured concrete topping is applied. Slabs of different thicknesses can be supported by forming of a raised concrete bearing for the thinner slab at the fabrication plant.

It is recommended to design the beam support levels 20 mm lower than required and then use shims to raise the bearing level during installation. This provides tolerance for level.

Any cross holes for shear connections in the beams should be checked prior to installation to check that they are clean and free of debris. If contaminated, they should be cleaned before installation.

Hybridbeams normally need no additional support while installing the floor. Only when the slab span extend over 12 m, sometimes is can be required an auxiliary support in the bearing zone of the beam. If the Hybridbeams are placed in final position the hollow core slabs are placed on elastomer strip of the bottom flange. The continuity reinforcement is installed in Hybridbeam and floor slabs according to design documentation. The joint, gaps and connection voids with infill concrete to ensure full filling. After hardening the floor slab is available for using in full strength for live loads.

4. CONCLUSIONS

- Hybridbeam is composite element acting in three bond steps.
- Optimised material combination reinforcement bars, high-strength self-compacting concrete, u-shaped steel element and the floor slab for high load bearing performance.
- Elimination of visible support beams as flush soffit.
- High degree of prefabrication promises a ready-to-install composite component
- High stiffness means no job site propping necessary.
- Increased torsional rigidity already during installation on job site grants free assembly sequence of slab elements.
- Suitable for most slab systems with less deflection because camber in advance
- Highly efficient use of materials.
- Independent first technical performance assessment in Poland Corrosion protection and effective fire protection properties between 1 and 2 hours gives time for evacuating buildings.

The effects of combining all materials and methods of connecting show the efficiency of the whole structure to more than the pure sum of them.

REFERENCES

[1] EN 1991-1-7 Eurocode 1: Actions on structures - Part 1-7: General actions - Accidental actions
[2] EN 1992-1-1:2010 Eurocode 2: Design of concrete structures – Part 1-2: General rules – Structural fire design
[3] EN 1993-1-1:2009 Eurocode 3: Design of steel structures – Part 1-1: General rules and rules for buildings
[4] EN 1994-1-2 Eurocode 4: Design of composite steel and concrete structures – Part 1-2: General rules – Structural fire design
[5] PFEIFER Hybridbeam – Wide spanned to the future, PFEIFER Steel Production Poland, brochure 12-2018, Wroclaw

SPONSORS AND SUPPORT

UNIVERSITY OF ZAGREB
FACULTY OF CIVIL ENGINEERING

100
Years

1919-2019

www.grad.unizg.hr

Mision, Vision and Strategy

Mission

The Faculty of Civil Engineering of the University of Zagreb is the oldest civil engineering faculty in Croatia conducting university education at an undergraduate, graduate and postgraduate level in all branches of civil engineering. It is continually developing and advancing higher education, scientific research activities and overall education, and actively participates in the development of the profession and implementation of new technologies.

Vision

- to retain and strengthen the leading position as a university and scientific-research centre in the country, which covers all branches of civil engineering
- to achieve international recognisability by developing a culture of quality higher education and research work by implementing the best European and world practices, promoting the mobility of students and researchers, and by becoming one of the regional centres of excellence in individual disciplines, as well as a "cooperation bridge" for countries of the European Union and the region
- to retain and strengthen cooperation with the business sector in high-expertise tasks and developmental projects, specialised life-long higher education, and the development of an alumni network for mutual support and progress

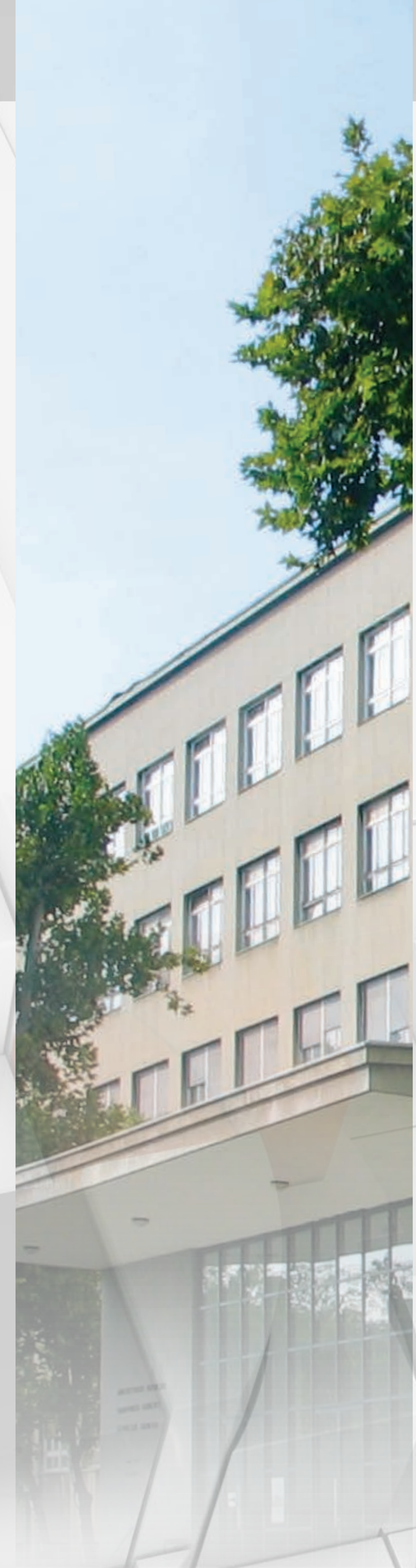

Objectives

- further harmonisation of the outcome of learning with the demands of the profession and market, with continual modernisation of the teaching process and content
- connecting and expanding cooperation with related university institutions and scientific institutions, primarily in the European Union, along with promoting the international mobility of students and researchers
- participation in joint research projects and joint studies with partners from EU countries and the region
- founding individual study programmes in the English language, and organising life-long learning and non-formal education in the English language
- development and modernisation, and certification of laboratories
- increasing spatial and personnel capacities for teaching and research needs
- further ties with the business sector and searching for adequate organisational forms

BE SURE. BUILD SURE.

ENABLING BETTER CONSTRUCTION AND REPAIR

Each individual product can have a critical effect on an entire structure or its repair. Choosing the wrong solutions or applying them incorrectly can lead to component and structural damage and, in extreme cases, even endanger life.
Planners, engineers and applicators therefore have a significant responsibility to bear, of which we are only too aware.
It is not only your own good name that is at stake; businesses and people also have to be protected.
Hence – through reliable and sound technical advice and product solutions – we dedicate our fullest efforts, care and attention to ensuring that each project performed by our customers is executed to their enduring satisfaction and peace of mind. Because part of being MC really does mean accepting responsibility for lives and reputations.

We take building seriously.
BE SURE. BUILD SURE.

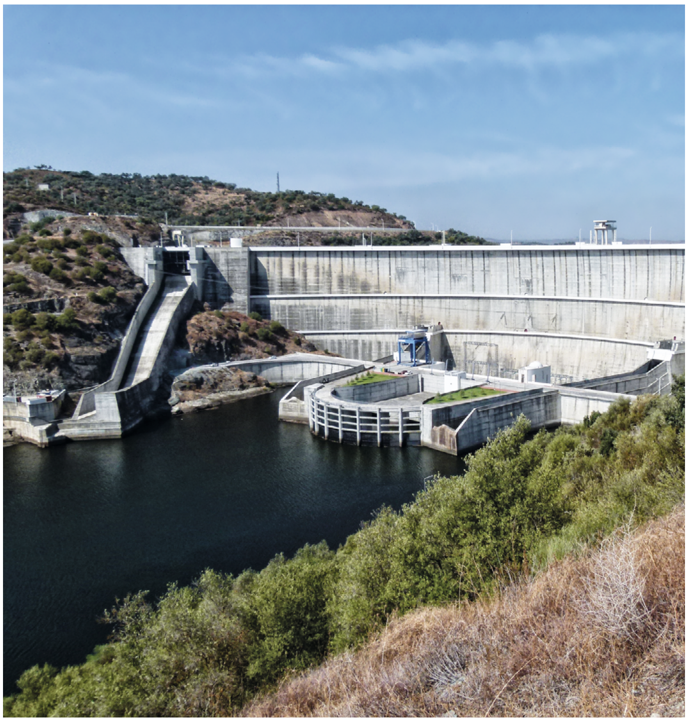

Injection systems

Admixtures for precast concrete

Admixtures
Concrete cosmetics
Grouting mortar

Admixtures
Concrete cosmetics

Floor coatings
Epoxy, Polyurethane

Injection systems
Concrete repair

Floor coatings
Waterproofing
Surface protection

MC solutions in demand throughout the world

MC solutions have been used in major construction and repair projects around the world for more than 50 years now. Developers, promoters, architects, planning engineers and applicators know they can rely both on the advice of our experienced consultants and on the high quality of our product systems.

MC – Building Chemicals d.o.o.
Kovinska 4a, 10090 Zagreb
Tel. +385 (1) 5587 797

www.mc-bauchemie.hr
infocro@mc-bauchemie.com

CONFERENCE EXHIBITORS

CORTEC CORPORATION — Environmentally Safe VpCI®/MCI® Technologies

KNAUF INSULATION

Beton Lučko

PermeaTORR ACTIVE CELL

METTLER TOLEDO

RO-TEHNOLOGIJA — RO - TECHNOLOGIES AG

Toni Technik

ISSN: 0350-2465 (print) ISSN: 1333-9095 (on-line)

GRAĐEVINAR

Journal of the Croatian Association of Civil Engineers

Editor-in-Chief
Prof. **Stjepan Lakusic**
University of Zagreb
Faculty of Civil Engineering

stjepan.lakusic@grad.hr

Journal GRADEVINAR (eng. CIVIL ENGINEER) is a scientific/professional journal with a strong focus on all aspects of Civil Engineering

12 issues/year
3500 copies/issue

The journal GRADEVINAR is a monthly publication that has been regularly appearing **12 times a year** without interruption for three decades now. As the journal is published each month, the publication process of reviewed and accepted papers is relatively fast. The Journal uses the **double blind review** process for evaluation of papers. All papers are printed in Croatian language, but the online edition of the journal features full versions of all papers in English language as well.

The journal GRADEVINAR encourages submission of good papers, not only to help disseminate technical information useful in the field of civil engineering, but also to provide authors with the opportunity to have their paper reviewed by peers and, when published, receive proper recognition for their efforts. The scientific/professional papers are grouped into four categories, depending on their contribution to the advancement of research or professional work.

According to its circulation (3,500 copies), GRADEVINAR is the biggest scientific/professional journal in the field of technical engineering in Croatia and wider region, and is **Indexed in Science Citation Index Expanded.**

On the homepage of Journal GRADEVINAR you can:

- Find all information about the journal
- Acquire information about the journal's most read papers
- Read all papers free of charge
- Find submission information

For more information and for submission guidelines, please visit us at www.casopis-gradjevinar.hr

Editorial address:
Berislavićeva 6, Zagreb, Croatia

phone: +385 1 4872-502
fax: +385 1 4872-526

e-mail: gradjevinar@hsgi.org
www.casopis-gradjevinar.hr

International Conference on Sustainable Materials, Systems and Structures (SMSS2019) – 20-22 March 2019 – Rovinj, Croatia
Challenges in Design and Management of Structures

Edited by Ana Mandić Ivanković, Marija Kušter Marić, Alfred Strauss, Tomislav Kišiček

RILEM Proceedings PRO 128
ISBN: 978-2-35158-217-6
VOL 4. ISBN: 978-2-35158-226-8
e-ISBN: 978-2-35158-218-3
2019 Edition

Conference segment Challenges in Design and Management of Structures provides a forum for discussion on problems related to structural performance for the whole life cycle of the civil engineering structures. It covers advances in design of new and assessment of existing structures based on lessons learned from practice, from collapses, from successes, aiming optimization of structural life cycle management decisions.

Rating and weighting of performance indicators from component, through system, up to network level is a crucial for optimal management of structures aiming their safety, durability and reliability, security and serviceability, availability and maintainability.

Application of scientific achievements in linear and nonlinear analysis methods, numerical modelling and simulation, data updating and processing, semi and full probabilistic based methods with adequate treatment of uncertainties is envisaged to improve design of new and assessment and maintenance of existing infrastructures.

RILEM Publications S.a.r.l.
4 avenue du Recteur Poincaré
75016 Paris - FRANCE
Tel: + 33 1 42 24 64 46 Fax: + 33 9 70 29 51 20
E-mail : dg@rilem.net